# Dyslipidemia, inflammation and the link with metabolism in driving atherosclerosis

Schnitzler, J.G.

**Publication date**
2021

**Document Version**
Final published version

**License**
Other

# Dyslipidemia, inflammation and the link with metabolism in driving atherosclerosis

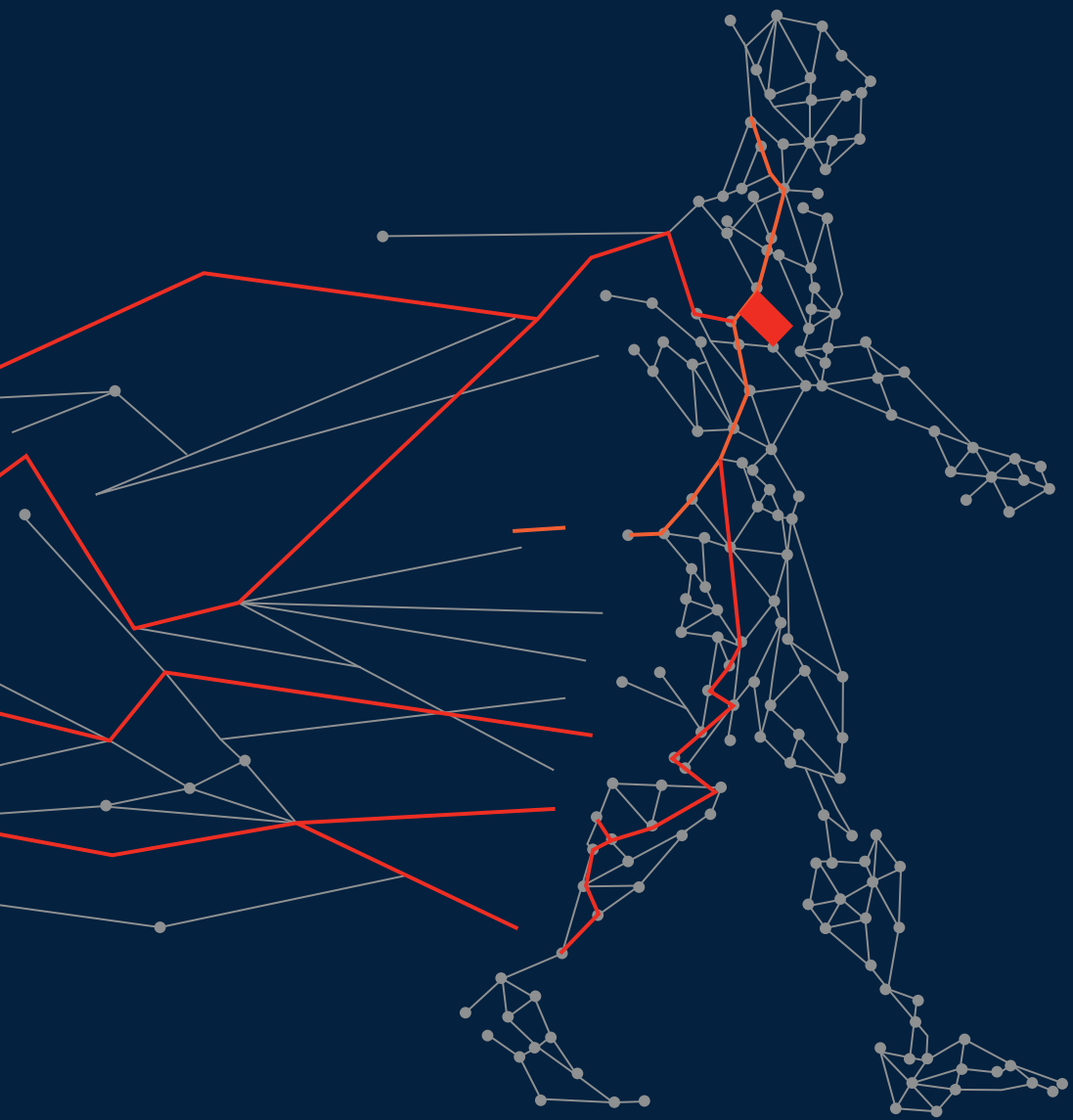

Johan Gustaaf Schnitzler

# Dyslipidemia, inflammation and the link with metabolism in driving atherosclerosis

Johan Gustaaf Schnitzler

## Colofon



Author: Johan Gustaaf Schnitzler

Cover: Marit Janssen

Lay-out: Johan Gustaaf Schnitzler

Printing: Ridderprint | www.ridderprint.nl

ISBN: 978-94-6416-350-6

The research described in this thesis was kindly supported by the AMC and Stichting tot Steun Promovendi Vasculaire Geneeskunde

# Dyslipidemia, inflammation and the link with metabolism in driving atherosclerosis

ACADEMISCH PROEFSCHRIFT

ter verkrijging van de graad van doctor

aan de Universiteit van Amsterdam

op gezag van de Rector Magnificus

prof. dr. ir. K.I.J. Maex

ten overstaan van een door het College voor Promoties ingestelde commissie,

in het openbaar te verdedigen in de Agnietenkapel

op donderdag 14 januari 2021, te 13.00 uur

door

Johan Gustaaf Schnitzler

geboren te Naarden

## Promotiecommissie

| | | |
|---|---|---|
| **Promotor:** | Prof. dr. E.S.G. Stroes | AMC-UvA |
| **Copromotor:** | Dr. J. Kroon | AMC-UvA |
| **Overige leden:** | Prof. dr. R.H.L. Houtkooper | AMC-UvA |
| | Prof. dr. M.P.J. de Winther | AMC-UvA |
| | Dr. S. Huveneers | AMC-UvA |
| | Prof. dr. J.J.P. Kastelein | AMC-UvA |
| | Prof. dr. C.J.M. de Vries | AMC-UvA |
| | Prof. dr. G. Pasterkamp | Universiteit van Utrecht |

**Faculteit der Geneeskunde**

# Dyslipidemia, inflammation and the link with metabolism in driving atherosclerosis

Johan Gustaaf Schnitzler

# Table of contents

# CHAPTER I

General introduction and outline of the thesis

Schnitzler JG

# General introduction

Cardiovascular disease (CVD) is the number one cause of mortality worldwide according to the World Health Organization [1]. The major underlying condition predisposing CVD is atherosclerosis; a chronic lipid-driven low-grade inflammatory disease of the bigger arteries. Atherosclerosis comprises complex interplay with lipids, immune cells, smooth muscle cells and endothelial cells eventually leading to atherosclerotic plaque formation. The combination and interplay of these crucial players ultimately determines the stability of the plaque. Clinically unfavorable vulnerable plaques are prone to rupture and thereby are able to cause myocardial infarction or stroke [2]. Unraveling the mechanisms contributing to atherosclerosis paves the way for identifying new therapeutic options for the treatment of CVD.

*Inflammation*

Classically, atherosclerosis was considered a lipid-driven disease characterized by retention and modification of lipids in the intima. Elevation of low-density (LDL) is a, besides hypertension, smoking and diabetes, well-described risk factor for developing CVD, as seen in patients with familial hypercholesterolemia (FH) [3]. The reputation of high-density lipoprotein (HDL) remains a point of discussion as studies indicate discrepancy with regards to causality in CVD[4].

In line with HDL, triglyceride (TG) levels are an enigmatic issue as very high levels of TG induce to a lesser regard CVD which is most likely attributed to their size [5]. During postprandial hypertriglyceridemia, TG levels rise within hours and stay elevated, making TG levels yet another risk factor for developing CVD [6]. TG mainly enter the body by oral intake, next TG are encapsulated in chylomicrons (CM) for metabolic modification. In severe hypertriglyceridemia, big CM particles are the main carriers of TG and cholesterol but due to their size, ranging up to 600nm, these particles are unable to enter the intima and therefore exert less atherogenic properties. Once metabolized, TGs are carried in smaller remnant cholesterol particles and suddenly become more atherogenic as they now can pass the arterial wall [7]. As TGs are important sources of energy, they are quickly taken up by a variety of cells however, the remaining cholesterol content (or remnant cholesterol) is also considered a causal risk factor for CVD as they are, similar to LDL, retained in the vessel wall and induce inflammation which accelerates atherogenesis. As lipids are retained in the intima of the vessel wall, they undergo oxidic modifications which in turn can be recognized by immune cells as danger-associated molecules or DAMPs [8]. As these cells internalize more and more of these modified lipids, they become foam cells and eventually

become apoptotic which recruits even more immune cells. All these processes are pivotal in the progression of atherosclerosis [9].

Another, revived lipoprotein particle, that is currently gaining more interest is lipoprotein(a) [Lp(a)]. Lp(a) consists of an LDL-like particle with an apolipoprotein(a) protein tail covalently bound to it. Lp(a) levels are genetically determined, and when elevated a causal risk factor for developing CVD. This is attributed to its LDL-entity, which is able to accumulate in the intima, but recent data emerges that in addition, the presence of oxidized phospholipids (OxPLs) present on apo(a) could evoke an inflammatory response [10]. Apo(a), the preferential carrier of OxPLs are marked recognized as DA,MPS by immune cells thereby provoking an immune response [11].

*Current lipid-lowering therapies*

Lowering LDL levels has proved to be a major success in reducing cardiovascular events and all-cause mortality in CVD [12] however, despite potent lipid-lowering therapies, a large inflammatory residual risk remains. This could be ascribed to persistent low-grade inflammation as was shown in the CANTOS-trial where the pro-inflammatory C-reactive protein levels remained increased in patients with CVD despite a strong decrease in LDL levels [13]. Further reduction of LDL decreases the number of CV death yet the residual risk remains apparent [14]. Interestingly, this is amongst others attributed to the potential of LDL to affect stem cell functioning and hematopoiesis, thereby altering their commitment. In the case of LDL, an increased skewing towards the myeloid lineage has been observed [15]. Preclinical data indicates that this remains even without presence of increased LDL levels, indicating LDL-induced persistent activation of the bone marrow which is the main source of hematopoiesis[16]. In case of Lp(a), to date no FDA-approved lowering therapies have been in use however, some interesting new antisense-based therapies emerge [17]. Therefore, the remaining residual risk for developing CVD requires further investigation to treat patients.

*Metabolism*

Nowadays, it is likely to think that the process of atherogenesis is an energy demanding process. As under these inflammatory conditions, both immune cells and endothelial cells secrete cytokines, need to remodel their actin cytoskeleton and have to produce biomass in order to sustain a state of inflammation [2]. Therefore, cells rewire their metabolism to generate sufficient adenosine triphosphate (ATP) to supply energy [18]. Pioneering research over the past years have shown that during atherogenesis, intraplaque macrophages have distinct anti- and proinflammatory

phenotypes which are closely intertwined with specific metabolic traits. As such, proinflammatory macrophages rewire their metabolism from mitochondrial oxidative phosphorylation to the rapid, albeit it less efficient aerobic glycolysis with regards to ATP production. It is important to mention that this 'metabolic switch' occurs despite oxygen being abundantly present. The rate of glycolytic flux is predominantly regulated by the allosteric enzyme 6-phosphofructo-2-kinase/fructose-2,6-biphosphatase-3 (PFKFB3) [18]. This enzyme is pivotal as it converts fructose-6-phosphate (F6P) into fructose 2,6-bisphosphate (F2,6,P2) which in turn increases affinity of 6-phosphofructo-1-kinase (PFK-1). PFK-1 is the first rate-limiting enzyme in glycolysis [19]. Interestingly, PFKFB3 increases the glycolytic flux via a 'glycolytic' loop and thereby not affecting basal glycolysis. This characteristic could pave the way for the use of a potential glycolytic inhibitor as normal glycolysis would not be affected upon inhibition [20]. However, to date this phenomenon has only been described in immune cells which are pivotal in the onset of atherosclerosis once they interact with cells of the vessels.

The inner lining of the vessel wall consists of endothelial cells (ECs), which together comprise a monolayer of cells. In the context of metabolism, an increasing body of evidence indicates glycolysis as main source of energy for ECs, thereby outcompeting the more efficient pathway of OXPHOS [20]. During cancer angiogenesis, specialized ECs (tip cells) have directional migratory traits which, together with proliferating stalk cells, form new vessels to supply tumors with nutrients and oxygen. Landmark papers by the group of Prof. Carmeliet have shown that deletion of inhibition of PFKFB3 is in tip cells, significantly impairs angiogenesis, emphasizing the role of glycolysis in tip-cell migration and angiogenic sprout formation [21].

In the context of atherosclerosis, investigation of endothelial metabolism is a largely underexplored field. However, it has been shown that shear stress is an important factor in controlling EC glycolysis. As ECs are exposed to laminar shear stress, the transcription factor Krüpple-like factor (KLF)2 increases which in turn induces an atheroprotective EC phenotype [22], characterized by endothelial cell alignment in the direction of flow. As such, specific endothelial deletion KLF2 in mice leads to increased glucose uptake and glycolytic flux, all indicative of a glycolytic phenotype. This process is mediated by KLF2 which represses the promotor region of PFKFB3 which is extremely important in angiogenic sprouting and network formation [22]. In atherosclerotic lesions however, predisposed at sites of disturbed blood flow (i.e. vessel branch points and bifurcations) ECs are unable to align and as a functional

consequence become inflamed, secrete pro-inflammatory cytokines such as interleukin (IL) 6, IL8 and monocyte chemoattractant protein (MCP) 1 and upregulate amongst others, the adhesion molecules intercellular adhesion molecule-1 (ICAM-1) and vascular adhesion molecule-1 (VCAM-1) [23]. These cytokines are important in the process of atherogenesis by recruiting immune cells [24]. Since both these as well as angiogenic ECs are activated we hypothesize that ECs in atherosclerosis rely on glycolysis in order to be activated and maintain a pro-inflammatory phenotype.

## OUTLINE OF THE THESIS

In this thesis the first part shines a light on how different subsets of lipoproteins affect and drive immune cell inflammation (see figure 1). This part describes how these lipoproteins are involved in inflammation of immune cells and endothelial cells and how the latter facilitates transmigration of monocytes to contribute to the process of atherosclerosis (**chapter 2**). Next, we describe that LDL induces lipid droplet formation in monocytes (**chapter 3**) and **chapter 4** focuses on the role of remnant cholesterol in context of arterial wall inflammation. **Chapter 5** discusses how postprandial inflammation affects monocytes in patients with metabolic syndrome. Finally, the effect of Lp(a) on hematopoietic activity is investigated in **chapter 6**.

The second part of this thesis reveals how lipid-induced inflammation is fueled by cellular metabolic alterations (see figure 1). First, the interaction of lipoproteins with immune- and endothelial cells is investigated and subsequently how these cells rewire their metabolism as a response to inflammation is studied (**chapter 7**). Subsequently, we investigated the potential of OxPL-Lp(a) to induce inflammation in endothelial cells and the ability of these cells to increase glycolysis after Lp(a) exposure. Furthermore, we show that inhibition of glycolysis leads to decreased inflammation in ECs and thereby decreased monocyte transmigration (**chapter 8**). Next, we reveal that *in vivo* inhibition of glycolysis in hypercholesterolemic mice leads to decreased atherogenesis and increased plaque stability (**chapter 9**). Finally, **chapter 10** comprises the general discussion of this thesis, which summarizes and discusses the main findings of this thesis.

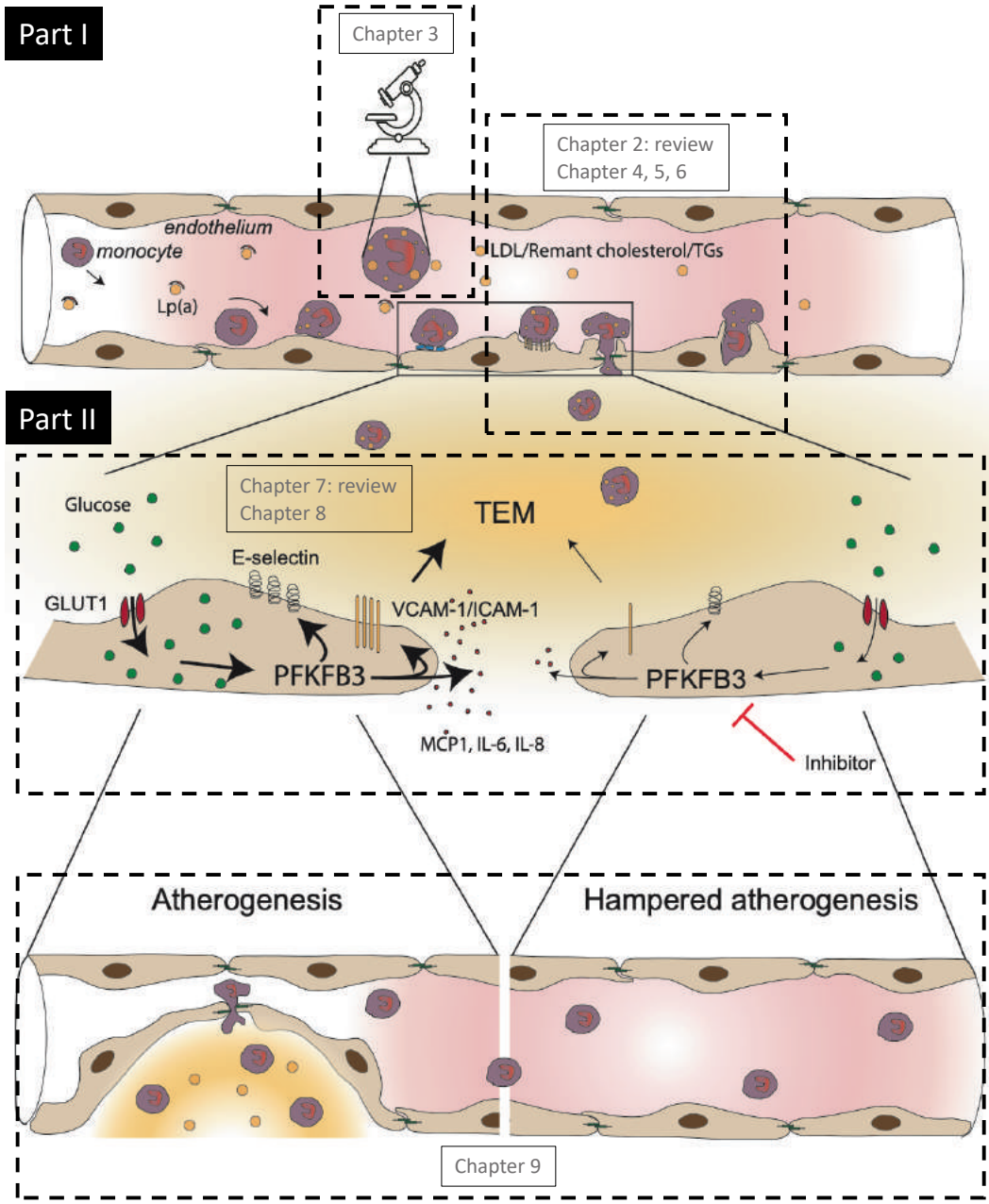
Part I
Chapter 3
Chapter 2: review
Chapter 4, 5, 6
endothelium
monocyte
Lp(a)
LDL/Remant cholesterol/TGs
Part II
Chapter 7: review
Chapter 8
Glucose
TEM
E-selectin
GLUT1
VCAM-1/ICAM-1
PFKFB3
PFKFB3
MCP1, IL-6, IL-8
Inhibitor
Atherogenesis
Hampered atherogenesis
Chapter 9

## References


1. Organisation WH. World Health Organisation. Cardiovascular diseases (CVDs). *https://www.who.int/news-room/fact-sheets/detail/cardiovascular-diseases-(cvds)* 2017;
2. Geovanini GR, Libby P. Atherosclerosis and inflammation: overview and updates. *Clin Sci (Lond)* England; 2018;**132**:1243–1252.
3. Hobbs HH, Brown MS, Goldstein JL. Molecular genetics of the LDL receptor gene in familial hypercholesterolemia. *Hum Mutat* 1992;
4. Voight BF, Peloso GM, Orho-Melander M, Frikke-Schmidt R, Barbalic M, Jensen MK, Hindy G, Hólm H, Ding EL, Johnson T, Schunkert H, Samani NJ, Clarke R, Hopewell JC, Thompson JF, Li M, Thorleifsson G, Newton-Cheh C, Musunuru K, Pirruccello JP, Saleheen D, Chen L, Stewart AFR, Schillert A, Thorsteinsdottir U, Thorgeirsson G, Anand S, Engert JC, Morgan T, Spertus J, et al. Plasma HDL cholesterol and risk of myocardial infarction: a mendelian randomisation study. *Lancet (London, England)* Lancet Publishing Group; 2012;**380**:572–580.
5. Nordestgaard BG, Zilversmit DB. Large lipoproteins are excluded from the arterial wall in diabetic cholesterol-fed rabbits. *J Lipid Res* United States; 1988;**29**:1491–1500.
6. Nordestgaard BG, Freiberg JJ. Clinical relevance of non-fasting and postprandial hypertriglyceridemia and remnant cholesterol. *Curr Vasc Pharmacol* United Arab Emirates; 2011;**9**:281–286.
7. Dallinga-Thie GM, Kroon J, Borén J, Chapman MJ. Triglyceride-Rich Lipoproteins and Remnants: Targets for Therapy? *Curr Cardiol Rep* 2016;**18**:67.
8. Varbo A, Benn M, Tybjaerg-Hansen A, Jorgensen AB, Frikke-Schmidt R, Nordestgaard BG. Remnant cholesterol as a causal risk factor for ischemic heart disease. *J Am Coll Cardiol* United States; 2013;**61**:427–436.
9. Libby P. Inflammation in atherosclerosis. *Nature* England; 2002;**420**:868–874.
10. Tsimikas S. A Test in Context: Lipoprotein(a): Diagnosis, Prognosis, Controversies, and Emerging Therapies. *J Am Coll Cardiol* United States; 2017;**69**:692–711.
11. Serbulea V, Upchurch CM, Ahern KW, Bories G, Voigt P, DeWeese DE, Meher AK, Harris TE, Leitinger N. Macrophages sensing oxidized DAMPs reprogram their metabolism to support redox homeostasis and inflammation through a TLR2-Syk-ceramide dependent mechanism. *Mol Metab* Germany; 2018;**7**:23–34.
12. Pedersen TR, Kjekshus J, Berg K, Haghfelt T, Faergeman O, Faergeman G, Pyörälä K, Miettinen T, Wilhelmsen L, Olsson AG, Wedel H. Randomised trial of cholesterol lowering in 4444 patients with coronary heart disease: the Scandinavian Simvastatin Survival Study (4S). 1994. *Atheroscler Suppl* Netherlands; 2004;**5**:81–87.
13. Ridker PM, MacFadyen JG, Everett BM, Libby P, Thuren T, Glynn RJ. Relationship of C-reactive protein reduction to cardiovascular event reduction following treatment with canakinumab: a secondary analysis from the CANTOS randomised controlled trial. *Lancet (London, England)* England; 2018;**391**:319–328.
14. Ridker PM. Residual inflammatory risk: addressing the obverse side of the atherosclerosis prevention coin. *Eur Heart J* England; 2016;**37**:1720–1722.
15. Valk FM van der, Kuijk C, Verweij SL, Stiekema LCA, Kaiser Y, Zeerleder S, Nahrendorf M, Voermans C, Stroes ESG. Increased haematopoietic activity in patients with atherosclerosis. *Eur Heart J* England; 2017;**38**:425–432.
16. Seijkens T, Hoeksema MA, Beckers L, Smeets E, Meiler S, Levels J, Tjwa M, Winther MPJ de, Lutgens E. Hypercholesterolemia-induced priming of hematopoietic stem and progenitor cells aggravates atherosclerosis. *FASEB J Off Publ Fed Am Soc Exp Biol* United States; 2014;**28**:2202–2213.
17. Tsimikas S, Karwatowska-Prokopczuk E, Gouni-Berthold I, Tardif J-C, Baum SJ, Steinhagen-Thiessen E, Shapiro MD, Stroes ES, Moriarty PM, Nordestgaard BG, Xia S, Guerriero J, Viney NJ, O'Dea L, Witztum JL. Lipoprotein(a) Reduction in Persons with Cardiovascular Disease. *N Engl J Med* United States; 2020;**382**:244–255.
18. Ali L, Schnitzler JG, Kroon J. Metabolism: The road to inflammation and atherosclerosis. *Curr Opin Lipidol* England; 2018;**29**:474–480.
19. Bock K De, Georgiadou M, Carmeliet P. Role of endothelial cell metabolism in vessel sprouting. *Cell Metab* United States; 2013;**18**:634–647.
20. Bock K De, Georgiadou M, Schoors S, Kuchnio A, Wong BW, Cantelmo AR, Quaegebeur A, Ghesquiere B, Cauwenberghs S, Eelen G, Phng L-K, Betz I, Tembuyser B, Brepoels K, Welti J, Geudens I, Segura I, Cruys B, Bifari F, Decimo I, Blanco R, Wyns S, Vangindertael J, Rocha S, Collins RT, Munck S, Daelemans D, Imamura H, Devlieger R, Rider M, et al. Role of PFKFB3-driven glycolysis in vessel sprouting. *Cell* United States; 2013;**154**:651–663.
21. Li X, Kumar A, Carmeliet P. Metabolic Pathways Fueling the Endothelial Cell Drive. *Annu Rev Physiol* United States; 2019;**81**:483–503.
22. Doddaballapur A, Michalik KM, Manavski Y, Lucas T, Houtkooper RH, You X, Chen W, Zeiher AM, Potente M, Dimmeler S, Boon RA. Laminar shear stress inhibits endothelial cell metabolism via KLF2-mediated repression of PFKFB3. *Arterioscler Thromb Vasc Biol* United States; 2015;**35**:137–145.
23. Hahn C, Schwartz MA. The role of cellular adaptation to mechanical forces in atherosclerosis. *Arterioscler Thromb Vasc Biol* United States; 2008;**28**:2101–2107.
24. Schnitzler JG, Dallinga-Thie GM, Kroon J. The Role of (Modified) Lipoproteins in Vascular Function: A Duet Between Monocytes and the Endothelium. *Curr Med Chem* United Arab Emirates; 2019;**26**:1594–1609.

# Part I

*Dyslipidemia, inflammation and monocytes*

# Chapter 2

## The role of (modified) lipoproteins in vascular function: a duet between monocytes and the endothelium

Johan G. Schnitzler, Geesje M. Dallinga-Thie, Jeffrey Kroon

*Current Medicinal Chemistry. 2019;26(9):1594-1609*

## Abstract

Over the last century, many studies have demonstrated that low-density lipoprotein (LDL) is a key risk factor of cardiovascular diseases (CVD) related to atherosclerosis. Thus, for these CVD patients, LDL lowering agents are commonly used in the clinic to reduce the risk for CVD. LDL, upon modification, will develop distinct inflammatory and pro-atherogenic potential, leading to impaired endothelial behavior and subsequent increased foam cell formation. LDL can also directly affect circulating monocyte composition, rendering them in a more favorable position to migrate and accumulate in the subendothelial space. It has become apparent that other lipoprotein particles, such as triglyceride-rich remnants (TRL) and lipoprotein (a) [Lp(a)] may also impact on atherogenic pathways. Evidence is accumulating that Lp(a) can promote peripheral monocyte activation, leading to increased transmigration capacity through the endothelium. Similarly, remnant cholesterol has been identified to play a key role in endothelial dysfunction and monocyte behavior. In this review, we will discuss recent developments in understanding the role of different lipoproteins in the context of inflammation at both the monocyte and the level of the endothelial cell.

**Keywords:** lipoproteins, apoB, Lp(a), oxidized phospholipids, remnants, atherogenesis, monocytes, endothelial cells

## Introduction

Lipoproteins and inflammation of the vasculature are closely intertwined and underlie the pathobiology of atherosclerosis. Depending on their size and composition, most lipoproteins are able to transmigrate through the endothelium, a monolayer of cells lining the lumen of the vessel.[1] This elicits an inflammatory response upon lipoprotein modification, eventually leading to atherogenesis.[2]

Lipoproteins are the main carriers of water insoluble cholesterol (C), cholesterol esters (CE) and triglycerides (TG). The size and density of lipoprotein particles vary and are dependent upon the ratio of CE and TG. The liver acts as a factory where TG, C and CE are packaged into apoB100-containing very low-density lipoproteins (VLDL). Once released in the circulation, the TG moiety will be used for fueling extrahepatic target tissues [3]. During this process, Lipoprotein Lipase (LPL) bound to glycosylphosphatidylinositol high-density lipoprotein (HDL) binding protein1 (GPIHBP1) on the luminal site of the endothelial cell surface drives TG hydrolysis leading to the generation of fatty acids that can be taken up by different cells by CD36.[4-6] Hydrolysis of TG results into smaller cholesterol-enriched VLDL remnant particles. Further lipolysis leads to the generation of cholesterol-enriched low density lipoprotein (LDL) particles by Hepatic Lipase.[7] These particles will be cleared by the liver through uptake via the LDL receptor (LDLR) and subsequent secretion of the cholesterol into the bile [8]. Excess LDL, however, will be taken up in extrahepatic tissues.

Exogenous derived dietary lipids are packaged in apoB48-containing chylomicrons (CMs) in the intestines [5]. Although these CMs are synthetized constitutively in enterocytes, its content is drastically altered in the postprandial state. Once CM are packaged with lipids they are secreted in the lymphatics before being released in the blood circulation.[9] Similar to VLDL, TG in CM will be hydrolyzed by LPL and the fatty acids are directed to energy-demanding tissues leading to a CM-remnant particle which in turn is cleared by the liver [10].

The level of plasma LDL-C is the most important risk factor for cardiovascular disease (CVD). If hepatic clearance of LDL is insufficient, particles will circulate longer in the plasma, which results in oxidative modification of the lipid moiety This is one of the first processes occurring in the pathobiology of CVD.[11] There are multiple mechanisms contributing to the atherogenicity of excess LDL, including its ability to change peripheral monocyte properties and its involvement in macrophage homeostasis after direct intima intravasation.[12] In addition, TG-rich remnant lipoproteins (TRL) are also contributing to the CVD phenotype.[13-16]

Although the best-known driver of atherosclerosis is elevated LDL-C, another important player is Lp(a), which is composed of a single copy apolipoprotein (apo)(a) covalently bound to apoB-100.[17] How Lp(a) assembly occurs is poorly understood. *In vitro* studies show that apo(a) synthesis occurs in hepatocytes and binding of apo(a) with apolipoprotein (apo)B-100 at the cell surface via the lysine-binding pockets or in

the extra hepatic space.[18, 19] However, there is also support for intracellular assembly of Lp(a) as summarized elsewhere.[20]
Recently, Lp(a) has gained major interest because of the development of successful antisense therapies directed against apo(a) synthesis, resulting in decreased Lp(a) particle generation.[21-24] So far, little is known about the pathophysiology of Lp(a), although an increasing number of studies reported that the oxidized phospholipids (OxPLs) are the atherogenic entities carried by Lp(a).[25, 26]. A strong, independent and causal relationship exists between elevated Lp(a) and myocardial infarction, stroke and peripheral artery disease.[27-30] Interestingly, Lp(a) levels are only minimally (~10%) influenced by inflammatory- or fasting state, age and sex [31]. Plasma Lp(a) levels however, are determined by the number of kringle-IV type 2 repeats in the *LPA* gene, resulting in differences in molecular weight of apo(a) protein.[32] Furthermore, apo(a) comprises a serine-protease domain, similar to plasminogen.[33]
Besides these atherogenic apoB-containing lipoprotein particles, HDL particles are known to act as "good" cholesterol.[34, 35] Endogenous HDL assembly starts with the formation of apoAI in the liver or intestine. ApoAI binds to adenosine triphosphate-binding cassette (ABC) transporters AI (ABCA1) at the cell surface resulting in the transfer of cholesterol to apoAI micelles generating pre-mature HDL particles. Free cholesterol is converted into CE by lecithin cholesterol acyltransferase (LCAT). Further maturation occurs via binding to the ABCG1 receptor, allowing further cholesterol enrichment of the particle. Cholesteryl ester transfer protein (CETP) enables the exchange between VLDL-TG and HDL-cholesterol esters.[36]
In this review, we will discuss recent developments in understanding the role of different lipoproteins in the context of inflammation at both the monocyte and endothelial cell level.

## Flow disturbances dictate the sites of vessel wall activation

The endothelium functions as the main regulator of vascular wall homeostasis and serves as a mechanical barrier between blood components and the underlying tissue.[37, 38] Endothelial cells are highly responsive to changes in the direction and magnitude of blood flow, which is an important modulator of vascular integrity.[39, 40] Therefore, the nature and extent of flow-induced shear stress, caused by blood flow, circulating blood cells and plasma factors, play a pivotal role in long-term maintenance, structure and function of the blood vessel.[41] In linear parts of the vessel, endothelial cells are subjected to high laminar shear forces, which are known to be anti-inflammatory and atheroprotective.[42] In contrast, in the vicinity of branch points, bifurcations and curvatures, a disturbed low shear stress pattern is observed, leading to cellular changes within the endothelium.[39, 43, 44]. One well-known example is the downregulation of the anti-inflammatory transcription factor Krüppel-like Factor 2 (KLF2). Consequently, endothelial nitric oxide (NOS3) stability is impaired, leading to a reduction in the production and availability of the vasodilator nitric oxide (NO).[45] This gives rise to increased reactive oxygen species (ROS)

production, enhanced chronic inflammation and increased expression of leucocyte adhesion receptors on the apical membrane of endothelial cells. Interestingly, earlier data suggests that an increase in oxygen radicals could also modify lipoproteins, rendering them more atherogenic.[46, 47] Accordingly, this will lead to the recruitment of monocytes in the subendothelial space. This enhances local inflammation and allows for increased lipoprotein retention in the subendothelial space, thereby facilitating atherogenesis. In the next part, we will further discuss the process of lipoprotein retention leading to aberrant vascular function in the context of atherosclerosis.

### Subendothelial retention of LDL induces atherogenesis

Lipoprotein retention in the subendothelial space is an early event in the pathogenesis of atherosclerosis and occurs even prior to endothelial injury.[48, 49] Lipoproteins cross the intact endothelial barrier by a process termed transcytosis. This encompasses a cascade of reactions including endocytosis, vesicular transport through the cell and exocytosis of the particles at the basolateral site. Transcytosis can be mediated through specific receptors located in clathrin-coated pits or in caveolae, which are specialized membrane microdomains responsible for LDL retention in the subendothelial space.[50] These caveolae are enriched in cholesterol and sphingolipids. Caveolin-1 (Cav1), a prominent protein in caveolae, is not only involved in numerous signaling pathways, but also in plasma lipoprotein metabolism [51]. Interestingly, recent studies in *Cav1*$^{-/-}$ mice revealed attenuation of transcytosis of LDL, resulting in decreased atherosclerosis [52]. The caveolae, up to 100 nm in size, dictate the type of lipoproteins that cross the endothelium. Hence, this process is restricted to smaller VLDL particles, intermediate low-density lipoprotein (IDL;25-35 nm) and LDL (18-25 nm)[53]. In addition, the paracellular transport pathway has been shown to be even more restricted to macromolecules in the range of 3-6 nm. Although several studies have suggested that LDL is able to exit the vasculature via the paracellular route at sites where the endothelium is either damaged resulting in leaky junctions or in mitosis [54-56], recent published studies show only a minor function for the paracellular route in LDL trafficking.[57] These effects appear to be shear stress-dependent.[56] Instead, investigations on intact vessels reveal that fluorescently labelled LDL is transcellularly transported, most likely in a scavenger receptor-B1 (SR-B1)-dependent fashion.[57] Since reduction in SR-B1 expression does not completely abrogate LDL trafficking, the scavenger receptors CD36, scavenger receptor AI and AII (SR-AI/II), and lectin-like ox-LDL receptor (LOX-1), all expressed by endothelial cells, are likely to participate as well.[57] However, Velagapudi *et al*. clearly exclude a role for SR-BI in transcellular transport of LDL.[58] A novel pathway for LDL transcytosis has been recently described by Kraehling etal.[59] It involves Activin A Receptor Like 1 (ACVRL1 or ALK1) which is a novel low-affinity, high capacity receptor, expressed on endothelial cells, that binds LDL and promotes LDL transcytosis in a LDLr independent manner. In summary, the contribution of paracellular transport of LDL

across the vessel wall remains to be further elucidated.[54, 55] Future research will provide more insight in the underlying biology and importance of para- as well as trans-cellular lipoprotein transport. It is becoming increasingly clear that sub-endothelial retention of lipoproteins in the vessel wall appears to be a major determinant of atherogenesis [53, 60]. It has not been fully elucidated which subendothelial matrix molecules participate in the retention of apoB-containing lipoproteins. The extracellular matrix is composed of proteoglycans that consist of a core protein with one or more covalently attached glycosaminoglycan chains that vary in length and determines the properties of the proteoglycans. The most important proteoglycans in the vessel wall are Decorin, Biglycan, Perlecan, Versican and Syndecan-4.[53] Research performed in the mid-nineties by Borén and others demonstrated the importance of the interaction of the positively charged apoB-100 molecules and bridging proteins such as Lipoprotein Lipase and apoE with negatively charged sulphate or carbohydrate groups of glycosaminoglycans on proteoglycans.[61, 62] Interestingly, a single-point mutation in the C-terminal part of *APOB* (p.K3363E) drastically impacts on LDL-proteoglycan interaction, without affecting LDLR binding and provides support for the "response to retention" hypothesis for the initiation of atherosclerosis.[60, 61]. Surprisingly, despite the compelling evidence for its crucial role in promoting atherosclerosis, native LDL does not exert that many inflammatory properties.

The key process underlying the initiation of atherosclerosis, is the influx of monocytes into the vessel wall. In the next section, we will first describe the process of monocyte migration through the vessel wall. Next we will discuss the participation of lipoproteins.

### Monocyte migration: local interactions with the endothelium

Monocytes are key players in innate immunity, mostly known for their role in the promotion and resolution of inflammation.[63] As monocytes are one of the first immune cells to respond during inflammation, it is of importance that these leukocytes quickly reach sites of injury or inflammation. This process of leukocytes crossing the vessel wall is also known as leukocyte extravasation or transendothelial migration (TEM). The recruitment of leukocytes to sites of inflammation is tightly regulated and initiated by cytokines and chemokines, leading to a cascade of interactions between different leukocyte- and endothelial receptors.[64] The initial phase is characterized by rolling and tethering of leukocytes to the vessel wall, followed by chemokine-induced activation. This step provokes firm adhesion and subsequent leukocyte extravasation. Here, we will discuss the underlying processes and the pivotal role of lipoproteins that influence monocyte recruitment and transmigration.[65]

As a result of reduced shear stress or injury, endothelial cells become activated and express an inflammatory signature. In the primary phase of the leukocyte adhesion cascade, low-affinity interplay between L-selectin (CD62L) and P-selectin glycoprotein

ligand-1 (PSLG-1 or CD162) to their endothelial complementary molecules cause the monocyte to decelerate by promoting its rolling and tethering. Next, endothelial release of chemokines and cytokines ensure adhesion structures to be formed at the membrane, thereby enabling monocytes to adhere. This phase is characterized by endothelial-induced chemokine release of amongst others Monocyte Chemoattractant Protein 1(MCP1) and C-X3-C Motif Chemokine Ligand 1 (CX3CL1) which cause monocytes to surveil and roll over the endothelium via their respective counterparts C-C Motif Chemokine Receptor 2 (CCR2) and C-X-C Motif Chemokine Receptor 1 (CXCR1). Integrins, lymphocyte function-associated antigen-1 (LFA-1,$\boldsymbol{\alpha_L\beta_2}$, CD11a/CD18) and very late antigen-4 (VLA-4,$\boldsymbol{\alpha_4\beta_1}$, CD49d/CD29, CD11b) become upregulated and once ligated to their endothelial respective counterparts, intercellular adhesion molecule (ICAM)-1 or CD54 and vascular cell adhesion molecule (VCAM)-1 or CD106, firm adhesion arrest monocytes on the endothelium.[66-68] Subsequently, the majority of the monocytes migrate paracellularly through the endothelial layer whereas some pass the endothelium via the transcellular route.[69, 70] New data emerges that family members of the neuronal guidance cues (NGC) are crucial players involved in regulation of leukocyte transendothelial migration and specifically in steering the leukocyte-endothelium interaction.[71] Decreased expression of Netrin-1 and Semaphorin 3A (SEM3A) in atheroprone regions in *Ldlr*$^{-/-}$ mice was found.[72] Functionally, these findings were substantiated by Van Gils *et al.*, who showed decreased Netrin-1 and Sem3A expression in human coronary artery endothelial cells under pro-inflammatory conditions, whereas increased expression under laminar shear conditions was observed, thereby favoring an atheroprotective effect.[71] In contrast, EphrinB2 (EFNB2) was upregulated under pro-atherosclerotic flow conditions. Increased expression of Sem3A and Netrin-1 leads to reduced leukocyte migration and recruitment to atherosclerotic plaques. Another regulatory layer influencing monocyte TEM is mediated by platelets. Activated platelets, usually present at sites of vascular damage, have been shown to modulate monocyte rolling and tethering under physiological flow conditions. Not only platelets bound to the vessel wall mediate this process, but activated platelets in the circulation can form platelet-monocyte complexes and thereby mediate monocyte migration as well.[73-75] Thus, monocyte adhesion to the vessel wall is enhanced by platelet-monocyte complexes, mainly orchestrated by the interaction of P-selectin on platelets and PSGL-1 on monocytes.[76] Upon monocyte migration, these monocyte-platelet complexes dissociate.[77] OxLDL is able to mediate monocyte-platelet interaction.[78] Excessive passage of monocytes and leukocytes across the endothelium is a hallmark of atherosclerosis.[79, 80] Trapped monocytes will, in an environment with excess lipids, transform into lipid-laden foam cells. The developing synergetic cascade has already been initiated via local cytokine and chemokine release by cells of the immune system causing even more leukocyte accumulation, ultimately aggravating atherogenesis.[79, 81] In the next part, we will discuss the role of (modified) lipoproteins in regulating cellular responses in endothelial cells and how this affects atherogenesis.

## Different lipoproteins and their effect on the endothelium

*Native LDL*

LDL binds and is internalized mainly by the LDL receptor, expressed on a variety of cells, such as smooth muscle cells in atherosclerotic lesions, macrophages, monocytes and EC.[82] Besides native LDL, modified forms of LDL exist that display characteristics distinct from native LDL and have substantially increased pro-atherogenic and inflammatory potential.[83] LDL will be trapped in the subendothelial space where its lipid and protein moiety undergo modifications.[84] *In vitro* studies have shown that LDL exerts a pro-inflammatory effect on endothelial cells, although the actual response was relatively low when compared to the inflammatory capacity of modified LDL.[85] Only a significant increase in the adhesion molecule ICAM-1 was observed after long exposure of (> 4 days) of the cells to LDL.[85] Interestingly, LDL binding to the LDLR is able to induce an inflammatory signaling cascade mediated by the activator protein-1 (AP-1).[86, 87] LDL-induced AP-1 activation increases the leukocyte adhesion molecule VCAM-1 in human umbilical vein endothelial cells (HUVEC), an effect countered by anti-VCAM-1 antibodies.[88] In line with this, LDL, by binding to the LDLR, upregulates VCAM-1 expression in human coronary artery endothelial cells (HCAEC) and porcine aortic endothelial cells as well as VCAM-1 and E-selectin expression in human arterial endothelial cells (HAEC). The observed effects were abrogated by blocking the LDLR, signifying that the effects were attributed to LDL and minimally modified LDL (mmLDL) via binding to the LDLR. Of note, oxidized LDL (oxLDL) does not bind to the LDLR.[89, 90].

*Endothelial modulation upon oxLDL exposure*

The hypothesis of atherosclerosis postulates that oxidation of LDL retained in the subendothelial space is an early event in atherogenesis and is a causative factor in the development of atherosclerosis.[83, 91] OxLDL is present in plasma despite the fact that there are multiple antioxidant defenses present. For example, LDL contains alpha-tocopherol, an important molecule in the protection against oxidation [92] and Lipoprotein-phospholipase A2 (Lp-PLA2).[93, 94] Lipoprotein retention in the intima can lead to oxidation of lipids in LDL, a process mediated by exposure of lipids to oxidizing agents and enzymes. [53] Incubation of endothelial cells, smooth muscle cells, or peripheral blood mononuclear cells (PBMC) with LDL leads to modification of LDL-lipids, a process that could completely be prevented by chelating calcium ions in the medium.[95] Lipoprotein and lipid oxidation is mediated by enzymatic and non-enzymatic oxidative changes.[96, 97] For example, endothelial cells and neutrophils are able to oxidize LDL when NO bioavailability becomes low, which makes NO an essential anti-oxidant.[98] In addition, endothelial cell activation by various molecular stimuli, such as oscillatory shear stress, cytokines, pathogen-associated molecules, could lead to increased reactive oxygen species which in turn further enhance the oxidative modification of apoB-containing lipoproteins.[99] Both LDL and anti-oxidant/oxidant concentrations are in a delicate balance and determine if LDL

oxidation leads to the formation of minimally modified LDL or fully oxidized LDL.[100] Polyunsaturated fatty acids in LDL are prone to be oxidized and may lead to exposure of different epitopes on apoB100 due to conformational changes of the protein, which may result in inhibition of LDL binding to the LDLR on macrophages. Instead, LDL will bind to the scavenger receptors, marking a critical step in atherogenesis.[96, 101, 102] Not only are endothelial cells able to oxidize LDL, their inflammatory signature is also affected by oxLDL itself. Pioneering studies from the group of Orr *et al*. showed that oxLDL was able to influence the nuclear factor-□B (NF-□B) signaling pathway via extracellular matrix-mediated activation of p21 activated kinase, leading to an inflammatory phenotype and increased endothelial permeability via myosin contractility and VE-cadherin phosphorylation. All these effects were abrogated after blocking the fibronectin integrin □5□1. These data indicate that □5□1-mediated crosstalk between fibronectin and oxLDL regulates inflammation in early atherogenesis. [103, 104]. Interestingly, the binding of LDL to proteoglycans makes LDL even more susceptible to oxidation. Consecutively, oxLDL stimulates vascular smooth muscle cells to produce proteoglycans, leading to more LDL retention and more oxidation; an infinite process.[105]

OxLDL is able to trigger an inflammatory response in endothelial cells on multiple levels; it can have a direct effect via the oxLDL-induced release of cytokines by activated tissue resident cells.[100] An interesting new concept has been postulated by Fu etal who showed that oxLDL increases the release of endothelial derived microparticles containing ICAM-1. These particles interact with endothelial cells and results in increased ICAM-1 expression as well as increased monocyte recruitment in regions were oxLDL itself is limited.[106] Recently, it has been shown that the oxidized phospholipid component of oxLDL impairs endothelial function by uncoupling eNOS through inhibition of AKT phosphorylation, but also affects endothelial cell proliferation.[107-110] The major receptor for oxLDL on endothelial cells is LOX-1 although a putative role for the scavenger receptor CD36 has been described.[111-115] Although basal LOX-1 expression is very low, it can be upregulated by pro-inflammatory cytokines, such as tumor necrosis factor (TNF)□ and oxLDL itself.[116, 117] Once oxLDL binds to the receptor, endothelial cells become activated and facilitate increased binding of circulating leukocytes to the inflamed vessel wall. The recruitment of monocytes to the vessel wall involve both chemokines and adhesion molecules. Besides this, oxLDL/LOX-1 binding upregulate the adhesion molecules E-selectin, P-selectin, VCAM-1 and ICAM-1; key molecules involved in efficient leukocyte diapedesis oxLDL which are regulated in a NF-□B dependent manner.[118, 119] Additionally, oxLDL is able to increase Actin Related Protein 2/3 expression via LOX-1 signaling in a Rac-1 dependent fashion, leading to increased vessel wall permeability.[120] *In vitro* studies revealed that oxLDL also may induce endothelial cell apoptosis through LOX-1 dependent endoplasmatic reticulum stress response pathway.[121] Another layer of complexity in oxLDL induced endothelial responses is

regulated by different microRNAs. Its clinical relevance, however, remains to be established.[122-124]

*Lipoprotein (a)-mediated activation of the endothelium*

Lp(a) has been studied for many years but the underlying mechanisms by which it regulates its atherogenicity is poorly understood.[125] Elegant research from the group of Tsimikas and colleagues demonstrated that Lp(a) is the preferential lipoprotein carrier for oxidized phospholipids. This makes Lp(a) on an equimolar basis even more atherogenic than LDL.[26, 126, 127] HUVEC stimulated with Lp(a) increase the expression of CC chemokine I-309. The increase is mediated via its receptor CCR8 and is pivotal for monocyte chemotactic activity.[128] This effect was attributed to apo(a) and is absent after stimulation with solely LDL. These findings were substantiated by the detection of I-309 in human plaques implying that I-309 could lead to the attraction of monocytes into plaques. In addition, Lp(a) can also enhance the migratory capacity through the vessel wall by upregulating key adhesion molecules required for efficient leukocyte migration. Lp(a) induces the expression of the adhesion molecules E-selectin, ICAM-1, VCAM-1 and MCP-1 in bovine aortic endothelial cells. In line with this, Lp(a) increases VCAM-1 and E-selectin surface expression in a dose- and time-dependent manner in HCAEC. [129] This response is triggered by a rise of intracellular free calcium. Lp(a) is furthermore able to increase the expression of adhesion molecule P-selectin and ICAM-1 in HUVEC, but VCAM-1 and E-selectin were not affected.[130, 131] Interestingly, recombinant apo(a) (r-apo(a)) is able to increase vascular permeability. Binding of r-apo(a) to a putative receptor leads the activation of the small GTPase RhoA and its downstream effector Rho kinase (ROCK), eventually leading to a marked increase in endothelial cell contractility. This coincides with junction instability, characterized by internalization of the key endothelial junction molecule vascular endothelial (VE)-cadherin and increased junction leakage as measured with fluorescently labelled FITC-dextran over a transwell filter.[132] All these observed effects were abrogated using r-apo(a) lacking the strong lysine binding site which is responsible for oxPL binding. Taken together, although it is clear that oxPL-Lp(a) has pro-inflammatory effects on endothelial cells, its exact molecular mechanism remains largely unknown and requires further investigation.

*Remnant lipoproteins as potent mediators of endothelial inflammation*

In recent years, endothelial inflammatory pathways initiated by VLDL-remnant lipoproteins are a topic of extensive investigation. These days, remnant cholesterol reflects the cholesterol content in TG-rich lipoproteins such as IDL and VLDL, but also chylomicron remnants in a non-fasting state. Remnant particles transmigrate through the endothelial layer, get trapped, accumulate and are engulfed by macrophages which becomes foam cells.[1] Besides LDL, oxLDL and Lp(a), remnant particles have potent atherogenic properties leading to enhanced gene expression of VCAM-1, ICAM-1, E-selectin and MCP-1 but also increase the production of the pro-

inflammatory cytokines TNF-α and IL-1β by the endothelium.[133, 134] Interestingly, remnant particles derived from hypertriglyceridemic patients led to a more profound endothelial inflammatory response, compared to particles derived from healthy subjects, implicating that the lipid content of remnant particles is an important driver of endothelial inflammation.[135] Postprandial VLDL remnants have an even more profound effect as demonstrated by the observation that endothelial dysfunction occurs during postprandial hypertriglyceridemia.[136-139] The uptake of remnant particles in the endothelium is mainly mediated via LOX-1[133, 140] but remnants are also taken up by LDL receptor-mediated protein 1 (LRP1) located in lipid rafts. These lipid rafts cluster when exposed to remnant particles and therefore induce inflammatory signaling pathways in endothelial cells.[141] In addition, VLDL remnant particles have shown to activate NF-κB.[142] *In vivo* evidence of remnant particles participating in the process of atherosclerosis is the accumulation of $^{18}$F-fluorodeoxyglucose, a marker for arterial wall inflammation, in the arterial wall in patients with dysbetalipoproteinemia.[143, 144]. Together, these data indicate that remnant cholesterol is a key player of endothelial inflammation, both in the fasting- as in the non-fasting state.

*HDL and the endothelium*

Although the role of HDL on TEM is beyond the scope of this paper, we will briefly discuss this topic. Low plasma HDL cholesterol is associated with an increased risk for coronary heart disease which indicates an atheroprotective role for HDL.[145-147] Multiple functions of HDL, such as protection against oxidation, capacity to efflux cholesterol, protection against inflammation and modulation of vascular endothelial function, may all contribute to the anti-atherosclerotic properties.[148, 149] As an example, it has been shown that HDL protects the endothelium from the atherogenic effect of oxLDL or other inflammatory agents by attenuating the release of adhesion molecules.[150, 151] Furthermore HDL induces endothelium-dependent vasodilation through phosphorylation of eNOS, and attenuation nitric oxide synthesis and uncoupling of NADPH oxidation.[148] HDL also promotes vascular cell migration and proliferation but also recruitment of endothelial progenitor cells to the sites where vascular injury occurs although the latter function is still in debate since results are conflicting.

## Monocyte migration: systemic inflammation

*LDL-cholesterol: an alternative road to systemic inflammation*

Recent evidence emerged indicating that LDL in the circulation interacts with white blood cells, mainly monocytes, leading to an enhanced inflammatory state. Monocytes derived from patients with Familial Hypercholesterolemia (FH) have increased expression of CD11b, CD18, and chemokines receptors CX3CR1 and CCR2.[12] This increase in CCR2 expression is correlated markedly with elevated neutral lipid accumulation in the monocytes.[12, 152] An increase in peripheral lipid

accumulation was accompanied by elevated expression of cholesterol efflux proteins ABCA1 and ABCG1, suggesting a compensatory mechanism to overcome the increase in lipid content. These findings are similar to earlier findings showing an increased monocyte lipid accumulation in patients with FH, but also in hypercholesterolemic mice, although ABCA1 expression was decreased.[152] On the other hand, CCR2 mediates the propensity for trafficking of monocytes towards vascular sites of inflammation and is therefore pivotal in the process of atherogenesis.[153] The altered composition of monocytes derived from hypercholesterolemic patients results in different behavior as shown by *ex vivo* increased transmigration capacity across endothelium.[12] Twenty-four weeks of treatment with a monoclonal antibody against proprotein convertase subtilisin/kexin type 9 (PCSK9) resulted in significant plasma LDL reduction due to anti-PCSK9-induced increased availability of the hepatic LDL receptor. This coincided with reduced expression of CCR2 on the monocytes resulting in decreased monocyte transmigration. Taken together, LDL is an important driver of monocyte behavior.

*Remnant cholesterol elicits monocyte inflammation*

LDL particles are not solely responsible for observed effects on circulating monocytes but also triglyceride-rich remnant particles may participate in defining the lipid composition of circulating monocytes. Monocytes isolated from patients with familial dysbetalipoproteinemia, characterized with *APOE2E2* genotype and elevated levels of plasma TG and cholesterol, have a phenotypically inflamed profile as demonstrated by increased expression of CD11b/CD11c/CD18.[143] Similar observations have been made in the postprandial state [154] wherein monocytes isolated during the peak of the postprandial response have more lipid droplets. In support, *in vitro* uptake of TRLs by monocytes leads to enhanced internalization of TGRL, mainly via LRP1.[155] Treatment of THP1 cells with VLDL lipolysis products demonstrated that the origin of lipids in the droplets originates from hydrolysed VLDL-derived fatty acids. *Apoe*$^{-/-}$ mice fed a western diet also develop lipid-laden monocytes, which infiltrate into nascent atherosclerotic lesions in a CD11c-dependent manner.[156] A deficiency in CD11c led to decreased arrest of monocytes to VCAM-1 and E-selectin in a shear flow model, but also reduced monocyte and macrophage accumulation in atherosclerotic regions.[157] In conclusion, monocytes internalize lipids in the circulation and as a result express more CD11c leading to increased adhesion and migratory capacity to the vascular wall.

*Lp(a) drives monocyte activation*

Patients with elevated levels of plasma Lp(a) (>50 mg/dL) have monocytes with an inflammatory profile characterized by, amongst others, increased CD11c, CD11b, CD29, but also chemokine receptor CCR7 and increased potential to transmigrate.[25, 158] This was further substantiated with cross-sectional SPECT/CT imaging, showing autologous labelled $^{99m}$Tc-labeled PBMC accumulation in the

carotids and aorta of patients. Apo(a) can specifically interact with the ß2-integrin Mac1, thereby promoting the adhesion of monocytes resulting in increased TEM.[158] On the other hand, Lp(a) is the major carrier of oxidized phospholipids, and is known to act as a danger-associated molecular pattern by recognizing receptors on immune cells, leading to an pro-inflammatory stimulus.[127] Indeed, inactivation of oxPLs on Lp(a) leads to an attenuation of the inflammatory response of monocytes.[25] However, more research is required to fully understand the underlying pathobiology of Lp(a) action in monocyte activation.

*Anti-inflammatory properties of HDL on monocytes*

The role of HDL on macrophages in the intima is well described, however the interplay of HDL and circulating monocytes is less understood. Recombinant HDL infusion markedly attenuated the inflammatory monocyte phenotype in patients with type 2 diabetes.[159] This has been further investigated in a very recent study showing that HDL cholesterol levels are negatively associated with different monocyte cytokine markers.[160] Additionally, HDL suppressed monocyte migration towards MCP-1 and decreased monocyte f-actin content which is essential for transmigration.[161, 162]

## Lipoproteins intervene at hematopoietic level

Over the past few years, the importance of dysregulated hematopoiesis, the production of blood cells, as a strong driver of atherogenesis and plaque vulnerability has been emphasized. Monocytes are mainly derived from precursor cells in the bone marrow and are an important player in the underlying pathobiology of atherosclerosis. This process is a low-grade inflammatory disease of the arterial wall, largely driven by cholesterol-facilitated recruitment of bone-marrow derived monocytes into the atherosclerotic plaque.[37, 163-165]. Several research groups hypothesized that the fate of monocytes is already determined at the hematopoietic level. Hematopoiesis is tightly regulated by the bone marrow niche, consisting of multiple cell types which orchestrate the quiescence and activation of hematopoietic stem cells (HSCs).[166, 167] Once HSCs are activated, they generate monocytes which then can enter the circulation. Interestingly, previous studies have shown that common cardiovascular risk factors such as dyslipidemia [168] and hyperglycemia [169] can also modulate HSC cell fate. In most cases, HSC activation, as was found in patients with familial dysbetalipoproteinemia using $^{18}$F-FDG-PET/CT imaging, leads to increased monocyte production. [143] Similar findings were made in mice lacking ABCA1 and ABCG1, but after bone marrow transplantation to mice with elevated levels of HDL these adverse effects were abrogated.[170] Since HSC phenotype is already influenced in the bone marrow, it would be of great clinical interest to investigate whether and when monocytes obtain their mature inflammatory profile once exposed to common risk factors at the bone marrow level.

## Conclusion

It has become evident that circulating monocytes are playing a more important role in the pathobiology underlying atherosclerosis than has been anticipated so far. The composition of the monocytes will affect its function and is influenced by disturbed lipoprotein particles. Moreover, the migration of monocytes through the endothelial cell layer lining the vessel wall is a complex multilevel process. Different lipoproteins such as triglyceride-rich lipoprotein remnant, LDL, Lp(a) and HDL, which vary in size and function, mediate trans-endothelial migration via different pathways. A summarizing illustration of this important process can be found in Figure 1. In conclusion it is a great challenge to monitor monocyte behavior *in vivo* by improving imaging techniques, allowing a better understanding of the underlying pathobiology.


## Acknowledgements

The authors would like to thank Yasmin de Wit for assisting with the literature research. J.K is supported by the Amsterdam Cardiovascular Sciences (ACS) Postdoc Fellowship (2017). This project has received funding from the European Union's Horizon 2020 research and innovation programme under grant agreement No 667837.


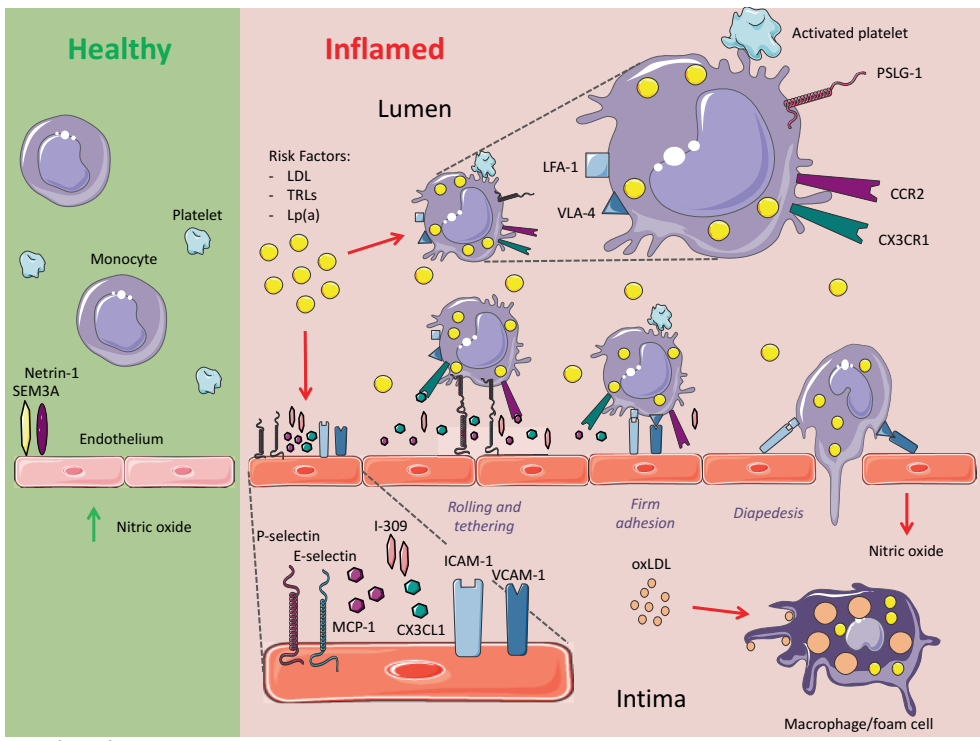


**Figure legend:**

**Transendothelial migration of monocytes.** Reduced expression of Netrin-1 and SEM3A together with decreased NO production, as a consequence of disturbed flow, progresses endothelial activation. Additionally, lipoproteins (LDL, TRLs and Lp(a)) may increase the inflammatory response of both EC and monocytes. Monocytes are able to internalize lipoproteins already in the

circulation and gain an inflammatory phenotype. Activated EC produce chemokines such as, MCP-1, I-309 and CX3CL1 to attract monocytes from the circulation. The chemokines are detected by monocytes expressing chemokine receptors CCR2 and CX3CR1. Next, the rolling phase is initiated by endothelial upregulation of P-selectin and E-selectin that bind PSGL-1 present on monocytes with low affinity. Now, firm adhesion occurs via LFA-1/ICAM-1 and VLA-4/VCAM-1 binding which renders firmly adhered monocytes prone for diapedesis. In addition, the process of TEM is in part orchestrated via activated platelets that form a complex with monocytes. Once in the intima, monocytes take up oxLDL and become macrophage/foam cells.

**Abbreviations:** CVD, cardio vascular disease; LDL, low-density lipoprotein; oxLDL, oxidized LDL; oxPL, oxidized phospholipids; VLDL, very low density lipoprotein; IDL, intermediate density lipoprotein; HDL, high density lipoprotein; TRL, triglyceride-rich lipoprotein; CM, chylomicron; Lp(a), lipoprotein(a); apo, apolipoprotein; LDLR, LDL receptor; LCAT, lecithin cholesterol acyl transferase; CETP, cholesterol ester transfer protein; TEM, trans endothelial migration; MCP-1, monocyte chemoattractant protein-1; CX3CL1, C-X3-C motif chemokine ligand1; CCR2, C-C motif chemokine receptor2; CX3CR1, C-X3-C motif chemokine receptor1; PSGL-1, P-selectin glycoprotein ligand-1; LFA-1, lymphocyte function-associated antigen-1; ICAM-1, intercellular adhesion molecule-1; VLA-4, very late antigen-4; VCAM-1, vascular cell adhesion molecule-1; NGC, neuronal guidance cues; SEM3A, semaphore 3 A; EFNB2, ephrin B2; KLF2, Krüppel like factor 2; NOS3, endothelial nitric oxide synthase; ACVRL1 or ALK1, Activin A Receptor Like Protein 1; ROS, reactive oxygen species; Cav1, caveolin 1; SR-B1, scavenger receptor B1; SR-AI, scavenger recptor AI; LOX-1, lectin-like ox-LDL receptor; AP-1, activator protein1; HUVEC, human umbiolical vene endothelial cell; HCAEC, human coronary artery andothelial cell; HAEC, human artery endothelial cell; Lp-PLA2, lipoprotein phospholipase A2; PBMC, peripheral blood mononuclear cells; TNF tissue nuclear factor; ROCK, ; LRP1, LDL receptor-like receptor protein; ABCA1 and ABCG1, adenosine triphosphate-binding cassette (ABC) transporters A1 and GI; PCSK9, proprotein convertase subtilisin/kexin type 9; HSC, human stem cells.

## Reference List


[1] Boren, J.; Williams, K.J., The central role of arterial retention of cholesterol-rich apolipoprotein-B-containing lipoproteins in the pathogenesis of atherosclerosis: a triumph of simplicity. *Curr Opin Lipidol*, **2016**, *27*, 473-483.

[2] Gistera, A.; Hansson, G.K., The immunology of atherosclerosis. *Nat Rev Nephrol*, **2017**, *13*, 368-380.

[3] Dallinga-Thie, G.M.; Franssen, R.; Mooij, H.L.; Visser, M.E.; Hassing, H.C.; Peelman, F.; Kastelein, J.J.; Peterfy, M.; Nieuwdorp, M., The metabolism of triglyceride-rich lipoproteins revisited: new players, new insight. *Atherosclerosis*, **2010**, *211*, 1-8.

[4] Young, S.G.; Zechner, R., Biochemistry and pathophysiology of intravascular and intracellular lipolysis. *Genes Dev*, **2013**, *27*, 459-484.

[5] Hussain, M.M., Intestinal lipid absorption and lipoprotein formation. *Curr Opin Lipidol*, **2014**, *25*, 200-206.

[6] Abumrad, N.A.; Goldberg, I.J., CD36 actions in the heart: Lipids, calcium, inflammation, repair and more? *Biochim Biophys Acta*, **2016**, *1861*, 1442-1449.

[7] Williams, K.J., Molecular processes that handle -- and mishandle -- dietary lipids. *J Clin Invest*, **2008**, *118*, 3247-3259.

[8] Goldstein, J.L.; Brown, M.S., Atherosclerosis: the low-density lipoprotein receptor hypothesis. *Metabolism*, **1977**, *26*, 1257-1275.

[9] Twickler, T.; Dallinga-Thie, G.M.; Chapman, M.J.; Cohn, J.S., Remnant lipoproteins and atherosclerosis. *Curr Atheroscler Rep*, **2005**, *7*, 140-147.

[10] Chatterjee, C.; Sparks, D.L., Hepatic lipase, high density lipoproteins, and hypertriglyceridemia. *Am J Pathol*, **2011**, *178*, 1429-1433.

[11] Ketelhuth, D.F.; Hansson, G.K., Cellular immunity, low-density lipoprotein and atherosclerosis: break of tolerance in the artery wall. *Thromb Haemost*, **2011**, *106*, 779-786.

[12] Bernelot Moens, S.J.; Neele, A.E.; Kroon, J.; van der Valk, F.M.; Van den Bossche, J.; Hoeksema, M.A.; Hoogeveen, R.M.; Schnitzler, J.G.; Baccara-Dinet, M.T.; Manvelian, G.; de Winther, M.P.J.; Stroes, E.S.G., PCSK9 monoclonal antibodies reverse the pro-inflammatory profile of monocytes in familial hypercholesterolaemia. *Eur Heart J*, **2017**, *38*, 1584-1593.

[13] Berglund, L.; Brunzell, J.D.; Goldberg, A.C.; Goldberg, I.J.; Sacks, F.; Murad, M.H.; Stalenhoef, A.F.; Endocrine, s., Evaluation and treatment of hypertriglyceridemia: an Endocrine Society clinical practice guideline. *J Clin Endocrinol Metab*, **2012**, *97*, 2969-2989.

[14] Freiberg, J.J.; Tybjaerg-Hansen, A.; Jensen, J.S.; Nordestgaard, B.G., Nonfasting triglycerides and risk of ischemic stroke in the general population. *JAMA*, **2008**, *300*, 2142-2152.

[15] Nordestgaard, B.G.; Benn, M.; Schnohr, P.; Tybjaerg-Hansen, A., Nonfasting triglycerides and risk of myocardial infarction, ischemic heart disease, and death in men and women. *JAMA*, **2007**, *298*, 299-308.

[16] Varbo, A.; Benn, M.; Tybjaerg-Hansen, A.; Jorgensen, A.B.; Frikke-Schmidt, R.; Nordestgaard, B.G., Remnant cholesterol as a causal risk factor for ischemic heart disease. *J Am Coll Cardiol*, **2013**, *61*, 427-436.

[17] Utermann, G.; Menzel, H.J.; Kraft, H.G.; Duba, H.C.; Kemmler, H.G.; Seitz, C., Lp(a) glycoprotein phenotypes. Inheritance and relation to Lp(a)-lipoprotein concentrations in plasma. *J Clin Invest*, **1987**, *80*, 458-465.

[18] White, A.L.; Lanford, R.E., Cell surface assembly of lipoprotein(a) in primary cultures of baboon hepatocytes. *J Biol Chem*, **1994**, *269*, 28716-28723.

[19] Lobentanz, E.M.; Dieplinger, H., Biogenesis of lipoprotein(a) in human and animal hepatocytes. *Electrophoresis*, **1997**, *18*, 2677-2681.

[20] Reyes-Soffer, G.; Ginsberg, H.N.; Ramakrishnan, R., The metabolism of lipoprotein (a): an ever-evolving story. *J Lipid Res*, **2017**, *58*, 1756-1764.

[21] Willeit, P.; Kiechl, S.; Kronenberg, F.; Witztum, J.L.; Santer, P.; Mayr, M.; Xu, Q.; Mayr, A.; Willeit, J.; Tsimikas, S., Discrimination and net reclassification of cardiovascular risk with lipoprotein(a): prospective 15-year outcomes in the Bruneck Study. *J Am Coll Cardiol*, **2014**, *64*, 851-860.

[22] Merki, E.; Graham, M.; Taleb, A.; Leibundgut, G.; Yang, X.; Miller, E.R.; Fu, W.; Mullick, A.E.; Lee, R.; Willeit, P.; Crooke, R.M.; Witztum, J.L.; Tsimikas, S., Antisense oligonucleotide lowers plasma levels of apolipoprotein (a) and lipoprotein (a) in transgenic mice. *J Am Coll Cardiol*, **2011**, *57*, 1611-1621.

[23] Nordestgaard, B.G.; Langsted, A., Lipoprotein (a) as a cause of cardiovascular disease: insights from epidemiology, genetics, and biology. *J Lipid Res*, **2016**, *57*, 1953-1975.

[24] Tsimikas, S., A Test in Context: Lipoprotein(a): Diagnosis, Prognosis, Controversies, and Emerging Therapies. *J Am Coll Cardiol*, **2017**, *69*, 692-711.

[25] van der Valk, F.M.; Bekkering, S.; Kroon, J.; Yeang, C.; Van den Bossche, J.; van Buul, J.D.; Ravandi, A.; Nederveen, A.J.; Verberne, H.J.; Scipione, C.; Nieuwdorp, M.; Joosten, L.A.; Netea, M.G.; Koschinsky, M.L.; Witztum, J.L.; Tsimikas, S.; Riksen, N.P.; Stroes, E.S., Oxidized Phospholipids on Lipoprotein(a) Elicit Arterial Wall Inflammation and an Inflammatory Monocyte Response in Humans. *Circulation*, **2016**, *134*, 611-624.

[26] Capoulade, R.; Chan, K.L.; Yeang, C.; Mathieu, P.; Bosse, Y.; Dumesnil, J.G.; Tam, J.W.; Teo, K.K.; Mahmut, A.; Yang, X.; Witztum, J.L.; Arsenault, B.J.; Despres, J.P.; Pibarot, P.; Tsimikas, S., Oxidized Phospholipids, Lipoprotein(a), and Progression of Calcific Aortic Valve Stenosis. *J Am Coll Cardiol*, **2015**, *66*, 1236-1246.

[27] Tsimikas, S.; Mallat, Z.; Talmud, P.J.; Kastelein, J.J.; Wareham, N.J.; Sandhu, M.S.; Miller, E.R.; Benessiano, J.; Tedgui, A.; Witztum, J.L.; Khaw, K.T.; Boekholdt, S.M., Oxidation-specific biomarkers, lipoprotein(a), and risk of fatal and nonfatal coronary events. *J Am Coll Cardiol*, **2010**, *56*, 946-955.

[28] Emerging Risk Factors, C.; Erqou, S.; Kaptoge, S.; Perry, P.L.; Di Angelantonio, E.; Thompson, A.; White, I.R.; Marcovina, S.M.; Collins, R.; Thompson, S.G.; Danesh, J., Lipoprotein(a) concentration and the risk of coronary heart disease, stroke, and nonvascular mortality. *JAMA,* **2009**, *302*, 412-423.
[29] Erqou, S.; Thompson, A.; Di Angelantonio, E.; Saleheen, D.; Kaptoge, S.; Marcovina, S.; Danesh, J., Apolipoprotein(a) isoforms and the risk of vascular disease: systematic review of 40 studies involving 58,000 participants. *J Am Coll Cardiol,* **2010**, *55*, 2160-2167.
[30] Kamstrup, P.R.; Benn, M.; Tybjaerg-Hansen, A.; Nordestgaard, B.G., Extreme lipoprotein(a) levels and risk of myocardial infarction in the general population: the Copenhagen City Heart Study. *Circulation,* **2008**, *117*, 176-184.
[31] Langsted, A.; Kamstrup, P.R.; Nordestgaard, B.G., Lipoprotein(a): fasting and nonfasting levels, inflammation, and cardiovascular risk. *Atherosclerosis,* **2014**, *234*, 95-101.
[32] Boerwinkle, E.; Leffert, C.C.; Lin, J.; Lackner, C.; Chiesa, G.; Hobbs, H.H., Apolipoprotein(a) gene accounts for greater than 90% of the variation in plasma lipoprotein(a) concentrations. *J Clin Invest,* **1992**, *90*, 52-60.
[33] Utermann, G., The mysteries of lipoprotein(a). *Science,* **1989**, *246*, 904-910.
[34] Tardif, J.C.; Gregoire, J.; L'Allier, P.L.; Ibrahim, R.; Lesperance, J.; Heinonen, T.M.; Kouz, S.; Berry, C.; Basser, R.; Lavoie, M.A.; Guertin, M.C.; Rodes-Cabau, J.; Effect of r, H.D.L.o.A.-S.; Efficacy, I., Effects of reconstituted high-density lipoprotein infusions on coronary atherosclerosis: a randomized controlled trial. *JAMA,* **2007**, *297*, 1675-1682.
[35] Libby, P., Managing the risk of atherosclerosis: the role of high-density lipoprotein. *Am J Cardiol,* **2001**, *88*, 3N-8N.
[36] Kontush, A.; Chapman, M.J., Functionally defective high-density lipoprotein: a new therapeutic target at the crossroads of dyslipidemia, inflammation, and atherosclerosis. *Pharmacol Rev,* **2006**, *58*, 342-374.
[37] Ross, R., Atherosclerosis--an inflammatory disease. *The New England Journal of Medicine,* **1999**, *340*, 115-126.
[38] Hahn, C.; Schwartz, M.A., The role of cellular adaptation to mechanical forces in atherosclerosis. *Arterioscler Thromb Vasc Biol,* **2008**, *28*, 2101-2107.
[39] Baratchi, S.; Khoshmanesh, K.; Woodman, O.L.; Potocnik, S.; Peter, K.; McIntyre, P., Molecular Sensors of Blood Flow in Endothelial Cells. *Trends Mol Med,* **2017**.
[40] Cunningham, K.S.; Gotlieb, A.I., The role of shear stress in the pathogenesis of atherosclerosis. *Lab Invest,* **2005**, *85*, 9-23.
[41] Traub, O.; Berk, B.C., Laminar shear stress: mechanisms by which endothelial cells transduce an atheroprotective force. *Arterioscler Thromb Vasc Biol,* **1998**, *18*, 677-685.
[42] Pan, S., Molecular mechanisms responsible for the atheroprotective effects of laminar shear stress. *Antioxid Redox Signal,* **2009**, *11*, 1669-1682.
[43] VanderLaan, P.A.; Reardon, C.A.; Getz, G.S., Site specificity of atherosclerosis: site-selective responses to atherosclerotic modulators. *Arterioscler Thromb Vasc Biol,* **2004**, *24*, 12-22.
[44] Zhou, J.; Li, Y.S.; Chien, S., Shear stress-initiated signaling and its regulation of endothelial function. *Arterioscler Thromb Vasc Biol,* **2014**, *34*, 2191-2198.
[45] Won, D.; Zhu, S.N.; Chen, M.; Teichert, A.M.; Fish, J.E.; Matouk, C.C.; Bonert, M.; Ojha, M.; Marsden, P.A.; Cybulsky, M.I., Relative reduction of endothelial nitric-oxide synthase expression and transcription in atherosclerosis-prone regions of the mouse aorta and in an in vitro model of disturbed flow. *Am J Pathol,* **2007**, *171*, 1691-1704.
[46] Heinecke, J.W.; Baker, L.; Rosen, H.; Chait, A., Superoxide-mediated modification of low density lipoprotein by arterial smooth muscle cells. *J Clin Invest,* **1986**, *77*, 757-761.
[47] Botti, H.; Trostchansky, A.; Batthyany, C.; Rubbo, H., Reactivity of peroxynitrite and nitric oxide with LDL. *IUBMB Life,* **2005**, *57*, 407-412.
[48] von Eckardstein, A.; Rohrer, L., Transendothelial lipoprotein transport and regulation of endothelial permeability and integrity by lipoproteins. *Curr Opin Lipidol,* **2009**, *20*, 197-205.
[49] Schwenke, D.C.; Carew, T.E., Initiation of atherosclerotic lesions in cholesterol-fed rabbits. I. Focal increases in arterial LDL concentration precede development of fatty streak lesions. *Arteriosclerosis,* **1989**, *9*, 895-907.
[50] Tabas, I.; Williams, K.J.; Boren, J., Subendothelial lipoprotein retention as the initiating process in atherosclerosis: update and therapeutic implications. *Circulation,* **2007**, *116*, 1832-1844.
[51] Sun, S.W.; Zu, X.Y.; Tuo, Q.H.; Chen, L.X.; Lei, X.Y.; Li, K.; Tang, C.K.; Liao, D.F., Caveolae and caveolin-1 mediate endocytosis and transcytosis of oxidized low density lipoprotein in endothelial cells. *Acta Pharmacol Sin,* **2010**, *31*, 1336-1342.
[52] Frank, P.G.; Pavlides, S.; Cheung, M.W.; Daumer, K.; Lisanti, M.P., Role of caveolin-1 in the regulation of lipoprotein metabolism. *Am J Physiol Cell Physiol,* **2008**, *295*, C242-248.
[53] Fogelstrand, P.; Boren, J., Retention of atherogenic lipoproteins in the artery wall and its role in atherogenesis. *Nutr Metab Cardiovasc Dis,* **2012**, *22*, 1-7.
[54] Cancel, L.M.; Fitting, A.; Tarbell, J.M., In vitro study of LDL transport under pressurized (convective) conditions. *Am J Physiol Heart Circ Physiol,* **2007**, *293*, H126-132.
[55] Dabagh, M.; Jalali, P.; Tarbell, J.M., The transport of LDL across the deformable arterial wall: the effect of endothelial cell turnover and intimal deformation under hypertension. *Am J Physiol Heart Circ Physiol,* **2009**, *297*, H983-996.
[56] Kang, H.; Cancel, L.M.; Tarbell, J.M., Effect of shear stress on water and LDL transport through cultured endothelial cell monolayers. *Atherosclerosis,* **2014**, *233*, 682-690.
[57] Armstrong, S.M.; Sugiyama, M.G.; Fung, K.Y.; Gao, Y.; Wang, C.; Levy, A.S.; Azizi, P.; Roufaiel, M.; Zhu, S.N.; Neculai, D.; Yin, C.; Bolz, S.S.; Seidah, N.G.; Cybulsky, M.I.; Heit, B.; Lee, W.L., A novel assay uncovers an unexpected role for SR-BI in LDL transcytosis. *Cardiovasc Res,* **2015**, *108*, 268-277.

[58] Velagapudi, S.; Yalcinkaya, M.; Piemontese, A.; Meier, R.; Norrelykke, S.F.; Perisa, D.; Rzepiela, A.; Stebler, M.; Stoma, S.; Zanoni, P.; Rohrer, L.; von Eckardstein, A., VEGF-A Regulates Cellular Localization of SR-BI as Well as Transendothelial Transport of HDL but Not LDL. *Arterioscler Thromb Vasc Biol,* **2017**, *37*, 794-803.
[59] Kraehling, J.R.; Chidlow, J.H.; Rajagopal, C.; Sugiyama, M.G.; Fowler, J.W.; Lee, M.Y.; Zhang, X.; Ramirez, C.M.; Park, E.J.; Tao, B.; Chen, K.; Kuruvilla, L.; Larrivee, B.; Folta-Stogniew, E.; Ola, R.; Rotllan, N.; Zhou, W.; Nagle, M.W.; Herz, J.; Williams, K.J.; Eichmann, A.; Lee, W.L.; Fernandez-Hernando, C.; Sessa, W.C., Genome-wide RNAi screen reveals ALK1 mediates LDL uptake and transcytosis in endothelial cells. *Nat Commun,* **2016**, *7*, 13516.
[60] Skalen, K.; Gustafsson, M.; Rydberg, E.K.; Hulten, L.M.; Wiklund, O.; Innerarity, T.L.; Boren, J., Subendothelial retention of atherogenic lipoproteins in early atherosclerosis. *Nature,* **2002**, *417*, 750-754.
[61] Boren, J.; Olin, K.; Lee, I.; Chait, A.; Wight, T.N.; Innerarity, T.L., Identification of the principal proteoglycan-binding site in LDL. A single-point mutation in apo-B100 severely affects proteoglycan interaction without affecting LDL receptor binding. *J Clin Invest,* **1998**, *101*, 2658-2664.
[62] Boren, J.; Lee, I.; Zhu, W.; Arnold, K.; Taylor, S.; Innerarity, T.L., Identification of the low density lipoprotein receptor-binding site in apolipoprotein B100 and the modulation of its binding activity by the carboxyl terminus in familial defective apo-B100. *J Clin Invest,* **1998**, *101*, 1084-1093.
[63] Gerhardt, T.; Ley, K., Monocyte trafficking across the vessel wall. *Cardiovasc Res,* **2015**, *107*, 321-330.
[64] Timmerman, I.; Daniel, A.E.; Kroon, J.; van Buul, J.D., Leukocytes Crossing the Endothelium: A Matter of Communication. *Int Rev Cell Mol Biol,* **2016**, *322*, 281-329.
[65] Woollard, K.J.; Geissmann, F., Monocytes in atherosclerosis: subsets and functions. *Nat Rev Cardiol,* **2010**, *7*, 77-86.
[66] Moore, K.J.; Sheedy, F.J.; Fisher, E.A., Macrophages in atherosclerosis: a dynamic balance. *Nat Rev Immunol,* **2013**, *13*, 709-721.
[67] Nourshargh, S.; Hordijk, P.L.; Sixt, M., Breaching multiple barriers: leukocyte motility through venular walls and the interstitium. *Nat Rev Mol Cell Biol,* **2010**, *11*, 366-378.
[68] Boring, L.; Gosling, J.; Cleary, M.; Charo, I.F., Decreased lesion formation in CCR2-/- mice reveals a role for chemokines in the initiation of atherosclerosis. *Nature,* **1998**, *394*, 894-897.
[69] Carman, C.V.; Springer, T.A., A transmigratory cup in leukocyte diapedesis both through individual vascular endothelial cells and between them. *J Cell Biol,* **2004**, *167*, 377-388.
[70] Carman, C.V.; Sage, P.T.; Sciuto, T.E.; de la Fuente, M.A.; Geha, R.S.; Ochs, H.D.; Dvorak, H.F.; Dvorak, A.M.; Springer, T.A., Transcellular diapedesis is initiated by invasive podosomes. *Immunity,* **2007**, *26*, 784-797.
[71] van Gils, J.M.; Ramkhelawon, B.; Fernandes, L.; Stewart, M.C.; Guo, L.; Seibert, T.; Menezes, G.B.; Cara, D.C.; Chow, C.; Kinane, T.B.; Fisher, E.A.; Balcells, M.; Alvarez-Leite, J.; Lacy-Hulbert, A.; Moore, K.J., Endothelial expression of guidance cues in vessel wall homeostasis dysregulation under proatherosclerotic conditions. *Arterioscler Thromb Vasc Biol,* **2013**, *33*, 911-919.
[72] Ly, N.P.; Komatsuzaki, K.; Fraser, I.P.; Tseng, A.A.; Prodhan, P.; Moore, K.J.; Kinane, T.B., Netrin-1 inhibits leukocyte migration in vitro and in vivo. *Proc Natl Acad Sci U S A,* **2005**, *102*, 14729-14734.
[73] Zwaginga, J.J.; Torres, H.I.; Lammers, J.; Sixma, J.J.; Koenderman, L.; Kuijper, P.H., Minimal platelet deposition and activation in models of injured vessel wall ensure optimal neutrophil adhesion under flow conditions. *Arterioscler Thromb Vasc Biol,* **1999**, *19*, 1549-1554.
[74] Huo, Y.; Schober, A.; Forlow, S.B.; Smith, D.F.; Hyman, M.C.; Jung, S.; Littman, D.R.; Weber, C.; Ley, K., Circulating activated platelets exacerbate atherosclerosis in mice deficient in apolipoprotein E. *Nat Med,* **2003**, *9*, 61-67.
[75] Langer, H.F.; Gawaz, M., Platelet-vessel wall interactions in atherosclerotic disease. *Thromb Haemost,* **2008**, *99*, 480-486.
[76] da Costa Martins, P.; van den Berk, N.; Ulfman, L.H.; Koenderman, L.; Hordijk, P.L.; Zwaginga, J.J., Platelet-monocyte complexes support monocyte adhesion to endothelium by enhancing secondary tethering and cluster formation. *Arterioscler Thromb Vasc Biol,* **2004**, *24*, 193-199.
[77] van Gils, J.M.; da Costa Martins, P.A.; Mol, A.; Hordijk, P.L.; Zwaginga, J.J., Transendothelial migration drives dissociation of plateletmonocyte complexes. *Thromb Haemost,* **2008**, *100*, 271-279.
[78] Badrnya, S.; Schrottmaier, W.C.; Kral, J.B.; Yaiw, K.C.; Volf, I.; Schabbauer, G.; Soderberg-Naucler, C.; Assinger, A., Platelets mediate oxidized low-density lipoprotein-induced monocyte extravasation and foam cell formation. *Arterioscler Thromb Vasc Biol,* **2014**, *34*, 571-580.
[79] Libby, P.; Ridker, P.M.; Hansson, G.K., Progress and challenges in translating the biology of atherosclerosis. *Nature,* **2011**, *473*, 317-325.
[80] Frohman, E.M.; Racke, M.K.; Raine, C.S., Multiple sclerosis--the plaque and its pathogenesis. *N Engl J Med,* **2006**, *354*, 942-955.
[81] Dutta, P.; Nahrendorf, M., Monocytes in myocardial infarction. *Arterioscler Thromb Vasc Biol,* **2015**, *35*, 1066-1070.
[82] Goldstein, J.L.; Brown, M.S., The low-density lipoprotein pathway and its relation to atherosclerosis. *Annu Rev Biochem,* **1977**, *46*, 897-930.
[83] Steinberg, D., Oxidative Modification of LDL in the Pathogenesis of Atherosclerosis. *Am J Geriatr Cardiol,* **1993**, *2*, 38-41.
[84] Gleissner, C.A.; Leitinger, N.; Ley, K., Effects of native and modified low-density lipoproteins on monocyte recruitment in atherosclerosis. *Hypertension,* **2007**, *50*, 276-283.
[85] Smalley, D.M.; Lin, J.H.; Curtis, M.L.; Kobari, Y.; Stemerman, M.B.; Pritchard, K.A., Jr., Native LDL increases endothelial cell adhesiveness by inducing intercellular adhesion molecule-1. *Arterioscler Thromb Vasc Biol,* **1996**, *16*, 585-590.

[86] Zhu, Y.; Lin, J.H.; Liao, H.L.; Friedli, O., Jr.; Verna, L.; Marten, N.W.; Straus, D.S.; Stemerman, M.B., LDL induces transcription factor activator protein-1 in human endothelial cells. *Arterioscler Thromb Vasc Biol,* **1998**, *18*, 473-480.
[87] Verna, L.; Ganda, C.; Stemerman, M.B., In vivo low-density lipoprotein exposure induces intercellular adhesion molecule-1 and vascular cell adhesion molecule-1 correlated with activator protein-1 expression. *Arterioscler Thromb Vasc Biol,* **2006**, *26*, 1344-1349.
[88] Lin, J.H.; Zhu, Y.; Liao, H.L.; Kobari, Y.; Groszek, L.; Stemerman, M.B., Induction of vascular cell adhesion molecule-1 by low-density lipoprotein. *Atherosclerosis,* **1996**, *127*, 185-194.
[89] Allen, S.; Khan, S.; Al-Mohanna, F.; Batten, P.; Yacoub, M., Native low density lipoprotein-induced calcium transients trigger VCAM-1 and E-selectin expression in cultured human vascular endothelial cells. *J Clin Invest,* **1998**, *101*, 1064-1075.
[90] Blacklow, S.C., Versatility in ligand recognition by LDL receptor family proteins: advances and frontiers. *Curr Opin Struct Biol,* **2007**, *17*, 419-426.
[91] Steinberg, D., The LDL modification hypothesis of atherogenesis: an update. *J Lipid Res,* **2009**, *50 Suppl*, S376-381.
[92] Saremi, A.; Arora, R., Vitamin E and cardiovascular disease. *Am J Ther,* **2010**, *17*, e56-65.
[93] Gregson, J.M.; Freitag, D.F.; Surendran, P.; Stitziel, N.O.; Chowdhury, R.; Burgess, S.; Kaptoge, S.; Gao, P.; Staley, J.R.; Willeit, P.; Nielsen, S.F.; Caslake, M.; Trompet, S.; Polfus, L.M.; Kuulasmaa, K.; Kontto, J.; Perola, M.; Blankenberg, S.; Veronesi, G.; Gianfagna, F.; Mannisto, S.; Kimura, A.; Lin, H.; Reilly, D.F.; Gorski, M.; Mijatovic, V.; consortium, C.K.; Munroe, P.B.; Ehret, G.B.; International Consortium for Blood, P.; Thompson, A.; Uria-Nickelsen, M.; Malarstig, A.; Dehghan, A.; group, C.i.w.; Vogt, T.F.; Sasaoka, T.; Takeuchi, F.; Kato, N.; Yamada, Y.; Kee, F.; Muller-Nurasyid, M.; Ferrieres, J.; Arveiler, D.; Amouyel, P.; Salomaa, V.; Boerwinkle, E.; Thompson, S.G.; Ford, I.; Wouter Jukema, J.; Sattar, N.; Packard, C.J.; Shafi Majumder, A.A.; Alam, D.S.; Deloukas, P.; Schunkert, H.; Samani, N.J.; Kathiresan, S.; consortium, M.E.; Nordestgaard, B.G.; Saleheen, D.; Howson, J.M.; Di Angelantonio, E.; Butterworth, A.S.; Danesh, J.; consortium, E.-C.; the, C.H.D.E.c., Genetic invalidation of Lp-PLA2 as a therapeutic target: Large-scale study of five functional Lp-PLA2-lowering alleles. *Eur J Prev Cardiol,* **2017**, *24*, 492-504.
[94] Tellis, C.C.; Tselepis, A.D., Pathophysiological role and clinical significance of lipoprotein-associated phospholipase A(2) (Lp-PLA(2)) bound to LDL and HDL. *Curr Pharm Des,* **2014**, *20*, 6256-6269.
[95] Steinbrecher, U.P.; Parthasarathy, S.; Leake, D.S.; Witztum, J.L.; Steinberg, D., Modification of low density lipoprotein by endothelial cells involves lipid peroxidation and degradation of low density lipoprotein phospholipids. *Proc Natl Acad Sci U S A,* **1984**, *81*, 3883-3887.
[96] Steinbrecher, U.P., Oxidation of human low density lipoprotein results in derivatization of lysine residues of apolipoprotein B by lipid peroxide decomposition products. *J Biol Chem,* **1987**, *262*, 3603-3608.
[97] Steinbrecher, U.P.; Witztum, J.L.; Parthasarathy, S.; Steinberg, D., Decrease in reactive amino groups during oxidation or endothelial cell modification of LDL. Correlation with changes in receptor-mediated catabolism. *Arteriosclerosis,* **1987**, *7*, 135-143.
[98] Lubos, E.; Handy, D.E.; Loscalzo, J., Role of oxidative stress and nitric oxide in atherothrombosis. *Front Biosci,* **2008**, *13*, 5323-5344.
[99] Berliner, J.A.; Heinecke, J.W., The role of oxidized lipoproteins in atherogenesis. *Free Radic Biol Med,* **1996**, *20*, 707-727.
[100] Chen, C.; Khismatullin, D.B., Oxidized low-density lipoprotein contributes to atherogenesis via co-activation of macrophages and mast cells. *PLoS One,* **2015**, *10*, e0123088.
[101] Esterbauer, H.; Jurgens, G.; Quehenberger, O.; Koller, E., Autoxidation of human low density lipoprotein: loss of polyunsaturated fatty acids and vitamin E and generation of aldehydes. *J Lipid Res,* **1987**, *28*, 495-509.
[102] Jurgens, G.; Hoff, H.F.; Chisolm, G.M., 3rd; Esterbauer, H., Modification of human serum low density lipoprotein by oxidation--characterization and pathophysiological implications. *Chem Phys Lipids,* **1987**, *45*, 315-336.
[103] Orr, A.W.; Hahn, C.; Blackman, B.R.; Schwartz, M.A., p21-activated kinase signaling regulates oxidant-dependent NF-kappa B activation by flow. *Circ Res,* **2008**, *103*, 671-679.
[104] Yurdagul, A., Jr.; Chen, J.; Funk, S.D.; Albert, P.; Kevil, C.G.; Orr, A.W., Altered nitric oxide production mediates matrix-specific PAK2 and NF-kappaB activation by flow. *Mol Biol Cell,* **2013**, *24*, 398-408.
[105] Flood, C.; Gustafsson, M.; Pitas, R.E.; Arnaboldi, L.; Walzem, R.L.; Boren, J., Molecular mechanism for changes in proteoglycan binding on compositional changes of the core and the surface of low-density lipoprotein-containing human apolipoprotein B100. *Arterioscler Thromb Vasc Biol,* **2004**, *24*, 564-570.
[106] Fu, Z.; Zhou, E.; Wang, X.; Tian, M.; Kong, J.; Li, J.; Ji, L.; Niu, C.; Shen, H.; Dong, S.; Liu, C.; Vermorken, A.; Willard, B.; Zu, L.; Zheng, L., Oxidized low-density lipoprotein-induced microparticles promote endothelial monocyte adhesion via intercellular adhesion molecule 1. *Am J Physiol Cell Physiol,* **2017**, *313*, C567-C574.
[107] Yan, F.X.; Li, H.M.; Li, S.X.; He, S.H.; Dai, W.P.; Li, Y.; Wang, T.T.; Shi, M.M.; Yuan, H.X.; Xu, Z.; Zhou, J.G.; Ning, D.S.; Mo, Z.W.; Ou, Z.J.; Ou, J.S., The oxidized phospholipid POVPC impairs endothelial function and vasodilation via uncoupling endothelial nitric oxide synthase. *J Mol Cell Cardiol,* **2017**, *112*, 40-48.
[108] Zhang, C.; Adamos, C.; Oh, M.J.; Baruah, J.; Ayee, M.A.A.; Mehta, D.; Wary, K.K.; Levitan, I., oxLDL induces endothelial cell proliferation via Rho/ROCK/Akt/p27kip1 signaling: opposite effects of oxLDL and cholesterol loading. *Am J Physiol Cell Physiol,* **2017**, *313*, C340-C351.
[109] Ahmadian, M.; Abbott, M.J.; Tang, T.; Hudak, C.S.; Kim, Y.; Bruss, M.; Hellerstein, M.K.; Lee, H.Y.; Samuel, V.T.; Shulman, G.I.; Wang, Y.; Duncan, R.E.; Kang, C.; Sul, H.S., Desnutrin/ATGL is regulated by AMPK and is required for a brown adipose phenotype. *Cell Metab,* **2011**, *13*, 739-748.
[110] Le Master, E.; Huang, R.T.; Zhang, C.; Bogachkov, Y.; Coles, C.; Shentu, T.P.; Sheng, Y.; Fancher, I.S.; Ng, C.; Christoforidis, T.; Subbaiah, P.V.; Berdyshev, E.; Qain, Z.; Eddington, D.T.; Lee, J.; Cho, M.; Fang, Y.; Minshall, R.D.; Levitan, I.,

Proatherogenic Flow Increases Endothelial Stiffness via Enhanced CD36 (Cluster of Differentiation 36)-Mediated OxLDL (Oxidized Low-Density Lipoprotein) Uptake. *Arterioscler Thromb Vasc Biol,* **2017**.
[111] Sawamura, T.; Kume, N.; Aoyama, T.; Moriwaki, H.; Hoshikawa, H.; Aiba, Y.; Tanaka, T.; Miwa, S.; Katsura, Y.; Kita, T.; Masaki, T., An endothelial receptor for oxidized low-density lipoprotein. *Nature,* **1997**, *386*, 73-77.
[112] Afonso Mda, S.; Castilho, G.; Lavrador, M.S.; Passarelli, M.; Nakandakare, E.R.; Lottenberg, S.A.; Lottenberg, A.M., The impact of dietary fatty acids on macrophage cholesterol homeostasis. *J Nutr Biochem,* **2014**, *25*, 95-103.
[113] Mollace, V.; Gliozzi, M.; Musolino, V.; Carresi, C.; Muscoli, S.; Mollace, R.; Tavernese, A.; Gratteri, S.; Palma, E.; Morabito, C.; Vitale, C.; Muscoli, C.; Fini, M.; Romeo, F., Oxidized LDL attenuates protective autophagy and induces apoptotic cell death of endothelial cells: Role of oxidative stress and LOX-1 receptor expression. *Int J Cardiol,* **2015**, *184*, 152-158.
[114] Marcovecchio, P.M.; Thomas, G.D.; Mikulski, Z.; Ehinger, E.; Mueller, K.A.L.; Blatchley, A.; Wu, R.; Miller, Y.I.; Nguyen, A.T.; Taylor, A.M.; McNamara, C.A.; Ley, K.; Hedrick, C.C., Scavenger Receptor CD36 Directs Nonclassical Monocyte Patrolling Along the Endothelium During Early Atherogenesis. *Arterioscler Thromb Vasc Biol*, **2017**, *37*, 2043-2052.
[115] Syvaranta, S.; Alanne-Kinnunen, M.; Oorni, K.; Oksjoki, R.; Kupari, M.; Kovanen, P.T.; Helske-Suihko, S., Potential pathological roles for oxidized low-density lipoprotein and scavenger receptors SR-AI, CD36, and LOX-1 in aortic valve stenosis. *Atherosclerosis,* **2014**, *235*, 398-407.
[116] Chen, M.; Masaki, T.; Sawamura, T., LOX-1, the receptor for oxidized low-density lipoprotein identified from endothelial cells: implications in endothelial dysfunction and atherosclerosis. *Pharmacol Ther,* **2002**, *95*, 89-100.
[117] Xu, S.; Ogura, S.; Chen, J.; Little, P.J.; Moss, J.; Liu, P., LOX-1 in atherosclerosis: biological functions and pharmacological modifiers. *Cell Mol Life Sci,* **2013**, *70*, 2859-2872.
[118] Lawrence, T., The nuclear factor NF-kappaB pathway in inflammation. *Cold Spring Harb Perspect Biol,* **2009**, *1*, a001651.
[119] Cominacini, L.; Pasini, A.F.; Garbin, U.; Davoli, A.; Tosetti, M.L.; Campagnola, M.; Rigoni, A.; Pastorino, A.M.; Lo Cascio, V.; Sawamura, T., Oxidized low density lipoprotein (ox-LDL) binding to ox-LDL receptor-1 in endothelial cells induces the activation of NF-kappaB through an increased production of intracellular reactive oxygen species. *J Biol Chem,* **2000**, *275*, 12633-12638.
[120] Tang, Y.; Zhao, J.; Shen, L.; Jin, Y.; Zhang, Z.; Xu, G.; Huang, X., ox-LDL induces endothelial dysfunction by promoting Arp2/3 complex expression. *Biochem Biophys Res Commun,* **2016**, *475*, 182-188.
[121] Hong, D.; Bai, Y.P.; Gao, H.C.; Wang, X.; Li, L.F.; Zhang, G.G.; Hu, C.P., Ox-LDL induces endothelial cell apoptosis via the LOX-1-dependent endoplasmic reticulum stress pathway. *Atherosclerosis,* **2014**, *235*, 310-317.
[122] Tang, F.; Yang, T.L.; Zhang, Z.; Li, X.G.; Zhong, Q.Q.; Zhao, T.T.; Gong, L., MicroRNA-21 suppresses ox-LDL-induced human aortic endothelial cells injuries in atherosclerosis through enhancement of autophagic flux: Involvement in promotion of lysosomal function. *Exp Cell Res,* **2017**, *359*, 374-383.
[123] Lv, J.; Yang, L.; Guo, R.; Shi, Y.; Zhang, Z.; Ye, J., Ox-LDL-Induced MicroRNA-155 Promotes Autophagy in Human Endothelial Cells via Repressing the Rheb/ mTOR Pathway. *Cell Physiol Biochem,* **2017**, *43*, 1436-1448.
[124] Qin, B.; Cao, Y.; Yang, H.; Xiao, B.; Lu, Z., MicroRNA-221/222 regulate ox-LDL-induced endothelial apoptosis via Ets-1/p21 inhibition. *Mol Cell Biochem,* **2015**, *405*, 115-124.
[125] Gencer, B.; Kronenberg, F.; Stroes, E.S.; Mach, F., Lipoprotein(a): the revenant. *Eur Heart J,* **2017**, *38*, 1553-1560.
[126] Leibundgut, G.; Scipione, C.; Yin, H.; Schneider, M.; Boffa, M.B.; Green, S.; Yang, X.; Dennis, E.; Witztum, J.L.; Koschinsky, M.L.; Tsimikas, S., Determinants of binding of oxidized phospholipids on apolipoprotein (a) and lipoprotein (a). *J Lipid Res,* **2013**, *54*, 2815-2830.
[127] Bergmark, C.; Dewan, A.; Orsoni, A.; Merki, E.; Miller, E.R.; Shin, M.J.; Binder, C.J.; Horkko, S.; Krauss, R.M.; Chapman, M.J.; Witztum, J.L.; Tsimikas, S., A novel function of lipoprotein [a] as a preferential carrier of oxidized phospholipids in human plasma. *J Lipid Res,* **2008**, *49*, 2230-2239.
[128] Haque, N.S.; Zhang, X.; French, D.L.; Li, J.; Poon, M.; Fallon, J.T.; Gabel, B.R.; Taubman, M.B.; Koschinsky, M.; Harpel, P.C., CC chemokine I-309 is the principal monocyte chemoattractant induced by apolipoprotein(a) in human vascular endothelial cells. *Circulation,* **2000**, *102*, 786-792.
[129] Nakagami, F.; Nakagami, H.; Osako, M.K.; Iwabayashi, M.; Taniyama, Y.; Doi, T.; Shimizu, H.; Shimamura, M.; Rakugi, H.; Morishita, R., Estrogen attenuates vascular remodeling in Lp(a) transgenic mice. *Atherosclerosis,* **2010**, *211*, 41-47.
[130] Zhao, S.P.; Xu, D.Y., Oxidized lipoprotein(a) enhanced the expression of P-selectin in cultured human umbilical vein endothelial cells. *Thromb Res,* **2000**, *100*, 501-510.
[131] Takami, S.; Yamashita, S.; Kihara, S.; Ishigami, M.; Takemura, K.; Kume, N.; Kita, T.; Matsuzawa, Y., Lipoprotein(a) enhances the expression of intercellular adhesion molecule-1 in cultured human umbilical vein endothelial cells. *Circulation,* **1998**, *97*, 721-728.
[132] Pellegrino, M.; Furmaniak-Kazmierczak, E.; LeBlanc, J.C.; Cho, T.; Cao, K.; Marcovina, S.M.; Boffa, M.B.; Cote, G.P.; Koschinsky, M.L., The apolipoprotein(a) component of lipoprotein(a) stimulates actin stress fiber formation and loss of cell-cell contact in cultured endothelial cells. *J Biol Chem,* **2004**, *279*, 6526-6533.
[133] Park, S.Y.; Lee, J.H.; Kim, Y.K.; Kim, C.D.; Rhim, B.Y.; Lee, W.S.; Hong, K.W., Cilostazol prevents remnant lipoprotein particle-induced monocyte adhesion to endothelial cells by suppression of adhesion molecules and monocyte chemoattractant protein-1 expression via lectin-like receptor for oxidized low-density lipoprotein receptor activation. *J Pharmacol Exp Ther,* **2005**, *312*, 1241-1248.
[134] Adams, D.H.; Shaw, S., Leucocyte-endothelial interactions and regulation of leucocyte migration. *Lancet,* **1994**, *343*, 831-836.

[135] Norata, G.D.; Grigore, L.; Raselli, S.; Seccomandi, P.M.; Hamsten, A.; Maggi, F.M.; Eriksson, P.; Catapano, A.L., Triglyceride-rich lipoproteins from hypertriglyceridemic subjects induce a pro-inflammatory response in the endothelium: Molecular mechanisms and gene expression studies. *J Mol Cell Cardiol,* **2006**, *40*, 484-494.
[136] Williams, C.M.; Maitin, V.; Jackson, K.G., Triacylglycerol-rich lipoprotein-gene interactions in endothelial cells. *Biochem Soc Trans,* **2004**, *32*, 994-998.
[137] Maggi, F.M.; Raselli, S.; Grigore, L.; Redaelli, L.; Fantappie, S.; Catapano, A.L., Lipoprotein remnants and endothelial dysfunction in the postprandial phase. *J Clin Endocrinol Metab,* **2004**, *89*, 2946-2950.
[138] Wilmink, H.W.; Twickler, M.B.; Banga, J.D.; Dallinga-Thie, G.M.; Eeltink, H.; Erkelens, D.W.; Rabelink, T.J.; Stroes, E.S., Effect of statin versus fibrate on postprandial endothelial dysfunction: role of remnant-like particles. *Cardiovasc Res,* **2001**, *50*, 577-582.
[139] Ceriello, A.; Assaloni, R.; Da Ros, R.; Maier, A.; Piconi, L.; Quagliaro, L.; Esposito, K.; Giugliano, D., Effect of atorvastatin and irbesartan, alone and in combination, on postprandial endothelial dysfunction, oxidative stress, and inflammation in type 2 diabetic patients. *Circulation,* **2005**, *111*, 2518-2524.
[140] Shin, H.K.; Kim, Y.K.; Kim, K.Y.; Lee, J.H.; Hong, K.W., Remnant lipoprotein particles induce apoptosis in endothelial cells by NAD(P)H oxidase-mediated production of superoxide and cytokines via lectin-like oxidized low-density lipoprotein receptor-1 activation: prevention by cilostazol. *Circulation,* **2004**, *109*, 1022-1028.
[141] Wang, L.; Sapuri-Butti, A.R.; Aung, H.H.; Parikh, A.N.; Rutledge, J.C., Triglyceride-rich lipoprotein lipolysis increases aggregation of endothelial cell membrane microdomains and produces reactive oxygen species. *Am J Physiol Heart Circ Physiol,* **2008**, *295*, H237-244.
[142] Dichtl, W.; Nilsson, L.; Goncalves, I.; Ares, M.P.; Banfi, C.; Calara, F.; Hamsten, A.; Eriksson, P.; Nilsson, J., Very low-density lipoprotein activates nuclear factor-kappaB in endothelial cells. *Circ Res,* **1999**, *84*, 1085-1094.
[143] Bernelot Moens, S.J.; Verweij, S.L.; Schnitzler, J.G.; Stiekema, L.C.A.; Bos, M.; Langsted, A.; Kuijk, C.; Bekkering, S.; Voermans, C.; Verberne, H.J.; Nordestgaard, B.G.; Stroes, E.S.G.; Kroon, J., Remnant Cholesterol Elicits Arterial Wall Inflammation and a Multilevel Cellular Immune Response in Humans. *Arterioscler Thromb Vasc Biol,* **2017**, *37*, 969-975.
[144] Tarkin, J.M.; Joshi, F.R.; Rudd, J.H., PET imaging of inflammation in atherosclerosis. *Nat Rev Cardiol,* **2014**, *11*, 443-457.
[145] Rosenson, R.S.; Brewer, H.B., Jr.; Ansell, B.J.; Barter, P.; Chapman, M.J.; Heinecke, J.W.; Kontush, A.; Tall, A.R.; Webb, N.R., Dysfunctional HDL and atherosclerotic cardiovascular disease. *Nat Rev Cardiol,* **2016**, *13*, 48-60.
[146] Haase, C.L.; Tybjaerg-Hansen, A.; Qayyum, A.A.; Schou, J.; Nordestgaard, B.G.; Frikke-Schmidt, R., LCAT, HDL cholesterol and ischemic cardiovascular disease: a Mendelian randomization study of HDL cholesterol in 54,500 individuals. *J Clin Endocrinol Metab,* **2012**, *97*, E248-256.
[147] Emerging Risk Factors, C.; Di Angelantonio, E.; Gao, P.; Pennells, L.; Kaptoge, S.; Caslake, M.; Thompson, A.; Butterworth, A.S.; Sarwar, N.; Wormser, D.; Saleheen, D.; Ballantyne, C.M.; Psaty, B.M.; Sundstrom, J.; Ridker, P.M.; Nagel, D.; Gillum, R.F.; Ford, I.; Ducimetiere, P.; Kiechl, S.; Koenig, W.; Dullaart, R.P.; Assmann, G.; D'Agostino, R.B., Sr.; Dagenais, G.R.; Cooper, J.A.; Kromhout, D.; Onat, A.; Tipping, R.W.; Gomez-de-la-Camara, A.; Rosengren, A.; Sutherland, S.E.; Gallacher, J.; Fowkes, F.G.; Casiglia, E.; Hofman, A.; Salomaa, V.; Barrett-Connor, E.; Clarke, R.; Brunner, E.; Jukema, J.W.; Simons, L.A.; Sandhu, M.; Wareham, N.J.; Khaw, K.T.; Kauhanen, J.; Salonen, J.T.; Howard, W.J.; Nordestgaard, B.G.; Wood, A.M.; Thompson, S.G.; Boekholdt, S.M.; Sattar, N.; Packard, C.; Gudnason, V.; Danesh, J., Lipid-related markers and cardiovascular disease prediction. *JAMA,* **2012**, *307*, 2499-2506.
[148] Campbell, S.; Genest, J., HDL-C: clinical equipoise and vascular endothelial function. *Expert Rev Cardiovasc Ther,* **2013**, *11*, 343-353.
[149] Annema, W.; von Eckardstein, A., Dysfunctional high-density lipoproteins in coronary heart disease: implications for diagnostics and therapy. *Transl Res,* **2016**, *173*, 30-57.
[150] Aviram, M., Atherosclerosis: cell biology and lipoproteins--inflammation and oxidative stress in atherogenesis: protective role for paraoxonases. *Curr Opin Lipidol,* **2011**, *22*, 243-244.
[151] Nofer, J.R.; Geigenmuller, S.; Gopfert, C.; Assmann, G.; Buddecke, E.; Schmidt, A., High density lipoprotein-associated lysosphingolipids reduce E-selectin expression in human endothelial cells. *Biochem Biophys Res Commun,* **2003**, *310*, 98-103.
[152] Mosig, S.; Rennert, K.; Buttner, P.; Krause, S.; Lutjohann, D.; Soufi, M.; Heller, R.; Funke, H., Monocytes of patients with familial hypercholesterolemia show alterations in cholesterol metabolism. *BMC Med Genomics,* **2008**, *1*, 60.
[153] Tacke, F.; Alvarez, D.; Kaplan, T.J.; Jakubzick, C.; Spanbroek, R.; Llodra, J.; Garin, A.; Liu, J.; Mack, M.; van Rooijen, N.; Lira, S.A.; Habenicht, A.J.; Randolph, G.J., Monocyte subsets differentially employ CCR2, CCR5, and CX3CR1 to accumulate within atherosclerotic plaques. *J Clin Invest,* **2007**, *117*, 185-194.
[154] den Hartigh, L.J.; Connolly-Rohrbach, J.E.; Fore, S.; Huser, T.R.; Rutledge, J.C., Fatty acids from very low-density lipoprotein lipolysis products induce lipid droplet accumulation in human monocytes. *J Immunol,* **2010**, *184*, 3927-3936.
[155] Gower, R.M.; Wu, H.; Foster, G.A.; Devaraj, S.; Jialal, I.; Ballantyne, C.M.; Knowlton, A.A.; Simon, S.I., CD11c/CD18 expression is upregulated on blood monocytes during hypertriglyceridemia and enhances adhesion to vascular cell adhesion molecule-1. *Arterioscler Thromb Vasc Biol,* **2011**, *31*, 160-166.
[156] Xu, L.; Dai Perrard, X.; Perrard, J.L.; Yang, D.; Xiao, X.; Teng, B.B.; Simon, S.I.; Ballantyne, C.M.; Wu, H., Foamy monocytes form early and contribute to nascent atherosclerosis in mice with hypercholesterolemia. *Arterioscler Thromb Vasc Biol,* **2015**, *35*, 1787-1797.
[157] Wu, H.; Gower, R.M.; Wang, H.; Perrard, X.Y.; Ma, R.; Bullard, D.C.; Burns, A.R.; Paul, A.; Smith, C.W.; Simon, S.I.; Ballantyne, C.M., Functional role of CD11c+ monocytes in atherogenesis associated with hypercholesterolemia. *Circulation,* **2009**, *119*, 2708-2717.

[158] Sotiriou, S.N.; Orlova, V.V.; Al-Fakhri, N.; Ihanus, E.; Economopoulou, M.; Isermann, B.; Bdeir, K.; Nawroth, P.P.; Preissner, K.T.; Gahmberg, C.G.; Koschinsky, M.L.; Chavakis, T., Lipoprotein(a) in atherosclerotic plaques recruits inflammatory cells through interaction with Mac-1 integrin. *FASEB J*, **2006**, *20*, 559-561.
[159] Patel, S.; Drew, B.G.; Nakhla, S.; Duffy, S.J.; Murphy, A.J.; Barter, P.J.; Rye, K.A.; Chin-Dusting, J.; Hoang, A.; Sviridov, D.; Celermajer, D.S.; Kingwell, B.A., Reconstituted high-density lipoprotein increases plasma high-density lipoprotein anti-inflammatory properties and cholesterol efflux capacity in patients with type 2 diabetes. *J Am Coll Cardiol*, **2009**, *53*, 962-971.
[160] Patel, V.K.; Williams, H.; Li, S.C.H.; Fletcher, J.P.; Medbury, H.J., Monocyte inflammatory profile is specific for individuals and associated with altered blood lipid levels. *Atherosclerosis*, **2017**, *263*, 15-23.
[161] Murphy, A.J.; Woollard, K.J.; Hoang, A.; Mukhamedova, N.; Stirzaker, R.A.; McCormick, S.P.; Remaley, A.T.; Sviridov, D.; Chin-Dusting, J., High-density lipoprotein reduces the human monocyte inflammatory response. *Arterioscler Thromb Vasc Biol*, **2008**, *28*, 2071-2077.
[162] Iqbal, A.J.; Barrett, T.J.; Taylor, L.; McNeill, E.; Manmadhan, A.; Recio, C.; Carmineri, A.; Brodermann, M.H.; White, G.E.; Cooper, D.; DiDonato, J.A.; Zamanian-Daryoush, M.; Hazen, S.L.; Channon, K.M.; Greaves, D.R.; Fisher, E.A., Acute exposure to apolipoprotein A1 inhibits macrophage chemotaxis in vitro and monocyte recruitment in vivo. *Elife*, **2016**, *5*.
[163] Ginhoux, F.; Jung, S., Monocytes and macrophages: developmental pathways and tissue homeostasis. *Nat Rev Immunol*, **2014**, *14*, 392-404.
[164] Dutta, P.; Sager, H.B.; Stengel, K.R.; Naxerova, K.; Courties, G.; Saez, B.; Silberstein, L.; Heidt, T.; Sebas, M.; Sun, Y.; Wojtkiewicz, G.; Feruglio, P.F.; King, K.; Baker, J.N.; van der Laan, A.M.; Borodovsky, A.; Fitzgerald, K.; Hulsmans, M.; Hoyer, F.; Iwamoto, Y.; Vinegoni, C.; Brown, D.; Di Carli, M.; Libby, P.; Hiebert, S.W.; Scadden, D.T.; Swirski, F.K.; Weissleder, R.; Nahrendorf, M., Myocardial Infarction Activates CCR2(+) Hematopoietic Stem and Progenitor Cells. *Cell Stem Cell*, **2015**, *16*, 477-487.
[165] Libby, P.; Nahrendorf, M.; Swirski, F.K., Leukocytes Link Local and Systemic Inflammation in Ischemic Cardiovascular Disease: An Expanded "Cardiovascular Continuum". *J Am Coll Cardiol*, **2016**, *67*, 1091-1103.
[166] Morrison, S.J.; Scadden, D.T., The bone marrow niche for haematopoietic stem cells. *Nature*, **2014**, *505*, 327-334.
[167] Suda, T.; Arai, F.; Hirao, A., Hematopoietic stem cells and their niche. *Trends Immunol*, **2005**, *26*, 426-433.
[168] Rahman, M.S.; Murphy, A.J.; Woollard, K.J., Effects of dyslipidaemia on monocyte production and function in cardiovascular disease. *Nat Rev Cardiol*, **2017**, *14*, 387-400.
[169] Blue, E.K.; Ballman, K.; Boyle, F.; Oh, E.; Kono, T.; Quinney, S.K.; Thurmond, D.C.; Evans-Molina, C.; Haneline, L.S., Fetal hyperglycemia and a high-fat diet contribute to aberrant glucose tolerance and hematopoiesis in adult rats. *Pediatr Res*, **2015**, *77*, 316-325.
[170] Yvan-Charvet, L.; Pagler, T.; Gautier, E.L.; Avagyan, S.; Siry, R.L.; Han, S.; Welch, C.L.; Wang, N.; Randolph, G.J.; Snoeck, H.W.; Tall, A.R., ATP-binding cassette transporters and HDL suppress hematopoietic stem cell proliferation. *Science*, **2010**, *328*, 1689-1693.

# Chapter 3

## Nile Red Quantifier: a novel and quantitative tool to study lipid accumulation in patient-derived circulating monocytes using confocal microscopy.

Johan G. Schnitzler, Sophie J. Bernelot Moens, Feiko Tiessens, Geesje M. Dallinga-Thie, Albert K. Groen, Erik S.G. Stroes and Jeffrey Kroon

*Journal of Lipid Research. 2017 Nov;58(11):2210-2219*

Abstract
The inflammatory profile of circulating monocytes is an important biomarker for atherosclerotic plaque vulnerability. Recent research revealed that peripheral lipid uptake by monocytes alters their phenotype towards an inflammatory state and this coincides with an increased lipid droplet (LD) content. Determination of lipid content of circulating monocytes is, however, not very well established. Based on Nile Red (NR) LD-imaging using confocal microscopy and computational analysis, we developed Nile Red Quantifier (NRQ); a novel quantification method to assess lipid droplet content in monocytes.

Freshly isolated circulating monocytes were used for the NR-staining procedure. In monocytes stained with NR, we clearly distinguish, based on 3D-imaging, phospho- and exclusively intracellular neutral lipids. Extraction of LDs and subsequent LD-composition analysis showed that LDs contain primarily, cholesterol esters and trigylcerides. Next, we developed and validated NRQ, a semi-automated quantification program which detects alterations in lipid accumulation after exposure of isolated monocytes to freshly derived low-density lipoproteins (LDL) in a time- and dose dependent fashion.

In conclusion, NR-staining is a suitable procedure to detect small differences in lipid droplet content in circulating monocytes using NRQ and could therefore be used as a potential biomarker for cardiovascular disease.

**Keywords:** circulating monocytes, lipid droplet, Nile Red, Nile Red Quantifier

## Introduction

Atherosclerosis is characterized by the recruitment of inflammatory cells into the intima, where excessive uptake of modified LDL particles, such as oxidized LDL (oxLDL) by monocytes and macrophages leads to foam cell formation [1], promoting the initiation of atherosclerotic lesions. Subsequent endothelial activation leads to continuous recruitment of circulating monocytes into the subintimal area, further increasing inflammatory activity of these lesions, leading to plaque progression and eventually plaque destabilization [2–4]. Recently, it has been suggested that migration of circulating monocytes is not merely a reflection of local endothelial activation near atherogenic areas, but circulating monocytes may also display pro-adhesive properties in patients at increased CV risk [5]. The factors leading to this systemic activation of circulating monocytes remain to be established. In dyslipidemic states, lipid accumulation is thought to contribute to the pro-adhesiveness of the circulating cells. In the postprandial state lipids were found to be taken up by circulating monocytes, resulting in increased expression of the integrin CD11c, binding partner of vascular adhesion molecule-1 (VCAM-1) [6], as well as increased monocyte-derived production of tumor necrosis factor **α** (TNF **α**) and interleukin 1**β** (IL1**β**) [7]. In this context, circulating monocytes may serve as biomarkers for atherosclerotic plaque vulnerability [1,8,9], whereas lipid accumulation in these cells may be an important driver for this systemic pro-inflammatory phenotype [6,7,10].

In cells, lipids are usually stored in lipid droplets (LDs) [11,12]. LDs have been identified as organelles that are actively involved in many essential cellular functions, such as cellular homeostasis (membrane biogenesis and lipoprotein synthesis), cell survival in a nutrient-poor milieu, protein storage and protection against lipotoxicity by scavenging free fatty acids and cholesterol [12]. LDs consist of a surrounding phospholipid layer, with similar composition to that of the ER membrane and it encloses a neutral lipid core of cholesterol, cholesterol esters and triglycerides in various ratios [13]. Lipid uptake must be tightly controlled in order to maintain cellular homeostasis by preventing lipid overload and subsequent cellular activation [14].

A number of techniques have been developed to detect lipids in cytoplasmic LDs [15,16]. One of the best known lipid dyes used to assess cytoplasmic lipid content in cells is Oil Red O (ORO), although it has become evident that ORO has multiple drawbacks [17,18]. Since ORO is very sensitive to preparation conditions, working solutions must be freshly prepared which is labor intensive [19], but more importantly quantification of lipid particles is arbitrary [15]. Another frequently used lipid dye is filipin, but is known to photobleach rapidly [20] whereas the fluorophore boron-dipyrromethene (BODIPY) can bind nonspecifically to other intracellular cell structures [16].

Here, we set out to develop a fast and quantitative lipid stain for circulating monocytes based on the lysochrome Nile Red (NR), an environment-sensitive fluorescent dye used to detect intracellular lipid particles with high sensitivity [21,22] in multiple cell types [11] by high-resolution confocal laser scanning microscopy. For quantification of the cytoplasmic neutral lipids, we developed Nile Red Quantifier (NRQ), a Matlab-based, freely available program for quick and easy assessment of lipid uptake.

## Materials and methods

*Monocyte isolation*

The study was approved by the institutional review board of the AMC and conducted according to the declaration of Helsinki. Written informed consent was obtained from all participants. Venous blood was drawn in ethylenediaminetetraacetic acid (EDTA)-coated Vacutainer® tubes (BD, Plymouth, UK). Peripheral blood mononuclear cells were obtained from whole blood samples through density centrifugation using Lymphoprep (D=1.077) as described in detail elsewhere [23]. In short, blood was diluted in a 1:1 ratio with Phosphate-Buffered Saline (PBS) 2 mM EDTA and subsequently added to a layer Ficoll-Paque PLUS (Axis-Shield). Next, cells were centrifuged for 20 minutes at 2200 RPM at RT with slow acceleration and no brake. The PBMC fraction was collected and washed twice with PBS 2 mM EDTA. Next, cells were counted using a Casy Counter (Roche Innovatis Casy TT, Bielefeld, Germany). Subsequently, monocytes were isolated using human CD14 magnetic beads and MACS® cell separation columns (Miltenyi, Bergisch Gladbach, Germany). In short, cells were resuspended in MACS buffer (0,5% Bovine Serum Albumin (Sigma-Aldrich, St. Louis, Missouri, USA) in PBS 2 mM EDTA). Next, CD14 MicroBeads (Miltenyi Biotec, Leiden, The Netherlands) were added and incubated for 30 minutes at 4°C. After incubation, the cells were washed with MACS buffer and resuspended in MACS buffer for CD14 bead isolation using MACS Separation Columns (Miltenyi Biotec, Leiden, The Netherlands). After isolation, cells were counted by means of a Casy Counter. Freshly-derived monocytes were kept in Iscove's Modified Dulbecco's Medium (IMDM; Thermo Fischer Scientific, Waltham, Massachussetts, USA) for further immunohistochemistry and immunofluorescent analysis.

*Lipid droplet and neutral lipid extraction*

Lipid droplet extraction on peripheral monocytes was performed on $10x10^6$ CD14+ monocytes according to manufacturer's instructions (#MET-5011: Cell Biolabs Inc, San Didgo, CA). Next, density gradient ultracentrifugation was performed for 3 hours at 20000 x g at 4°C using a Ultracentrifuge (Beckman, Uithoorn, The Netherlands). The top layer, containing the floating lipid droplets, were collected and used for neutral lipid extraction. Lipids were isolated as previously described by performing a Butanol-Methanol extraction [24]. Neutral lipids were separated from polar lipids by dissolving the nitrogen-dried lipid extract in heptane:methanol [98:2]. After vortexing, 300 µl Methanol: $H_2O$ + 1% $NH_3$ (of 23% $NH_3$ stock) was added and the upper phase, containing the neutral lipids, was collected and dried at 35 °C under a continuous flow of nitrogen gas.

*HPLC analysis*

The neutral lipid extractions were analyzed using a LC-4000 Series UHPLC system (Jasco, Tokyo, Japan). A volume of 5 ul sample was injected with a Jasco AS-4250 UHPLC autosampler (Jasco, Tokyo, Japan) on a Spherosorb 5.0 µM Sillica column (4.6 mm x 100mm) (Waters, Dublin, Ireland) which was temperature-regulated at 45 °C. A linear gradient was applied on the mobile phase by mixing phase A in 9 min from 0 % - 50 % with phase B at a continuous flow of 1.6 ml/min. Phase A consisted of a Heptane/Ethylacetate (98.8/0.2 %) whereas phase B of a Acetone/Ethylacetate (2:1) mixture (Merck Chemicals, Amsterdam, The Netherlands). Finally, the relative peak areas of the cholesterol and triglycerides were calculated using Chromnav v 2.0 software (Jasco, Tokyo, Japan).

*LDL isolation by ultracentrifugation*

Lipoprotein fractions were obtained from healthy normolipidemic volunteers, both male and female from different ages. Human LDL (d= 1.019-1.063 g/L) was isolated from plasma by density gradient ultracentrifugation (UC) as described previously [25]. Briefly, plasma was obtained after centrifugation of blood at 3000 rpm at 4°C for 15 minutes. Next, 1155 mg of potassium bromide and 75 mg of sucrose was dissolved in 3 mL of plasma to a final density of 1.25 g/mL. Then, 3 ml of high density plasma was pipetted into a Polystyrene SW41 tube (Beckman). Then the gradient was built by pipetting consecutively 2.0 mL KBr solution with d=1.225 , 4 mL KBr (d=1.100 g/ml) and 3 ml KBr (d=1.006g/ml) on top of the plasma. Ultracentrifugation was run at 29,000 rpm for 19 hours at 10°C in an Optima XPN-100 ultracentrifuge system (Beckman, Fullerton, CA, USA). After centrifugation, LDL fractions were harvested by tube slicing and cholesterol, triglycerides and ApoB concentrations were measured using commercially available assays (Diasys) on a Selectra system (Sopachem). Prior to the experiments, the fractions were dialyzed for 24 h in phosphate-buffered saline (PBS). Incubation experiments with LDL were normalized to ApoB concentrations. For the dose response and time incubation studies, monocytes were incubated on fibronectin-coated (FN; 30 µg/ml) glass microscope slides with either an increasing concentration of freshly isolated LDL for 1 h at 37°C, 5% $CO_2$ or a fixed concentration (50 µg/ml) of LDL for an increasing period of time at 37°C, 5% $CO_2$. In order to maintain similar volumes, IMDM was added to a final volume of 200 µl. After incubation, monocytes were fixed with 4% formaldehyde.

*Nile red lipid content staining of CD14+ monocytes*

The NR (9-diethylamino-5H-benzo [alpha] phenoxazine-5-one) staining solution (1mM) was prepared by dissolving 318 µg/mL NR in dimethyl sulfoxide (DMSO) and filtered through a 0.22 µm Minisart® Syringe Filter (Sartorius, Göttinger, Germany) in order to reduce fluorescent background. Aliquots were stored in aliquots at -20°C for at least 6 months. The working solution was prepared freshly by dissolving NR-stock solution in an isosmotic and isotonic solution (BD FACS buffer) to a final concentration of 10 µM and was protected from light. Freshly isolated monocytes were plated on FN-coated glass microscope slides after drawing a circle of approximately 1.5 cm with a DAKO hydrophobic pencil (Dako, Heverlee, Belgium). Monocytes were added in a concentration of $0.5*10^6$/mL and incubated for 1 h at 37°C, 5% $CO_2$, after which the adhered cells were fixed with 4% formaldehyde. Next, the cells were washed with PBS and stored at 4°C. Monocytes were then permeabilized for 5 min with 0.1% Triton-X100 and incubated with the lipid dye Nile Red (1 µg/mL; N3013-100MG, Sigma Aldrich, Zwijndrecht, The Netherlands) for 15 minutes. Cells were washed in PBS (pH 7.4) and mounted using fluorescent mounting medium (Dako, Heverlee, Belgium).

*Image acquisition*

Imaging was performed on a Leica TCS SP8 Confocal laser scanning DMI6000 inverted microscope (Leica Microsystems, Wetzlar, Germany) using a 63x/1.40 Oil CS2 objective coupled to a Hammamatsu camera. Phospholipids were excited at 590(600-700nm) and neutral lipids at 488(500-580nm). In addition, line averaging was used during image acquisition to minimize background noise. Quantification of LDs was performed by assessing total number of monocytes with lipid droplets per field of view (FOV), as well as the number of lipid droplets per positive monocyte in 6–10 FOVs. In order to visualize all LDs with sufficient resolution in the cell, z-stack images of 0.75 µm per stack were made (1024 pixels x

1024 pixels x 8 bit) and merged into a maximum intensity projection for quantification. A minimal number of eight images per sample were taken. For intracellular LD assessment an extensive z-stack was made of NR stained monocytes. Subsequently, for 3D-imaging, the software program Imaris® (version 7.7.0; Belfast, United Kingdom) was used for converting these extensive z-stack images into a 3D model.

*Quantification of lipid droplets using Matlab™ AMC Nile Red Quantifier*

The cell and lipid counter, named Nile Red Quantifier (NRQ) is a custom-made, stand-alone program, with in-house created code in Matlab™ 2015b (The MathWorks Inc., Natick, MA, United States). NRQ is based on a semi-automated segmentation where the user has to point out and click on the cells in the image, leaving a mark for recognition. With this program, the total number of lipids can be counted automatically, as well as the total number of cells and the number of lipid-positive cells per FOV. Obtained microscopic images, (RGB color, TIFF format), with a resolution of 1024x1024x pixels are first converted into grayscale, eliminating hue and saturation while retaining luminance. This grayscale image is morphological opened [26] using a disk structure with a user-defined size and subsequently the image is contrast enhanced. 2D cell segmentation is performed which enables monocyte detection (28) as well as removal of monocytes touching the edges, since lipid count is incomplete in these cells. This binary mask, dilated with a user-defined size, is visualized on the original image to check if LDs are within these masks. Lipid droplets are segmented as described (29) by creating a binary lipid-mask. Hue, Saturation and Value (HSV) segmentation method is used to identify boundaries of objects, making it suitable for segmentation and thus specific lipid droplet detection purposes (29) for which Value (color range) is modifiable to user preference or dye. Next, the background correction is applied by subtracting the inverse monocyte cell-mask from the lipid droplet-mask to avoid possible lipids located outside cell regions. Although lipid droplets in isolated monocytes are in general spherical shaped, the space between LDs can be small and segmentation can lead to overlapping lipids. To distinguish individual lipid droplets from connected lipid droplets in the mask, shape measurements are computed. Subsequently, the original image with (on top) the transparent monocyte cell-mask is displayed. A new binary monocyte cell-mask, with a user-defined octagonal size, is created using these marks.

*Validation of Nile Red lipid content assessment using Oil Red O*

The ORO staining solution was made by dissolving 50 mg of ORO in 10mL isopropanol and was incubated overnight at 56°C. Next, the stock solution was filtered with standard Whatman® filter paper (Sigma Aldrich) and was kept at room temperature. The working solution was prepared by mixing 6 parts of ORO-stock and 4 parts of MQ and subsequently filtered through standard Whatman® filter paper to remove precipitates. After monocyte isolation, cells were fixed with 4% formaldehyde and subsequently permealized for 5 minutes using 0.1% Triton X-100. Next, coverslips were incubated in 60% isopropanol for 5 minutes and subsequently exposed to Oil Red O and incubated for 15 minutes. Cells were destained with 60% isopropanol for 15 seconds, washed once with water and mounted. Imaging was performed on a Leica DM-RA wide-field microscope using a PLAN APO 40x/1.40 Oil PH3 objective and a Charge-Coupled-Device camera (Leica Microsystems) or a Leica TCS SP8 Confocal laser scanning DMI6000 inverted microscope for fluorescent ORO assessment (excited at 568 nm).

*Culturing THP1 cells*

The human THP-1 monocytic cell line [27] (ATCC, Manassas, Virginia, USA) was used as an *in vitro* model for investigating LD-formation and inflammatory response upon LDL-lipid exposure. THP-1 cells were cultured in RPMI 1640 GlutaMAX-medium (ThermoFisher Scientific, Waltham, Massachussetts, USA) supplemented with 10% fetal bovine serum (FBS; Bodinco, Alkmaar, The Netherlands), penicillin (pen; 100 U/ml; ThermoFisher Scientific) and streptomycin (strep; 100mg/ml; ThermoFisher Scientific) at 37°C at 5% $CO_2$. At least 24h prior experiments, THP-1 cells (passage 2-4) were incubated in RPMI-medium containing pen/strep and 1% lipid depleted FBS (Bodinco). Next, THP1 were seeded in a 12-wells plate (Costar, Corning, New York, USA) at a concentration of $1*10^6$ cells/ml and stimulated with 10 μg/ml oxLDL (BioConnect Life Sciences, Huissen, The Netherlands), 100 μg/ml freshly isolated LDL (isolation procedure as previously described in this paper) or left untreated for 24h at 37°C at 5% $CO_2$. Cells were prepped for FACS analysis or adhered to a microscope slide using a Cytospin cytocentrifuge (ThermoFisher Scientific) for two minutes and 550 RPM. After fixation, cells were incubated with Nile Red for subsequent lipid-driven LD formation analysis.

*Statistical analysis*

Data are presented as the mean ± standard error of the mean (SEM) and as number (percentage) for categorical variables, unless stated otherwise. Correlations were assessed using univariate linear regression. Time- and dose dependency experiments were assessed with a one-way ANOVA Dunnett's method for multiple comparisons. All other experiments were analyzed using student T-tests. All statistics were assessed using Graphpad Prism (v6.0h; La Jolla, CA). Statistical significance was reported for $p < 0.05$.

## Results

*NR imaging in peripheral human CD14+ monocytes*

The accumulation of lipids in circulating monocytes can be measured with the NR lipid dye which visualizes both phospholipids and neutral lipids by high resolution confocal microscopy imaging (Fig. 1A). Neutral lipids (cholesterol, cholesterol esters and triglycerides) are shown in green, whereas phospholipids are shown in red. In order to distinguish between membrane-bound cholesterol [28] (MBC) and neutral LDs, the fluorescent intensity of MBC was reduced until LDs alone were visible (Fig. S1A). The advantage of the phospholipid staining is that it results in a clear plasma membrane staining which can be used to assess if neutral lipids are stored within cell bodies, whereas other lipid dyes often require alternative fluorescent labels for this purpose [29]. To test if NR staining is similar to ORO, we examined lipid accumulation in isolated monocytes exposed to 50 μg/ml LDL for 1h and stained LDs using both ORO and NR. Imaging of ORO-stained monocytes using brightfield microscopy (Fig. 1B, left image; LDs indicated with white arrows) and confocal microscopy (Fig. 1B, right image) show intracellular LDs in red and green, respectively. NR imaging of LDs of the same monocyte pool (Fig. 1C) showed that both NR and ORO are able to stain intracellular LDs. However, the use of methanol in the ORO staining procedure promotes fusion of LDs [30].

It is crucial to examine if LDs are located within the isolated monocytes, since presence of artifacts (i.e. background signal outside of the cell perimeter) may result into false positive LD quantification. For this reason, we either treated isolated monocytes with or without 50 μg/ml

LDL and made an extensive Z-stack which is subsequently modelled into a 3D structure in order to establish the LD localization in great detail (Fig. 1D and Movie S1-2). Addition of freshly isolated LDL resulted in elevated intracellular neutral lipids when compared to non-treated monocytes, indicating that LDL particles are routed towards LDs and leads to a concomitant increase in intracellular LD content.

Thus, NR-staining allows us to visualize elevated intracellular neutral LDs upon LDL-lipid exposure to monocytes. To investigate neutral LD-composition, we isolated lipid droplets from LDL-lipid (0, 1 or 2 mg/ml) stimulated circulating monocytes. Next, phospholipids were separated from neutral lipids, and analysis of isolated neutral lipids via high performance liquid chromatography (HPLC) revealed an increase in cholesterol ester/triglyceride ratio (CE/TG; 3.46; 8.28 vs. 1.00-fold for 1, 2 vs. 0 mg/ml LDL, respectively) in a dose-dependent manner (Fig. S1B). This implies that increased lipid loading of monocytes corresponds with elevated cholesterol ester content upon monocyte exposure to LDL-lipids.

Although validation concerning LD composition and visualizing intracellular LDs have been established, analysis of intracellular lipid content remains time consuming and arbitrary.

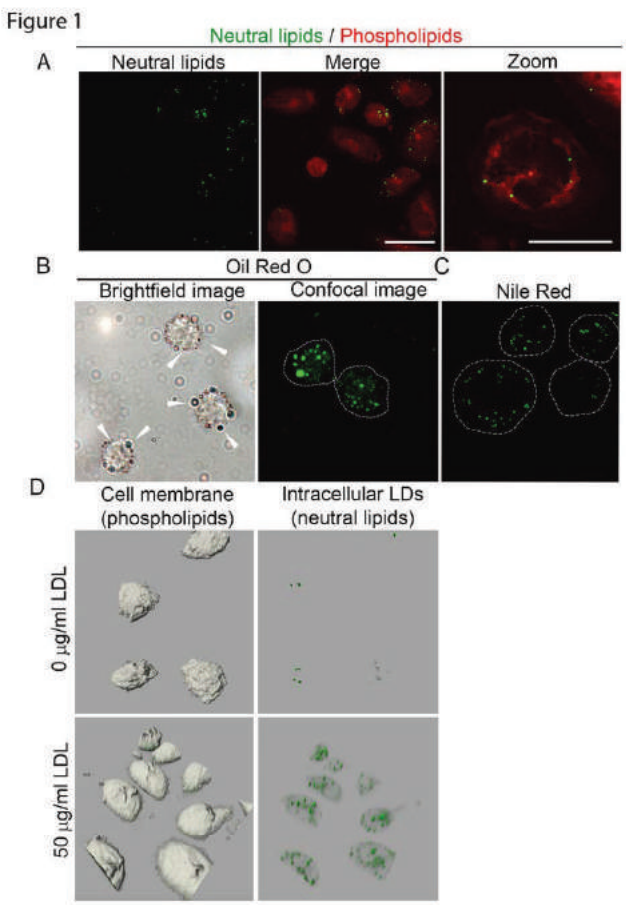


**Figure 1 Lipid droplet detection by Nile Red in human peripheral monocytes. (A)** Images of monocytes were stained with NR. Neutral lipids (left image) can be discriminated from phospholipids (middle image and right image, scale bars, 20 and 10 µm,

respectively); **(B)** Representative images of ORO-stained monocytes treated with 50 μg/ml LDL. The left image shows lipid droplets by brightfield microscopy, LDs are indicated with white arrows. The right image is obtained by confocal microscopy. LD are shown in green; **(C)** NR-stained monocytes treated with 50 μg/ml LDL; LDs are shown in green. Scale bar, 10 μm; **(D)** 3D images of monocytes (grey bodies shown on left images) untreated (upper images) and treated with 50 μg/ml LDL (lower images). LDs are shown in green.

*Validation of Nile Red Quantifier*

Automated quantification of NR-stained isolated monocytes provides a tool for automated counting in a standardized way. Here, we created and used a semi-automated segmentation to quantify lipid droplets in the cells using the Nile Red Quantifier. The multiple NRQ processing steps are shown in a flow diagram (Fig. 2A). Obtained microscopic images (Fig. 2B) are converted into grayscale and subsequently contrast-enhanced (Fig 2C). Next, lipid count of cells found in the perimeter of the image are excluded due to insufficient lipid count in these areas (Fig 2D). After counting all LDs found in the FOV (Fig 2E), based on the green channel (neutral lipids) in the RGB image, all LDs located outside the perimeter of the phospholipid monocyte membrane are excluded from the calculations, a process also known as background correction (Fig 2F). Although lipid droplets in isolated monocytes are in general spherical shaped, the space between LDs can be small and segmentation can lead to overlapping lipids. To distinguish individual LDs from connected LDs in the mask, shape measurements are computed. Next, thresholds are set for these measurements to complete lipid droplet count (Fig. S2 A-E). LD count is visualized by individual lipid droplets with a blue marked "x" and segmented areas that are counted twice and three times are displayed with a red circle and green circle, respectively (Fig. 2G). Monocytes can then be counted by creating marks close to the center of each monocyte. Subsequently, the original image with (on top) the transparent monocyte cell-mask is displayed. Next, lipid-positive monocytes are counted by subtracting the inverted binary lipid-mask of the new monocyte cell-mask. Every region in the new monocyte cell-mask that lost area pixels is now considered positive (yellow circle; Fig. S2 A-E). Further validation of NRQ revealed a strong correlation between automated and manual LD count for circulating monocytes (Fig. 2H; $r = 0.8123$). In addition, a robust correlation was observed in the frequently used THP-1 monocytic cell line as well (Fig. 2I; $r = 0.7213$). Both correlational analyses reveal that NRQ is suitable to asses LD content in both circulating monocytes and THP-1 cells.

Figure 2

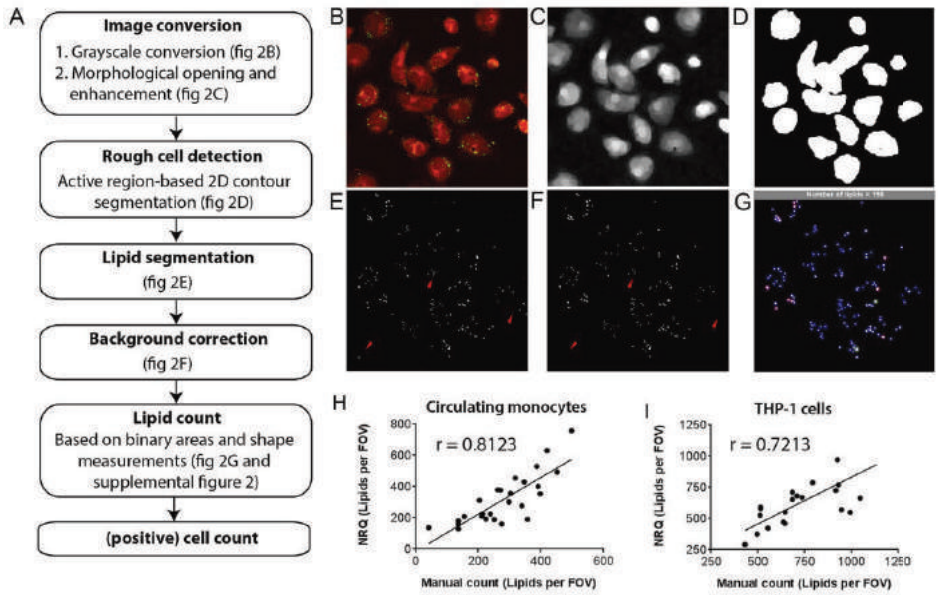


**Figure 2 Processing steps and validation of the Nile Red Quantifier**. **(A)** Overview of processing steps of NRQ; **(B)** Original image of the Nile Red stained monocytes; **(C)** After converting it to grayscale, morphological opening of the grayscales and enhancement is created; **(D)** Figure 1B is then used to segment the cells with a region-based active contour method. **(E** Segmentation of the original image using a HSV color coding segmentation **(F)** After background correction using Figure 1C, Figure 1F is obtained. Segmented lipid areas are then calculated with aid of shape measurements (Fig. S2 A-E); **(G)** Counted areas are visualized with a blue circle and areas counted twice show an additional red circle. Total amount of calculated LD is shown in the gray bar; **(H-I)** Pearson's correlation between manual and NRQ quantification of LDs in circulating monocytes (H) and THP-1 cells (H) with n=20-25 independent images.

*Ex vivo lipid uptake by human peripheral CD14+ monocytes*

To assess whether NR, as quantified by NRQ, was able to detect differences in lipid uptake in monocytes, a time course experiment was conducted. Isolated monocytes were incubated with 50 µg/ml LDL for different times as indicated and subsequently lipid accumulation (Fig. 3A) was analyzed by assessing the increase in intracellular LDs and the percentage of lipid-positive cells (Fig. 3B and 3C, respectively). Already after 5 minutes of incubation with 50 µg/ml, a significant increase of lipid droplets per positive monocyte was found (Fig. 3C). After 30 and 60 minutes, both the number of lipid-positive monocytes (Fig. 3B) as well as the amount of intracellular LD per positive monocyte (Fig. 3C) were significantly increased. This indicates that NR detects rapidly-formed lipid droplets upon lipid exposure in circulating monocytes.

Next, we examined the LDL-lipid uptake in a dose-dependent manner (Fig. 3D). An increase in both lipid-positive monocytes and in lipid content per lipid-positive monocyte is observed after 60 minutes of incubation with either 10, 20 or 50 µg/ml freshly isolated LDL (Fig. 3E and 3F). These data suggest that LDL-lipids are taken up by monocytes leading to intracellular lipid body formation detectable by NR. To study if the LDL-uptake process is due to receptor-mediated uptake and not passive diffusion the cells were incubated with 50 µg/ml LDL and either fixed with 4% paraformaldehyde or incubated at 4 °C to induce metabolic arrest

(Supplemental Fig. 3A-B and 3C-D, respectively). As expected, in both conditions, receptor-mediated LDL uptake is inhibited.

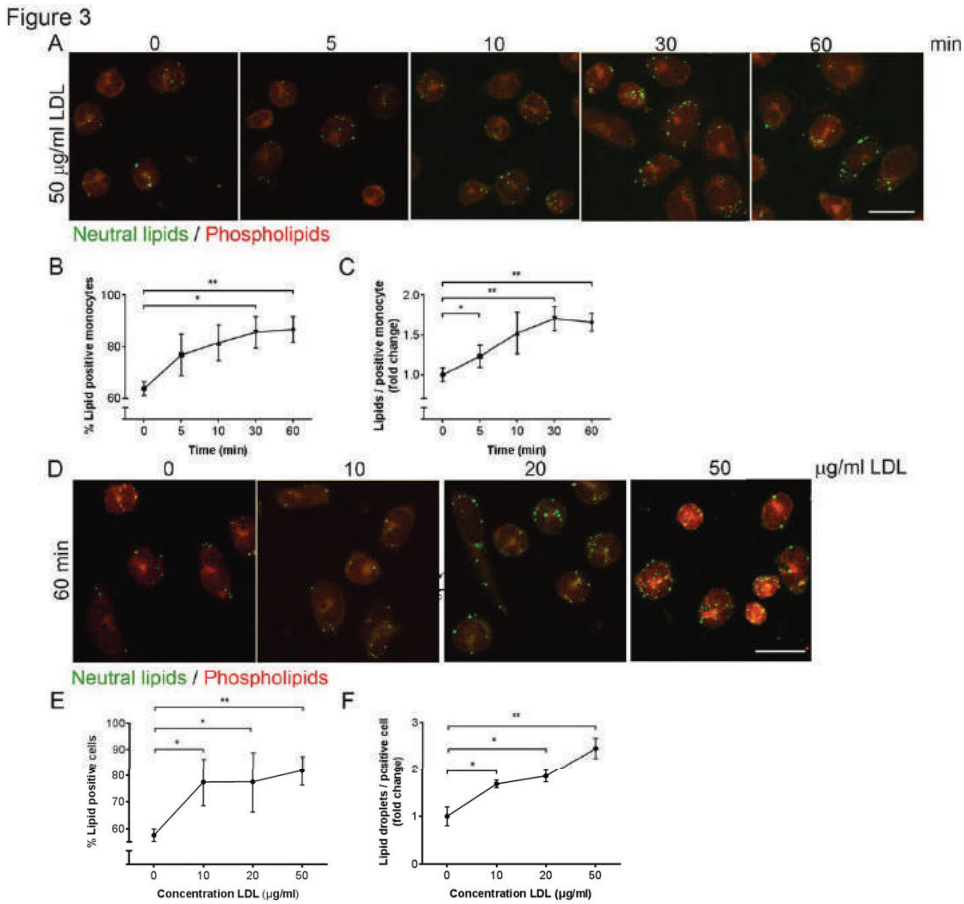


**Figure 3 NR detection of LD in monocytes in a time- and dose-dependent manner. (A)** Representative images of monocytes treated with 50 µg/ml LDL at different time points as indicated. Scale bar, 10 µm. LD and phospholipids are shown in green and red respectively. **(B)** Quantification of LD-positive monocytes after NR-staining; **(C)** Quantification of the amount of lipids per positive monocytes after NR-staining. **(D)** Representative images for dose dependent uptake of different concentrations of LDL as indicated for 60 minutes. Scale bar, 10 µm. LD are shown in green. Phospholipids in red; **(E-F)** Quantification of dose dependency experiments in amount of LD-positive monocytes (E) and number of LDs per LD-positive monocyte (F). $p < 0.05$ considered significant. Data are shown as mean ± SEM for n=5-7 independent experiments.

## Discussion

Here, we show that the lipid dye Nile red is suitable for assessment of intracellular lipid content in isolated circulating monocytes and we subsequently developed an automated-lipid quantification tool.

*Benefits of Nile Red*

In the present study NR staining was capable of detecting alterations in LDL-induced neutral lipid accumulation in a time (Fig. 3A-C) - and concentration-dependent manner (Fig. S1; Fig. 3D-F). These data validate NR-based LD measurement as a reliable tool to detect alterations

in LD accumulation in circulating monocytes. NR has several advantages over other lipid probes or dyes: (A) the lipophilic dye NR provides an inexpensive method to visualize intracellular lipid accumulation as compared to antibody-based lipid probes. (B) As shown in this study, cellular NR-staining is quick and easy to apply, whereas antibody-based procedures are time-consuming due to the multiple staining steps. (C) The fluorescence maxima fluctuate based on hydrophobicity of the cellular content NR allowing us to discriminate between neutral lipids and phospholipids. This enables us to specifically detect intracellular lipids stored in lipid droplets, whereas a lipid dye as BODIPY may bind nonspecifically [16], and allowed us to use the phospholipid staining to visualize the cell membrane [22]. (D) NR is an uncharged heterocyclic molecule and thus soluble in organic solvents [21]. Furthermore, the use of confocal microscopy allows us to visualize LD at different focal planes within monocytes. This is in contrast with ORO, a lipid-dye normally imaged using a brightfield microscope which often cannot image in the Z-dimension. Without this dimension, it is more difficult to count and quantify all the lipids within one cell, since most LDs are not located in one focal plane, resulting in potential difficulties in the quantification procedure of LD content. (E) Furthermore, validation of NR-applicability revealed its flexibility regarding staining of other cell types such as, THP-1 cells, murine bone marrow-derived macrophages but also human fibroblasts (data not shown).

*Automated image analysis using NRQ*

The NRQ quantification tool allows time-effective analysis of LD-content. We showed that NRQ is suitable to replace manual counting of intracellular LDs in circulating monocytes as well as THP-1 cells (Fig. 2H and I, respectively) when high quality images are captured, since low resolution of images complicates detection of green fluorescent LDs. In addition, both NRQ and the confocal settings used should remain identical within a study to perform objective analysis. For optimal use of NRQ one must take caution concerning the amount of cells per FOV. Too many cells per FOV could result in clusters that are too dense, which results in difficulties in semi-automated quantification of single cells. Therefore, we recommend to maximally seed $1x10^5$ monocytes/$cm^2$ for optimal usage of NRQ.

*Implications for clinical research*

Whereas until recently, research into lipid accumulation focused predominantly on plaque macrophages, recent findings highlight the importance of the interaction between lipoproteins and mononuclear cells already in the circulation [31]. Foamy monocytes have been shown to contribute to nascent atherosclerosis [32]. Cellular lipid accumulation actually induces β2-integrin (CD11c/CD18) surface expression [33], which plays an important role as a compatible structure for vascular cellular adhesion molecule on endothelial cells, supporting monocyte recruitment into atherosclerotic plaques [6,34]. This perspective makes NRQ a valuable tool for future research into the fate of these lipid laden cells.

*Limitations*

Although NR-staining and NRQ analysis offer a reproducible method for intracellular quantification of LD content, there are some considerations to discuss. One possible limitation is the broad emission spectrum of the dye, since fluorescent signal is observed 488nm up to the far red spectrum [35]. It is possible however, to use the dye in combination with fluorophores which can be excited in the violet spectrum (405nm) in order to perform dual localization

studies using NR [36,37]. The diameter of LDs in non-adipocytes generally range from 0.1-5 μm, but can be up to 100 μm in size in white adipocytes [38]. Since NRQ is developed to detect LDs based on fluorescent intensity and their correlated pixel size, NRQ is solely validated to image LDs in the nonadipocyte range when recorded with 1024x1024 pixels.

*Conclusion*

Altogether, we provide a new quantitative tool, the Nile Red Quantifier (NRQ), for quick and reproducible NR-based lipid detection in isolated patient-derived circulating monocytes. This procedure measures the total amount of lipids per FOV and the number of LD-positive cells. With these parameters one is able to quantify LD content on a per cell basis and the percentage of lipid positive cells. We also revealed that NRQ is applicable for THP-1 cells, besides circulating monocytes suggesting its potential for other cell types as well. Additionally, the NR staining procedure is sensitive to detect any changes in LD dynamics and NRQ is a useful tool for analysis of lipid-induced remodeling in patient-derived circulating monocytes. With the use of this tool it would be of great clinical interest to examine if increased lipid accumulation and hence increased pro-inflammatory phenotype could be used in the future as possible biomarker for CVD risk.

## Supplemental data

### Supplementary methods NRQ

Shape measurements performed on the lipid mask are; area, number of pixels in every region; perimeter, scalar that specifies distance around the boundary of the pixel region, solidity, scalar that is area divided by convex area (number of pixels that specifies the smallest convex polygon containing the region); bounding box, axis sizes of smallest rectangle containing area; eccentricity, scalar that specifies the eccentricity of the ellipse (Fig. S2). Some of the mentioned measurements are calculated using other measurements that follows out of all the shape measurements resulting from regionprops.m, a standard function from MATLAB (The MathWorks Inc., Natick, MA, United States). For example, the major axis length (Fig. S2B) of the mask is measured from which the eccentricity (a scalar) can be calculated using the ratio of the foci of the ellipse and the major axis length. The value can be between 0 and 1, in which an ellipse with an eccentricity of 0 actually is a circle and an eccentricity of 1 would mean a line segment. For individual lipids, the expectation for eccentricity is close to 0 and if it is close to 1 it is more likely to be a connected mask as lipids are thought to be more round shaped due to their hydrophobic core [39].

Upon inspection of individual lipids in the segmented lipid mask, it is clearly noticed that some lipid areas in the mask were connected and did not represent one lipid droplet. Therefore, because the calculation of lipids is based on individual areas in the mask, shape measurements could provide that extra information on discriminating lipids from one another. In Fig. S2A one can see an enlargement of two segmented areas in the lipid mask, which by human eye could be explained as three lipids. Measurements as major axis length, for calculating eccentricity 2), is performed as can be seen in Figure S2. The convex image is a rectangular cut-out version of the smallest polygon sized pixel region, adding more information about size and form of the segmented area (Fig. S2C). With these measurements, we can discriminate the lipids that are spherically shaped (thus one lipid) from those who are not or extremely large and thus are most likely to represent more than one lipid.

These different shape properties are used to set conditions for the analysis of the segmented regions. When these shape measurements are above all set thresholds, determined by visual inspection and exploration of the data, these lipids will be counted twice and marked (extra) with a red circle. In rare cases, if the size of the lipid mask exceeds 40 pixels ('AreaThreshold2'), 5 times the size of the average lipid, it will be counted as three lipids (maximum count of one mask) and additionally marked by a green circle (Fig. S2D-E). This method allows the user to more accurately count individual lipids.

Below is a list of the set thresholds for each measured parameter:
AreaThreshold1 = 16 (pixels)
AreaThreshold2 = 40 (pixels)

PerimeterThreshold = 11 (means 11 or higher)
SolidityThreshold = 1 (means below 1)
CVXimageThreshold = 20 (means 20 or higher)
EccentricityThreshold = 0.6 (or higher but 0.6 was seen as high [2])

## References


1. Passacquale G, Giosia P Di, Ferro A. The role of inflammatory biomarkers in developing targeted cardiovascular therapies: lessons from the cardiovascular inflammation reduction trials. *Cardiovasc Res* England; 2016;**109**:9–23.
2. Libby P, Ridke PM, Hansson GK. Progress and challenges in translating the biology of atherosclerosis. *Nature* England; 2011;**473**:317–325.
3. Lusis AJ. Atherosclerosis. *Nature* ENGLAND; 2000;**407**:233–241.
4. Libby P. Inflammation in atherosclerosis. *Nature* England; 2002;**420**:868–874.
5. Ghattas A, Griffiths HR, Devitt A, Lip GYH, Shantsila E. Monocytes in coronary artery disease and atherosclerosis: where are we now? *J Am Coll Cardiol* United States; 2013;**62**:1541–1551.
6. Gower RM, Wu H, Foster GA, Devaraj S, Jialal I, Ballantyne CM, Knowlton AA, Simon SI. CD11c/CD18 expression is upregulated on blood monocytes during hypertriglyceridemia and enhances adhesion to vascular cell adhesion molecule-1. *Arterioscler Thromb Vasc Biol* United States; 2011;**31**:160–166.
7. Hyson DA, Paglieroni TG, Wun T, Rutledge JC. Postprandial lipemia is associated with platelet and monocyte activation and increased monocyte cytokine expression in normolipemic men. *Clin Appl Thromb Hemost* United States; 2002;**8**:147–155.
8. Imanishi T, Ikejima H, Tsujioka H, Kuroi A, Ishibashi K, Komukai K, Tanimoto T, Ino Y, Takeshita T, Akasaka T. Association of monocyte subset counts with coronary fibrous cap thickness in patients with unstable angina pectoris. *Atherosclerosis* Ireland; 2010;**212**:628–635.
9. Kashiwagi M, Imanishi T, Tsujioka H, Ikejima H, Kuroi A, Ozaki Y, Ishibashi K, Komukai K, Tanimoto T, Ino Y, Kitabata H, Hirata K, Akasaka T. Association of monocyte subsets with vulnerability characteristics of coronary plaques as assessed by 64-slice multidetector computed tomography in patients with stable angina pectoris. *Atherosclerosis* Ireland; 2010;**212**:171–176.
10. Hartigh LJ den, Altman R, Norman JE, Rutledge JC. Postprandial VLDL lipolysis products increase monocyte adhesion and lipid droplet formation via activation of ERK2 and NFkappaB. *Am J Physiol Heart Circ Physiol* United States; 2014;**306**:H109-20.
11. Melo RCN, D'Avila H, Bozza PT, Weller PF. Imaging lipid bodies within leukocytes with different light microscopy techniques. *Methods Mol Biol* United States; 2011;**689**:149–161.
12. Fujimoto T, Ohsaki Y, Cheng J, Suzuki M, Shinohara Y. Lipid droplets: a classic organelle with new outfits. *Histochem Cell Biol* Germany; 2008;**130**:263–279.
13. Murphy DJ. The biogenesis and functions of lipid bodies in animals, plants and microorganisms. *Prog Lipid Res* England; 2001;**40**:325–438.
14. Murphy DJ, Vance J. Mechanisms of lipid-body formation. *Trends Biochem Sci* ENGLAND; 1999;**24**:109–115.
15. Mehlem A, Hagberg CE, Muhl L, Eriksson U, Falkevall A. Imaging of neutral lipids by oil red O for analyzing the metabolic status in health and disease. *Nat Protoc* England; 2013;**8**:1149–1154.
16. Daemen S, Zandvoort MAMJ van, Parekh SH, Hesselink MKC. Microscopy tools for the investigation of intracellular lipid storage and dynamics. *Mol Metab* Germany; 2016;**5**:153–163.
17. Fukumoto S, Fujimoto T. Deformation of lipid droplets in fixed samples. *Histochem Cell Biol* Germany; 2002;**118**:423–428.
18. Xu S, Huang Y, Xie Y, Lan T, Le K, Chen J, Chen S, Gao S, Xu X, Shen X, Huang H, Liu P. Evaluation of foam cell formation in cultured macrophages: an improved method with Oil Red O staining and DiI-oxLDL uptake. *Cytotechnology* Netherlands; 2010;**62**:473–481.
19. Spangenburg EE, Pratt SJP, Wohlers LM, Lovering RM. Use of BODIPY (493/503) to visualize intramuscular lipid droplets in skeletal muscle. *J Biomed Biotechnol* United States; 2011;**2011**:598358.
20. Maxfield FR, Wustner D. Analysis of cholesterol trafficking with fluorescent probes. *Methods Cell Biol* United States; 2012;**108**:367–393.
21. Greenspan P, Mayer EP, Fowler SD. Nile red: a selective fluorescent stain for intracellular lipid droplets. *J Cell Biol* UNITED STATES; 1985;**100**:965–973.
22. Fowler SD, Greenspan P. Application of Nile red, a fluorescent hydrophobic probe, for the detection of neutral lipid deposits in tissue sections: comparison with oil red O. *J Histochem Cytochem* UNITED STATES; 1985;**33**:833–836.
23. Munoz NM, Leff AR. Highly purified selective isolation of eosinophils from human peripheral blood by negative immunomagnetic selection. *Nat Protoc* England; 2006;**1**:2613–2620.
24. Löfgren L, Ståhlman M, Forsberg G-B, Saarinen S, Nilsson R, Hansson GI. The BUME method: a novel automated chloroform-free 96-well total lipid extraction method for blood plasma. *J Lipid Res* 2012;**53**:1690–1700.
25. Graaf J de, Vleuten GM van der, Avest E ter, Dallinga-Thie GM, Stalenhoef AFH. High plasma level of remnant-like particles cholesterol in familial combined hyperlipidemia. *J Clin Endocrinol Metab* United States; 2007;**92**:1269–1275.
26. Chan TF, Vese LA. Active contours without edges. *IEEE Trans Image Process* United States; 2001;**10**:266–277.
27. Tsuchiya S, Yamabe M, Yamaguchi Y, Kobayashi Y, Konno T, Tada K. Establishment and characterization of a human acute monocytic leukemia cell line (THP-1). *Int J cancer* DENMARK; 1980;**26**:171–176.
28. Simons K, Toomre D. Lipid rafts and signal transduction. *Nat Rev Mol Cell Biol* England; 2000;**1**:31–39.
29. Harris L-ALS, Skinner JR, Wolins NE. Imaging of neutral lipids and neutral lipid associated proteins. *Methods Cell Biol* United States; 2013;**116**:213–226.
30. DiDonato D, Brasaemle DL. Fixation methods for the study of lipid droplets by immunofluorescence microscopy. *J Histochem Cytochem* United States; 2003;**51**:773–780.

31. Jackson WD, Weinrich TW, Woollard KJ. Very-low and low-density lipoproteins induce neutral lipid accumulation and impair migration in monocyte subsets. *Sci Rep* England; 2016;**6**:20038.
32. Xu L, Dai Perrard X, Perrard JL, Yang D, Xiao X, Teng B-B, Simon SI, Ballantyne CM, Wu H. Foamy monocytes form early and contribute to nascent atherosclerosis in mice with hypercholesterolemia. *Arterioscler Thromb Vasc Biol* United States; 2015;**35**:1787–1797.
33. Wu H, Gower RM, Wang H, Perrard X-YD, Ma R, Bullard DC, Burns AR, Paul A, Smith CW, Simon SI, Ballantyne CM. Functional role of CD11c+ monocytes in atherogenesis associated with hypercholesterolemia. *Circulation* United States; 2009;**119**:2708–2717.
34. Timmerman I, Daniel AE, Kroon J, Buul JD van. Leukocytes Crossing the Endothelium: A Matter of Communication. *Int Rev Cell Mol Biol* 2016;**322**:281–329.
35. Listenberger LL, Studer AM, Brown DA, Wolins NE. Fluorescent Detection of Lipid Droplets and Associated Proteins. *Curr Protoc Cell Biol* United States; 2016;**71**:4.31.1-4.31.14.
36. Ostermeyer AG, Ramcharan LT, Zeng Y, Lublin DM, Brown DA. Role of the hydrophobic domain in targeting caveolin-1 to lipid droplets. *J Cell Biol* United States; 2004;**164**:69–78.
37. Ostermeyer AG, Paci JM, Zeng Y, Lublin DM, Munro S, Brown DA. Accumulation of caveolin in the endoplasmic reticulum redirects the protein to lipid storage droplets. *J Cell Biol* United States; 2001;**152**:1071–1078.
38. Fujimoto T, Parton RG. Not Just Fat: The Structure and Function of the Lipid Droplet. *Cold Spring Harb Perspect Biol* 2011;**3**.
39. Penno A, Hackenbroich G, Thiele C. Phospholipids and lipid droplets. *Biochim Biophys Acta* Netherlands; 2013;**1831**:589–594.
2. Weisstein, Eric W. "Eccentricity." From *MathWorld*--A Wolfram Web Resource. http://mathworld.wolfram.com/Eccentricity.html

Supplemental Figure S1

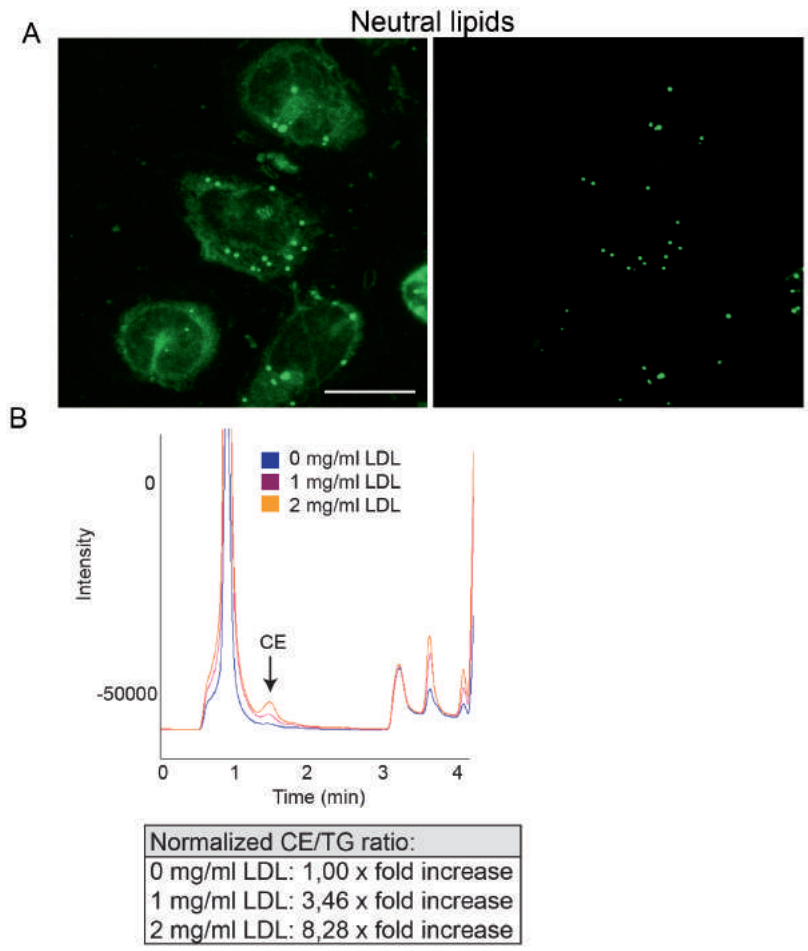


| Normalized CE/TG ratio: |
|---|
| 0 mg/ml LDL: 1,00 x fold increase |
| 1 mg/ml LDL: 3,46 x fold increase |
| 2 mg/ml LDL: 8,28 x fold increase |

**Supplemental Figure S1 (A)** Green fluorescence reveals both membrane bound- and intracellular neutral lipids (lef image; neutral lipids in green). For analysis of intracellular LDs, fluorescent intensity was decreased until solely LDs were visible (right image); **(B)** HPLC-analysis reveals elevated cholesterol ester content upon LDL-lipid loading. The relative peak areas of CE/TG ratio were calculated in monocytes stimulated with 0 (blue line), 1 (purple line) and 2 mg/ml LDL (orange line). CE/TG ratio increased in a dose-dependent fashion once stimulated with LDL. HPLC, high performance liquid chromatography; LDL, low-density lipoprotein; CE, cholesterol ester; TG, triglyceride

Supplemental Figure S2

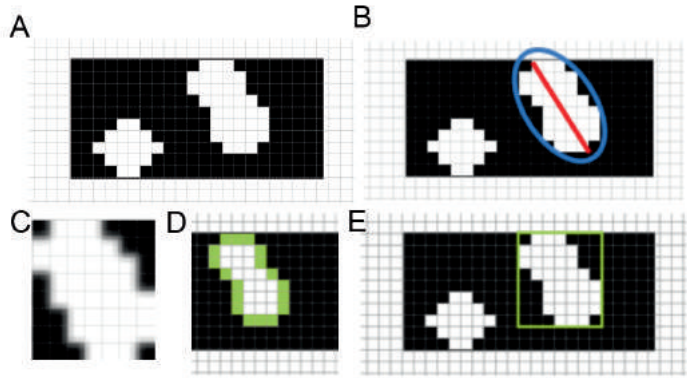


**Supplemental Figure S2 Example of shape measurements applied** on **(A)** Segmented lipid areas; **(B)** From the right area the major axis length is depicted by the red line across the area from which the eccentricity of the ellipse (blue) is calculated; **(C)** A small image which only contains the smallest polygon sized area of that segmented lipid area; **(D-E)** The perimeter and bounding box in green, respectively.

Supplemental Figure S3

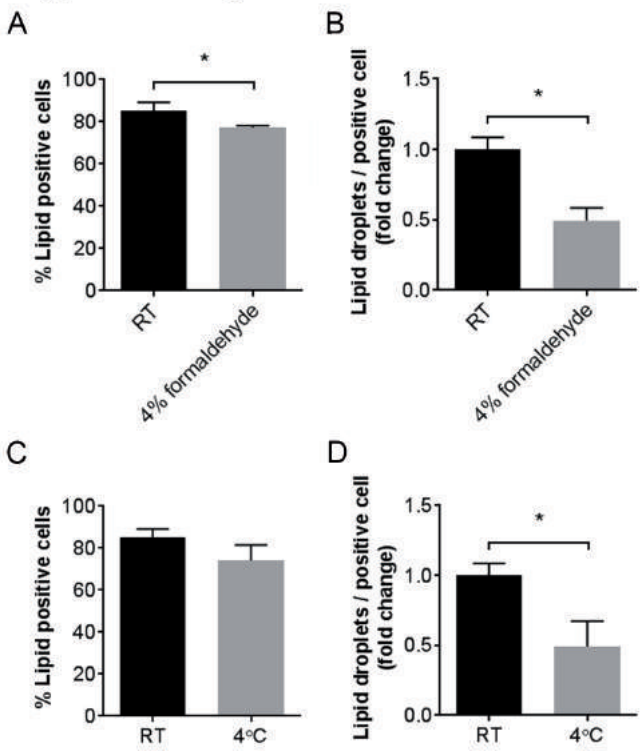

**Supplemental Figure S3 Metabolic arrest leads to inhibition of intracellular LDL-initiated LD formation**. **(A-B)** 4% Formaldehyde fixed samples showed less LD-positive monocytes (A) and less LDs per LD-positive monocyte compared to non-fixed monocytes; **(C-D)** Samples incubated at 4°C lead to decreased number of LD-positive monocytes (C) and declined number of LDs per LD-positive monocyte. LDL, low-density lipoprotein; LD, lipid droplet

**Supplemental Movies LDL-lipid uptake increased intracellular LDL-mediated LD formation in circulating monocytes.** Monocytes were stimulated with 50 μg/ml LDL and 3D-modeling revealed an elevated of lipid uptake **(1)** compared to unstimulated monocytes (**2**). Monocytes are shown in grey, whereas LD are in green. Scale bar, 7 μm. LDL, low-density lipoprotein; LD, lipid droplet
*https://www.ncbi.nlm.nih.gov/pmc/articles/PMC5665660/bin/supp_58_11_2210__index.html*

# Chapter 4

## Remnant cholesterol as a direct mediator of cellular and arterial wall inflammation

Sophie J. Bernelot Moens*, Simone L. Verweij*, Johan G. Schnitzler, Lotte C.A. Stiekema, Merijn Bos, A. Langsted, Carlijn Kuijk, Carlijn Voermans, Hein J. Verberne, Siroon Bekkering, Borge Nordestgaard, Erik S.G. Stroes, Jeffrey Kroon

*Arteriosclerose, Thrombosis, and Vascular Biology. 2017 May;37(5):969-975*

## Abstract

**Background** Mendelian randomization studies revealed a causal role for remnant cholesterol in cardiovascular disease. Remnant particles accumulate in the arterial, potentially propagating local and systemic inflammation.
**Objectives** We evaluated the impact of remnant cholesterol on arterial wall inflammation, circulating monocytes, and bone marrow in patients with familial dysbetalipoproteinemia (FD).
**Methods** Arterial wall inflammation and bone marrow activity was measured using $^{18}$F-FDG PET/CT. Monocyte phenotype was assessed with flow cytometry. The correlation between remnant levels and hematopoietic activity was validated in the Copenhagen General Population Study.
**Results** We found a 1.2-fold increase of $^{18}$F-FDG uptake in the arterial wall in FD patients (n=17, age 60±8, remnant cholesterol: 3.26[2.07-5.71]) compared with controls (n=17, age 61±8, remnant cholesterol 0.29[0.27-0.40]). Monocytes from FD patients showed increased lipid accumulation (lipid positive monocytes: FD patients 92% [86-95], controls 76% [66-81], p=0.001, with an increase in lipid droplets per monocyte), and a higher expression of surface integrins (CD11b, CD11c, CD18). FD patients also exhibited monocytosis and leukocytosis, accompanied by a 1.2-fold increase of $^{18}$F-FDG uptake in bone marrow. Additionally, we found a strong correlation between remnant levels and leukocyte counts in the Copenhagen General Population Study (n=103.953, p for trend $5*10^{-276}$). *In vitro* experiments substantiated that remnant cholesterol accumulates in human hematopoietic stem and progenitor cells which coincides with myeloid skewing.
**Conclusions** FD patients have increased arterial wall and cellular inflammation. These findings indicate an important inflammatory component to the atherogenicity of remnant cholesterol, contributing to the increased CVD risk in FD patients.

**Key words**: remnant cholesterol, arterial wall inflammation, cardiovascular disease, monocytes, hematopoietic stem and progenitor cells

List of abbreviations

| | |
|---|---|
| BMI | Body Mass Index |
| CD | Cluster of differentiation |
| CFU-GM | colony forming unit – granulocyte monocyte |
| CRP | C-reactive protein |
| CGPS | Copenhagen General Population Study |
| CVD | cardiovascular disease |
| FD | familial dysbetalipoproteinemia |
| $^{18}$F-FDG PET/CT scan | $^{18}$F-fluordeoxyglucose positron emission tomography/ computed tomography |
| FOV | field of view |
| HDL-c | high density lipoprotein cholesterol |
| HSPCs | hematopoietic stem and progenitor cells |
| IQR | interquartile range |
| LDL-c | low density lipoprotein cholesterol |
| MFI | mean fluorescent intensity |
| PBS | phosphate buffered saline |
| SD | standard deviation |
| SUV | standard uptake value |
| TBR | target to background ratio |
| TRLs | triglyceride rich lipoproteins |
| VLDL | very low density lipoprotein |

## Introduction

After lowering of low-density lipoprotein cholesterol (LDL-c) to recommended levels, a significant cardiovascular disease (CVD) burden remains unaddressed. This residual risk has been attributed partly to triglyceride-rich lipoproteins (TRLs), particularly in the non-fasting state [1]. In plasma, triglycerides are initially carried in very-low-density-lipoproteins (VLDL) or chylomicrons. Following lipolysis of triglycerides, TRLs are converted to 'remnant' particles, enriched in cholesterol [2]. Recently, Mendelian randomization studies suggested a causal association between remnant cholesterol and ischemic heart disease [3]. The mechanisms contributing to the atherogenicity of remnant particles has been suggested to relate to subendothelial accumulation of remnant cholesterol (comparable to LDL-c) and/or the induction of an inflammatory state [4]. In support of the latter, an association was reported between remnant cholesterol and CRP levels [5].

The potential mechanisms by which remnant cholesterol particles may induce inflammatory changes remain to be established. Remnant cholesterol can be readily taken up by plaque macrophages without prior oxidation of the particle [6], thereby promoting arterial inflammation [7]. This reaction propagates continued influx of circulating immune cells, predominantly monocytes, into atherosclerotic lesions in both experimental models [8] as well as patients [9], leading to a multi-level inflammatory response [10]. Recent data supports that remnant cholesterol can also be taken up by circulating monocytes, eliciting a pro-adhesive phenotype [11]. Upstream, this heightened activation status is maintained by augmented hematopoietic activity, as has been shown in CVD patients [12].

In the present study, we set out to evaluate the impact of elevated levels of remnant cholesterol on multi-level inflammatory activation in patients with familial dysbetalipoprotenemia (FD), who are characterized by genetically elevated levels of remnant cholesterol [13]. Inflammatory activity of the arterial wall and activity of the bone marrow was assessed using $^{18}$F-fluordeoxyglucose positron emission tomography computed tomography ($^{18}$F-FDG PET/CT) [14]. In parallel, we also assessed the phenotype of circulating monocytes using flow cytometry and remnant-induced changes in hematopoietic activity.

## Methods

*Study population and design*

We performed an observational case-control study in 17 patients, 50 years or older, with a molecular diagnosis of FD [13], based on the presence of the ApoE2/E2 genotype and remnant cholesterol levels > 0.7 mmol/l (>27.3mg/dl). Exclusion criteria comprised any chronic inflammatory disease, diabetes mellitus, chronic kidney disease and the use of lipid lowering drugs 6 weeks prior to study inclusion. In order to minimize radiation exposure, age and gender matched healthy controls were selected from a concurrent cohort at our department who were scanned using the same protocol and the same scanner. For *ex vivo* monocyte experiments matched

healthy controls were included on the same day as the FD patients. The study protocol was approved by the institutional review board of the Academic Medical Center in Amsterdam, The Netherlands. Written informed consent was obtained from each participant.

*Baseline characteristics*

Patients underwent cardiovascular risk assessment including the presence of risk factors, family history and medication use. Vital parameters, including weight, height and blood pressure, were measured. Lipid levels were measured using fast protein liquid chromatography (FPLC) as described in the supplemental methods [15]. In this study remnant cholesterol is defined as the non-HDL and non-LDL lipoprotein class [2].

*$^{18}$F-FDG PET/CT studies*

$^{18}$F-FDG PET/CT scans were performed on a dedicated scanner (Philips, Best, the Netherlands). Patients were fasted for at least 6 hours before infusion of 100 MBq $^{18}$F-FDG. 90 minutes post-infusion, a PET scan was performed in combination with a low-dose, non-contrast enhanced CT for attenuation, correction and anatomic co-registration. Images were analyzed by experienced readers blinded for patient data, using dedicated software (OsiriX, Geneva, Switzerland; http://www.osirix-viewer.com). $^{18}$F-FDG uptake was assessed in both carotids, the ascending aorta and the bone marrow. The maximal target-to-background-ratio ($TBR_{max}$) of both arterial segments were determined as described previously [16]. The maximal standard uptake ($SUV_{max}$) in the bone marrow was assessed by drawing 5 regions of interest within the vertebrae T1 to L5. The bone marrow activity was calculated as the mean of $SUV_{max}$ of these five vertebrae [17].

<u>Flow cytometric analysis of monocytes</u>

Red blood cells were lysed with red blood cell lysis buffer (Affymetrix, eBioscience, San Diego, USA). Leukocytes were incubated with fluorochrome labelled antibodies (supplemental table 1) for 15 minutes and washed with phosphate buffered saline (PBS). Samples were analyzed using BD FACS Canto II (Becton, Dickinson, Fanklin Lakes, New Jersey). Monocytes were classified according to HLA-DR, CD14 and CD16 expression [18]. Subsequently, surface markers involved in monocyte chemotaxis were determined (supplemental table 1). Samples were analyzed using FlowJo software (version 10.0 FlowJO, LLC, Ashland, OR). Delta median fluorescence intensity (MFI) was obtained by subtracting the MFI from the isotype control from the MFI of the marker.

*Monocyte isolation and Intracellular lipid accumulation*

Monocytes were isolated through density centrifugation using Lymphoprep™ (Axis-Shield, Dundee, Scotland) followed by human CD14 magnetic beads and MACS® cell separation columns (Miltenyi, Bergisch Gladbach, Germany).

Subsequently cells were stained to assess intracellular lipid content using the lipid dye Nile Red and subsequently imaged using high resolution confocal laser scanning microscopy, as described in the supplemental material.

*In vitro effect of remnant cholesterol on HSPC progenitor potential*
Leukapheresis material of healthy donors treated with G-CSF was used to obtain CD34+ cells and were subsequently enriched by magnetic activated cell sorting (see supplemental material). At day 0 CD34+ cells were stimulated once with pooled remnant cholesterol (isolated using ultracentrifugation) of either two FD patients or two healthy controls. All cells were cultured at 37°C at 5% CO2. At day one, cells were fixated and intracellular lipid accumulation was assessed. At day seven, cells were counted and flow cytometric assays were performed as described in detail previously [12].

*Validation in the Copenhagen General Population Study*
Data were collected from the Copenhagen general population study (CGPS), a prospective study of general Danish population. We extracted information on remnant cholesterol levels, leukocyte count and leukocyte differentiation from 103.953 participants. Participants with diabetes were excluded. The data of the CGPS study were analyzed using stata (version 11.2). Participants were divided into 5 groups, based on remnant cholesterol levels (<0.5; 0.5-0.99; 1.0-1.49; 1.5-1,99; >2.0 mmol/L). Data are presented as median with interquartile range (IQR), and corrected for the following confounders: units of alcohol per week, smoking status, time since last meal and body mass index (BMI).

*Statistical analysis*
All data, except the data of the CGPS study, were analyzed using Prism version 6.0e (GraphPad software, LaJolla, California) and SPSS version 23.0 (SPSS Inc., Chicago, Illinois). Data are presented as the mean ± standard deviation (SD) for normally distributed data, the median with IQR for non-normally distributed data or as a number (percentage) for categorical variables. To examine differences in clinical characteristics and monocyte phenotype (except for flow cytometry) and functions between FD patients and healthy controls we performed student T-tests or Mann Whitney U tests for respectively normal and non-normal distributed variables. Differences in TBR were assessed with linear regression analysis, correcting for systolic blood pressure and BMI.
A two-way ANOVA with Bonferroni post-hoc analysis was performed for all flow cytometry analysis. A 2-sided *P*-value<0.05 was considered statistically significant.

## Results
*Study population*

We included 17 FD patients (age 60±8 years, 70% male) and 17 healthy controls matched for age and gender (age 61±8 years, 59% male). Baseline characteristics are listed in table 1. FD patients had higher levels of total cholesterol and triglycerides and, as expected, lower levels of HDL-c and LDL-c. This translated in significantly higher levels of remnant cholesterol (FD patients 3.26[2.07-5.71] mmol/l versus controls 0.29[0.27-0.4] mmol/l, p=<0.001). FD patients had an adverse CV risk profile, with elevated systolic blood pressure (FD patients: 138±13 mmHg versus controls: 128±11 mmHg, P=0.028) and an increased BMI (FD patients 27.3±3.7 kg/m$^2$ versus controls 24.4±3.8 kg/m$^2$, p=0.034). We found a non-significant increase in CRP levels (FD patients 2.6[1.1-3.9] mg/dl versus controls 1.5[0.6-2.0] mg/dl, p=0.152). FD patients also had increased leukocyte counts with distinct alterations in leukocyte differentiation compared to controls.

Table 1 baseline characteristics

| Characteristics | Control (n=17) | Patient with FD (n=17) | P-value |
|---|---|---|---|
| Sex, male/female | 10/7 | 12/5 | 0.360 |
| Age, y | 61±8 | 60±8 | 0.704 |
| Body mass index, kg/m² | 24.4±3.6 | 27.3±3.7 | 0.034 |
| Smoking, yes/no | 3/13 | 4/13 | 0.537 |
| Peripheral SBP, mm Hg | 128±11 | 138±13 | 0.028 |
| Peripheral DPB, mm Hg | 82±7 | 86±10 | 0.206 |
| Total cholesterol, mmol/L | 5.58±0.98 | 7.27±2.5 | 0.017 |
| LDL cholesterol, mmol/L | 3.35±0.7 | 2.08±0.62 | <0.001 |
| HDL cholesterol, mmol/L | 1.91±0.55 | 1.42±0.35 | 0.004 |
| Remnant cholesterol, mmol/L | 0.29[0.27-0.4] | 3.26[2.07-5.71] | <0.001 |
| Triglycerides, mmol/L | 1.09[0.71-1.35] | 4.30[2.81-5.3] | <0.001 |
| Lp(a), mg/L | 93[47-223] | 120[71-400] | 0.652 |
| CRP, mg/dl | 1.5[0.6-2.0] | 2.6[1.1-3.9] | 0.152 |
| WBC, 10E9/L | 4.9±0.9 | 6.4±0.9 | <0.001 |
| - Lymphocytes | 1.6±0.38 | 2.19±0.57 | 0.001 |
| - Neutrophils | 2.73±0.77 | 3.5±0.62 | 0.003 |
| - Monocytes | 0.43±0.12 | 0.56±0.11 | 0.004 |

*Values are n, mean ± SD or median [IQR] for non-normally distributed data. FD indicates familial dysbetalipoproteinemia, SBP; systolic blood pressure, DBP; diastolic blood pressure, WBC; white blood cell count*

*Enhanced arterial wall inflammation in FD patients*

Baseline characteristics of the additional control cohort of the PET/CT study are listed in supplemental table 3 and were comparable to the cohort used for the monocyte studies.

FD patients showed a 1.2 fold higher uptake of $^{18}$F-FDG in the arterial wall of both the aorta and carotid arteries ($TBR_{max}$ aorta: FD patients 2.83±0.42 versus control 2.33±0.22, p<0.001; $TBR_{max}$ carotid: FD patients 2.02±0.35 versus control 1.63±0.27, p=0.002 (all analyses were adjusted for systolic blood pressure and BMI) (figure 1A,C). $^{18}$F-FDG uptake in the most diseased segment (MDS) revealed a similar pattern ($TBR_{MDS}$ aorta: FD patients 2.93±0.45 versus control 2,41±0.25, p<0.001. $TBR_{MDS}$ carotid: FD patients 2.11±0.37 versus control 1.73±0.29, p=0.005) (figure 1B,D).

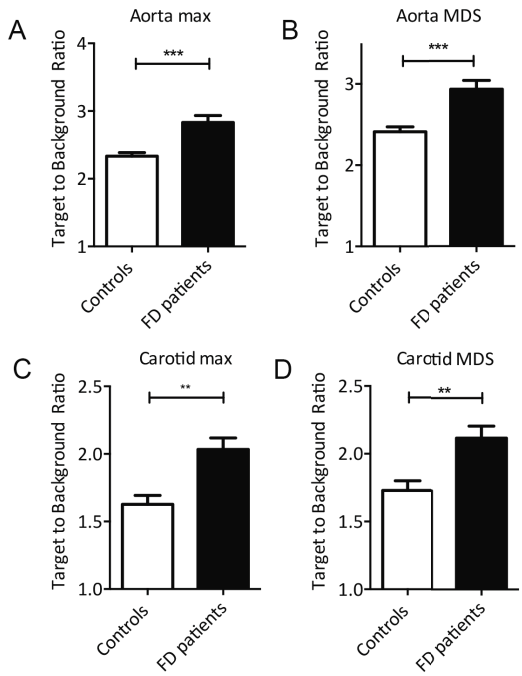


**Figure 1: Increased arterial wall inflammation in patients with elevated levels of remnant cholesterol**
Assessment of $^{18}$F-FDG uptake, represented as Target-to-Background ratio (TBR), revealed increased uptake in the aorta and carotid arteries (**A,C**) of FD patients compared to controls, with similar differences in the most disease segment (MDS) (**B,D**). *p<0.05, **p<0.01, ***p<0.001
*FD indicates familial dysbetalipoproteinemia; MDS: most disease segment; TBR: target to background ratio*

*Increased integrin expression on monocytes in FD patients*

Since postprandial lipids were previously found to induce skewing of monocytes towards a pro-inflammatory phenotype [11], we also assessed monocyte phenotype in FD patients. Using flow cytometry, we found that distribution of the pro-inflammatory classical monocyte (Mon1: $CD14^{++}CD16^{-}$), intermediate monocyte (Mon2:

$CD14^{++}CD16^{+}$) and non-classical monocyte subset (Mon3: $CD14^{+}CD16^{+}$) was comparable between FD patients and controls (figure 2A,B). However, in FD patients, expression of integrins CD11b and CD18 – involved in adhesion of monocytes to the vessel wall - was significantly increased in the classical and intermediate monocyte subset (figure 2C,D), where elevated CD11c expression levels was observed in the intermediate monocyte subset (figure 2E).

*Intracellular lipid accumulation*

As it waspreviously suggested that increased integrin expression is the result of excessive intracellular lipid accumulation [19], we assessed the lipid content of circulating monocytes in FD patients using Nile Red lipid staining and high resolution confocal laser scanning microscopy. The percentage of monocytes containing lipids was significantly increased in FD patients (92% (86-95) versus 76%(66-81) in controls, p=0.001) (figure 2F,G), with a concomitant increase in the number of lipid droplets (shown in green) per positive monocyte (FD patients 7.6(6.35-10.5), controls 6(4.9-7.0) lipid droplets per monocyte, p=0.016) (figure 2H). To validate these *in vivo* findings, we incubated human monocytes *in vitro* with various concentrations of remnant cholesterol (supplemental figure S1A). Incubation of monocytes with remnant cholesterol resulted in a dose-dependent increase in the percentage lipid positive cells (supplemental figure S1B), as well as the number of lipids per positive cell (supplemental figure S1C).

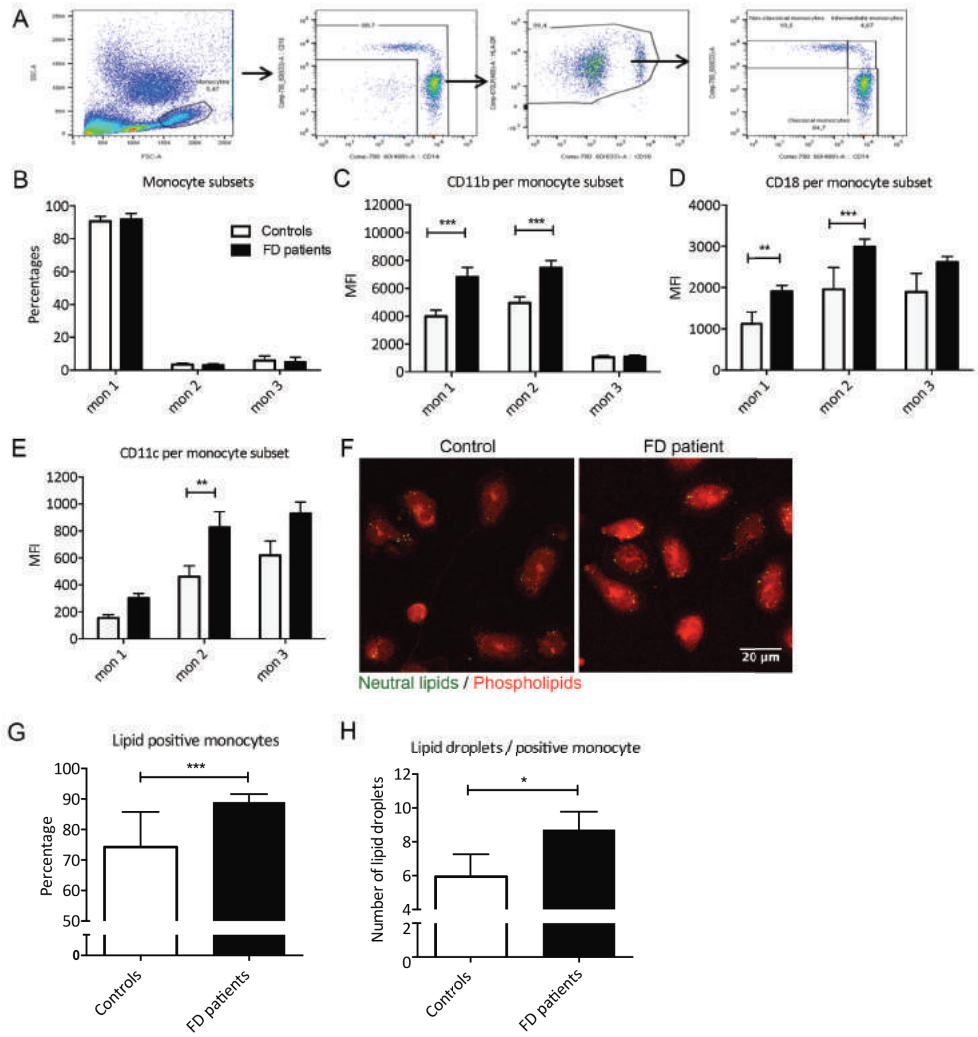


**Figure 2: Remnant cholesterol induces lipid accumulation and an adhesive phenotype in monocytes**

Flow cytometry on whole blood was performed to study monocyte subsets and surface expression markers. We distinguish classical (Mon1: $CD14^{++}CD16^{-}$), intermediate (Mon2: $CD14^{++}CD16^{+}$) and 'non-classical' (Mon3: $CD14^{+}CD16^{+}$) monocytes **(A).** FD patients and controls have the same distribution of monocyte subsets **(B)**. In FD patients the surface expression of CD11b and CD18 is significant increased on the classical and intermediate monocytes (**C,D**), whereas CD11c is significant increased on the classical monocytes (**E**).

Lipid accumulation was quantified with Nile Red staining, in which the red color represents the phospholipids (and therefore stains the cell membrane) and the neutral lipids are shown in green (**F**). Data are shown as percentage lipid positive monocytes (**G**) and number of droplets per positive monocyte (**H**). FD patients show increased numbers of lipid positive monocytes and this is concomitant with a significant increase of number of lipid droplets per monocyte. Data are represented as mean±SEM, *p<0.05, **p<0.01, ***p<0,001.

*FD indicates familial dysbetalipoproteinemia; MFI: median fluorescence intensity*

## *FD patients show enhanced bone-marrow activity and leukocytosis*

Murine data suggested that lipid accumulation in HSPCs resulted in an expansion of the hematopoietic lineage [20]. We therefore assessed leukocyte counts and bone

marrow activity in FD patients and controls. As shown in table 1, FD patients showed significantly increased white blood cell counts throughout the hematopoietic lineage compared with controls. Using $^{18}$F-FDG uptake in the bone marrow as an index of metabolic-activity, we observed an 1.2 fold higher uptake of $^{18}$F-FDG in the bone marrow of FD patients compared with controls ($SUV_{max}$ FD patients: 2.7±0.5, control: 2.2±0.3, p=0.028, figure 3A,B). Moreover, in FD patients increased FDG uptake in the bone marrow correlated significantly to leukocyte counts (r=0.410, p=0.03).
In order to examine if remnant cholesterol can also accumulate in human HSPCs, we performed *in vitro* experiments incubating GCSF harvested human HSPCs with remnant cholesterol from either FD patients or healthy controls. This revealed increased numbers of lipid droplets in human HSPCs following 24 hour incubation with remnant cholesterol isolated from FD patients compared to controls (figure 3C,D). Incubation of human HSPCs with patient-derived remnant cholesterol coincided with elevated skewing towards the myeloid lineage, as assessed by increased expression of the myeloid expression markers CD13 and CD33 by flow cytometry analysis (figure 3E).

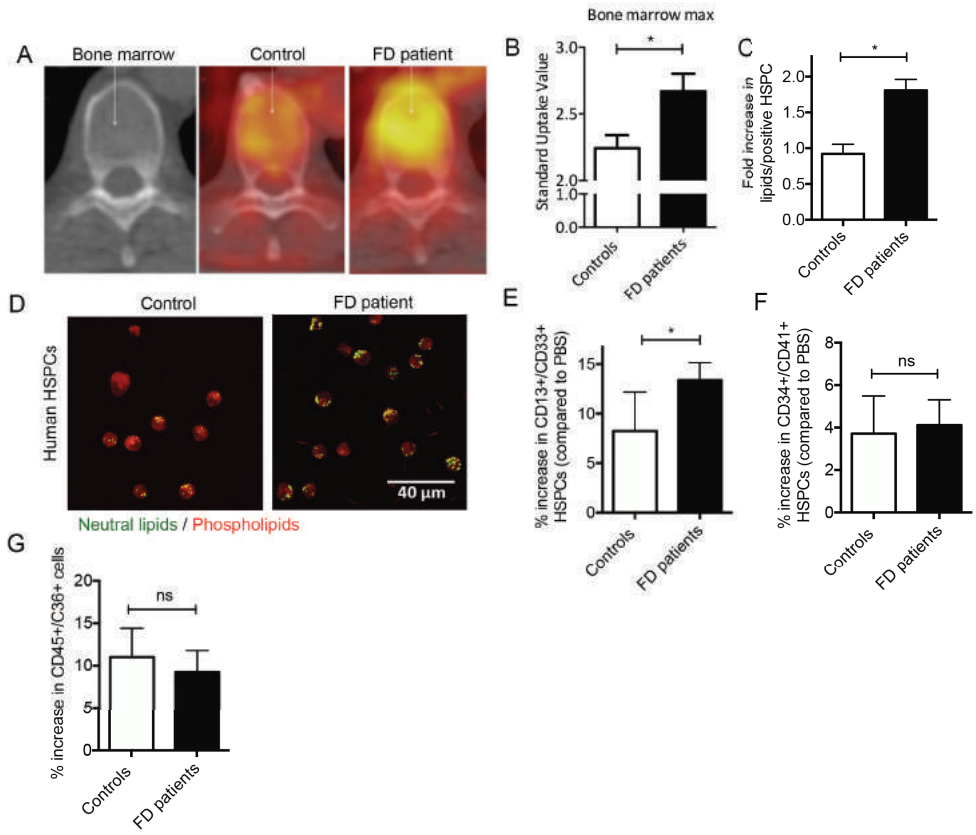

**Figure 3: Increased bone marrow activity**

$^{18}$F-FDG uptake in the bone marrow, (yellow color in **A**) was quantified as standardized uptake value (SUV). FD patients have significantly increased $SUV_{max}$ in the bone marrow compared with controls (**B**). *In vitro* experiments showed an increased lipid accumulation in HSPCs after 24 hour incubation with patient-derived remnant cholesterol compared with control-derived remnant cholesterol (**C,D**). After 7 days this co-incubation resulted in increased expression of CD13/CD33 positive HSPCs, a marker for the myeloid lineage **(E)**. *p<0.05

*FD indicates familial dysbetalipoproteinemia; HSPCs: hematopoietic stem and progenitor cells; SUV: standard uptake value*

*Validation in the Copenhagen General Population study*

Finally, we determined the correlation of remnant cholesterol and leukocyte lineage count in the Copenhagen General Population Study (CGPS). Table 2 shows a significant association with leukocyte counts ranging from $6.8*10^{-9}$/L (5.8-7.9) in the lowest quintile of remnant cholesterol level to $7.4 *10^{-9}$/L (6.4-8.9) in the highest quintile ($p=5*10^{-276}$), divided into monocytes ($p=1*10^{-155}$), lymphocytes ($p=4*10^{-238}$) and neutrophils ($p=4*10^{-126}$).

Table 2 Validation in Copenhagen Population Study in 103,953 individuals

| Remnant cholesterol, mmol/L | <0.5 | 0.5-0.99 | 1.00-1.49 | 1.5-1.99 | ≥2 | P for trend |
|---|---|---|---|---|---|---|
| **Number** | 36,446 | 46,969 | 14,818 | 4514 | 1206 | |
| **Leukocytes, $1*10^{-9}$/L** | 6.8(5.8-7.9) | 7.0(6.0-8.2) | 7.2(6.2-8.4) | 7.4(6.3-8.6) | 7.4(6.4-8.9) | $5*10^{-276}$ |
| **Monocytes, $1*10^{-9}$/L** | 0.39(0.32-0.47) | 0.40(0.33-0.49) | 0.42(0.34-0.51) | 0.42(0.34-0.52) | 0.43(0.35-0.52) | $1*10^{-155}$ |
| **Lymphocytes, $1*10^{-9}$/L** | 2.0(1.7-2.4) | 2.1(1.7-2.5) | 2.2(1.8-2.6) | 2.2(1.8-2.7) | 2.3(1.9-2.8) | $4*10^{-238}$ |
| **Neutrophils, $1*10^{-9}$/L** | 3.9(3.2-4.8) | 4.1(3.3-4.9) | 4.1(3.4-5.1) | 4.2(3.5-5.1) | 4.2(3.5-5.2) | $4*10^{-126}$ |

Values are shown as median (interquartile range). Blood leukocytes, monocytes, lymphocytes and neutrophils were adjusted for units alcohol per week, smoking status, time since last meal and for body mass index

## Discussion

Observational and Mendelian randomization studies revealed a strong, causal relationship between elevated levels of remnant cholesterol and CV-risk [3]. In the present study, we provide the first human validation of several hypotheses underlying this association. We show that i) FD patients have increased arterial wall inflammation; ii) monocytes of these patients show increased intracellular lipid accumulation with a

concomitant adhesive phenotype, as well as iii) an increased metabolic activity of the bone marrow in FD patients, with a corresponding increase in circulating leukocytes, suggesting increased proliferation; iv) *in vitro* stimulation of human HSPCs with patient-derived remnant cholesterol results in intracellular lipid accumulation. Finally, in a large population cohort, remnant levels were shown to correlate to leukocyte as well as monocyte levels.

*Lipid driven atherogenesis*

The trapping of apoB containing lipoproteins in the arterial intimal space is the key initiating factor in the formation of atherosclerotic lesions [21]. Elevated LDL-c levels were previously associated with increased arterial wall inflammation [22]. Here we show that patients with elevated levels of remnant cholesterol, but low levels of LDL-c, are also characterized by increased arterial wall inflammation. In contrast to larger TRLs such as chylomicrons, TRL remnants particles can enter the arterial wall [4]. This arterial retention will lead to enhanced plaque formation, whereas it has also been proposed to elicit an inflammatory response [723].

Besides a local inflammatory effect in the arterial wall, we also report increased expression of the integrins CD11b/CD11c/CD18 on the surface of circulating monocytes in FD patients, which coincided with a marked increase of intracellular lipid accumulation in plasma monocytes. These findings in patients with genetically determined, elevated remnant levels show a striking resemblance to those by Ballantyne and colleagues, reporting increased expression of CD11c/CD18 on monocytes in healthy volunteers after consuming a high-fat meal. These pro-adhesive changes were attributed to accumulation of lipids in circulating monocytes [11]. The relation between remnant cholesterol accumulation and phenotypical changes in monocytes is supported by our *in vitro* findings, showing a dose-dependent increase in intracellular lipid accumulation, which is in line with pro-adhesive changes reported by Gower et all [11]. Xu and colleagues showed that these 'foamy' monocytes promote the formation of atherosclerotic lesions in mice, whereas upregulation of CD11c plays a key role in the migration of these monocytes into the arterial wall [19]. As it was recently shown that white blood cells also home towards atherosclerotic lesions in patients with atherosclerotic disease [9], the remnant-cholesterol induced monocyte phenotype in our study can be expected to contribute to the increase of arterial inflammatory activity observed in patients with elevated remnant cholesterol levels.

*Hematopoiesis*

Besides activation of circulating monocytes, we also observed an increased leukocyte count with a marked monocytosis in FD patients. Experimental studies previously showed that apoE$^{-/-}$ mice also exhibited excessive proliferation and myeloid skewing of HSPCs as a result of cholesterol trapping [20]. By lowering LDL-c in humans using statins, the number of circulating HSPCs is reduced, supporting the reversibility of LDL-associated bone marrow activation in humans as well [24]. In the present study, we

show increased metabolic activity ($^{18}$F-FDG PET/CT) in the bone marrow of FD patients, correlating with plasma leukocyte number. *In vitro*, incubation of HSPCs with remnant cholesterol induced intracellular cholesterol accumulation. Together, these data suggest that remnant cholesterol may also induce increased proliferation at the bone marrow level. Interestingly, in addition to an overall increase in numbers, lipid accumulation may also induce early skewing towards the monocyte lineage, as suggested by the flow cytometry experiments. The robustness of this observation is underscored by the correlation between remnant cholesterol and hematopoietic activity in the CGPS. These findings in a large population-based cohort show that also in moderate phenotypes, fluctuations in remnant cholesterol affect the myeloid bone marrow – plasma axis, leading to elevated leukocyte numbers. Previous data from the CGPS reported causal associations between remnant cholesterol, ischemic heart diseases and levels of inflammation using a Mendelian randomization approach [5], which was attributed to the ability of remnant cholesterol to accumulate in plaque macrophages without prior oxidation. Our data substantiates this hypothesis by demonstrating the capability of remnant cholesterol to accumulate in immune cells, inducing increased leukocyte levels and a pro-atherogenic phenotype in circulating monocytes.

*Limitations*

Our study has several limitations. First, we studied a relatively modest number of patients with genetically determined levels of remnant cholesterol based on FD in a case-control design. However, this small group is very well defined with high levels of remnant cholesterol and low levels of LDL-c, no diabetes mellitus or other conditions confounding the results, thereby enabling us to specifically address the effect of elevated remnant levels. Second, the definition of remnant cholesterol remains a matter of debate. Varbo and colleagues described remnant cholesterol as total cholesterol minus HDL-c minus LDL-c [2], which is a readily applicable method. However, this simplified method also introduces the lack of particle specificity. Specific components of the remnant cholesterol particles predisposing to atherogenicity remain to be elucidated. Finally, the use of $^{18}$F-FDG PET/CT to assess bone marrow activity has not been linked to specific pathophysiological process in the bone marrow. Therefore, the use of increased FDG uptake as a marker of increased progenitor potential should be interpreted with caution. Conversely, the linear relation between increased FDG-bone marrow uptake and circulating leukocyte levels supports this assumption in the present study.

## Clinical implications

Although the FD population is an extreme model, elevated levels of (non-fasting) remnant cholesterol are present in 38% of men and 20% of woman in the general population [25], emphasizing the importance of better understanding its relationship to CVD. Our study provides important novel pathophysiological insights in the

atherogenicity of remnant cholesterol, showing a direct relationship to arterial inflammation and a link between remnant cholesterol and bone marrow activition. These findings indicate an important multi-level inflammatory component to the atherogenicity of remnant cholesterol, which may contribute to its relation with increased CV risk.

## Perspectives

Competency in medical knowledge: Inflammation has been established as an important element of atherosclerotic CVD. $^{18}$F-FDG PET/CT is a validated way to measure inflammation in atherosclerotic plaques with predictive value for cardiovascular events. Patients with elevated levels of remnant cholesterol have increased arterial wall inflammation.

Translational outlook: Inflammation is an important component of the atherogenicity of remnant cholesterol, contributing to its relationship with increased CVD risk.

## Acknowledgements

The authors thank M. Versloot for assisting in flow cytometry experiments, S. Bekkering for her input on the *in vitro* incubation experiments and M.F. Lam for performing PET/CT scans.

## References


1. M.J. C, H.N. G, P. A, F. A, J. B, a.L. C, O.S. D, E. F, P.T. K, J.a. K, P. L, L. M, B.G. N, K.K. R, Z. R, M.-R. T, L. T, a. T-H, G.F. W. Triglyceride-rich lipoproteins and high-density lipoprotein cholesterol in patients at high risk of cardiovascular disease: Evidence and guidance for management. *Eur Heart J* Oxford University Press (Great Clarendon Street, Oxford OX2 6DP, United Kingdom); 2011;**32**:1345–1361.
2. Varbo A, Benn M, Nordestgaard BG. Remnant cholesterol as a cause of ischemic heart disease: evidence, definition, measurement, atherogenicity, high risk patients, and present and future treatment. *Pharmacol Ther* Elsevier Inc.; 2014;**141**:358–367.
3. Varbo A, Benn M, Tybjaerg-Hansen A, Jorgensen AB, Frikke-Schmidt R, Nordestgaard BG. Remnant cholesterol as a causal risk factor for ischemic heart disease. *J Am Coll Cardiol* United States; 2013;**61**:427–436.
4. Nordestgaard BG, Varbo A. Triglycerides and cardiovascular disease. *Lancet (London, England)* England; 2014;**384**:626–635.
5. Varbo A, Benn M, Tybjaerg-Hansen A, Nordestgaard BG. Elevated Remnant Cholesterol Causes Both Low-Grade Inflammation and Ischemic Heart Disease, Whereas Elevated Low-Density Lipoprotein Cholesterol Causes Ischemic Heart Disease Without Inflammation. *Circulation* 2013;**128**:1298–1309.
6. Nakajima K, Nakano T, Tanaka A. The oxidative modification hypothesis of atherosclerosis: the comparison of atherogenic effects on oxidized LDL and remnant lipoproteins in plasma. *Clin Chim Acta* 2006;**367**:36–47.
7. Batt K V, Avella M, Moore EH, Jackson B, Suckling KE, Botham KM. Differential effects of low-density lipoprotein and chylomicron remnants on lipid accumulation in human macrophages. *Exp Biol Med* 2004;**229**:528–537.
8. Dutta P, Courties G, Wei Y, Leuschner F, Gorbatov R, Robbins CS, Iwamoto Y, Thompson B, Carlson AL, Heidt T, Majmudar MD, Lasitschka F, Etzrodt M, Waterman P, Waring MT, Chicoine AT, Laan AM van der, Niessen HWM, Piek JJ, Rubin BB, Butany J, Stone JR, Katus HA, Murphy SA, Morrow DA, Sabatine MS, Vinegoni C, Moskowitz MA, Pittet MJ, Libby P, et al. Myocardial infarction accelerates atherosclerosis. *Nature* England; 2012;**487**:325–329.
9. Valk FM van der, Kroon J, Potters W V, Thurlings RM, Bennink RJ, Verberne HJ, Nederveen AJ, Nieuwdorp M, Mulder WJM, Fayad ZA, Buul JD van, Stroes ESG. In vivo imaging of enhanced leukocyte accumulation in atherosclerotic lesions in humans. *J Am Coll Cardiol* United States; 2014;**64**:1019–1029.
10. Dutta P, Nahrendorf M. Regulation and consequences of monocytosis. *Immunol Rev* 2014;**262**:167–178.
11. Gower RM, Wu H, Foster GA, Devaraj S, Jialal I, Ballantyne CM, Knowlton AA, Simon SI. CD11c/CD18 Expression Is Upregulated on Blood Monocytes During Hypertriglyceridemia and Enhances Adhesion to Vascular Cell Adhesion Molecule-1. *Arterioscler Thromb Vasc Biol* 2011;**31**:160–166.
12. Valk FM van der, Kuijk C, Verweij SL, Stiekema LCA, Kaiser Y, Zeerleder S, Nahrendorf M, Voermans C, Stroes ESG. Increased haematopoietic activity in patients with atherosclerosis. *Eur Heart J* 2016;
13. Marais AD, Solomon GAE, Blom DJ. Dysbetalipoproteinaemia: a mixed hyperlipidaemia of remnant lipoproteins due to mutations in apolipoprotein E. *Crit Rev Clin Lab Sci* England; 2014;**51**:46–62.
14. Tawakol A, Migrino RQ, Bashian GG, Bedri S, Vermylen D, Cury RC, Yates D, LaMuraglia GM, Furie K, Houser S, Gewirtz H, Muller JE, Brady TJ, Fischman AJ. In Vivo 18F-Fluorodeoxyglucose Positron Emission Tomography Imaging Provides a Noninvasive Measure of Carotid Plaque Inflammation in Patients. *J Am Coll Cardiol* 2006;**48**:1818–1824.
15. Hasty a H, Linton MF, Swift LL, Fazio S. Determination of the lower threshold of apolipoprotein E resulting in remnant lipoprotein clearance. *J Lipid Res* 1999;**40**:1529–1538.
16. Rudd JHF, Myers KS, Bansilal S, Machac J, Rafique A, Farkouh M, Fuster V, Fayad Z a. (18)Fluorodeoxyglucose positron emission tomography imaging of atherosclerotic plaque inflammation is highly reproducible: implications for atherosclerosis therapy trials. *J Am Coll Cardiol* 2007;**50**:892–896.
17. Emami H, Singh P, MacNabb M, Vucic E, Lavender Z, Rudd JHF, Fayad ZA, Lehrer-Graiwer J, Korsgren M, Figueroa AL, Fredrickson J, Rubin B, Hoffmann U, Truong QA, Min JK, Baruch A, Nasir K, Nahrendorf M, Tawakol A. Splenic metabolic activity predicts risk of future cardiovascular events: demonstration of a cardiosplenic axis in humans. *JACC Cardiovasc Imaging* United States; 2015;**8**:121–130.
18. Abeles RD, McPhail MJ, Sowter D, Antoniades CG, Vergis N, Vijay GKM, Xystrakis E, Khamri W, Shawcross DL, Ma Y, Wendon J a., Vergani D. CD14, CD16 and HLA-DR reliably identifies human monocytes and their subsets in the context of pathologically reduced HLA-DR expression by CD14hi/CD16neg monocytes: Expansion of CD14hi/CD16pos and contraction of CD14lo/CD16pos monocytes in acute liver fail. *Cytom Part A* 2012;**81 A**:823–834.
19. Xu L, Dai Perrard X, Perrard JL, Yang D, Xiao X, Teng BB, Simon SI, Ballantyne CM, Wu H. Foamy monocytes form early and contribute to nascent atherosclerosis in mice with hypercholesterolemia. *Arterioscler Thromb Vasc Biol* 2015;**35**:1787–1797.
20. Tall AR, Yvan-charvet L. Cholesterol, inflammation and innate immunity. *Nat Rev Immunol* Nature Publishing Group;

2015;**15**:104–116.

21. Tabas I, Williams KJ, Borén J. Subendothelial lipoprotein retention as the initiating process in atherosclerosis: update and therapeutic implications. *Circulation* 2007;**116**:1832–1844.

22. Wijk DF van, Sjouke B, Figueroa A, Emami H, Valk FM van der, MacNabb MH, Hemphill LC, Schulte DM, Koopman MG, Lobatto ME, Verberne HJ, Fayad Z a, Kastelein JJP, Mulder WJM, Hovingh GK, Tawakol A, Stroes ESG. Nonpharmacological lipoprotein apheresis reduces arterial inflammation in familial hypercholesterolemia. *J Am Coll Cardiol* 2014;**64**:1418–1426.

23. Goldberg IJ, Eckel RH, McPherson R. Triglycerides and heart disease: Still a hypothesis? Arterioscler. Thromb. Vasc. Biol. 2011. p. 1716–1725.

24. Cimato TR, Palka BA, Lang JK, Young RF. LDL Cholesterol Modulates Human CD34+ HSPCs through Effects on Proliferation and the IL-17 G-CSF Axis. *PLoS One* 2013;**8**.

25. Kolovou GD, Mikhailidis DP, Kovar J, Lairon D, Nordestgaard BG, Ooi TC, Perez-Martinez P, Bilianou H, Anagnostopoulou K, Panotopoulos G. Assessment and clinical relevance of non-fasting and postprandial triglycerides: an expert panel statement. *Curr Vasc Pharmacol* 2011;**9**:258–270.

# Chapter 5

## Short-term regulation of hematopoiesis by lipoprotein(a) results in the production of pro-inflammatory monocytes

Johan G. Schnitzler*, Kikkie Poels*, Lotte C.A. Stiekema, Calvin Yeang, Sotirios Tsimikas, Jeffrey Kroon, Erik S.G. Stroes, Esther Lutgens, Tom T.P. Seijkens

*International Journal of Cardiology. 2020 May 7;S0167-5273(20)31189-X*

## Abstract

*Background*

Lipoproteins are important regulators of hematopoietic stem and progenitor cell (HSPC) biology, predominantly affecting myelopoiesis. Since myeloid cells, including monocytes and macrophages, promote the inflammatory response that propagates atherosclerosis, it is of interest whether the atherogenic low-density lipoprotein (LDL)-like particle lipoprotein(a) [Lp(a)] contributes to atherogenesis via stimulating myelopoiesis.

*Methods & Results*

To assess the effects of Lp(a)-priming on long-term HSPC behavior we transplanted BM of Lp(a) transgenic mice, that had been exposed to elevated levels of Lp(a), into lethally-irradiated C57Bl6 mice and hematopoietic reconstitution was analyzed. No differences in HSPC populations or circulating myeloid cells were detected ten weeks after transplantation. Likewise, *in vitro* stimulation of C57Bl6 BM cells for 24 hours with Lp(a) did not affect colony formation, total cell numbers or myeloid populations 7 days later.

To assess the effects of elevated levels of Lp(a) on myelopoiesis, C57Bl6 bone marrow (BM) cells were stimulated with Lp(a) for 24 hours, and a marked increase in granulocyte-monocyte progenitors, pro-inflammatory Ly6$^{high}$ monocytes and macrophages was observed. Seven days of continuous exposure to Lp(a) increased colony formation and enhanced the formation of pro-inflammatory monocytes and macrophages. Antibody-mediated neutralization of oxidized phospholipids abolished the Lp(a)-induced effects on myelopoiesis.

*Conclusion*

Lp(a) enhances the production of inflammatory monocytes at the bone marrow level but does not induce cell-intrinsic long-term priming of HSPCs. Given the short-term and direct nature of this effect, we postulate that Lp(a)-lowering treatment has the capacity to rapidly revert this multi-level inflammatory response.

**Keywords** Lipoprotein (a) [Lp(a)], atherosclerosis, inflammation, hematopoiesis, monocytes

## Introduction

Atherosclerosis, a major cause of cardiovascular disease (CVD), is a chronic inflammatory disease of the arterial wall. Myeloid cells, particularly monocytes and macrophages, have a critical role in the local and systemic inflammatory process that driving atherosclerosis [1]. Epidemiological and experimental studies have demonstrated that circulating myeloid cell numbers are associated with an increased cardiovascular risk [2]. Monocytes are derived from hematopoietic stem and progenitor cells (HSPC), which are located in the bone marrow (BM) [2]. During atherogenesis, hematopoiesis, the process that results in the formation of mature immune cells, is skewed towards the myeloid lineages [2, 3], thereby increasing circulating inflammatory monocyte number and aggravating atherosclerotic lesion formation [2, 3]. Pioneering studies in the last decade have demonstrated that lipoproteins including low-density lipoprotein cholesterol LDL-C and high-density lipoprotein cholesterol (HDL-C) are important regulators of HSPC biology during atherogenesis [4]. Hypercholesterolemia induces cell intrinsic priming of HSPCs, which enhances stem cell proliferation and the production of pro-inflammatory monocytes, whereas HDL-C promotes HSPC quiescence [2-4].

The LDL-like particle lipoprotein(a) [Lp(a)] is an independent risk factor for CVD, and several mechanisms by which Lp(a) mediates CVD are proposed, including pro-inflammatory and pro-thrombotic effects [5-6]. Most notably, Lp(a) has strong pro-inflammatory properties, predominantly provoked by the pro-inflammatory oxidized phospholipids (OxPL) bound to Lp(a) [5]. Lp(a) not only exerts a local inflammatory response in atherosclerotic plaques, but also has the potential to activate monocytes in the circulation, leading to enhanced monocyte migration into atherosclerotic lesions [7, 8]. We hypothesize that Lp(a) also influences myelopoiesis, leading to an enhanced production of pro-atherogenic monocytes, thereby fueling the detrimental innate immune response in atherosclerosis.

## Materials & Methods

A comprehensive material & methods section can be found in the supplemental material. In brief, one day prior to the bone marrow transplantation (BMT), recipient mice were lethally irradiated. The next day, $1x10^6$ BM cells obtained from transgenic mice expressing both apo(a) and human apoB-100 (apoB), which assemble to form Lp(a), or from C57Bl6 donors were intravenously injected in the recipients [9]. Hematopoietic reconstitution was analysed in BM and peripheral blood 10 weeks after the BMT. All animal experiments were approved by the local Animal Experimentation Ethics Committee. Results are shown as mean standard error of the mean. A p-value $< 0.05$ was considered statistically significant.

## Results

*Lp(a) does not induce long-term priming of HSPCs*

To investigate if Lp(a) induces cell intrinsic priming of HSPC *in vivo*, we transplanted BM cells of Lp(a) transgenic mice with elevated plasma Lp(a) levels or control BM cells obtained from C57Bl6 mice with undetectable levels of plasma Lp(a) in lethally irradiated C57Bl6 recipients. Mice do not contain the LPA gene and in these transgenic mice, Lp(a) is produced by the liver, resulting in high circulating levels of Lp(a) and high levels of OxPLs (9). The donor BM was exposed for 8 weeks to Lp(a) before harvest, our BMT approach is therefore an appropriate model to study priming of BM by Lp(a). Ten weeks post-BMT, HSPC population counts in the BM and circulating myeloid population counts did not differ between the two groups, reflecting absence of long-term Lp(a)-induced HSPC priming (Fig. 1A, B).
To confirm that Lp(a) has indeed no intrinsic priming effects on HSPCs, or that the potentially weaker priming effect of Lp(a) was abolished by the transplantation itself, *in vitro* stimulation assays with wild type BM cells and Lp(a) were performed. C57Bl6 BM was exposed to Lp(a) (1 mg/ml) for 24 hours and this Lp(a)-primed BM was analyzed in colony forming unit (CFU) assays. After 7 days no differences in colony formation (Fig. 1C) or total myeloid cell numbers (Fig. 1D) were observed between control and Lp(a)-primed BM. Additionally, flow cytometry revealed no differences in granulocytes, monocyte subsets or macrophages (Fig. 1E), indicating absence of Lp(a)-induced HSPC priming.

Figure 1.

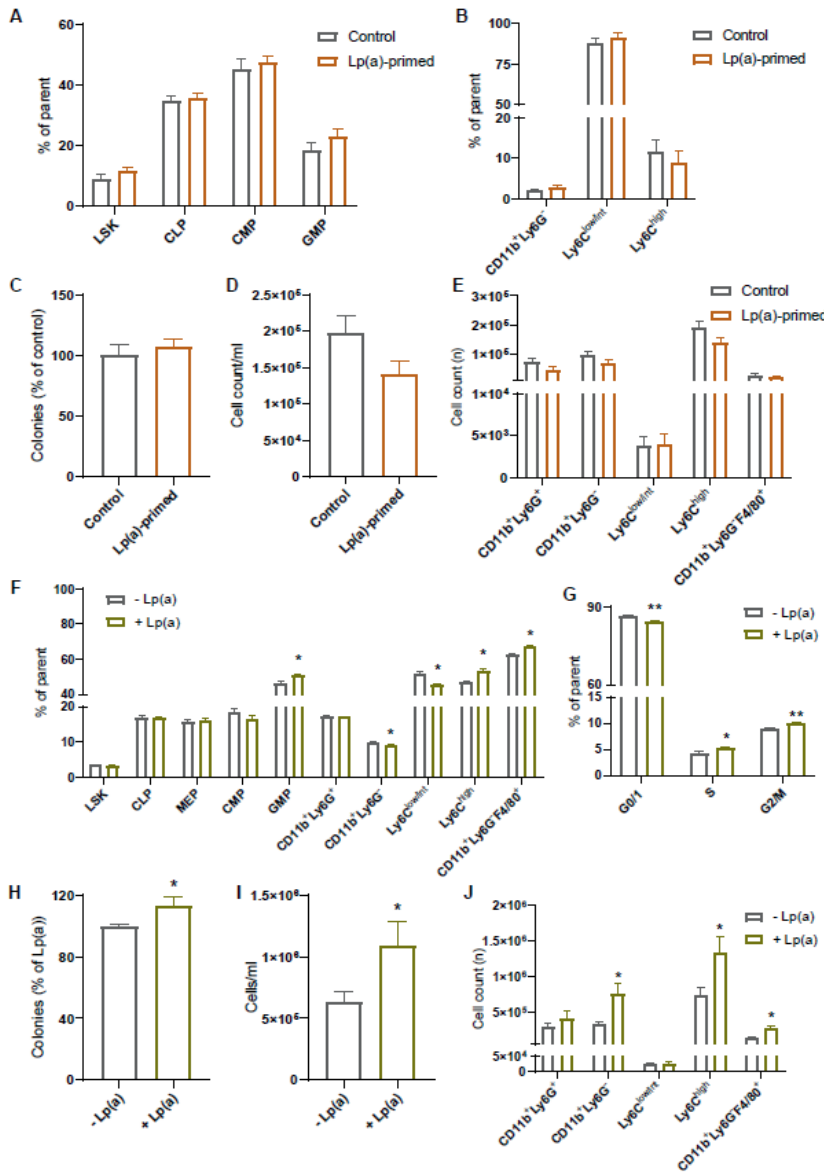


**Figure 1. Lp(a) promotes myelopoiesis but does not induce long-term priming of HSPCs. (A)** Lp(a) exposure did not affect the reconstitution of HSPC populations within the BM of C57Bl6 mice (n = 12), *LSK*: *Lin⁻Sca-1⁺cKit⁺*; *CLP: Lin⁻cKit⁺Sca-1⁺CD135⁺CD127⁺ Lin⁻cKit⁺Sca-1⁺CD135⁺CD127⁺*; *CMP: Lin⁻cKit⁺CD16/32⁺CD34⁺ Lin⁻cKit⁺CD16/32⁺CD34⁺*; *GMP: Lin⁻cKit⁺CD16/32^intCD34^int*. (**B**) Lp(a) exposure did not affect the reconstitution of circulating monocyte (*CD11b⁺Ly6G⁻*) populations at week 10 post-BMT (n = 12). (**C**) Colony forming unit (CFU) assays demonstrated that short-term (24 hours) exposure of BM cells to Lp(a) did not affect colony formation after 7 days. (**D**) No differences in total cell counts and (**E**) myeloid populations were observed (n = 10), *monocytes: CD11b⁺Ly6G⁺*, *granulocytes: CD11b⁺Ly6G⁺*, *macrophages CD11b⁺Ly6G⁻F4/80⁺*. (**F**) After 24 hours of stimulation with Lp(a), increased granulocyte-monocyte progenitor, Ly6C^high monocytes and macrophages was observed. The relative number of total monocytes decreased and the number of Ly6C^low/int monocytes decreased due to the shift towards Ly6C^high monocytes (n = 10). (**G**) Continuous exposure to Lp(a) for 7 days induced proliferation of BM cells, as

shown by PI flow cytometry, which resulted in increased colony formation (**H**) and total cell numbers in CFU assays (**I**) (n = 8). (**J**) Continuous exposure to Lp(a) for 7 days increased pro-inflammatory monocyte and macrophage numbers (n = 8). *Data represented as mean ± SEM. * p < 0.05, ** p < 0.01, *** p < 0.001.*

*Lp(a) directly promotes myelopoiesis and enhances the production of inflammatory monocytes*

Next, BM cells were analyzed directly after 24 hours of stimulation with Lp(a) *in vitro*; an 8.6% increase in granulocyte-monocyte progenitors was observed, without affecting other progenitor populations, including common lymphoid progenitors (Fig. 1F). Analysis of mature myeloid populations showed a 14.4% increase in pro-inflammatory Ly6$^{high}$ monocytes and 6.7% increase in macrophages (Fig. 1F). Total monocytes slightly decreased, possibly due to increased differentiation into macrophages (Fig. 1F). Continuous exposure to Lp(a) for 7 days induced a proliferative BM profile, characterized by a 20.5% increase in BM cells in the S-phase and 10.6% increase in BM cells in the G2/M-phase of the cell cycle (Fig. 1G). Accordingly, colony formation of Lp(a)-stimulated BM was increased by 13.3% (Fig. 1H). The production of mature myeloid cells (Fig. 1I), especially inflammatory Ly6C$^{high}$ monocytes and macrophages (Fig. 1J) increased upon Lp(a) stimulation.

To investigate if the hematopoietic effects of Lp(a) depended on its oxidized phospholipid content, the monoclonal antibody E06, which binds the phosphocholine moiety of oxidized phospholipid and blocks its inflammatory effects, was included in the BM culture assays. Antibody-mediated blockage of oxidized phospholipids on Lp(a) prevented the Lp(a)-induced increase in colony formation (Fig. 2A), total cell numbers (Fig. 2B), as well as the production of mature myeloid cells, in particular granulocytes and Ly6C$^{high}$ monocytes (Fig. 2C). Together these data demonstrate that Lp(a) enhances the formation of inflammatory myeloid cells *in vitro*, which is mediated by its oxidized phospholipid content.

## Figure 2

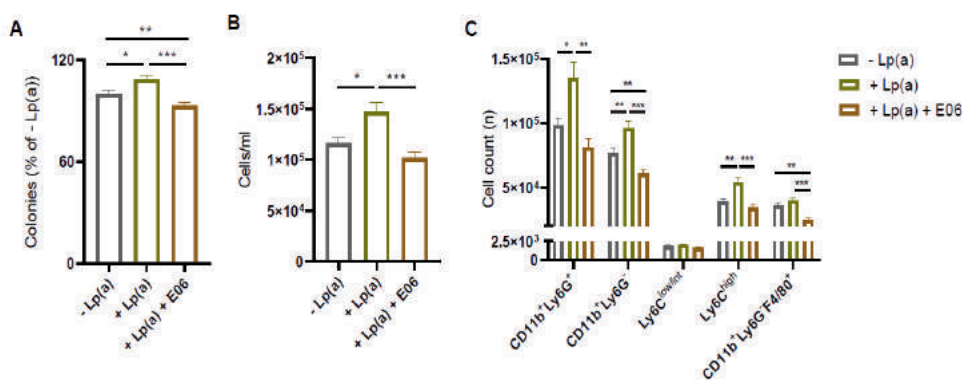


**Figure 2. Antibody-mediated blockage of oxidized phospholipids abolishes the Lp(a)-induced effects on myelopoiesis.** CFU assays demonstrated that E06 prevented the LP(a)-induced increase in colony formation (**A**), total cell counts (**B**), and mature myeloid cells, in particular CD11b$^{+}$Ly6G$^{+}$, CD11b$^{+}$Ly6G$^{-}$ and CD11b$^{+}$Ly6G$^{-}$Ly$C^{high}$ cells (**C**) (n = 10). *Data represented as mean ± SEM. * p < 0.05, ** p < 0.01, *** p < 0.001.*

*Discussion*

A few conclusions can be drawn from these studies. First, Lp(a)-stimulated HSPC produce pro-inflammatory monocytes, which indicates that direct interaction of Lp(a) with monocytes in the circulation leads to monocyte activation, but also that Lp(a) affects their production on the marrow level. Second, although LDL-C exerts *long-term* priming effects of HSPC that persist in a normocholesterolemic environment, Lp(a) has a *short-term* effect on HSPC [3]. We hypothesize that this is attributed to the relative low concentrations of Lp(a) compared to LDL concentrations used in other experiments and therefore the lack of Lp(a)-induced priming. This relies on the fact that the inflammatory effects of Lp(a) are mainly attributed to the signaling capacity of its oxidized phospholipid content and not due to NLRP3 inflammasome activation resulting from intracellular cholesterol accumulation, which is the mechanism of LDL-C-induced intrinsic priming of myeloid cells and their progenitors [10, 11]. Previous data suggest that besides the LDL-entity of Lp(a), the apo(a) tail of Lp(a) does not induce cellular activation without presence of OxPLs [7]. Furthermore, Lp(a) was able to activate HSPCs directly (i.e. 24h and 7 days), however, once the Lp(a) stimulus was absent (i.e. 24h stimulation and 6 days without stimulus or BMT experiment) HSPC activity exerted normal function further indicating that Lp(a) does not induce NLRP3 activation but its mode of action is via OxPLs. These oxidized phospholipids represent danger-associated molecular patterns, recognized by a variety of pattern recognition receptors, including Toll-like receptor 4 (TLR4) and scavenger receptor-B1 (SR-B1), which are expressed on HSPC and regulate their biology [12]. For example, TLR4 engagement on HSPCs skews hematopoiesis towards the myeloid lineage, whereas SR-B1 activation limits HSPC proliferation and the production of inflammatory cells, indicating that activation of pattern recognition receptors on HSPCs has diverse effects that may be ligand-dependent [13, 14]. Although our data demonstrate that the oxidized phospholipid content of Lp(a) promotes myelopoiesis, the pattern recognition receptor for these oxidized phospholipids on HSPCs has yet to be discovered.

Our data imply that depleting the HSPC microenvironment of Lp(a) will lead to a rapid reversal of the activated monocyte profile that is attributed to elevated Lp(a) levels, while the LDL-induced hematopoietic effects will persist for a much longer period following LDL-C reduction. This concept concurs with the attenuation of transendothelial migration of monocytes by an approximately 70% Lp(a) reduction following 12 weeks of apo(a) antisense therapy in Lp(a) patients, whereas an approximately 44% LDL-C reduction following 14 weeks of statin therapy is still characterized by an unchanged, hyperinflammatory monocyte phenotype in patients with genetic LDL-C elevation [15, 16].

Study limitations: this proof of concept study in mice identifies direct effects of Lp(a) on BM proliferation, myelopoiesis and the formation of inflammatory monocytes, and additional studies are needed to elucidate the underlying mechanisms of these Lp(a)-

induced hematopoietic effects. Clinical studies are required to determine if the activated monocyte profile in patients with elevated Lp(a) levels results from aberrations in HSPC biology.
In conclusion, this study proposes that in addition to direct activation of monocytes in the circulation, Lp(a) also enhances the production of activated monocytes on bone marrow level. Given the short-term and direct nature of this effect on hematopoiesis, we postulate that Lp(a)-lowering treatment has the capacity to rapidly revert this multi-level inflammatory response.

Acknowledgement of grant support
This project received support from the European Union's Horizon 2020 research and innovation program under grant agreement No 667837 (REPROGRAM). T.T.P.S. received a MD/PhD grant from Amsterdam Cardiovascular Sciences, a Young@heart grant from The Netherlands Heart Institute and a Dr. Dekker Physician-in-specialty-training grant from the Dutch Heart Foundation. JK received a VENI grant from ZonMW (91619098).

Conflicts of interest
E.S.G.S. reports that his institution has received lecturing fees and advisory board fees from Amgen Inc., Regeneron, Sanofi, Akcea, Novartis and Esperion. ST is a co-inventor and receives royalties from patents owned by UCSD on oxidation-specific antibodies and of biomarkers related to oxidized lipoproteins, has a dual appointment at UCSD and Ionis Pharmaceuticals, is a co-founder of Oxitope, Inc and Kleanthi LLC, and is a consultant to Boston Heart Diagnostics. The other authors have nothing to disclose.

## References


1. Lutgens E, Atzler D, Doring Y, Duchene J, Steffens S, Weber C. Immunotherapy for cardiovascular disease. European heart journal. 2019;40(48):3937-46.
2. Morgan PK, Fang L, Lancaster GI, Murphy AJ. Hematopoiesis is regulated by cholesterol efflux pathways and lipid rafts: connections with cardiovascular diseases. Journal of lipid research. 2019.
3. Seijkens T, Hoeksema MA, Beckers L, Smeets E, Meiler S, Levels J, Tjwa M, de Winther MP, Lutgens E. Hypercholesterolemia-induced priming of hematopoietic stem and progenitor cells aggravates atherosclerosis. FASEB journal : official publication of the Federation of American Societies for Experimental Biology. 2014;28(5):2202-13.
4. Oguro H. The Roles of Cholesterol and Its Metabolites in Normal and Malignant Hematopoiesis. Frontiers in endocrinology. 2019;10:204.
5. Tsimikas S. A Test in Context: Lipoprotein(a): Diagnosis, Prognosis, Controversies, and Emerging Therapies. Journal of the American College of Cardiology. 2017;69(6):692-711.
6. Arsenault BJ, Pelletier W, Kaiser Y, Perrot N, Couture C, Khaw KT, Wareham NJ, Bosse Y, Pibarot P, Stroes ESG, Mathieu P, Theriault S, Boekholdt SM. Association of Long-term Exposure to Elevated Lipoprotein(a) Levels With Parental Life Span, Chronic Disease-Free Survival, and Mortality Risk: A Mendelian Randomization Analysis. JAMA network open. 2020;3(2):e200129.
7. van der Valk FM, Bekkering S, Kroon J, Yeang C, Van den Bossche J, van Buul JD, Ravandi A, Nederveen AJ, Verberne HJ, Scipione C, Nieuwdorp M, Joosten LA, Netea MG, Koschinsky ML, Witztum JL, Tsimikas S, Riksen NP, Stroes ES. Oxidized Phospholipids on Lipoprotein(a) Elicit Arterial Wall Inflammation and an Inflammatory Monocyte Response in Humans. Circulation. 2016;134(8):611-24.
8. van Dijk RA, Kolodgie F, Ravandi A, Leibundgut G, Hu PP, Prasad A, Mahmud E, Dennis E, Curtiss LK, Witztum JL, Wasserman BA, Otsuka F, Virmani R, Tsimikas S. Differential expression of oxidation-specific epitopes and apolipoprotein(a) in progressing and ruptured human coronary and carotid atherosclerotic lesions. Journal of lipid research. 2012;53(12):2773-90.
9. Schneider M, Witztum JL, Young SG, Ludwig EH, Miller ER, Tsimikas S, Curtiss LK, Marcovina SM, Taylor JM, Lawn RM, Innerarity TL, Pitas RE. High-level lipoprotein [a] expression in transgenic mice: evidence for oxidized phospholipids in lipoprotein [a] but not in low density lipoproteins. Journal of lipid research. 2005;46(4):769-78.
10. Que X, Hung M-Y, Yeang C, Gonen A, Prohaska TA, Sun X, Diehl C, Määttä A, Gaddis DE, Bowden K, Pattison J, MacDonald JG, Ylä-Herttuala S, Mellon PL, Hedrick CC, Ley K, Miller YI, Glass CK, Peterson KL, Binder CJ, Tsimikas S, Witztum JL. Oxidized phospholipids are proinflammatory and proatherogenic in hypercholesterolaemic mice. Nature. 2018;558(7709):301-6.
11. Christ A, Gunther P, Lauterbach MAR, Duewell P, Biswas D, Pelka K, Scholz CJ, Oosting M, Haendler K, Bassler K, Klee K, Schulte-Schrepping J, Ulas T, Moorlag S, Kumar V, Park MH, Joosten LAB, Groh LA, Riksen NP, Espevik T, Schlitzer A, Li Y, Fitzgerald ML, Netea MG, Schultze JL, Latz E. Western Diet Triggers NLRP3-Dependent Innate Immune Reprogramming. Cell. 2018;172(1-2):162-75.e14.
12. Miller YI, Choi SH, Wiesner P, Fang L, Harkewicz R, Hartvigsen K, Boullier A, Gonen A, Diehl CJ, Que X, Montano E, Shaw PX, Tsimikas S, Binder CJ, Witztum JL. Oxidation-specific epitopes are danger-associated molecular patterns recognized by pattern recognition receptors of innate immunity. Circulation research. 2011;108(2):235-48.
13. Esplin BL, Shimazu T, Welner RS, Garrett KP, Nie L, Zhang Q, Humphrey MB, Yang Q, Borghesi LA, Kincade PW. Chronic exposure to a TLR ligand injures hematopoietic stem cells. Journal of immunology (Baltimore, Md : 1950). 2011;186(9):5367-75.
14. Feng Y, Schouteden S, Geenens R, Van Duppen V, Herijgers P, Holvoet P, Van Veldhoven PP, Verfaillie CM. Hematopoietic stem/progenitor cell proliferation and differentiation is differentially regulated by high-density and low-density lipoproteins in mice. PloS one. 2012;7(11):e47286.
15. Viney NJ, van Capelleveen JC, Geary RS, Xia S, Tami JA, Yu RZ, Marcovina SM, Hughes SG, Graham MJ, Crooke RM, Crooke ST, Witztum JL, Stroes ES, Tsimikas S. Antisense oligonucleotides targeting apolipoprotein(a) in people with raised lipoprotein(a): two randomised, double-blind, placebo-controlled, dose-ranging trials. Lancet (London, England). 2016;388(10057):2239-53.
16. Bekkering S, Stiekema LCA, Bernelot Moens S, Verweij SL, Novakovic B, Prange K, Versloot M, Roeters van Lennep JE, Stunnenberg H, de Winther M, Stroes ESG, Joosten LAB, Netea MG, Riksen NP. Treatment with Statins Does Not Revert Trained Immunity in Patients with Familial Hypercholesterolemia. Cell metabolism. 2019;30(1):1-2.

## Supplemental material

*Bone marrow transplantation*

All animal experiments were approved by the local Animal Experimentation Ethics Committee. C57Bl6 mice were bred in the local animal facility. All mice were aged-matched males. C57Bl6 recipient mice were housed in filter-top cages and received water containing antibiotics (polymyxine B sulfate, 60,000 U/L, and neomycin, 100 mg/L) for 5 weeks, starting 1 week before the bone marrow transplantation (BMT). One day prior to the BMT, the mice were lethally irradiated (9.5 Gy, 0.5 Gy/min; Philips MU15F/225 kV; Philips). The next day, $1x10^6$ BM cells obtained from transgenic mice expressing both apo(a) and human apoB-100 (apoB) (Schneider, JLR, 2005), which assemble to form Lp(a) or from C57Bl6 donors in the recipients. Hematopoietic reconstitution was analysed in BM and peripheral blood 10 weeks after the BMT.

*Flow cytometry*

Bone marrow (BM) was harvested in cold phosphate buffered saline (PBS) and a BM cell suspension was prepared and filtered through a 70-µm nylon mesh (BD Falcon, BD Biosciences, Breda, The Netherlands). Lineage depletion by magnetic bead isolation was performed according to the manufacturer's instructions (Lineage Cell Depletion Kit, Miltenyi Biotec, Teterow, Germany). Cell suspensions were treated with red blood cell lysis buffer that contained 8.4 g NH4Cl and 0.84 g NaHCO3 per liter distilled water. Staining was performed with anti-mouse antibodies against the following antigens: lineage cocktail (Miltenyi Biotec, Teterow, Germany); Ly6G (clone 1A8), CD11b (clone M1/70), CD127 (clone HIL-7R-M21) and Gr-1 (clone RB6-8C5) (BD Pharmingen, Breda, The Netherlands); CD117 (clone 2B8), CD34 (clone RAM34, F4/80 (clone BM8) and CD32/16 (clone 93) (Ebioscience, Vienna, Austria); Sca-1 (clone D7) and CD135 (A2F10) (aBiolegend, San Diego, CA, USA); and Ly6C (clone 1G7.G10) (Miltenyi Biotech, Teterow, Germany). Nonspecific binding was prevented by pre-incubation of the cells with an Fc receptor-blocking antibody (Ebioscience, Vienna, Austria). For cell-cycle analysis, bone marrow cells were fixed in 70% ethanol for 24 hours and treated with propidium iodide/RNase buffer according to the manufacture's protocol (BD Biosciences, San Jose, CA, USA). Staining was analysed by flow cytometry (FACS Canto II; BD Biosciences, San Jose, CA, USA) and FlowJo software version 7.6.5 (Treestar, Ashland, OR, USA).

*Lp(a) isolation*

Lp(a) was isolated from plasma of healthy volunteers. Blood was collected in EDTA (ethylenediaminetetraacetic acid (EDTA)-containing 10 mL Vacutainer tubes. Lp(a) was obtained after KBr (VWR, Radnor, Pennsylvania, USA)-density gradient ultracentrifugation. Here plasma was adjusted to d=1.25 g/mL with solid KBr solution and a discontinuous gradient was formed by carefully layering 2 mL of d=1.225 KBr solution, followed by 4 mL of d=1.100 KBr solution and a 3 mL of d=1.006 KBr solution and centrifuged at vacuum for 19 hours at 29.000 rpm at 10°C in a SW 41 Ti rotor without brake (Beckman Coulter Inc., CA). Next, Lp(a) was isolated and was filter sterilized (0.2 μm pore size; Sartorius, Göttingen, Germany) and concentrated using Amicon centrifugal filter units filter (10.000 MWCO; Millipore). Lp(a) concentration was measured using commercially available immunoturbidimetric enzymatic assays (Diasys, Holzheim, Germany) on a Selectra system (Sopachem, Ochten, The Netherlands).

*Colony-forming unit (CFU) assays*

BM was isolated from C57Bl6 mice and a single-cell suspension was prepared as described above. BM cells ($1\times10^4$) were cultured in 2 ml semisolid methylcellulose medium supplemented with growth factors (MethoCult; Stem Cell Technologies, Grenoble, France) at 37°C in 98% humidity and 5% CO2 for 7 days. Total colonies were scored after 7 days using an inverted microscope in a blinded protocol. In selected experiments, BM cells were co-cultured with Lp(a) (1 mg/ml) and/or E06 (100 μg/ml; Avanti Polar Lipids, Inc., Alabaster, AL, USA), as indicated in the figures.

*Statistical analysis*

Results are shown as mean standard error of the mean. A p-value $< 0.05$ was considered statistically significant. Data (mean ± SEM) were analysed by an unpaired, 2-tailed Student's t test. Grahphad Prism 5 software (GraphPad Software, La Jolla, CA, USA) was used for statistical analysis.

# Chapter 6

## Oral Vancomycin Treatment Does Not Alter Markers of Postprandial Inflammation in Lean and Obese Subjects

Guido J. Bakker, Johan G. Schnitzler, Siroon Bekkering, Nicolien C. de Clercq, Annefleur M. Koopen, Annick V. Hartstra, Emma C.E. Meessen, Torsten P. Scheithauer, Maaike Winkelmeijer, Geesje M. Dallinga-Thie, Patrice D. Cani, Elles Marleen Kemper, Maarten R. Soeters, Jeffrey Kroon, Albert K. Groen, Daniël H. van Raalte, Hilde Herrema , Max Nieuwdorp

*Physiology Reports. 2019 Aug;7(16):e14199*

Abstract

**Introduction** Intake of a high-fat meal induces a systemic inflammatory response in the postprandial which is augmented in obese subjects. However, the underlying mechanisms of this response have not been fully elucidated. We aimed to assess the effect of gut microbiota modulation on the postprandial inflammatory response in lean and obese subjects.

**Methods** Ten lean and ten obese, metabolic syndrome subjects received oral vancomycin 500 mg four times per day for seven days. Oral high-fat meal tests (50 g fat/$m^2$ body surface area) were performed before and after vancomycin intervention. Gut microbiota composition, leukocyte counts, plasma lipopolysaccharides (LPS), LPS-binding protein (LBP), IL-6 and MCP-1 concentrations and monocyte CCR2 and cytokine expression were determined before and after the high-fat meal.

**Results** Oral vancomycin treatment resulted in profound changes in gut microbiota composition and significantly decreased bacterial diversity in both groups (phylogenetic diversity pre- versus post-intervention: lean, 56.9 ± 7.8 versus 21.4 ± 6.6, $p<0.001$; obese, 53.9 ± 7.8 versus 21.0 ± 5.9, $p<0.001$). After intervention, fasting plasma LPS significantly increased (lean, median [IQR] 0.81 [0.63-1.45] EU/mL versus 2.23 [1.33-3.83] EU/mL, $p=0.017$; obese, median [IQR] 0.76 [0.45-1.03] EU/mL versus 1.44 [1.11-4.24], $p=0.014$). However, postprandial increases in leukocytes and plasma LPS were unaffected by vancomycin in both groups. Moreover, we found no changes in plasma LBP, IL-6 and MCP-1 or in monocyte CCR2 expression.

**Conclusion** Despite major vancomycin-induced disruption of the gut microbiota and increased fasting plasma LPS, the postprandial inflammatory phenotype in lean and obese subjects was unaffected in this study.

## Introduction

In the past decade, a plethora of animal and human studies have shown an important link between the composition of the gut microbiota and metabolic diseases, such as obesity and type 2 diabetes mellitus (T2D) (1-4). These diseases are characterized by a chronic state of low-grade systemic inflammation (5, 6). Translocation of metabolites derived from intestinal bacteria into the systemic circulation has been suggested to underlie the pathophysiology of this inflammatory state (7, 8). For example, mice fed a high-fat diet for 4 weeks had increased amounts of bacterial DNA in both circulating blood and mesenteric visceral adipose tissue (9). In humans, plasma concentrations of lipopolysaccharide (LPS, also referred to as endotoxin), a cell wall component of Gram-negative bacteria, have been associated with obesity (10), T2D (11) and cardiovascular disease (12). Similarly, plasma LPS-binding protein (LBP), a marker of LPS exposure, has been associated with obesity and insulin resistance (13, 14). Translocation of intestinal LPS into the blood is actively mediated by enterocytes through the apical scavenger receptor class B type 1 (SR-BI), which binds LPS and mediates incorporation of LPS in chylomicrons (15, 16). Thus, endotoxemia may especially occur after a meal enriched with fat.

Indeed, several human studies have shown, after administration of a high-fat meal, a postprandial increase in plasma LPS (17-19), accompanied by a systemic increase in IL-6 (19-22) and TNF-**α** (23) and a shift towards a pro-inflammatory phenotype of circulating monocytes (24). This postprandial inflammatory response was found to be increased in obesity and T2D with the transient postprandial rise in LPS being significantly higher in obese (25, 26) and T2D (27) individuals compared to lean participants. Moreover, consumption of a high-fat meal increased plasma IL-6 and TNF-**α** concentrations to a greater extent in T2D compared to healthy subjects (23). Notably, in these trials endotoxin concentrations were closely related to postprandial plasma chylomicrons (CMs), further suggesting postprandial cotransport of LPS with dietary lipids.

As abundance of Gram-negative bacteria is the main driver of intestinal LPS concentration, we hypothesized that the composition of gut microbiota is an important factor in LPS translocation in the postprandial phase. In order to test this hypothesis, we treated our subjects with oral vancomycin, a broad-spectrum antibiotic that targets Gram-positive bacteria, resulting in overgrowth of Gram-negative strains and increasing luminal LPS concentrations. In this study, we aimed to assess the effect of oral vancomycin on postprandial LPS translocation and the inflammatory response in lean subjects and in obese subjects who fulfil the metabolic syndrome criteria.

## Methods

*Study design*

Lean (body mass index (BMI) between 18.5 and 25 kg/m$^2$) and obese (BMI ≥30 kg/m$^2$), metabolic syndrome (≥3/6 criteria: waist circumference >102 cm; blood pressure

≥130 mmHg systolic or ≥85 mmHg diastolic; fasting plasma glucose ≥5.6 mmol/L; high-density lipoprotein cholesterol (HDL-C) <1.03 mmol/L; fasting triglycerides ≥1.7 mmol/L; HOMA-IR >2.2) male subjects aged 18-75 years were recruited via local advertisements. Subjects were excluded if they met one of the following criteria: use of any medication; use of antibiotics or proton pump inhibitors in the past 3 months; a medical history of type 1 or 2 diabetes, stroke, myocardial infarction, pacemaker, or cholecystectomy; smoking; use of >5 units of alcohol daily; recreational drug use; use of pre-, pro- or synbiotics. All participants received oral vancomycin 500 mg four times a day for seven days. High-fat meal tests were scheduled before and after vancomycin intervention. To ensure a complete wash-out of the study medication, post-intervention visits were scheduled two days after cessation of vancomycin. Subjects were asked to refrain from strenuous exercise during the study and to keep 3-day online food diaries in the days preceding the study visits. All participants gave written informed consent for participation in the study. The study was approved by the Institutional Review Board of the Amsterdam UMC, location AMC in Amsterdam, The Netherlands, and conducted in accordance with the Declaration of Helsinki (version 2013).

*High-fat meal tests*

Subjects visited the hospital after an overnight fast of at least 10 h. After measurement of height, weight, waist and hip circumference, and blood pressure, a cannula was inserted into the antecubital vein for blood sampling. Blood samples were collected before (t = 0 h) and after (t = 2 h and t = 4 h) ingestion of the liquid high-fat meal (fresh cream, 35% fat, Albert Heijn, Zaandam, The Netherlands, 93 E% fat, 4 E% carbohydrate, 3 E% protein) containing 335 kcal, 35 g fat of which 23 g saturated and 12 g mono-unsaturated, 3.0 g carbohydrate of which 3.0 g sugars, and 2.5 g protein per 100 mL in a dosage of 50 g of fat per square meter body surface area (BSA) (28). BSA was calculated using the following formula: BSA ($m^2$) = $\sqrt{}$ ((height in cm * weight in kg) / 3600) (29). During the high-fat meal tests, subjects were not allowed to eat or drink, except water, and refrained from physical activity.

*Biochemical analyses*

Blood was collected in Vacutainer® tubes containing heparin, EDTA, or spray-coated silica and a polymer gel for serum separation (Beckton Dickinson, Franklin Lakes, New Jersey, U.S.A.), centrifuged at 1550 g (15 min, 4°C) and plasma and serum were stored at -80°C until further analyses. Plasma glucose was determined with a commercial assay on the Cobas 8000 c702 analyzer (Roche, Basel, Switzerland). Plasma insulin was determined using the ADVIA Centaur XP Immunoassay System (Siemens, Erlangen, Germany), according to the manufacturer's protocol. Plasma total cholesterol, HDL-C, and triglycerides were determined using commercial assays (Diasys and WAKO) on the Selectra® (Sopachem, Ochten, The Netherlands) according to the manufacturer's instructions. Low-density lipoprotein cholesterol

(LDL-c) levels were calculated using the Friedewald formula. Apolipoprotein (apo) B and apo A1 were analyzed using a commercial nephelometric assay on the Selectra® autoanalyzer.
Plasma for LPS measurements was transferred and stored using endotoxin-free materials only. LPS concentrations (*i.e.* endotoxin activity in EU/mL) were determined using the Endosafe-MCS (Charles River Laboratories, Lyon, France) based on the Limulus Amebocyte Lysate (LAL) kinetic chromogenic methodology measuring color intensity directly related to the endotoxin activity present in a sample as previously described (30). Briefly, plasma was first diluted 1/10 with endotoxin-free buffer (Charles River Laboratories, Lyon, France) and endotoxin-free LAL reagent water (Charles River Laboratories, Lyon, France) to minimize interferences in the reaction and then heated for 15 min at 70°C. Each sample was further diluted with LAL water and treated in duplicate. The dilution was chosen in order to fully recover the LPS spikes (>70%). Two spikes for each sample were included in the determination. All samples were validated for the recovery and the coefficient variation. The lower limit of detection was 0.005 EU/mL. Plasma concentrations of IL-6, MCP-1, and LBP were determined using commercially available ELISA kits (IL-6 Human ELISA Kit, High Sensitivity, Thermo Fisher Scientific, Waltham, Massachusetts, U.S.A.; Human CCL2 (MCP-1) ELISA Ready-SET-Go!®, eBioscience, San Diego, California, U.S.A; LBP, Human, ELISA kit, Hycult Biotech Inc., Plymouth Meeting, Pennsylvania, U.S.A., respectively) according to the manufacturer's instruction. Blood cell counts were determined automatically using a XN-9000 analyzer (Kobe, Hyōgo Prefecture, Japan) according to the manufacturer's instructions within 45 min after collection in EDTA-coated tubes that were kept at room temperature.

*Gut microbiota analyses*
Fecal samples were collected by the participants at home, stored at 4°C, transported to the hospital within 24 hours and stored at -80°C until further processing. Before collection, subjects received three feces collection tubes (Faeces tubes 76x20mm, Nümbrecht, Germany) and sample collection instruction. Total genomic DNA was isolated from 250 mg of feces using an adapted repeated bead-beating method (31). 16S genes were amplified with index primers with an adapted PCR method (32). After confirmation of PCR products on agarose gel the samples were purified and equal molar pooled before being analyzed by Illumina Miseq (V3,600) sequencing (32) (see Supplemental Information).
To allow interpretation of the sequences, forward and reverse reads were length trimmed at 240 and 210 nucleotides respectively and amplicon sequence variants (ASVs) were inferred and merged using dada2 V1.5.2 (33). Taxonomy was assigned using dada2 implementation of the RDP classifier (34) and SILVA (35) 16S ribosomal database V128. Microbiota data were further analyzed and visualized using phyloseq (36), vegan (37) and picante (38). Differences in beta-diversity were tested with permutational multivariate analysis of variance using weighted UniFrac (39). All

statistical tests concerning alpha- and beta-diversity were performed on rarefied ASV tables.

To determine the abundance of intact bacteria before and after vancomycin, fecal bacteria were stained with the nucleic acid stain SytoBC (ThermoFisher Scientific, Invitrogen, Carlsbad, California, U.S.A.). Frozen fecal samples (100 mg) were diluted 1:10 in phosphate buffered saline (PBS) with cOmpleteTM Protease Inhibitory Cocktail (Roche, Basel, Switzerland). All steps were performed on ice. Samples were vigorously shaken for 10 min to obtain a homogenized solution which was centrifuged at 400 g for 5 min to separate the bacteria from large debris. Next, 100 µL of the supernatant was taken and centrifuged for 5 min at 8000 g to pellet the bacteria. The pellet was washed with 1 mL of PBS. Lastly, bacteria were stained with 1:4000 diluted SytoBC stain in a 0.9% NaCl solution with 0.1 mol/L (4-(2-hydroxyethyl)-1-piperazineethanesulfonic acid) (HEPES). Stained bacteria were measured on a BD FACS Canto II (Becton, Dickinson, Franklin Lakes, New Jersey, U.S.A.) and analyzed using FlowJo software (version 10.0 FlowJo, LLC, Ashland, Oregon, U.S.A.). Threshold settings were set to the minimal allowable voltage for side scatter to be able to measure small particles. At least 50.000 events were counted. The gating strategy is outlined in Supplemental Figure S1).

*Monocyte flow cytometry*

700 µL whole blood was lysed in 6.3 mL red blood cell lysis buffer (Affymetrix, eBioscience, San Diego, California, U.S.A.) for 15 min. The reaction was stopped by the addition of 28 mL PBS. After centrifugation at 387 g (5 min, 4°C) the peripheral blood mononuclear cells (PBMCs) were harvested. The PBMCs were suspended in 200 µL PBS and incubated with fluorochrome labeled antibodies (PE-Cy7, mouse anti-human CD14, BD Pharmingen, clone: M5E2 , ref# 557742 , lot# 6273595, 1/50 dilution; APC-H7, mouse anti-human CD16, BD Pharmingen, clone: 3G8, ref# 560195, lot# 5061807, 1/50 dilution; PerCP-Cy5.5, mouse anti-human HLA-DR, BD Pharmingen, clone: G46-6, ref# 560652, lot# 6098644, 1/50 dilution; Alexa Fluor 647, mouse anti-human CD192 (CCR2), BD Pharmingen, clone: 48607, ref# 558406, lot# 6165900, 1/50 dilution) for 15 min (room temperature, dark). After incubation, the labeled cells were washed with 140 µL PBS and centrifuged at 441 g (3 min, 4°C). The cell pellet was resuspended in 200 µL PBS. Samples were analyzed on the BD FACS Canto II (Becton, Dickinson, Franklin Lakes, New Jersey, U.S.A.). 5000 monocyte events were counted per sample. Monocyte subsets (*i.e.* classical, intermediate, and non-classical monocytes) were classified according to HLA-DR, CD14, and CD16 expression (classical: CD14++, CD16–; intermediate: CD14++, CD16+; non-classical: CD14+, CD16+). The gating strategy is outlined in Supplemental Figure S2. Within the monocyte subsets the expression of C-C chemokine receptor type 2 (CCR2) was determined. The delta median fluorescence intensity (DMFI = MFI surface staining - MFI backbone (CD14, CD16, HLA-DR)) was analyzed using FlowJo software (version 10.0 FlowJo, LLC, Ashland, Oregon, U.S.A.).

*Ex vivo monocyte stimulation*

PBMCs were isolated using a LymphoprepTM (Axis-Shield, Dundee, Scotland) density gradient and subsequent CD14+ monocyte isolation was conducted by magnetic activated cell sorting (MACS) using human CD14-coated MicroBeads according to manufacturer's instructions (MACS, Miltenyi Biotec, Leiden, The Netherlands). Next, monocytes were counted (Casy TT, Roche Innovatis, Basel, Switzerland) and plated into a 96-well flat-bottom plate (1E5 monocytes/well), followed by culturing in Roswell Park Memorial Institute (RPMI) + GlutaMAX supplemented with 25 mmol/L HEPES and 1% penicillin/streptomycin (Gibco, Dun Laoghaire, County Dublin, Ireland). Subsequently, monocytes were stimulated for 24 h with either RPMI, 10 ng/mL LPS or 10 µg/mL Pam3Cys at 37°C, 5% CO2 after which the supernatants were collected and stored at -20°C. Cytokine production (IL-1**β**, TNF-**α**, MCP-1, IL-6 and IL-10) was determined in supernatants by LEGENDplexTM bead-based immunoassay according to the manufacturer's instructions (Biolegend, San Diego, California, U.S.A.).

*Statistical analyses*

Data were checked for normality with the Shapiro-Wilk test and by visually assessing histograms and normality plots. Effects of vancomycin on fasting parameters were assessed using the paired t-test for normal continuous variables and the Wilcoxon signed rank test for other variables. One-way ANOVA for repeated measures (rm-ANOVA) for normal continuous variables and the Friedman test for other variables, with Bonferroni post hoc testing, was used to assess effects of the high-fat meal on postprandial parameters. Two-way rm-ANOVA with Bonferroni post hoc testing with time after the meal (time) and treatment (pre- versus post-intervention) as factors was used to determine effect of treatment (time * treatment interaction) on postprandial parameters. Statistical analyses were performed using SPSS Statistics software, version 24 (IBM, Armonk, New York). Data are provided as mean with standard deviation (SD) or median with interquartile range (IQR). *P*-values <0.05 were considered statistically significant. All authors had access to the study data and reviewed and approved the final manuscript.

## Results

We included ten lean and ten obese Caucasian males. Baseline characteristics are summarized in Table 1. All obese subjects met the metabolic syndrome criteria and were insulin resistant (HOMA-IR score ≥ 2.2). All subjects completed the study. No side effects of vancomycin treatment were reported, apart from a mild increase in stool frequency in eight subjects (four subjects in each group). Caloric intake and body weight remained unchanged in both groups throughout the study period (data not shown).

Table 1. Baseline characteristics.

| | Lean (n = 10) | Obese (n = 10) |
|---|---|---|
| Age (years) | 28.7 (8.7) | 58.5 (7.3) |
| BMI (kg/m$^2$) | 22.8 (1.1) | 34.6 (4.2) |
| BSA (m$^2$) | 1.99 (0.16) | 2.41 (0.26) |
| Waist circumference (cm) | 79.5 (6.0) | 114.1 (14.5) |
| Waist/hip ratio | 0.92 (0.04) | 1.06 (0.06) |
| Systolic blood pressure (mmHg) | 130.8 (10.3) | 155.9 (14.7) |
| Diastolic blood pressure (mmHg) | 78.0 (9.9) | 93.8 (12.3) |
| Leukocytes (10E9/L) | 5.3 (0.8) | 6.0 (1.1) |
| Fasting glucose (mmol/L) | 4.8 (0.2) | 6.1 (0.7) |
| Fasting insulin (pmol/L)* | 29 [15-43] | 89 [66-128] |
| HOMA-IR* | 0.9 [0.5-1.4] | 3.4 [2.6-4.5] |
| Dietary intake | | |
| - Energy (kcal/day) | 2359 (652) | 2046 (289) |
| - Fat (g/day) | 86.8 (30.9) | 74.6 (18.0) |
| - Carbohydrates (g/day) | 279.3 (81.4) | 218.0 (58.4) |
| - Protein (g/day) | 92.8 (31.2) | 97.3 (12.8) |
| - Fiber (g/day) | 25.1 (9.7) | 16.6 (25.1) |

Data are represented as mean (SD) unless otherwise specified. BMI, body mass index; BSA, body surface area; HOMA-IR, homeostasis model assessment of insulin resistance; n, number of patients. *Data are represented as median [IQR].

*Vancomycin significantly alters fecal microbiota composition*

As expected, vancomycin significantly altered the relative abundance of several bacterial groups (Figure 1A). Specifically, major Gram-positive taxa such as Clostridia and Bacteroidia decreased, while Gram-negative taxa (Negativicutes and Proteobacteria) and vancomycin-resistant Gram-positive taxa such as Bacilli increased. Vancomycin decreased bacterial diversity (Faith's phylogenetic diversity pre- and post-intervention respectively: lean, 56.9 ± 7.8 versus 21.4 ± 6.6, $p<0.001$; obese, 53.9 ± 7.8 versus 21.0 ± 5.9, $p<0.001$; Figure 1B). Non-metric multidimensional scaling (NMDS) ordination of the weighted UniFrac distances showed a significant shift of gut microbiota composition after treatment (lean, $p=0.001$; obese, $p=0.001$; Figure 1C). The percentage of intact fecal bacteria as measured by SytoBC positivity was also significantly reduced (lean, 82.4 ± 5.8% versus 38.4 ± 11.4%, $p<0.001$; obese 76.1 ± 15.7% versus 35.4 ± 9.0%, $p<0.001$).

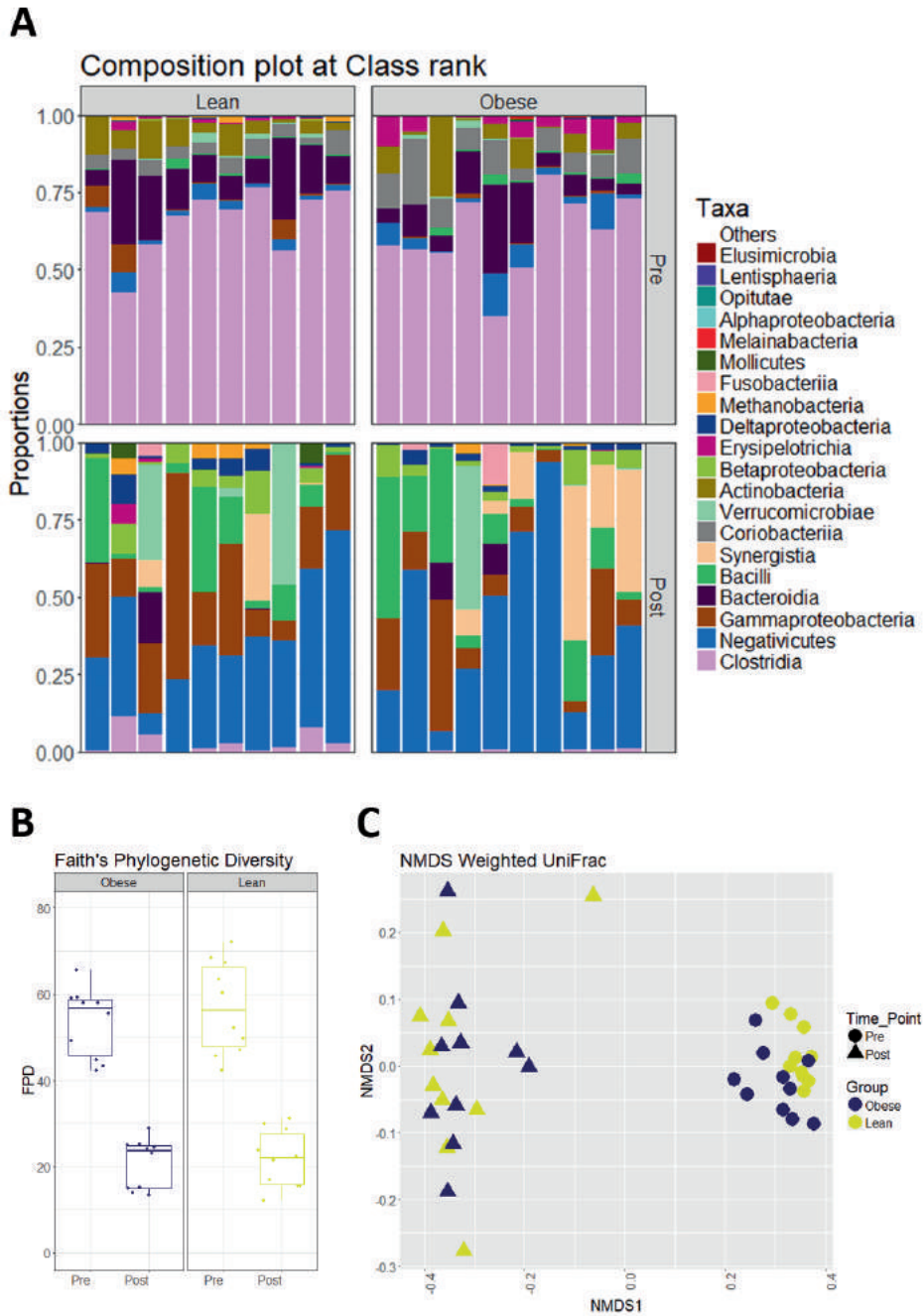


**Figure 1. Effect of vancomycin on gut microbiota composition.** Fecal microbial community characteristics of obese and lean subjects before and after treatment. Vancomycin treatment resulted in significant changes in gut microbiota composition in both groups. **(A)** microbial composition showing the 20 most abundant bacterial classes (upper part, pre-intervention; lower part, post-intervention). **(B)** Faith's phylogenetic diversity distribution showed a significant decrease in alpha-diversity (lean, $p<0.001$; obese, $p<0.001$). **(C)** NMDS ordination of the weighted UniFrac distances showed a significant shift in beta-diversity (lean, $p=0.001$; obese, $p=0.001$).

*Vancomycin increases fasting LPS, without significantly affecting the inflammatory state*

After vancomycin treatment, fasting LPS significantly increased in both groups (lean, median [IQR]: 0.81 [0.63-1.45] versus 2.23 [1.33-3.83], *p*=0.017; obese, median [IQR]: 0.76 [0.45-1.03] versus 1.44 [1.11-4.24], *p*=0.014; Figure 2). However, plasma LBP, IL-6 and MCP-1 did not change significantly (Table 2 and Supplemental Table ST1). On a cellular level, there was no effect on leukocyte counts (Table 2), leukocyte subtypes (Supplemental Table ST2) and distribution of monocyte subtypes (*i.e.* classical, intermediate and non-classical, Supplemental Table ST3). Monocyte expression of CCR2, which was previously shown to be positively correlated with lipid levels and inflammation (40, 41), did not differ significantly in the fasting state upon vancomycin treatment in the lean subjects but decreased in the obese group (Table 2). Finally, vancomycin treatment resulted in lower monocyte production of MCP-1 only in the lean group upon *ex vivo* stimulation with LPS (Supplemental Figure S3). IL-1**β** production was nonsignificantly reduced in Toll-like receptor (TLR) 2-stimulated monocytes after treatment compared to baseline in both the lean and obese subjects. Production of other cytokines (*i.e.* IL-6 and TNF-**α**) upon stimulation with either TLR4 or TLR2 ligands did not change after the intervention (Supplemental Figure S3).

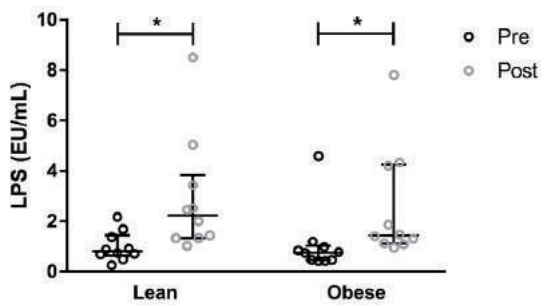


**Figure 2. Effect of vancomycin on fasting plasma LPS.** Vancomycin treatment significantly increased fasting plasma LPS in both groups (Wilcoxon signed rank test; lean, *p*=0.017; obese, *p*=0.014). Lines at median and IQR.

**Table 2. Effect of vancomycin on fasting leukocyte counts, LBP, and inflammatory markers.**

| | | Pre-intervention | Post-intervention | *p* |
|---|---|---|---|---|
| Leukocytes (10E9/L) | Lean | 5.3 (0.8) | 5.4 (1.0) | 0.752 |
| | Obese | 6.0 (1.1) | 6.1 (0.6) | 0.718 |
| LBP | Lean | 10.44 (1.46) | 11.04 (2.30) | 0.258 |
| | Obese | 12.03 (2.55) | 11.86 (2.61) | 0.811 |
| IL-6 (pg/mL) | Lean | 0.83 (1.82) | 1.07 (1.56) | 0.417 |
| | Obese | 2.03 (2.57) | 2.16 (3.04) | 0.720 |
| MCP-1 (pg/mL) | Lean | 44.2 (25.5) | 50.3 (21.9) | 0.538 |
| | Obese | 111.5 (107.9) | 91.6 (118.4) | 0.361 |
| CCR2 (MFI) | Lean | 628.0 (194.2) | 611.2 (149.1) | 0.649 |
| | Obese | 617.2 (195.6) | 518.2 (145.7) | 0.029 |

Fasting blood leukocyte counts, plasma inflammatory markers and monocyte CCR2 expression before and after vancomycin treatment. CCR2, chemokine receptor 2; IL-6, interleukin-6; LBP, lipopolysaccharide-binding protein; MCP-1, monocyte chemoattractant protein 1. n = 10 per group. Data are represented as mean (SD).

*Effect of a high-fat meal on postprandial lipids*

Plasma triglycerides significantly increased after a high-fat meal in both groups. This increase was unaffected by the intervention (Supplemental Figure S4). Plasma HDL-cholesterol decreased slightly but significantly after the meal. LDL-cholesterol levels decreased by about 10% after the meal in both groups (Supplemental Table ST4). There was no effect of vancomycin on postprandial plasma lipid concentrations (Supplemental Table ST4).

*Postprandial translocation of LPS is unaffected by vancomycin treatment*

LPS concentrations did not increase after a high-fat meal in both groups (lean, median [IQR] at t = 0 h, t = 2 h and t = 4 h, respectively: 0.81 [0.63-1.45], 1.19 [0.60-1.65] and 0.58 [0.46-0.63]; Friedman test $p$=0.016; post hoc pairwise comparisons: t = 0 h versus t = 2 h, $p$=1.000; t = 0 h versus t = 4 h, $p$=0.055, t = 2 h versus t = 4 h, $p$=0.029. Obese: median [IQR] at t = 0 h, t = 2 h and t = 4 h, respectively: 0.76 [0.45-1.03], 0.54 [0.38-0.98] and 0.71 [0.51-1.52]; Friedman test $p$=0.407). Although fasting LPS concentrations increased after treatment in both groups, there was no effect of vancomycin treatment on postprandial LPS concentrations (Figure 3). LBP did not increase after the high-fat meal, and vancomycin did not affect postprandial LBP concentrations (Supplemental Table ST1).

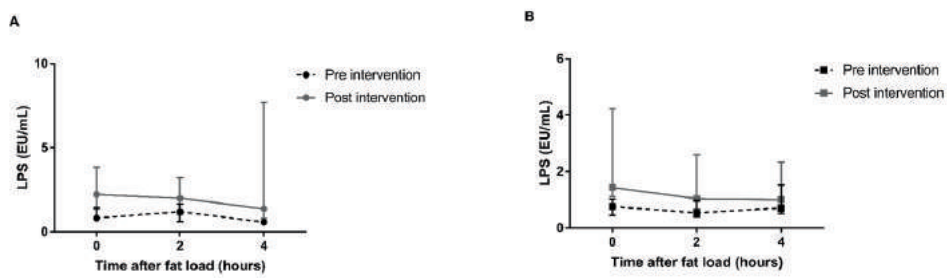


**Figure 3. Postprandial LPS concentrations.** LPS concentrations did not increase after the high-fat meal in both the lean **(A)** and obese **(B)** group. Vancomycin treatment did not affect postprandial LPS concentrations (two-way rm-ANOVA, time * treatment interaction: lean, $p$=0.318, obese, $p$=0.714). Lines show median and IQR.

*Postprandial monocyte activation is unaffected by vancomycin treatment*

Blood leukocyte counts significantly increased after the high-fat meals in both groups, with no differences between pre- and post-vancomycin treatment (Figure 4 and Supplemental Table ST2). This increase was mainly mediated by neutrophils (Supplemental Table ST2). The increase in postprandial leukocyte counts was not accompanied by an increase in plasma IL-6 or MCP-1 and vancomycin did not affect the concentrations of these cytokines in the postprandial period (Supplemental Table

ST1). Distribution of monocyte types and monocyte CCR2 expression (classical, intermediate, non-classical) also did not change after the intervention (Supplemental Table ST3).

*Ex vivo* stimulation experiments revealed that the production of several cytokines by monocytes significantly changed upon a high-fat meal challenge and vancomycin treatment (Figure 5) in the obese group but not in the lean group. First of all, before intervention, there was a decrease of MCP-1 production (upon stimulation with medium only) in the obese group after a high-fat meal. Furthermore, a high-fat meal resulted in a non-significant downregulation of both IL-1**β** and TNF-**α** upon TLR2 stimulation with Pam3Cys. Upon vancomycin treatment, these effects were even more pronounced. IL-6 production upon TLR2 stimulation was also downregulated in the obese group, but vancomycin treatment blunted this effect. Other cytokines were not affected by either the high-fat meal or vancomycin treatment (Figure 5).

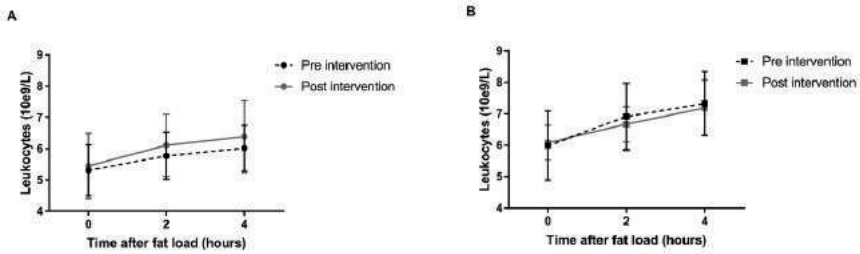


**Figure 4. Postprandial blood leukocyte counts.** Leukocyte counts significantly increased after the meal in both the lean **(A)** and obese **(B)** group (one-way rm-ANOVA: lean, $p$=0.006 pre-intervention and $p$=0.001 post-intervention; obese, $p$=0.001 pre-intervention and $p$=0.003 post-intervention). Vancomycin treatment did not affect postprandial leukocyte counts. Graphs show mean and SD.

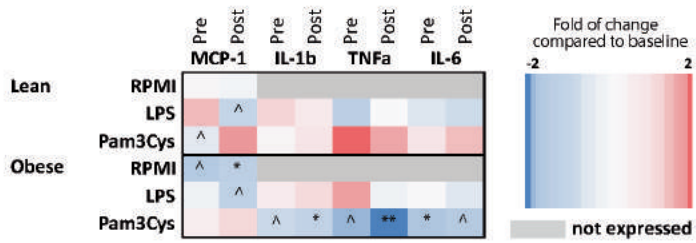


**Figure 5. Effect of a high-fat meal on monocyte cytokine production.** Monocytes of lean and obese subjects were isolated before (t = 0 h) and after (t = 4 h) a high-fat meal. Monocytes were stimulated with RPMI (negative control), LPS (TLR4 stimulation) or Pam3Cys (TLR2 stimulation). After 24 h, concentrations of MCP-1, IL-1**β**, TNF-**α** and IL-6 were measured in the supernatant. The heatmap shows the effects of the meal on monocyte cytokine production before (pre) and after (post) vancomycin treatment. Red indicates upregulated cytokine production after the meal compared to before the meal. Blue indicates a downregulation of cytokine production after the meal compared to before the meal. n = 10 per group. ^$p$<0.1, *$p$<0.05, **$p$<0.01.

## Discussion

In this study, we investigated the effect of manipulation of the gut microbiota by vancomycin on the inflammatory response in the postprandial state. Despite large shifts in fecal microbiota composition with a bloom in Gram-negative bacteria and a concomitant significant increase in fasting LPS, we did not observe a change in several postprandial inflammatory markers after a high-fat meal in lean and obese subjects with the metabolic syndrome. This suggests that LPS translocation may not play a large role in the short-term postprandial response in these groups.

Previously, several groups assessed the effects of meals of varying composition on postprandial inflammation. To our knowledge, we are the first to assess the effect of manipulation of the gut microbiota on postprandial inflammation. For example, it was shown that in lean and obese subjects, that a high-fat meal consisting of bread, palm fat, salami, and boiled eggs of 1500 kcal resulted in a significant increase in plasma IL-6 only in the obese group (42). Another study found an average increase of plasma LPS of 50% after a high-fat meal consisting of three slices of toast with 50 g butter in 12 healthy subjects, although there was no clear timepoint of maximum LPS concentration (17). Deopurkar et al. reported increased plasma LPS concentrations in healthy subjects 3 h after a meal consisting of cream, but not after intake of an isocaloric glucose drink or orange juice (43). Studies comparing T2D patients to healthy controls found stronger increases in T2D in postprandial plasma IL-6 (23) and LPS (27) levels. Taken together, these studies indicate that after a high-fat meal plasma LPS as well as inflammatory markers may increase, but they cannot confer a causal relationship between postprandial LPS translocation and low-grade inflammation observed after acute consumption of dietary fat.

Our findings add to previous insights on the pathophysiology of the inflammatory response in the postprandial period. We observed several changes induced by a high-fat meal in both the lean and the obese group. For example, leukocyte counts significantly increased after the meal in lean as well as in obese subjects, as was previously described (28). Moreover, the meal influenced *ex vivo* production of several cytokines by monocytes in the obese group. Specifically, MCP-1 production in unstimulated monocytes and IL-1**β**, TNF-**α** and IL-6 production in TLR2-stimulated monocytes were lower 4 h after a high-fat meal. We were unable to reproduce previous observations of a postprandial increase in monocyte activation (24, 44, 45), although in those studies, monocyte CCR2 expression was not assessed. Moreover, we did not observe an increase in plasma LPS, IL-6 or MCP-1 after the high-fat meal, which is in accordance with some (24, 46-48) but not other (18, 19, 49) studies.

Oral vancomycin treatment significantly changed the composition of the gut microbiota as shown previously (50, 51), with a relative overgrowth of potentially pathogenic Gram-negative taxa such as Proteobacteria. Concomitantly, we found increases in fasting plasma LPS levels, possibly due to the increased presence of Gram-negative bacteria inducing an excess of LPS in the intestinal lumen. Interestingly, *ex vivo* MCP-1 production by monocytes that were incubated with LPS

slightly decreased after vancomycin treatment only in lean fasting subjects. Similarly, a 7-day treatment of 12 healthy subjects with ciprofloxacin, vancomycin and metronidazole was shown to lower fasting LPS-induced TNF-**α** production in isolated monocytes (52). Nevertheless, in the postprandial phase, production of cytokines by stimulated monocytes was unaffected by the intervention in our study. Moreover, both fasting and postprandial leukocyte counts, monocyte activation markers and plasma IL-6 and MCP-1 were unaffected by vancomycin treatment. Finally, postprandial LPS concentrations as well as LBP levels were unaffected by treatment, suggesting that manipulation of the gut microbiota did not increase postprandial bacterial translocation.

Apart from LPS measurement, quantification or sequencing of 16S rDNA in plasma is sometimes used as marker of translocation. Although this would be interesting to assess, this is not the only way to do so, nor the gold standard. Moreover, in tissues with low microbial biomass, there may be the issue of contamination (53).

LPS toxicity is related to several factors, such as bacterial origin (54) and binding to plasma proteins (*e.g.* LBP, lipoproteins, CD14, endotoxin core antibodies) (55). As LBP may be upregulated after LPS exposure in a setting of septic shock (56), it is sometimes used as a marker of LPS exposure. While LBP can augment LPS-induced activation of monocytes by accelerating binding to CD14 at low concentration, it has inhibitory effects in high concentrations (57-59). In our study we observed increased fasting plasma LPS after vancomycin intervention. However, this was not accompanied by increase in LBP. Concomitantly, no change in inflammatory markers was found.

It should be noted that we investigated the effect of a short-term intervention (7 days) on the postprandial response to a single high-fat meal. Although this duration is sufficient to significantly alter gut microbiota composition (51), it cannot be ruled out that long-term microbiota manipulation may alter postprandial inflammatory mechanisms. The exact role of the gut microbiota in inflammation in high-fat diets as opposed to a single high-fat meal in humans is unclear. Previously, it was shown that in mice, a chronic high-fat diet increased endotoxemia 2-3-fold (7). Similarly, 18 healthy subjects that were overfed (+760 kcal/day) for 8 weeks showed increased postprandial endotoxemia upon a high-fat meal (60). Thus, even though we did not see an effect of the intervention on postprandial inflammation in this study, we cannot rule out a role for long-term changes in intestinal microbiota composition or intestinal permeability in postprandial inflammation.

Our study has several strengths and weaknesses. As vancomycin treatment induced large shifts in gut microbiota composition, we were able to directly assess a potential causal role of intestinal microbes in postprandial inflammation. Moreover, our meal was high in fat content, which was reflected by a significant increase of postprandial triglycerides in both groups. Thus, our study was well suited to test the hypothesis of postprandial chylomicron-associated LPS translocation. However, it should be noted that we were only able to assess the effect of the intervention on the fecal microbiota.

As lipid uptake predominantly takes place in the small intestine, we cannot rule out that the intervention was not sufficient to increase luminal LPS concentrations and potentially alter LPS translocation in the small intestine. Of note, the increase in fasting plasma LPS could both reflect increased luminal LPS concentrations due to overgrowth of Gram-negative bacteria or increased intestinal permeability. In this study, we did not assess intestinal permeability.

Secondly, we evaluated the postprandial inflammatory response in a lean healthy group and in an obese, metabolic syndrome group, as these groups were previously shown to have a different postprandial inflammatory response. However, as the groups had significantly different characteristics, such as age, dietary intake and baseline inflammatory parameters, we could not directly compare these two groups in this study. Instead, we assessed the effect of a vancomycin intervention in both groups separately, allowing us to do paired observations within the groups. Therefore, the study had significant power to detect differences between pre- and post-intervention, despite the groups being relatively small. Nevertheless, adding a placebo-arm would have increased the power. Thus, it would be interesting to perform a similar placebo-controlled study in age-matched lean and obese subjects.

In conclusion, manipulation of the gut microbiota by a short-term course of broad-spectrum antibiotics led to a large shift in gut microbiota composition and a significant increase in plasma LPS, but did not affect the physiology of postprandial inflammation in lean or obese subjects in this study. This suggests that LPS translocation may not drive the postprandial inflammatory response upon a single high-fat meal.

## References


1. Turnbaugh PJ, Hamady M, Yatsunenko T, Cantarel BL, Duncan A, Ley RE, et al. A core gut microbiome in obese and lean twins. Nature. 2009;457(7228):480-4.
2. Qin J, Li Y, Cai Z, Li S, Zhu J, Zhang F, et al. A metagenome-wide association study of gut microbiota in type 2 diabetes. Nature. 2012;490(7418):55-60.
3. Tremaroli V, Backhed F. Functional interactions between the gut microbiota and host metabolism. Nature. 2012;489(7415):242-9.
4. Karlsson FH, Tremaroli V, Nookaew I, Bergstrom G, Behre CJ, Fagerberg B, et al. Gut metagenome in European women with normal, impaired and diabetic glucose control. Nature. 2013;498(7452):99-103.
5. Chawla A, Nguyen KD, Goh YP. Macrophage-mediated inflammation in metabolic disease. Nat Rev Immunol. 2011;11(11):738-49.
6. Gregor MF, Hotamisligil GS. Inflammatory mechanisms in obesity. Annu Rev Immunol. 2011;29:415-45.
7. Cani PD, Amar J, Iglesias MA, Poggi M, Knauf C, Bastelica D, et al. Metabolic endotoxemia initiates obesity and insulin resistance. Diabetes. 2007;56(7):1761-72.
8. Cani PD, Bibiloni R, Knauf C, Waget A, Neyrinck AM, Delzenne NM, et al. Changes in gut microbiota control metabolic endotoxemia-induced inflammation in high-fat diet-induced obesity and diabetes in mice. Diabetes. 2008;57(6):1470-81.
9. Amar J, Chabo C, Waget A, Klopp P, Vachoux C, Bermudez-Humaran LG, et al. Intestinal mucosal adherence and translocation of commensal bacteria at the early onset of type 2 diabetes: molecular mechanisms and probiotic treatment. EMBO Mol Med. 2011;3(9):559-72.
10. Basu S, Haghiac M, Surace P, Challier JC, Guerre-Millo M, Singh K, et al. Pregravid obesity associates with increased maternal endotoxemia and metabolic inflammation. Obesity (Silver Spring). 2011;19(3):476-82.
11. Pussinen PJ, Havulinna AS, Lehto M, Sundvall J, Salomaa V. Endotoxemia is associated with an increased risk of incident diabetes. Diabetes Care. 2011;34(2):392-7.
12. Pussinen PJ, Tuomisto K, Jousilahti P, Havulinna AS, Sundvall J, Salomaa V. Endotoxemia, immune response to periodontal pathogens, and systemic inflammation associate with incident cardiovascular disease events. Arterioscler Thromb Vasc Biol. 2007;27(6):1433-9.
13. Sun L, Yu Z, Ye X, Zou S, Li H, Yu D, et al. A marker of endotoxemia is associated with obesity and related metabolic disorders in apparently healthy Chinese. Diabetes Care. 2010;33(9):1925-32.
14. Moreno-Navarrete JM, Ortega F, Serino M, Luche E, Waget A, Pardo G, et al. Circulating lipopolysaccharide-binding protein (LBP) as a marker of obesity-related insulin resistance. Int J Obes (Lond). 2012;36(11):1442-9.
15. Vishnyakova TG, Bocharov AV, Baranova IN, Chen Z, Remaley AT, Csako G, et al. Binding and internalization of lipopolysaccharide by Cla-1, a human orthologue of rodent scavenger receptor B1. J Biol Chem. 2003;278(25):22771-80.
16. Beaslas O, Cueille C, Delers F, Chateau D, Chambaz J, Rousset M, et al. Sensing of dietary lipids by enterocytes: a new role for SR-BI/CLA-1. PLoS One. 2009;4(1):e4278.
17. Erridge C, Attina T, Spickett CM, Webb DJ. A high-fat meal induces low-grade endotoxemia: evidence of a novel mechanism of postprandial inflammation. Am J Clin Nutr. 2007;86(5):1286-92.
18. Ghanim H, Abuaysheh S, Sia CL, Korzeniewski K, Chaudhuri A, Fernandez-Real JM, et al. Increase in plasma endotoxin concentrations and the expression of Toll-like receptors and suppressor of cytokine signaling-3 in mononuclear cells after a high-fat, high-carbohydrate meal: implications for insulin resistance. Diabetes Care. 2009;32(12):2281-7.
19. Laugerette F, Vors C, Geloen A, Chauvin MA, Soulage C, Lambert-Porcheron S, et al. Emulsified lipids increase endotoxemia: possible role in early postprandial low-grade inflammation. J Nutr Biochem. 2011;22(1):53-9.
20. Blackburn P, Despres JP, Lamarche B, Tremblay A, Bergeron J, Lemieux I, et al. Postprandial variations of plasma inflammatory markers in abdominally obese men. Obesity (Silver Spring). 2006;14(10):1747-54.
21. Lundman P, Boquist S, Samnegard A, Bennermo M, Held C, Ericsson CG, et al. A high-fat meal is accompanied by increased plasma interleukin-6 concentrations. Nutr Metab Cardiovasc Dis. 2007;17(3):195-202.
22. Khoury DE, Hwalla N, Frochot V, Lacorte JM, Chabert M, Kalopissis AD. Postprandial metabolic and hormonal responses of obese dyslipidemic subjects with metabolic syndrome to test meals, rich in carbohydrate, fat or protein. Atherosclerosis. 2010;210(1):307-13.
23. Nappo F, Esposito K, Cioffi M, Giugliano G, Molinari AM, Paolisso G, et al. Postprandial endothelial activation in healthy subjects and in type 2 diabetic patients: role of fat and carbohydrate meals. J Am Coll Cardiol. 2002;39(7):1145-50.
24. Gower RM, Wu H, Foster GA, Devaraj S, Jialal I, Ballantyne CM, et al. CD11c/CD18 expression is upregulated on blood monocytes during hypertriglyceridemia and enhances adhesion to vascular cell adhesion molecule-1. Arterioscler Thromb Vasc Biol. 2011;31(1):160-6.
25. Clemente-Postigo M, Queipo-Ortuno MI, Murri M, Boto-Ordonez M, Perez-Martinez P, Andres-Lacueva C, et al. Endotoxin increase after fat overload is related to postprandial hypertriglyceridemia in morbidly obese patients. J Lipid Res. 2012;53(5):973-8.
26. Vors C, Pineau G, Drai J, Meugnier E, Pesenti S, Laville M, et al. Postprandial Endotoxemia Linked With Chylomicrons and Lipopolysaccharides Handling in Obese Versus Lean Men: A Lipid Dose-Effect Trial. J Clin Endocrinol Metab. 2015;100(9):3427-35.
27. Harte AL, Varma MC, Tripathi G, McGee KC, Al-Daghri NM, Al-Attas OS, et al. High fat intake leads to acute postprandial exposure to circulating endotoxin in type 2 diabetic subjects. Diabetes Care. 2012;35(2):375-82.
28. Klop B, van de Geijn GJ, Njo TL, Janssen HW, Rietveld AP, van Miltenburg A, et al. Leukocyte cell population data (volume conductivity scatter) in postprandial leukocyte activation. Int J Lab Hematol. 2013;35(6):644-51.

29. Mosteller RD. Simplified calculation of body-surface area. N Engl J Med. 1987;317(17):1098.
30. Everard A, Belzer C, Geurts L, Ouwerkerk JP, Druart C, Bindels LB, et al. Cross-talk between Akkermansia muciniphila and intestinal epithelium controls diet-induced obesity. Proc Natl Acad Sci U S A. 2013;110(22):9066-71.
31. Salonen A, Nikkila J, Jalanka-Tuovinen J, Immonen O, Rajilic-Stojanovic M, Kekkonen RA, et al. Comparative analysis of fecal DNA extraction methods with phylogenetic microarray: effective recovery of bacterial and archaeal DNA using mechanical cell lysis. J Microbiol Methods. 2010;81(2):127-34.
32. Kozich JJ, Westcott SL, Baxter NT, Highlander SK, Schloss PD. Development of a dual-index sequencing strategy and curation pipeline for analyzing amplicon sequence data on the MiSeq Illumina sequencing platform. Appl Environ Microbiol. 2013;79(17):5112-20.
33. Callahan BJ, McMurdie PJ, Rosen MJ, Han AW, Johnson AJ, Holmes SP. DADA2: High-resolution sample inference from Illumina amplicon data. Nat Methods. 2016;13(7):581-3.
34. Wang Q, Garrity GM, Tiedje JM, Cole JR. Naive Bayesian classifier for rapid assignment of rRNA sequences into the new bacterial taxonomy. Appl Environ Microbiol. 2007;73(16):5261-7.
35. Quast C, Pruesse E, Yilmaz P, Gerken J, Schweer T, Yarza P, et al. The SILVA ribosomal RNA gene database project: improved data processing and web-based tools. Nucleic Acids Res. 2013;41(Database issue):D590-6.
36. McMurdie PJ, Holmes S. phyloseq: an R package for reproducible interactive analysis and graphics of microbiome census data. PLoS One. 2013;8(4):e61217.
37. Oksanen J, Guillaume Blanchet F, Friendly MK, R., Legendre P, McGlinn D, Minchin PR, et al. Package Vegan: Community Ecology Package. Version 2.5-2. 2018.
38. Kembel SW, Ackerly DD, Blomberg SP, Cornwell WK, Cowan PD, Helmus MR, et al. Package Picante: R tools for integrating phylogenies and ecology. Version 1.7. 2014.
39. Lozupone C, Knight R. UniFrac: a new phylogenetic method for comparing microbial communities. Appl Environ Microbiol. 2005;71(12):8228-35.
40. Bernelot Moens SJ, Neele AE, Kroon J, van der Valk FM, Van den Bossche J, Hoeksema MA, et al. PCSK9 monoclonal antibodies reverse the pro-inflammatory profile of monocytes in familial hypercholesterolaemia. Eur Heart J. 2017;38(20):1584-93.
41. Verweij SL, Duivenvoorden R, Stiekema LCA, Nurmohamed NS, van der Valk FM, Versloot M, et al. CCR2 expression on circulating monocytes is associated with arterial wall inflammation assessed by 18F-FDG PET/CT in patients at risk for cardiovascular disease. Cardiovasc Res. 2018;114(3):468-75.
42. Schwander F, Kopf-Bolanz KA, Buri C, Portmann R, Egger L, Chollet M, et al. A dose-response strategy reveals differences between normal-weight and obese men in their metabolic and inflammatory responses to a high-fat meal. J Nutr. 2014;144(10):1517-23.
43. Deopurkar R, Ghanim H, Friedman J, Abuaysheh S, Sia CL, Mohanty P, et al. Differential effects of cream, glucose, and orange juice on inflammation, endotoxin, and the expression of Toll-like receptor-4 and suppressor of cytokine signaling-3. Diabetes Care. 2010;33(5):991-7.
44. Alipour A, van Oostrom AJ, Izraeljan A, Verseyden C, Collins JM, Frayn KN, et al. Leukocyte activation by triglyceride-rich lipoproteins. Arterioscler Thromb Vasc Biol. 2008;28(4):792-7.
45. Esser D, van Dijk SJ, Oosterink E, Muller M, Afman LA. A high-fat SFA, MUFA, or n3 PUFA challenge affects the vascular response and initiates an activated state of cellular adherence in lean and obese middle-aged men. J Nutr. 2013;143(6):843-51.
46. Meher D, Dutta D, Ghosh S, Mukhopadhyay P, Chowdhury S, Mukhopadhyay S. Effect of a mixed meal on plasma lipids, insulin resistance and systemic inflammation in non-obese Indian adults with normal glucose tolerance and treatment naive type-2 diabetes. Diabetes Res Clin Pract. 2014;104(1):97-102.
47. Fogarty CL, Nieminen JK, Peraneva L, Lassenius MI, Ahola AJ, Taskinen MR, et al. High-fat meals induce systemic cytokine release without evidence of endotoxemia-mediated cytokine production from circulating monocytes or myeloid dendritic cells. Acta Diabetol. 2015;52(2):315-22.
48. Milan AM, Pundir S, Pileggi CA, Markworth JF, Lewandowski PA, Cameron-Smith D. Comparisons of the Postprandial Inflammatory and Endotoxaemic Responses to Mixed Meals in Young and Older Individuals: A Randomised Trial. Nutrients. 2017;9(4).
49. van Dijk SJ, Mensink M, Esser D, Feskens EJ, Muller M, Afman LA. Responses to high-fat challenges varying in fat type in subjects with different metabolic risk phenotypes: a randomized trial. PLoS One. 2012;7(7):e41388.
50. Vrieze A, Out C, Fuentes S, Jonker L, Reuling I, Kootte RS, et al. Impact of oral vancomycin on gut microbiota, bile acid metabolism, and insulin sensitivity. J Hepatol. 2014;60(4):824-31.
51. Reijnders D, Goossens GH, Hermes GD, Neis EP, van der Beek CM, Most J, et al. Effects of Gut Microbiota Manipulation by Antibiotics on Host Metabolism in Obese Humans: A Randomized Double-Blind Placebo-Controlled Trial. Cell Metab. 2016;24(1):63-74.
52. Lankelma JM, Belzer C, Hoogendijk AJ, de Vos AF, de Vos WM, van der Poll T, et al. Antibiotic-Induced Gut Microbiota Disruption Decreases TNF-alpha Release by Mononuclear Cells in Healthy Adults. Clin Transl Gastroenterol. 2016;7(8):e186.
53. Kim D, Hofstaedter CE, Zhao C, Mattei L, Tanes C, Clarke E, et al. Optimizing methods and dodging pitfalls in microbiome research. Microbiome. 2017;5(1):52.
54. Schromm AB, Brandenburg K, Loppnow H, Zahringer U, Rietschel ET, Carroll SF, et al. The charge of endotoxin molecules influences their conformation and IL-6-inducing capacity. J Immunol. 1998;161(10):5464-71.

55. Thompson PA, Berbee JF, Rensen PC, Kitchens RL. Apolipoprotein A-II augments monocyte responses to LPS by suppressing the inhibitory activity of LPS-binding protein. Innate Immun. 2008;14(6):365-74.
56. Opal SM, Scannon PJ, Vincent JL, White M, Carroll SF, Palardy JE, et al. Relationship between plasma levels of lipopolysaccharide (LPS) and LPS-binding protein in patients with severe sepsis and septic shock. J Infect Dis. 1999;180(5):1584-9.
57. Gutsmann T, Muller M, Carroll SF, MacKenzie RC, Wiese A, Seydel U. Dual role of lipopolysaccharide (LPS)-binding protein in neutralization of LPS and enhancement of LPS-induced activation of mononuclear cells. Infect Immun. 2001;69(11):6942-50.
58. Zweigner J, Gramm HJ, Singer OC, Wegscheider K, Schumann RR. High concentrations of lipopolysaccharide-binding protein in serum of patients with severe sepsis or septic shock inhibit the lipopolysaccharide response in human monocytes. Blood. 2001;98(13):3800-8.
59. Thompson PA, Kitchens RL. Native high-density lipoprotein augments monocyte responses to lipopolysaccharide (LPS) by suppressing the inhibitory activity of LPS-binding protein. J Immunol. 2006;177(7):4880-7.
60. Laugerette F, Alligier M, Bastard JP, Drai J, Chanseaume E, Lambert-Porcheron S, et al. Overfeeding increases postprandial endotoxemia in men: Inflammatory outcome may depend on LPS transporters LBP and sCD14. Mol Nutr Food Res. 2014;58(7):1513-8.

## Supplemental material

*Gut microbiota DNA isolation and 16S sequencing*

Total genomic DNA was isolated from 250 mg of feces using an adapted repeated bead beating method based on a protocol previously described (1). Fecal samples were placed in bead-beating tubes and extracted twice in lysis buffer (STARbuffer, Roche, Basel, Switzerland) with bead-beating at 5.5 m/s for 60 s, 3 times in 20 s intervals in a Precellys 24 (Bertin). After each bead-beating cycle, samples were heated to 95°C for 15 min and then centrifuged at full speed for 5 min at 4°C. Supernatants from the two extractions were pooled and purified with the Maxwell RSC Blood DNA kit (Promega, Madison, Wisconsin, U.S.A.). Amplicons containing the barcoded V4 region of 16S genes were amplified using an adapted one-step PCR method (2). Forward Index Primer (Illumina Adapter, Index, pad, link, 16Sf) and Reverse Index Primer (Illumina Adapter, Index, pad, link, 16Sr) were used (3).

Twenty ng of template DNA was used in the PCR mix: 6 µL 5× HF buffer (Thermo Fisher Scientific, Waltham, Massachusetts, U.S.A.), 0.75 µL PCR Grade Nucleotide Mix (10 µM) (Thermo Fisher Scientific, Waltham, Massachusetts, U.S.A.), 0.3 µL Phusion DNA Polymerase (2 U/µL), 18.95 µL nuclease free water, 1.5 µL Forward Index Primer (10 µM) and 1.5 µL Reverse Index Primer (10 µM). The amplification program: initial denaturation at 98°C for 30 s; 25 cycles of denaturation at 98°C for 10 s, annealing at 55°C for 20 s, elongation at 72°C for 90 s; extension at 72°C for 10 min (1). PCR was performed using a Biometra Thermocycler (Westburg, Leusden, The Netherlands). To confirm the presence of the PCR product, the amplification product was tested on a 1% agarose gel. PCR products were purified using the Biomek FX robot (Beckman Coulter, Brea, California, U.S.A.) with Ampure XP beads (Beckman Coulter, Brea, California, U.S.A.). Amplicons were quantified using the Qubit® dsDNA BR Assay Kit (Thermo Fisher Scientific, Waltham, Massachusetts, U.S.A.). The samples, each labeled with a unique index, were equal molar pooled. The quality and quantity of the pooled library was checked using a High Sensitive DNA chip (Agilent, Santa Clara, California, U.S.A.) on the Bioanalyzer 21000 (Agilent, Santa Clara, California, U.S.A.) and Qubit® dsDNA BR Assay Kit. The Pooled library was sequenced by Illumina Miseq (V3,600) sequencing (3).

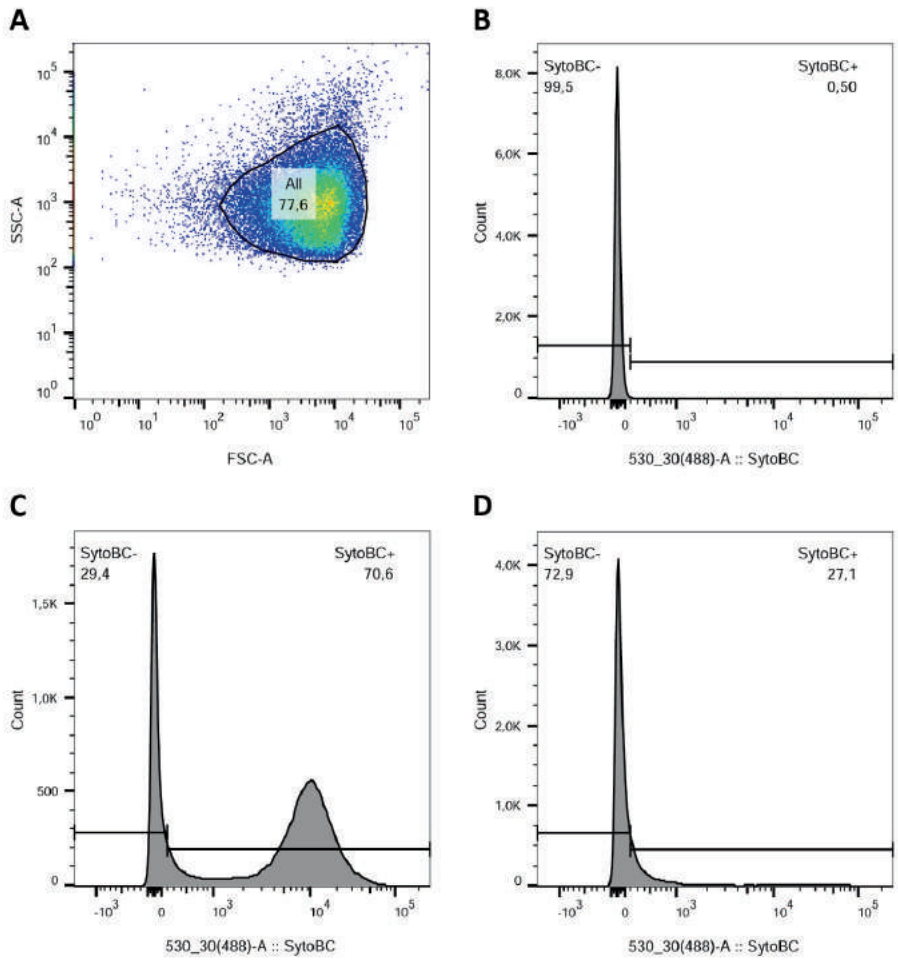


**Figure S1. Flow cytometry gating strategy for bacteria in fecal sample.** Forward and side scatter **(A)**, SytoBC histogram with negative control (no stain) **(B)**, example of stained bacteria from a pre-vancomycin fecal sample **(C)** and example from a post-vancomycin fecal sample **(D)**.

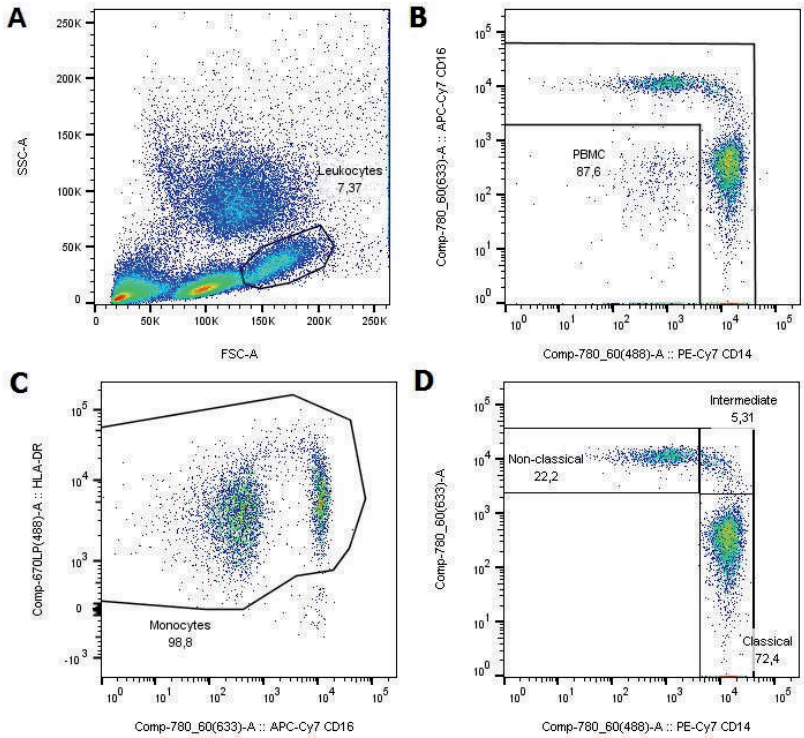


**Figure S2. Flow cytometry gating strategy for monocytes and their subtypes in a PBMC sample.** Leukocytes were gated using forward and side scatter **(A)**, monocytes were selected using CD14, CD16 and HLA-DR **(B and C)** and finally the monocyte subtypes were gated. We distinguished classical (CD14++ CD16-), intermediate (CD14++, CD16+) and non- classical (CD14+ CD16+) monocytes **(D)**.

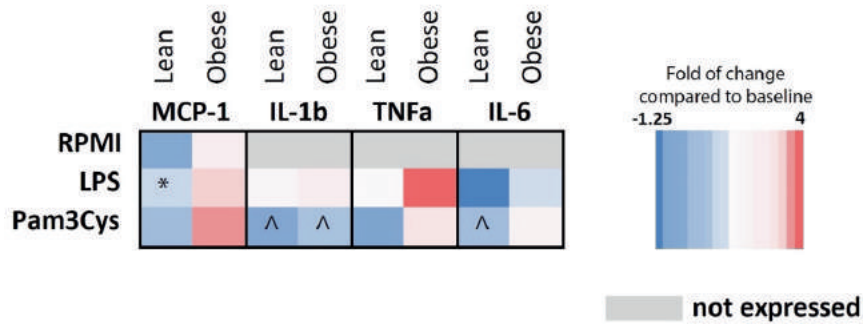


**Figure S3.** Monocytes of fasting lean and obese subjects were isolated and stimulated with RPMI (negative control), LPS (TLR4 stimulation) or Pam3Cys (TLR2 stimulation). After 24 h, concentrations of MCP-1, IL-1b, TNF-α and IL-6 were measured in the supernatant. The heatmap shows the effects of vancomycin on monocyte cytokine production. Red indicates upregulated cytokine production after treatment compared to before treatment. Blue indicates a downregulation of cytokine production after treatment compared to before treatment. n = 10 per group. ^$p$<0.1, *$p$<0.05.

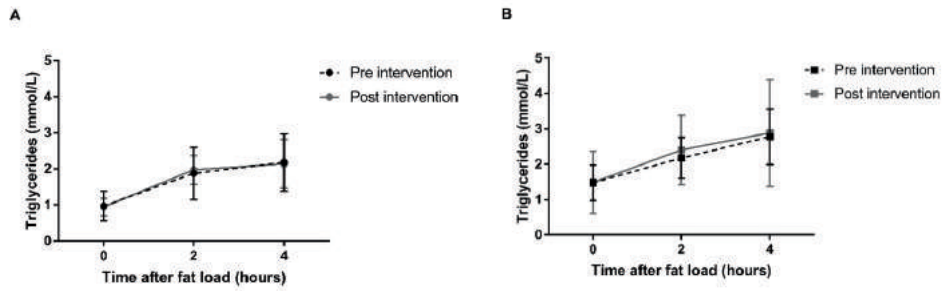


**Figure S4.** Triglycerides significantly increased after the meal in both the lean **(A)** and obese **(B)** group (one-way repeated measurements-ANOVA: lean, $p<0.001$ both pre- and post-intervention; obese, $p<0.001$ both pre- and post-intervention). There was no effect of vancomycin on postprandial triglyceride concentrations (two-way repeated measures ANOVA, time * treatment interaction: lean, $p=0.436$, obese, $p=0.483$). Graphs show mean and SD.

**Table ST1.**

| | | Lean (n = 10) | | | | | Obese (n = 10) | | | | |
|---|---|---|---|---|---|---|---|---|---|---|---|
| | | t = 0 | t = 2 | t = 4 | *p* meal | *p* inter-vention | t = 0 | t = 2 | t = 4 | *p* meal | *p* inter-vention |
| **LBP** | Pre | 10.44 (1.46) | 10.55 (1.23) | 10.99 (1.50) | 0.096 | 0.128 | 12.03 (2.55) | 11.79 (1.97) | 11.86 (1.94) | 0.623 | 0.332 |
| | Post | 11.04 (2.30) | 10.93 (1.58) | 10.76 (1.58) | 0.556 | | 11.86 (2.61) | 11.39 (2.37) | 11.87 (2.50) | 0.037 | |
| **IL-6** | Pre | 0.83 (1.82) | 1.15 (2.08) | 0.95 (1.76) | 0.153 | 0.347 | 2.03 (2.57) | 3.20 (5.67) | 2.66 (3.84) | 0.417 | 0.339 |
| | Post | 1.07 (1.56) | 0.80 (1.46) | 0.87 (1.46) | 0.496 | | 2.16 (3.04) | 1.96 (3.04) | 2.21 (3.34) | 0.347 | |
| **MCP-1** | Pre | 44.2 (25.5) | 32.0 (27.5) | 42.4 (15.9) | 0.053 | 0.084 | 111.5 (107.9) | 69.5 (101.6) | 69.6 (94.6) | 0.013 | 0.488 |
| | Post | 50.3 (21.9) | 40.9 (22.6) | 58.7 (26.5) | 0.037 | | 91.6 (118.4) | 73.4 (76.7) | 91.3 (100.0) | 0.286 | |

Plasma LBP and cytokines fasting at fasting, 2 and 4 h after an oral fat load before (pre) and after (post) vancomycin treatment. IL-6, Interleukin-6. LBP, lipopolysaccharide-binding protein; MCP-1, monocyte chemoattractant protein 1; *p* meal represents differences between t = 0 h, t = 2 h, and t = 4 h (one-way repeated measures ANOVA). *P* intervention represents the overall intervention effect (two-way rm-ANOVA, time * treatment interaction). Data are mean (SD).

**Table ST2.**

| | | Lean (n = 10) | | | | | Obese (n = 10) | | | | |
|---|---|---|---|---|---|---|---|---|---|---|---|
| | | t = 0 | t = 2 | t = 4 | *p* meal | *p* inter-vention | t = 0 | t = 2 | t = 4 | *p* meal | *p* inter-vention |
| Leukocytes (10E9/L) | Pre | 5.3 (0.8) | 5.8 (0.8) | 6.0 (0.7) | 0.006 | 0.478 | 6.0 (1.1) | 6.9 (1.0) | 7.3 (1.0) | 0.001 | 0.753 |
| | Post | 5.4 (1.0) | 6.1 (1.0) | 6.4 (1.1) | 0.001 | | 6.1 (0.6) | 6.7 (0.6) | 7.2 (0.9) | 0.003 | |
| Neutrophils (10E9/L) | Pre | 2.7 (0.7) | 3.3 (0.8) | 3.5 (0.9) | <0.001 | 0.886 | 3.5 (1.1) | 4.3 (1.2) | 4.4 (0.8) | 0.008 | 0.543 |
| | Post | 3.0 (0.9) | 3.6 (1.0) | 3.7 (1.0) | 0.003 | | 3.5 (0.7) | 4.0 (0.7) | 4.1 (0.7) | <0.001 | |
| Lymphocytes (10E9/L) | Pre | 1.9 (0.4) | 1.8 (0.4) | 1.9 (0.4) | 0.233 | 0.104 | 1.8 (0.4) | 1.9 (0.5) | 2.2 (0.6) | 0.010 | 0.825 |
| | Post | 1.7 (0.3) | 1.8 (0.3) | 1.9 (0.3) | 0.095 | | 1.7 (0.5) | 1.9 (0.5) | 2.2 (0.7) | <0.001 | |
| Monocytes (10E9/L) | Pre | 0.5 (0.1) | 0.5 (0.1) | 0.5 (0.1) | 0.748 | 0.383 | 0.5 (0.2) | 0.5 (0.2) | 0.6 (0.2) | 0.168 | 0.267 |

| | | | | | | | | | | | |
|---|---|---|---|---|---|---|---|---|---|---|---|
| | Post | 0.5 (0.1) | 0.5 (0.1) | 0.5 (0.1) | 0.227 | | 0.5 (0.1) | 0.5 (0.1) | 0.6 (0.1) | 0.016 | |

Blood differentiated leukocyte counts at fasting, 2 and 4 hours after an oral fat load before (pre) and after (post) vancomycin treatment. *P* meal represents differences between t = 0 h, t = 2 h, and t = 4 h (one-way rm-ANOVA). *P* intervention represents the overall intervention effect (two-way rm-ANOVA, time * treatment interaction). Data are mean (SD).

**Table ST3.**

| | | Lean (n = 10) | | | | Obese (n = 10) | | | |
|---|---|---|---|---|---|---|---|---|---|
| | | t = 0 | t = 4 | *p* meal | *p* intervention | t = 0 | t = 4 | *p* meal | *p* intervention |
| Monocyte type 1 (%) | Pre | 89.9 (3.7) | 88.9 (3.6) | 0.154 | 0.633 | 85.8 (6.2) | 86.4 (5.2) | 0.313 | 0.778 |
| | Post | 91.2 (3.9) | 90.4 (3.4) | 0.304 | | 84.3 (9.0) | 85.6 (4.0) | 0.695 | |
| Monocyte type 2 (%) | Pre | 2.5 (0.8) | 2.6 (0.6) | 0.778 | 0.185 | 3.7 (1.4) | 3.1 (1.4) | 0.006 | 0.064 |
| | Post | 2.4 (1.2) | 2.7 (1.0) | 0.186 | | 3.6 (1.6) | 3.3 (1.7) | 0.278 | |
| Monocyte type 3 (%) | Pre | 7.2 (3.0) | 8.1 (2.9) | 0.159 | 0.225 | 10.2 (5.6) | 10.3 (4.8) | 0.804 | 0.203 |
| | Post | 6.2 (3.0) | 6.6 (2.5) | 0.456 | | 9.2 (4.7) | 10.8 (3.8) | 0.134 | |
| Monocyte CCR2 expression (AU) | Pre | 628 (194) | 667 (184) | 0.187 | 0.543 | 617 (196) | 708 (190) | 0.014 | 0.124 |
| | Post | 611 (149) | 668 (119) | 0.109 | | 518 (146) | 543 (143) | 0.262 | |

Monocyte type distribution based on flow cytometry at fasting and 4 hours after an oral fat load before (pre) and after (post) vancomycin treatment. Monocytes were categorized as type 1 (classical), type 2 (intermediate) or type 3 (non-classical) based on CD14/CD16 expression (type 1, CD14++ CD16; type 2, CD14++CD16+; type 3, CD14+CD16+). CCR2, C-C chemokine receptor type 2. *P* meal represents differences between t = 0 h and t = 4 h (paired t-test). *P* intervention represents difference in delta (t = 4 h minus t = 0 h) between pre and post intervention (paired t-test). Data are mean (SD).

**Table ST4.**

| | | Lean (n = 10) | | | | | Obese (n = 10) | | | | |
|---|---|---|---|---|---|---|---|---|---|---|---|
| | | t = 0 | t = 2 | t = 4 | *p* meal | *p* intervention | t = 0 | t = 2 | t = 4 | *p* meal | *p* intervention |
| Total cholesterol (mmol/L) | Pre | 4.19 (0.59) | 4.37 (0.63) | 4.41 (0.66) | <0.001 | 0.663 | 5.49 (0.84) | 5.62 (0.94) | 5.64 (0.89) | 0.060 | 0.575 |
| | Post | 4.34 (0.72) | 4.53 (0.73) | 4.53 (0.73) | <0.001 | | 5.38 (0.82) | 5.56 (0.90) | 5.62 (0.90) | 0.009 | |
| HDL-c (mmol/L) | Pre | 1.23 (0.26) | 1.30 (0.28) | 1.19 (0.25) | 0.003 | 0.658 | 1.25 (0.18) | 1.24 (0.21) | 1.15 (0.21) | <0.001 | 0.407 |
| | Post | 1.27 (0.22) | 1.36 (0.27) | 1.21 (0.27) | 0.001 | | 1.19 (0.22) | 1.24 (0.16) | 1.13 (0.28) | 0.047 | |
| LDL-c (mmol/L) | Pre | 2.51 (0.46) | 2.21 (0.49) | 2.23 (0.49) | <0.001 | 0.490 | 3.56 (0.91) | 3.39 (0.90) | 3.22 (0.80) | 0.005 | 0.419 |
| | Post | 2.64 (0.58) | 2.26 (0.53) | 2.34 (0.55) | <0.001 | | 3.50 (0.89) | 3.23 (0.98) | 3.17 (1.00) | 0.002 | |
| Triglycerides (mmol/L) | Pre | 0.97 (0.41) | 1.87 (0.73) | 2.18 (0.80) | <0.001 | 0.436 | 1.48 (0.50) | 2.17 (0.58) | 2.78 (0.79) | <0.001 | 0.483 |
| | Post | 0.96 (0.24) | 1.97 (0.41) | 2.13 (0.67) | <0.001 | | 1.49 (0.88) | 2.40 (0.98) | 2.88 (1.51) | <0.001 | |
| Apo A1 (mg/dL) | Pre | 148 (20) | 153 (22) | 154 (22) | 0.013 | 0.732 | 149 (22) | 148 (19) | 149 (22) | 0.723 | 0.123 |
| | Post | 153 (20) | 159 (23) | 159 (23) | 0.023 | | 146 (21) | 150 (19) | 151 (20) | 0.013 | |
| Apo B (mg/dL) | Pre | 67.0 (13.4) | 69.5 (14.2) | 68.9 (14.4) | 0.002 | 0.899 | 104 (19) | 105 (22) | 105 (21) | 0.533 | 0.622 |

| | | | | | | | | | | | |
|---|---|---|---|---|---|---|---|---|---|---|---|
| | Post | 68.5 (14.1) | 71.1 (14.5) | 70.8 (14.6) | 0.004 | | 101 (21) | 103 (22) | 104 (22) | 0.083 | |

Plasma concentrations of lipids fasting and 2 and 4 h after an oral fat load before (pre) and after (post) vancomycin treatment. HDL-c, high density lipoprotein cholesterol; LDL-c, low-density lipoprotein cholesterol; n, number of patients. *P* meal represents differences between t = 0 h, t = 2 h, and t = 4 h (one-way repeated measures ANOVA). *P* intervention represents the overall intervention effect (two-way repeated measures ANOVA, time * treatment interaction). Data are mean (SD).

## Supplemental references


1. Salonen A, Nikkila J, Jalanka-Tuovinen J, Immonen O, Rajilic-Stojanovic M, Kekkonen RA, Palva A, and de Vos WM. Comparative analysis of fecal DNA extraction methods with phylogenetic microarray: effective recovery of bacterial and archaeal DNA using mechanical cell lysis. J Microbiol Methods 81: 127-134, 2010.
2. Ramiro-Garcia JH, G.D.A.; Giatsis, C.; Sipkema, D.; Zoetendal, E.G.; Schaap, P.J.; Smidt, H. NG-tax, a highly accurate and validated pipeline for analysis of 16S rRNA amplicons from complex biomes [version 1; referees: awaiting peer review]. F1000Research 5: 1791, 2016.
3. Kozich JJ, Westcott SL, Baxter NT, Highlander SK, and Schloss PD. Development of a dual-index sequencing strategy and curation pipeline for analyzing amplicon sequence data on the MiSeq Illumina sequencing platform. Appl Environ Microbiol 79: 5112-5120, 2013.

# *Part II*

*Lipid-induced metabolic reprogramming*

# Chapter 7

## Metabolism and the road to inflammation and atherosclerosis

Johan G. Schnitzler*, Lubna Ali* and Jeffrey Kroon

*Current Opinion in Lipidology. 2018 Dec;29(6):474-480*

Abstract

**Purpose of review** Evidence accumulates suggesting that cellular metabolic alterations fuel and dictate the inflammatory state of cells. In this review we provide an overview of the observed metabolic reprogramming in endothelial cells and innate immune cells upon interaction with modified lipoproteins, thereby contributing to the progression of atherosclerosis.

**Recent findings** Inflammatory endothelial cells at sites exposed to disturbed flow patterns show increased glycolytic activity. Atherogenic factors further enhance these metabolic changes by upregulating the mitochondrial energy production and thereby facilitating increased energy expenditure. Metabolic alterations are pivotal for monocyte and macrophage function as well. Exposure to atherogenic particles such as oxidized phospholipids lead to a regulatory metabolic pro-inflammatory phenotype, mediated via Toll-like receptor (TLR) 2 and the transcription factor erythroid 2-related factor (Nrf) 2 signaling. Translational studies underpinned the importance of metabolic alterations, since high-risk atherosclerotic plaques in the carotids showed an increased glycolytic signature.

**Summary** Alterations in cellular metabolism play an important role in controlling and steering the inflammatory state of both endothelial cells and immune cells. Targeting glycolysis may therefore provide an interesting route to attenuate the progression of atherosclerosis.

**Keywords:** Immunometabolism, metabolism, inflammation, atherosclerosis, inducible glycolysis

## Introduction

*General cellular metabolism*

Cellular metabolism comprises an intricate network of thousands of different metabolites and enzymes necessary for the generation of nucleic acids, proteins, lipids, carbohydrates and energy for the cell. Metabolism plays a pivotal role in maintaining homeostasis, proliferation and cellular activation. It has been generally acknowledged that perturbations in metabolic pathways underlie a wide variety of diseases. The need to produce energy in the form of ATP for cellular function is essential for both quiescent as well as activated cells and is tightly orchestrated by the integrated metabolic pathways of glycolysis, the tricarboxylic acid (TCA) cycle and the pentose-phosphate pathway (PPP).

*What have we learned so far?*

Early studies in the field of oncology provided researchers with fundamental insights on how alterations in the cell's metabolism steers the fate of the cell. Where glucose via the glycolytic pathway feeds into the TCA cycle and thereby drives mitochondrial oxidative phosphorylation (OXPHOS), highly proliferative tumor cells in cancer rely predominantly on glycolysis. This is remarkable, since sufficient oxygen is present to sustain the OXPHOS pathway. This phenomenon is known as 'the Warburg effect' or aerobic glycolysis [1,2]. Although OXPHOS generates adenosine triphosphate (ATP) more efficiently when compared to aerobic glycolysis, the latter is able to provide the cell not only with ATP, but also with metabolites that serve as building blocks required for proliferation and synthesis of other cellular products. In addition, recent findings show that the Warburg is also crucial in endothelial cells (EC) cells, monocytes and macrophages [3,4]. This interplay between metabolism and immunology, also known as immunometabolism, is rapidly emerging due to recent insights revealing that cellular metabolism has a major impact on the functional behavior of cells.

Despite this significant progress in the field of oncology, the role of cellular- and immunometabolism in the cardiovascular arena remains largely unexplored. In atherosclerosis, immune cells and ECs drive this chronic lipid-driven disease, hallmarked by low-grade inflammation of the arterial wall [5,6]. In this review, we provide an overview of the recent literature describing the role of atherogenic lipoproteins in affecting metabolic reprogramming of both macrophages and endothelial cells and thereby contributing to the progression of atherosclerosis.

## Metabolism determines the fate of endothelial cells

Pioneering research by the group of Carmeliet showed that glycolysis and not OXPHOS is the main source of ATP during angiogenic sprouting of ECs and even show a high glycolytic flux when quiescent. In agreement with this, it was shown that ECs have relatively low mitochondrial content (2-6% of total cytoplasm volume). This substantiates the finding why ECs rely on glycolysis to generate 2 ATP molecules and lactate per glucose molecule [7,8] and underpin the importance of glycolysis as primary

energy source in these cells [9]. However, the role of endothelial cell metabolism in the context of cardiovascular disease, especially the role of EC glycolysis in dictating disease progression, remains elusive to date.

Previous studies substantiated that vulnerable atherogenic regions, predominantly found near branch points and bifurcations are characterized by low shear stress or a disturbed (non-laminar) flow patterns [10–12]. Regions exposed to low shear stress patters were associated with alterations in endothelial cells (EC) metabolism and dysfunction in human umbilical vein ECs (HUVECs) [13,14]. Feng and colleagues showed that these atheroprone regions show increased glycolysis, marked by increased expression of the glycolytic regulators hexokinase (HK) 2, enolase 2, glucose transporter (GLUT) 1 and 6-phosphofructo-2-kinase/fructose-2,6-biphosphatase (PFKFB) 3; and (as a direct measurement for glycolysis) an increased extracellular acidification rate (ECAR). Furthermore, IκBα overexpression in ECs led to diminished nuclear factor κB (NFκB) activity and reduced hypoxia-inducible factor (HIF)1α expression, a regulator allowing rapid ATP generation [15,16]. Together this implies a direct link between the endothelial metabolic and inflammatory axis. In addition, the carotid arteries of hypercholesterolemic *ApoE*$^{-/-}$ mice displayed a distinct glycolytic phenotype (e.g. increased mRNA levels of HK2, enolase 2, GLUT1 and PFKFB3). This coincided with a 50% increased lesion size in the carotid arteries compared to mice with an endothelial specific deletion of HIF1α (HIF1α$^{EC\text{-}cKO}$ *ApoE*$^{-/-}$) which thereby validated that metabolic alterations underlie experimental atherosclerotic progression *in vivo* [13]. In summary, these data support the concept that the inflammatory NFκB -and metabolic HIF1α -axis are of utmost importance in atherogenesis. Considering the prominent role of HIF1a and NFkB, these data signify that inhibiting increased glycolysis may serve as an interesting target in order to reduce inflammation and thereby atherosclerosis.

By combining experimental data with a systems biology approach, Hitzel *et al* constructed molecular causal network models in order to study EC metabolism and thereby to predict key molecular drivers of inflammation [17,18]. Via this approach the authors sought to investigate the metabolic response of human aortic ECs (HAECs) to oxidized 1-palmitoyl-2-arachidonoyl-sn-glycero-3-phosphocholine (oxPAPC) [19]. The oxidized lipid epitopes on oxPAPC serve as endogenous danger-associated molecular patterns (DAMP) recognized by various receptors expressed by innate immune cells, which will be described in the next section [20,21]. OxPAPC was found to perturb the amino acid metabolism of HAECs, regulated via mitochondrial methylenetetrahydrofolate dehydrogenase/cyclohydrolase (MTHFD2) leading to increased glycine formation. *In vivo* MTHFD2 expression was increased in both the carotid arteries of *ApoE-/-* mice as well as in HAECs that were *ex vivo* stimulated with atherogenic lipid particles isolated from stable CAD patients. Based on this, it appears that glycolysis is not the sole driver of EC cell dysfunction, as mitochondrial activity plays a pivotal role dictating the phenotype of ECs (Figure 1). The increase in glycolysis during endothelial cell proliferation, angiogenesis or during endothelial

dysfunction (as described above) or its inhibition, leads to uncoupling of OXPHOS. In addition, some of the glucose intermediates can enter the PPP via glucose-6-phosphate where oxidative PPP can produce nicotinamide adenine dinucleotide phosphate. Via this pathway, oxidative PPP can scavenge reactive oxygen species (ROS), reduce oxidative stress (Spolarics Z. 1997) and can furthermore fuel nitric oxide (NO) synthesis.

The inflammatory phenotype of the endothelium, caused by flow disturbances and (modified) lipoproteins facilitates the adhesion and migration of immune cells such as monocytes. Upon migration through the vessel wall, monocytes are able to internalize lipids via, amongst others, scavenger receptor SR-A and CD36 and differentiate to macrophages [16,22,23].

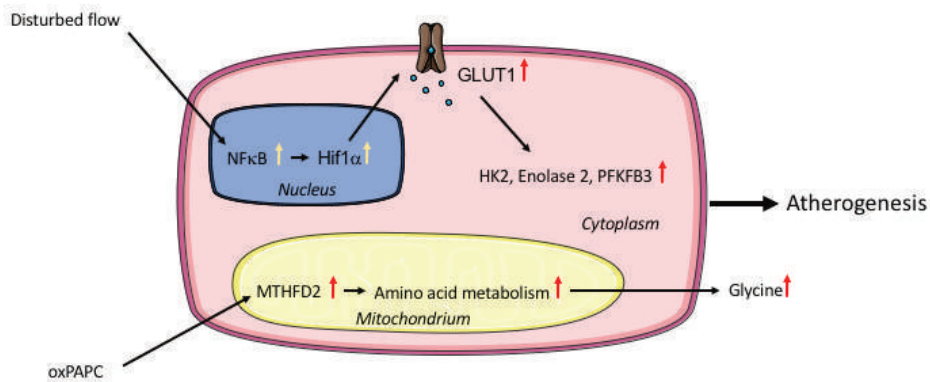


**Figure 1. Flow disturbance and OxPAPC cause altered endothelial cell metabolism.**
Disturbed flow cause increased glycolysis via NFκB and HIF1α for subsequent increased expression of the glycolytic regulators HK 2, enolase 2, GLUT1 and PFKFB3. This induced NFκB-HIF1α-axis increases endothelial inflammation which contributes to atherosclerotic disease development. On the other hand, endothelial mitochondrial metabolism is induced upon OxPAPC exposure. OxPAPC increases MTHFD2, which in turn leads to increased amino acid metabolism as glycine production is increased. Both increased glycolysis as mitochondrial activity contribute to the progression of atherosclerosis.
*OxPAPC, oxidized 1-palmitoyl-2-arachidonoyl-sn-glycero-3-phosphocholine; NFκB, nuclear factor κ B; HIF1α, hypoxia-inducible factor 1α; HK2, hexokinase 2; GLUT1, glucose transporter 1; PFKFB3, 6-phosphofructo-2-kinase/fructose-2,6-biphosphatase 3; MTHFD2, methylenetetrahydrofolate dehydrogenase/cyclohydrolase.*

## Macrophages in atherosclerosis

### *Metabolic rewiring in macrophages*

Generally, macrophage show two different phenotypes: classically versus alternatively activated macrophages. Classically activated macrophages display pro-inflammatory properties fuelled by primarily by glycolysis, whereas alternatively activated macrophages are associated with anti-inflammatory processes driven by OXPHOS [24]. Interestingly, the plasticity of macrophages can be explained by their ability to undergo metabolic rewiring depending on signals from their micro-environment [25]. In atherosclerosis, hyperlipidaemia and hypoxia are dominant factors that influence the

metabolic activation of macrophages residing in atherosclerotic plaques. Hypoxic conditions in plaques cause stabilization of transcription factor HIF1α and increased glycolysis by up regulating glucose transporter GLUT1. Furthermore, HIF1α induces the expression of the key glycolytic enzymes HK2 and pyruvate dehydrogenase kinase 1 (PDK1), driving glycolytic metabolism [26] and hence, functionally, increased glycolytic activity [27]. However, the importance of HIF1α in atherosclerosis was further established by a myeloid specific knock-down of HIF1α in *Ldlr*$^{-/-}$ mice [28], leading to reduced atherosclerotic plaque formation [29]. [30]. Moreover, metabolically rewired macrophages residing in plaque regions furthermore showed altered lipid metabolism. Finally, Bekkering et al., reported increased glycolytic activity (increased mRNA levels of HK2 and PFKFB3) in monocytes derived from patients with severe coronary artery disease (CAD) (REF Siroon 2016), underscoring the importance of the metabolic rewiring towards increased glycolysis in the context of atherosclerosis.

*Oxidized lipids elicit a Mox macrophage phenotype*

Accumulation of modified lipids causes macrophages to differentiate into foam cells. Oxidation of Apo-B-containing particles seems to be the key inductor of a pro-inflammatory phenotype observed in macrophages. Oxidation of Apo-B-containing particles occurs in a non-enzymatic fashion, creating oxidized epitopes on lipids serving as DAMPs. These are recognized by pattern recognition receptors (PRR) such as SR-A, CD36, TLR2, TLR4 and CD14 present on innate immune cells [20,21](REF TOEVOEGEN). To date, the exact pathophysiological effects of oxidized phospholipids (OxPLs) are unknown and no natural occurring enzyme inhibitors or small molecules neutralizing or inhibiting oxidation have been described. Work by Leitinger et al. revealed that OxPL stimulated macrophages acquire a unique phenotype characterized by increased expression of redox regulated genes Srx1, Gclc, Gclm, Txnrd1 and HO-1. These macrophages are also known as Mox macrophages [31]. An important step in acquiring this phenotype is that during oxidative stress, Nrf2 translocates to the nucleus and induces transcription of antioxidant genes such as HO-1. This in turn drives the synthesis of antioxidants glutamate-cysteine ligase, glutathione S-transferase and Txnrd1 in order to cope with the increased levels of oxygen radicals [32]. In line, with this, Serbulea et al., studied the metabolic response of macrophages upon OxPL or OxPAPC stimulation. They revealed that both OxPAPC and OxPL stimulated macrophages exert pro-inflammatory features, however, not to the same extent as classically activated macrophages. Oxidized lipids drive Mox macrophages to glutathione synthesis. Additionally, OxPAPC induces the expression of GLUT1, suggesting increased glucose metabolism. Remarkably, ECAR was shown to be significantly reduced in OxPAPC stimulated cells. However, pre-treatment of bone marrow derived macrophages (BMDMs) with 2-deoxy glucose (2DG) -a glycolytic inhibitor- abolished OxPAPC induced Ho1, Srxn1 and Txnrd1 expression. These results imply an important role for glucose metabolism in anti-oxidant production. These data indicate

that Mox macrophages rely on glycolytic flux to produce intermediate metabolites to fuel the PPP for anti-oxidant production rather than lactate production as seen in classically activated macrophages. In these macrophages, HIF1α stabilization induces IL-1β production and supports pro-inflammatory properties. However, BMDMs from HIF1α KO mice express increased IL-1β mRNA expression upon OxPAPC stimulation, indicating a pro-inflammatory phenotype independent of HIF1α [33]. In 2008, Dennehy et al., showed that spleen tyrosine kinase (Syk) induced cytokine production and more recently, Syk has been implicated in the production of pro-inflammatory cytokines through TLR2 signaling [34]. Indeed, OxPAPC challenged BMDMs from Syk deficient mice failed to induce inflammatory gene expression while anti-oxidant related genes remained unaffected. Moreover, inhibition of Syk using the tyrosine kinase inhibitor piceatannol eliminated OxPAPC-induced inflammatory gene expression [33]. Further relevance of OxPL-induced inflammation came from landmark studies by Tsimikas and Witztum in which they revealed the importance of the antibody E06 in neutralizing PC head groups [35]. Targeting these PC head groups with E06 in an atherosclerotic mouse model led to a striking 57-28% reduction in atherosclerosis after 4, 7 and 12 months. In addition, *in vivo* uptake of labeled-oxLDL by macrophages and its consequent inflammatory properties were markedly reduced in E06 transgenic mice. Finally, macrophages derived from *Ldlr*$^{-/-}$ mice displayed a phenotype associated with classical activated macrophages whereas, macrophages from *Ldlr*$^{-/-}$-E06 mice showed features of alternatively activated macrophages [36].
In summary, these data indicate that the importance of the HIF1α-pathway in the metabolism-inflammation-axis in both monocytes as macrophages. Furthermore, pro-inflammatory Mox macrophages rely on glycolytic flux to fuel the PPP for anti-oxidant production and thereby discriminates them from classically activated macrophages (Figure 2).

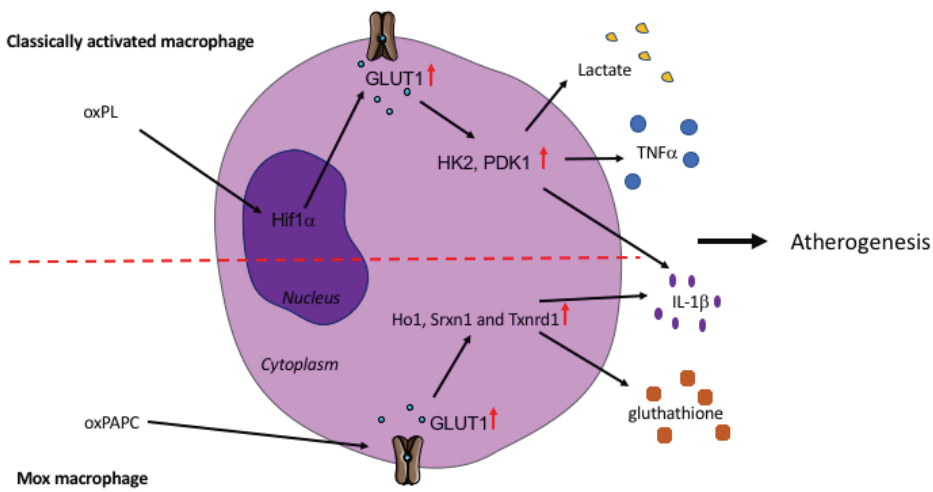

**Figure 2. OxPL and OxPAPC-induced activation of macrophages.** Classically activated macrophages initiate HIF1α stabilization in the nucleus. Subsequent upregulation of GLUT1 is induced for the uptake of glucose which in turn increases glycolysis via HK2 and PDK1 expression. This leads to increased production of pro-inflammatory cytokines TNFα and IL-1β. OxPAPC-activated Mox macrophages are independent of HIF1α and its pathway comprises increased expression of Ho1, Srxn1 and Txnrd1 in order to produce IL-1β and gluthathione. Despite metabolic differences, both macrophage subtypes ultimately attribute to the progression of atherosclerosis.
*OxPL, oxidized phospholipids; OxPAPC, oxidized 1-palmitoyl-2-arachidonoyl-sn-glycero-3-phosphocholine; HIF1α, hypoxia-inducible factor 1α; GLUT1, glucose transporter 1; HK2, hexokinase 2; PDK1, pyruvate dehydrogenase kinase 1; TNFα, tumour necrosis factor α; IL-1β, interleukin-1β*

## Clinical evidence for altered metabolism in atherosclerotic cardiovascular disease

The majority of lipoproteins undergo oxidative modification in the intima. However, another lipoprotein, lipoprotein(a) [Lp(a)] is the main carrier of OxPLs in the blood circulation [37]. Lp(a), a low-density (LDL)-like particle covalently bound to the hydrophilic glycoprotein apolipoprotein(a) [apo(a)](Dube, Curr. Opin. Lipidol. 2012; Hoover-Plow, metabolism, 2013), is nowadays been widely acknowledged to be an independent and causal risk factor for cardiovascular disease (CVD) (Nordestgaard, Eur Heart Journal, 2010). Twenty percent of the general population has elevated Lp(a) levels (>50 mg/dL) [38–41]. Patients with elevated Lp(a) undergoing $^{18}$F-fluorodeoxyglucose (FDG) positron emission tomography/computed tomography (CT) imaging, a glucose analogue that is being used as surrogate marker for CVD progression [42], showed increased $^{18}$F-FDG uptake in the carotid arteries and aorta [43]. This clearly shows that athero-prone areas are metabolically active and that increased metabolism may cause the state of inflammation in patients with elevated levels of Lp(a). One can envision that this increased glycolytic activity in athero-prone areas, shown by $^{18}$F-FDG PET/CT imaging, is an important regulator of other lipid driven diseases as well. Furthermore, single photon emission CT/CT imaging of patients with elevated Lp(a) revealed intimal accumulation of autologous peripheral blood mononuclear cells . It must be noted however, that metabolic alterations in these atherogenic areas were not addressed in this study (REF Fleur). Previously it was shown that $^{18}$F-FDG uptake in macrophages is strongly related to increased glycolysis. These macrophages were marked by both elevated GLUT1 expression and lactate production upon oxLDL exposure *in vitro* which was orchestrated by HIF1α [44]. These data corroborate with a previous study revealing a shift to glycolytic metabolism in activated leukocytes of CAD patients [45]. In summary, this data suggests that Lp(a)-induced inflammation is closely intertwined with increased glycolysis. Although the inflammatory properties of Lp(a) have gained increasing interest, it would be of great value to unravel its contribution to immunometabolism in atherosclerosis.

Recently, the importance of glycolysis was highlighted in a translational setting by Tomas and colleagues who highlighted the importance of cellular (immune)metabolism in high vs. low risk atherosclerotic plaques from patients after endarterectomy [46]. First, discrimination between the two plaque phenotypes revealed that high risk atherosclerotic plaques were strongly associated with clinical symptoms and characterized by histological evidence of vulnerability. Second, these high-risk plaques showed an inflammatory signature characterized by increased levels of

cytokines IL-6, IL-18 and IL-1β, chemokines monocyte chemoattractant 1 and macrophage inflammatory protein-1B, although levels of TNF did not differ. This inflammatory phenotype coincided with increased metabolic activity, in particular glycolysis, as measured by decreased hexose sugars and elevated lactate production. This strongly suggests enhanced glucose uptake in high-risk plaques, attributed to increased expression of the key-glycolytic transcription factors Myc and HIF1α. Interestingly, the net intracellular ATP content between low- and high-risk plaques did not differ, indicating a glycolytic switch rather than a net increase in metabolic activity. This data implies that inducible glycolysis in atherosclerotic plaques is an interesting target to counter the process of atherosclerosis in humans.

### Targeting increased glycolysis as potential therapeutic strategy to reduce endothelial inflammation

*In vivo* studies in mice showed that genetic and pharmacological blockade of PFKFB3 by 3-(3-pyridinyl)-1-(4-pyridinyl)-2-propen-1-one (3PO), a key-driver of endothelial glycolysis (only decreases glycolysis partial and transient by ~40%) did not alter tumor growth, but did however reduce cancer cell invasion, intravasation and metastasis by normalizing tumor vessels. Daily intraperitoneal injections with 3PO (50 mg/kg/day) for 15 d in C57BL/6 mice furthermore did not induce striking differences in biochemical blood parameters (liver, renal and hematological parameters) nor it induced histological abnormalities. These data were validated in a phase I clinical trial where PFK158 treatment, the first-in-human and first-in-class PFKFB3 inhibitor, reduced the growth of advanced solid tumors. It is important to note that only <2,5% of the total ATP in the body is produced by glycolysis, suggesting that most other cells rely on non-glycolytic metabolic pathways for ATP production. These data imply that inducible glycolysis in atherosclerotic plaques could be an interesting target to counter the process of atherosclerosis in humans. In summary, as Carmeliet and his team also states, it remains crucial to assess contra-indications and assessment of potential toxicity based on partial and transient glycolytic inhibitions.

### Conclusion

Metabolic transformations in ECs, monocytes and macrophages may have a profound impact on the inflammatory phenotype of these cells, determining their contribution to progression of atherosclerosis. The implementation of lipid-lowering therapies is hallmarked by a significant residual risk in patients at increased cardiovascular risk, partly attributed to the low grade chronic inflammation [47] [48]. The CANTOS trial revealed that targeting IL-1β with Canakinumab reduced the risk for recurrent events, indicating that anti-inflammatory strategies may hold a great promise [49]. Since inflammation and metabolic alteration are closely intertwined in both immune cells as well as endothelial cells, therapeutic targets aiming at altering cellular metabolism of activated cells may hold a great potential in the treatment of CV-patients.

Key points:

- Despite the low mitochondrial content in endothelial cells, both mitochondrial activation and increased glycolysis could be crucial in driving CVD, since its activity is increased in CVD patients.
- Different types of oxidized phospholipids are able to induce pro-inflammatory macrophages displaying distinct metabolic phenotypes.
- Atherogenic regions of the arteries are characterized by increased metabolic activity, where high-risk atherosclerotic plaques show an enhanced a glycolytic signature.

Acknowledgements

We would like to thank Prof. E.S.G Stroes and Prof. A.K. Groen for critically reading the manuscript.

Final support and sponsorship

Funding was provided by European Union's Horizon 2020 research and innovation program under grant agreement No 667837 (REPROGRAM). J.K received a VENI grant from ZonMW (91619098) and is supported by the Amsterdam Cardiovascular Sciences (ACS) Postdoc Fellowship (2017).

Conflict of interest

There are no conflicts of interest.

## References

• of special interest
•• of outstanding interest


1. Andrejeva G, Rathmell JC. Similarities and Distinctions of Cancer and Immune Metabolism in Inflammation and Tumors. *Cell Metab* United States; 2017;**26**:49–70.
2. Warburg O, Wind F, Negelein E. THE METABOLISM OF TUMORS IN THE BODY. *J Gen Physiol* United States; 1927;**8**:519–530.
3. Stienstra R, Netea-Maier RT, Riksen NP, Joosten LAB, Netea MG. Specific and Complex Reprogramming of Cellular Metabolism in Myeloid Cells during Innate Immune Responses. *Cell Metab* United States; 2017;**26**:142–156.
4. Koelwyn GJ, Corr EM, Erbay E, Moore KJ. Regulation of macrophage immunometabolism in atherosclerosis. *Nat Immunol* United States; 2018;**19**:526–537.
5. Nilsson J. Atherosclerotic plaque vulnerability in the statin era. *Eur Heart J* England; 2017;**38**:1638–1644.
6. Geovanini GR, Libby P. Atherosclerosis and inflammation: overview and updates. *Clin Sci (Lond)* England; 2018;**132**:1243–1252.
7. Mertens S, Noll T, Spahr R, Krutzfeldt A, Piper HM. Energetic response of coronary endothelial cells to hypoxia. *Am J Physiol* United States; 1990;**258**:H689-94.
8. Dobrina A, Rossi F. Metabolic properties of freshly isolated bovine endothelial cells. *Biochim Biophys Acta* Netherlands; 1983;**762**:295–301.
9. Bock K De, Georgiadou M, Schoors S, Kuchnio A, Wong BW, Cantelmo AR, Quaegebeur A, Ghesquiere B, Cauwenberghs S, Eelen G, Phng L-K, Betz I, Tembuyser B, Brepoels K, Welti J, Geudens I, Segura I, Cruys B, Bifari F, Decimo I, Blanco R, Wyns S, Vangindertael J, Rocha S, Collins RT, Munck S, Daelemans D, Imamura H, Devlieger R, Rider M, et al. Role of PFKFB3-driven glycolysis in vessel sprouting. *Cell* United States; 2013;**154**:651–663.
10. Abe J, Berk BC. Novel mechanisms of endothelial mechanotransduction. *Arterioscler Thromb Vasc Biol* United States; 2014;**34**:2378–2386.
11. Malek AM, Alper SL, Izumo S. Hemodynamic shear stress and its role in atherosclerosis. *JAMA* United States; 1999;**282**:2035–2042.
12. Chiu J-J, Chien S. Effects of disturbed flow on vascular endothelium: pathophysiological basis and clinical perspectives. *Physiol Rev* United States; 2011;**91**:327–387.
13. Feng S, Bowden N, Fragiadaki M, Souilhol C, Hsiao S, Mahmoud M, Allen S, Pirri D, Ayllon BT, Akhtar S, Thompson AAR, Jo H, Weber C, Ridger V, Schober A, Evans PC. Mechanical Activation of Hypoxia-Inducible Factor 1alpha Drives Endothelial Dysfunction at Atheroprone Sites. *Arterioscler Thromb Vasc Biol* United States; 2017;**37**:2087–2101.
14. Dai G, Kaazempur-Mofrad MR, Natarajan S, Zhang Y, Vaughn S, Blackman BR, Kamm RD, Garcia-Cardena G, Gimbrone MAJ. Distinct endothelial phenotypes evoked by arterial waveforms derived from atherosclerosis-susceptible and -resistant regions of human vasculature. *Proc Natl Acad Sci U S A* United States; 2004;**101**:14871–14876.
15. Bock K De, Georgiadou M, Carmeliet P. Role of endothelial cell metabolism in vessel sprouting. *Cell Metab* United States; 2013;**18**:634–647.
16. Eelen G, Zeeuw P de, Simons M, Carmeliet P. Endothelial cell metabolism in normal and diseased vasculature. *Circ Res* United States; 2015;**116**:1231–1244.
17. Makinen V-P, Civelek M, Meng Q, Zhang B, Zhu J, Levian C, Huan T, Segre A V, Ghosh S, Vivar J, Nikpay M, Stewart AFR, Nelson CP, Willenborg C, Erdmann J, Blakenberg S, O'Donnell CJ, Marz W, Laaksonen R, Epstein SE, Kathiresan S, Shah SH, Hazen SL, Reilly MP, Lusis AJ, Samani NJ, Schunkert H, Quertermous T, McPherson R, Yang X, et al. Integrative genomics reveals novel molecular pathways and gene networks for coronary artery disease. *PLoS Genet* United States; 2014;**10**:e1004502.
18. Zhu J, Zhang B, Smith EN, Drees B, Brem RB, Kruglyak L, Bumgarner RE, Schadt EE. Integrating large-scale functional genomic data to dissect the complexity of yeast regulatory networks. *Nat Genet* United States; 2008;**40**:854–861.
19. Hitzel J, Lee E, Zhang Y, Bibli SI, Li X, Zukunft S, Pfluger B, Hu J, Schurmann C, Vasconez AE, Oo JA, Kratzer A, Kumar S, Rezende F, Josipovic I, Thomas D, Giral H, Schreiber Y, Geisslinger G, Fork C, Yang X, Sigala F, Romanoski CE, Kroll J, Jo H, Landmesser U, Lusis AJ, Namgaladze D, Fleming I, Leisegang MS, et al. Oxidized phospholipids regulate amino acid metabolism through MTHFD2 to facilitate nucleotide release in endothelial cells. *Nat Commun* England; 2018;**9**:2292.
20. Lee S, Birukov KG, Romanoski CE, Springstead JR, Lusis AJ, Berliner JA. Role of phospholipid oxidation products in atherosclerosis. *Circ Res* United States; 2012;**111**:778–799.
21. Miller YI, Choi S-H, Wiesner P, Fang L, Harkewicz R, Hartvigsen K, Boullier A, Gonen A, Diehl CJ, Que X, Montano E, Shaw PX, Tsimikas S, Binder CJ, Witztum JL. Oxidation-specific epitopes are danger-associated molecular patterns recognized by pattern recognition receptors of innate immunity. *Circ Res* United States; 2011;**108**:235–248.
22. Libby P, Ridker PM, Hansson GK. Progress and challenges in translating the biology of atherosclerosis. *Nature* England; 2011;**473**:317–325.
23. Lusis AJ. Atherosclerosis. *Nature* ENGLAND; 2000;**407**:233–241.
24. Galvan-Pena S, O'Neill LAJ. Metabolic reprograming in macrophage polarization. *Front Immunol* Switzerland; 2014;**5**:420.
25. Kelly B, O'Neill LAJ. Metabolic reprogramming in macrophages and dendritic cells in innate immunity. *Cell Res* England; 2015;**25**:771–784.

26. Kim J, Tchernyshyov I, Semenza GL, Dang C V. HIF-1-mediated expression of pyruvate dehydrogenase kinase: a metabolic switch required for cellular adaptation to hypoxia. *Cell Metab* United States; 2006;**3**:177–185.
27. Chen C, Pore N, Behrooz A, Ismail-Beigi F, Maity A. Regulation of glut1 mRNA by hypoxia-inducible factor-1. Interaction between H-ras and hypoxia. *J Biol Chem* United States; 2001;**276**:9519–9525.
28. Li C, Wang Y, Li Y, Yu Q, Jin X, Wang X, Jia A, Hu Y, Han L, Wang J, Yang H, Yan D, Bi Y, Liu G. HIF1alpha-dependent glycolysis promotes macrophage functional activities in protecting against bacterial and fungal infection. *Sci Rep* England; 2018;**8**:3603.
29. Aarup A, Pedersen TX, Junker N, Christoffersen C, Bartels ED, Madsen M, Nielsen CH, Nielsen LB. Hypoxia-Inducible Factor-1alpha Expression in Macrophages Promotes Development of Atherosclerosis. *Arterioscler Thromb Vasc Biol* United States; 2016;**36**:1782–1790.
30. Bekkering S, Munckhof I van den, Nielen T, Lamfers E, Dinarello C, Rutten J, Graaf J de, Joosten LAB, Netea MG, Gomes MER, Riksen NP. Innate immune cell activation and epigenetic remodeling in symptomatic and asymptomatic atherosclerosis in humans in vivo. *Atherosclerosis* Ireland; 2016;**254**:228–236.
31. Kadl A, Meher AK, Sharma PR, Lee MY, Doran AC, Johnstone SR, Elliott MR, Gruber F, Han J, Chen W, Kensler T, Ravichandran KS, Isakson BE, Wamhoff BR, Leitinger N. Identification of a novel macrophage phenotype that develops in response to atherogenic phospholipids via Nrf2. *Circ Res* United States; 2010;**107**:737–746.
32. Itoh K, Wakabayashi N, Katoh Y, Ishii T, Igarashi K, Engel JD, Yamamoto M. Keap1 represses nuclear activation of antioxidant responsive elements by Nrf2 through binding to the amino-terminal Neh2 domain. *Genes Dev* United States; 1999;**13**:76–86.
33. Serbulea V, Upchurch CM, Ahern KW, Bories G, Voigt P, DeWeese DE, Meher AK, Harris TE, Leitinger N. Macrophages sensing oxidized DAMPs reprogram their metabolism to support redox homeostasis and inflammation through a TLR2-Syk-ceramide dependent mechanism. *Mol Metab* Germany; 2018;**7**:23–34.
34. Dennehy KM, Ferwerda G, Faro-Trindade I, Pyz E, Willment JA, Taylor PR, Kerrigan A, Tsoni SV, Gordon S, Meyer-Wentrup F, Adema GJ, Kullberg B-J, Schweighoffer E, Tybulewicz V, Mora-Montes HM, Gow NAR, Williams DL, Netea MG, Brown GD. Syk kinase is required for collaborative cytokine production induced through Dectin-1 and Toll-like receptors. *Eur J Immunol* Germany; 2008;**38**:500–506.
35. Friedman P, Horkko S, Steinberg D, Witztum JL, Dennis EA. Correlation of antiphospholipid antibody recognition with the structure of synthetic oxidized phospholipids. Importance of Schiff base formation and aldol condensation. *J Biol Chem* United States; 2002;**277**:7010–7020.
36. Que X, Hung M-Y, Yeang C, Gonen A, Prohaska TA, Sun X, Diehl C, Maatta A, Gaddis DE, Bowden K, Pattison J, MacDonald JG, Yla-Herttuala S, Mellon PL, Hedrick CC, Ley K, Miller YI, Glass CK, Peterson KL, Binder CJ, Tsimikas S, Witztum JL. Oxidized phospholipids are proinflammatory and proatherogenic in hypercholesterolaemic mice. *Nature* England; 2018;**558**:301–306.
37. Tsimikas S, Brilakis ES, Miller ER, McConnell JP, Lennon RJ, Kornman KS, Witztum JL, Berger PB. Oxidized phospholipids, Lp(a) lipoprotein, and coronary artery disease. *N Engl J Med* United States; 2005;**353**:46–57.
38. Danesh J, Collins R, Peto R. Lipoprotein(a) and coronary heart disease. Meta-analysis of prospective studies. *Circulation* United States; 2000;**102**:1082–1085.
39. Kamstrup PR, Tybjaerg-Hansen A, Steffensen R, Nordestgaard BG. Genetically elevated lipoprotein(a) and increased risk of myocardial infarction. *JAMA* United States; 2009;**301**:2331–2339.
40. Nordestgaard BG, Chapman MJ, Ray K, Boren J, Andreotti F, Watts GF, Ginsberg H, Amarenco P, Catapano A, Descamps OS, Fisher E, Kovanen PT, Kuivenhoven JA, Lesnik P, Masana L, Reiner Z, Taskinen M-R, Tokgozoglu L, Tybjaerg-Hansen A. Lipoprotein(a) as a cardiovascular risk factor: current status. *Eur Heart J* England; 2010;**31**:2844–2853.
41. Nordestgaard BG, Langsted A. Lipoprotein (a) as a cause of cardiovascular disease: insights from epidemiology, genetics, and biology. *J Lipid Res* United States; 2016;**57**:1953–1975.
42. Tarkin JM, Joshi FR, Rudd JHF. PET imaging of inflammation in atherosclerosis. *Nat Rev Cardiol* England; 2014;**11**:443–457.
43. Valk FM Van Der, Bekkering S, Kroon J, Yeang C, Bossche J Van Den, Buul JD Van, Ravandi A, Nederveen AJ, Verberne HJ, Scipione C, Nieuwdorp M, Joosten LAB, Netea MG, Koschinsky ML, Witztum JL, Tsimikas S, Riksen NP, Stroes ESG. Oxidized phospholipids on Lipoprotein(a) elicit arterial wall inflammation and an inflammatory monocyte response in humans. *Circulation* 2016;**134**.
44. Lee SJ, Thien Quach CH, Jung K-H, Paik J-Y, Lee JH, Park JW, Lee K-H. Oxidized low-density lipoprotein stimulates macrophage 18F-FDG uptake via hypoxia-inducible factor-1alpha activation through Nox2-dependent reactive oxygen species generation. *J Nucl Med* United States; 2014;**55**:1699–1705.
45. Shirai T, Nazarewicz RR, Wallis BB, Yanes RE, Watanabe R, Hilhorst M, Tian L, Harrison DG, Giacomini JC, Assimes TL, Goronzy JJ, Weyand CM. The glycolytic enzyme PKM2 bridges metabolic and inflammatory dysfunction in coronary artery disease. *J Exp Med* United States; 2016;**213**:337–354.
46. Tomas L, Edsfeldt A, Mollet IG, Perisic Matic L, Prehn C, Adamski J, Paulsson-Berne G, Hedin U, Nilsson J, Bengtsson E, Goncalves I, Bjorkbacka H. Altered metabolism distinguishes high-risk from stable carotid atherosclerotic plaques. *Eur Heart J* England; 2018;**39**:2301–2310.
47. Ridker PM. Residual inflammatory risk: addressing the obverse side of the atherosclerosis prevention coin. *Eur Heart J* England; 2016;**37**:1720–1722.
48. Ridker PM, Thuren T, Zalewski A, Libby P. Interleukin-1beta inhibition and the prevention of recurrent cardiovascular

events: rationale and design of the Canakinumab Anti-inflammatory Thrombosis Outcomes Study (CANTOS). *Am Heart J* United States; 2011;**162**:597–605.

49. Ridker PM, MacFadyen JG, Everett BM, Libby P, Thuren T, Glynn RJ. Relationship of C-reactive protein reduction to cardiovascular event reduction following treatment with canakinumab: a secondary analysis from the CANTOS randomised controlled trial. *Lancet (London, England)* England; 2018;**391**:319–328.

# Chapter 8

## Atherogenic lipoprotein(a) increases vascular glycolysis, thereby facilitating inflammation and leukocyte extravasation

Johan G. Schnitzler, Renate M. Hoogeveen, Lubna Ali, Koen H.M. Prange, Farahnaz Waissi, Michel van Weeghel, Julian C. Bachmann, Miranda Versloot, Matthew J. Borrelli, Calvin Yeang, Dominique P.V. De Kleijn, Riekelt H. Houtkooper, Marlys L. Koschinsky, Menno P.J. de Winther, Albert K. Groen, Joseph L. Witztum, Sotirios Tsimikas, Erik S.G. Stroes and Jeffrey Kroon

*Circulation Research. 2020;126:1346–1359*

Abstract

**Rationale**: Patients with elevated levels of lipoprotein(a) [Lp(a)] are hallmarked by increased metabolic activity in the arterial wall on positron emission tomography/computed tomography, indicative of a pro-inflammatory state.

**Objective**: We hypothesized that Lp(a) induces endothelial cell (EC) inflammation by rewiring endothelial metabolism.

**Methods and results**: We evaluated the impact of Lp(a) on the endothelium and describe that Lp(a), through its oxidized phospholipid content, activates arterial ECs, facilitating increased transendothelial migration (TEM) of monocytes. Transcriptome analysis of Lp(a)-stimulated human arterial ECs revealed upregulation of inflammatory pathways comprising monocyte adhesion and migration, coinciding with increased 6-phophofructo-2-kinase/fructose-2,6-biphosphatase (PFKFB)3-mediated glycolysis. Intercellular adhesion molecule (ICAM)-1 and PFKFB3 were also found to be upregulated in carotid plaques of patients with elevated levels of Lp(a). Inhibition of PFKFB3 abolished the inflammatory signature with concomitant attenuation of TEM.

**Conclusions**: Collectively, our findings show that Lp(a) activates the endothelium by enhancing PFKFB3-mediated glycolysis, leading to a pro-adhesive state, that can be reversed by inhibition of glycolysis. These findings pave the way for therapeutic agents targeting metabolism aimed at reducing inflammation in patients with cardiovascular disease.

**Keywords**: Lipoprotein(a), inflammation, endothelial cell, metabolism, glycolysis

## Non-standard Abbreviations and Acronyms

| | |
|---|---|
| Lp(a) | Lipoprotein(a) |
| TEM | Transendothelial migration |
| LDL | Low-density lipoprotein |
| apo(a) | apolipoprotein(a) |
| apoB | apolipoprotein B-100 |
| OxPL | Oxidized phospholipid |
| EC | Endothelial cell |
| HAEC | Human aortic endothelial cell |
| PC | Phosphocholine |
| LBS | Lysine binding site |
| Lp(a)-Tg | Lp(a) transgenic mice |
| LBS-Lp(a)-Tg | Lp(a) transgenic mice lacking the ability to bind OxPLs to Lp(a) |
| $^{18}$F-FDG | $^{18}$F-fluorodeoxyglucose |

## Introduction

Lipoprotein(a) [Lp(a)] is a low-density lipoprotein (LDL)-like particle characterized by covalently bound apolipoprotein(a) [(apo(a)] to apolipoprotein B-100 (apoB) of LDL. On an equimolar basis, Lp(a) is considered more atherogenic than LDL due to the presence of phosphocholine (PC) containing oxidized phospholipids (OxPLs) bound to apo(a) [1,2]. OxPLs are recognized as endogenous danger-associated molecular patterns [3]. Bound to Lp(a), OxPLs are capable of activating circulating monocytes, rendering them highly inflammatory leading to enhanced monocyte transendothelial migration (TEM) [4]. Lp(a) elevation (≥50 mg/dL, >125 nmol/L) is a highly prevalent condition [5,6] which is associated with a 2- to 4-fold increase in cardiovascular morbidity and mortality [7,8]. Lp(a) levels are inversely correlated to the number of kringle repeats found in the apo(a) entity of Lp(a) [9,10]. The mechanisms by which Lp(a) mediates enhanced arterial inflammation and accelerated atherogenesis may comprise accumulation of Lp(a) in atherosclerotic plaques, enhanced thrombogenic potential and pro-inflammatory effects from its content of OxPLs [2]. Whereas we and others have focused on the interaction of Lp(a) with immune cells and coagulation [4,11], functional data on the impact of Lp(a) on the endothelium, the first line of defense against atherosclerosis, remain scarce [12–18].

In the context of atherosclerosis, it became evident that monocytes rewire their metabolism as a common mechanism required to provide energy and building blocks for inflammatory reactions [4,19–21]. In contrast, the impact of Lp(a) on endothelial cells (ECs) with respect to changes in metabolism have not been studied. Since tumor angiogenesis has been found to coincide with EC metabolic alterations [22], we hypothesize that Lp(a) induces EC activation fueled by metabolic alterations in order to sustain a pro-inflammatory state.

In the present study, we reveal a novel role of Lp(a) and in particular, Lp(a)-bound OxPLs in driving EC-inflammation. Targeting these Lp(a)-induced endothelial metabolic alterations provides a fruitful strategy to reverse endothelial cell inflammation which may eventually help to reduce the atherogenic risk in patients.

## Methods

A detailed description of the methods is available in the Online Data Supplement. The RNA sequencing data generated in this study are available at the NCBI Gene Expression Omnibus (GEO) database under accession number GSE145898.

## Results

*Lp(a) elicits a pro-inflammatory response in endothelial cells*

To determine whether Lp(a) elicits endothelial cell activation leading to increased transmigration of monocytes, we stimulated human aortic ECs (HAECs) for 18h with a physiological relevant concentration of 100 mg/dL of Lp(a). Subsequently, healthy

monocytes were added to ECs incubated with Lp(a) (Lp(a)-ECs) or unstimulated ECs. The rate of adhesion of monocytes to the endothelium doubled in Lp(a)-ECs compared to control ECs (Fig. 1, A and B), with a concomitant 5-fold increase in TEM of monocytes in the Lp(a)-EC condition (Fig.1, A and C). To visualize transcriptional changes in Lp(a)-ECs, we incubated HAECs with either low (5 mg/dL) or high Lp(a) (100 mg/dL) and performed RNA sequencing. Heat-map analysis of Lp(a)-ECs upregulated transcripts revealed an activated EC-phenotype, with clustering of genes involved in leukocyte chemotaxis and migration (Fig. 1D and Online Fig I-A). Furthermore, two distinct groups were separated by principle component analysis (Online Fig. I-B). Volcano plot analysis showed 270 differentially expressed genes (134 genes upregulated and 136 genes downregulated) (Online Fig. I-C). Validation of key molecules involved in TEM (Fig. 1E) by targeted qPCR confirmed significantly increased expression of *SELE (E-selectin)*, *ICAM1* and *VCAM1* in Lp(a)-ECs (Fig. 1F). In addition, expression of *MCP1* showed a 3-fold increase, cytokines *IL6* and *IL8* revealed a 2- and 20-fold increase, respectively (Fig. 1G). Functionally, this resulted in increased secretion of IL-6 and IL-8 (Fig.1H) and a 3.5-fold increase in ICAM-1 protein (Fig. 1I). ICAM-1 is essential for efficient monocyte TEM as a knock-down of ICAM-1 in HAECs led to decreased TEM of monocytes (Online Fig. I-D). Secretion of MCP-1, IL-6 and IL-8 significantly increased over time as well (Online Fig. I-E). In addition, the observed effects of Lp(a) were independent of factors present in human serum (Online Fig. II-A). Together these data show that Lp(a) induces a pro-inflammatory signature of ECs.

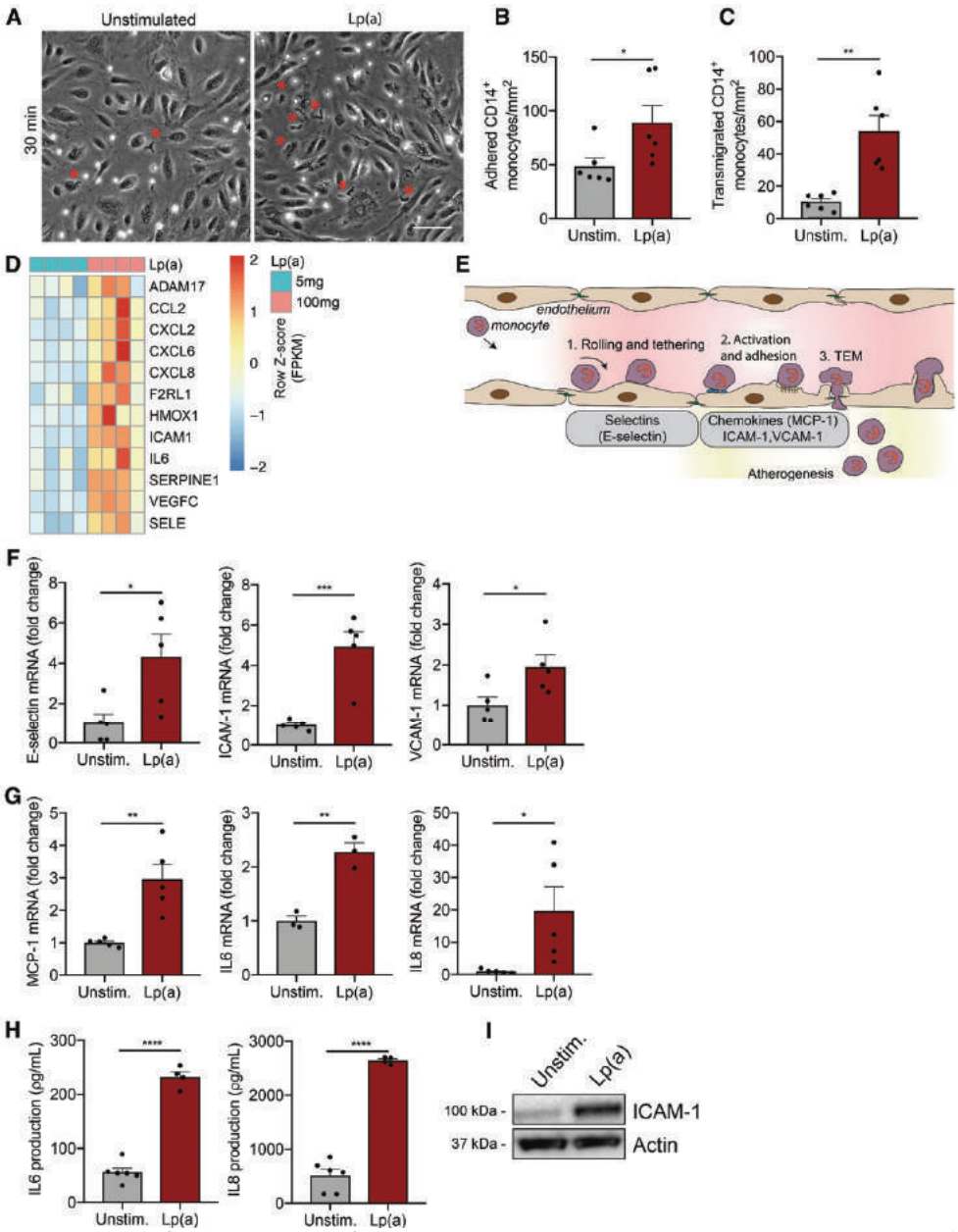


*Figure 1. Increased inflammation in Lp(a)-ECs facilitates excessive monocyte transmigration.* **(A)** Representative DIC images of TEM in unstimulated ECs (left image) compared to Lp(a)-stimulated ECs (Lp(a)-EC) for 18h. Transmigrated monocytes are visualized as black cells with a red asterisk and adhered monocytes as white cells. White bar, 200 μm. **(B)** Quantification of adhered (n=6; P=0.0466) and **(C)** transmigrated monocytes (n=6; P=0.0014). Data were analyzed using two-tailed Student unpaired T-test. **(D)** Heatmap of selected genes involved in TEM and leukocyte chemotaxis of 5mg/dL Lp(a)-EC compared to 100 mg/dL Lp(a)-EC (6h stimulation; n=4). **(E)** Schematic overview of the key steps and molecules involved in leukocyte TEM. **(F)** Genes important in rolling and tethering of leukocytes are upregulated in Lp(a)-ECs relative to unstimulated ECs. Data were analyzed using two-tailed Student unpaired T-test. (6h stimulation; n=5; P=0.0253 for *E-selectin*; P=0.0008 for *ICAM1*; P=0.0333 for *VCAM1*). **(G)** Chemotactic gene expression is elevated in Lp(a)-ECs compared to unstimulated ECs. Data were analyzed using two-tailed Student unpaired T-test. (6h stimulation; n= 3 for *IL6* and rest is n=5; P=0.0030 for *MCP1*; P=0.0025 for *IL6*; P=0.0368

for *IL8*). **(H)** IL-6 and IL-8 cytokine secretion in cell medium increased in Lp(a)-ECs (n=4) vs. unstimulated ECs (n=6). Data were analyzed using two-tailed Student unpaired T-test. (P<0.0001 for IL-6; P<0.0001 for IL8; 18h stimulation). **(I)** Representative immunoblot revealing increased EC ICAM-1 protein expression after incubation with 100 mg/dL Lp(a) compared to unstimulated ECs (18h stimulation).
Lp(a), lipoprotein(a); TEM, transendothelial migration; MCP-1, monocyte chemoattractant protein 1; ICAM-1, intercellular adhesion molecule 1; VCAM-1, vascular adhesion molecule 1; IL6, interleukin 6; IL8, interleukin 8.All data are mean ± SEM. *P< 0.05; **P< 0.005; ***P< 0.0005; ****P< 0.00005

*OxPLs carried by Lp(a) drive endothelial inflammation*

In view of the recently reported role of OxPLs in Lp(a) and its effects on immune cells [3], we investigated which moiety of the Lp(a) particle mediates the inflammatory response in the endothelium. To this end, we used either the 17-kringle recombinant apo(a) species 17K r-apo(a), containing OxPLs, or 17KΔLBS r-apo(a), which lacks OxPL-binding capacity due to a mutation in the lysine binding site (LBS; Online Fig. II-B) [4,23]. Gene expression revealed that TEM-associated expression of *SELE* (*E-selectin)*, *MCP1*, *ICAM1*, *VCAM1*, *IL6* and *IL8* were increased if ECs were exposed to 17K r-apo(a) treatment (Fig. 2A; red bars). In contrast, 17KΔLBS r-apo(a) had no significant effect on inflammatory gene expression (Fig. 2A; green bars). To functionally assess these changes, we determined adhesion and migration of healthy monocytes and found that monocyte adhesion was significantly increased when ECs were incubated with 17K apo(a), whereas no significant difference was found between unstimulated- and 17KΔLBS-stimulated ECs (Fig. 2B and C). Furthermore, 17K apo(a) significantly increased TEM 7-fold compared to 17KΔLBS apo(a) (Fig. 2B and D), underlining the importance of OxPL-Lp(a) in mediating the proinflammatory responses. To validate the importance of OxPLs carried by Lp(a), both OxPL-apoB and OxPL-apo(a) levels were measured in the isolated Lp(a) fraction of used donors. The OxPL-apo(a) content was similar between donors and correspondingly, the OxPL-apoB levels were comparable in different donors (Online Fig. II-C). To confirm if OxPLs bound to Lp(a) are driving EC activation, we co-incubated Lp(a)-ECs with the murine IgM monoclonal antibody E06 (100 μg/mL), which binds the PC moiety of OxPLs [24,25]. Blocking E06-detectable OxPLs abolished Lp(a)-induced *ICAM1*, *VCAM1*, *IL6* and *IL8* gene expression (Fig. 2E). Blocking OxPLs by the antibody E06 led to a significant reduction in both monocyte adhesion as well as TEM (Fig. 2F and 2G). In contrast, isolated LDL did not significantly change endothelial phenotype compared to the same concentration of Lp(a) based on apo(a) (Online Fig. II-D). However, incubation of LDL based on apoB levels did lead to a small, albeit significant increase in IL-8 expression compared to control ECs (Online Fig. II-E and II-F). Collectively, these data indicate that the activated state of ECs needed for monocyte TEM, is primarily orchestrated by OxPLs present on Lp(a).

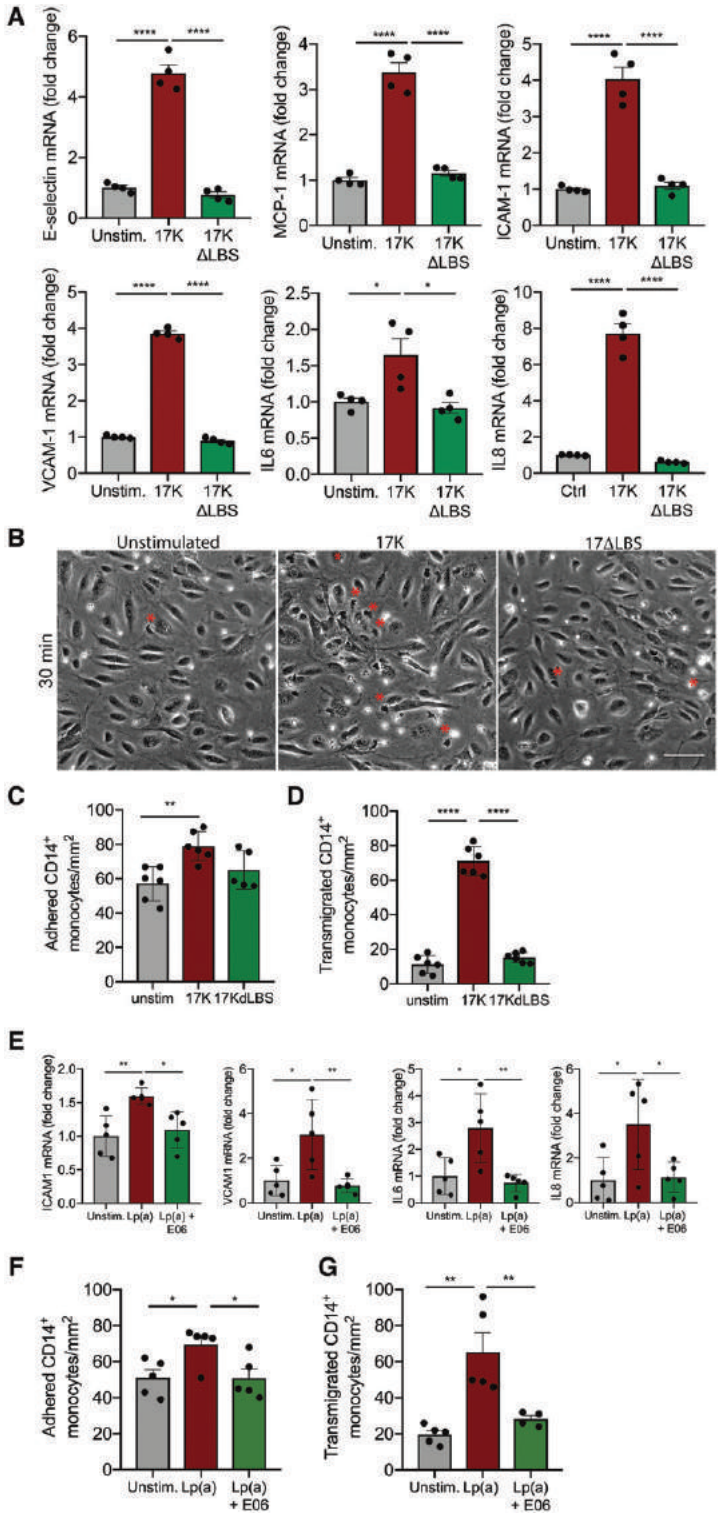


***Figure 2. OxPLs induce a pro-inflammatory EC phenotype and thereby facilitate monocyte TEM.*** **(A)** Recombinant 17K apo(a) induces increased expression of TEM-associated genes (50 μg/mL; red bars). No differences were observed in ECs stimulated with 17KΔLBS (50 μg/mL; green bars). Data were analyzed using one-way ANOVA with Tukey's correction (for *E-selectin* P<0.0001 for unstimulated vs 17K, P<0.0001 for 17K vs. 17KΔLBS; for *MCP1* P<0.0001 for unstimulated vs 17K, P<0.0001 for 17K vs. 17KΔLBS; for *ICAM1* P<0.0001 for unstimulated vs 17K, P<0.0001 for 17K vs. 17KΔLBS; for *VCAM1* P<0.0001 for unstimulated vs 17K, P<0.0001 for 17K vs. 17KΔLBS; for *IL6* P=0.037 for unstimulated vs 17K, P=0.0156 for 17K vs. 17KΔLBS; for *IL8* P<0.0001 for unstimulated vs 17K, P<0.0001 for 17K vs. 17KΔLBS 6h stimulation; n=4). **(B)** Representative DIC images of unstimulated ECs, 17K-stimulated ECs and 17KΔLBS-stimulated HAECs. Transmigrated monocytes are visualized as black cells with a red asterisk and adhered monocytes as white cells. (18h stimulation; n=6; white bar = 200 μm). **(C)** Quantification of adhered monocytes. Data were analyzed using one-way ANOVA with Tukey's correction. P=0.0049 for unstimulated vs 17K (17K, red bars; 17KΔLBS, green bars) and **(D)** transmigrated monocytes. Data were analyzed using one-way ANOVA with Tukey's correction. P<0.0001 for unstimulated vs 17K, P<0.0001 for 17K vs. 17KΔLBS (18h stimulation; n=6). **(E)** Monoclonal antibody E06 (100 μg/mL), decreased expression of *ICAM1*, *VCAM1*, *IL6* and *IL8* in Lp(a)-ECs (green bars) vs Lp(a)-ECs (red bars). Data were analyzed using one-way ANOVA with Tukey's correction. For *ICAM1* P=0,0059 for unstimulated vs Lp(a), P=0.0173 for Lp(a) vs. Lp(a)+E06; for *VCAM1*

P=0,0187 for unstimulated vs Lp(a), P=0.0099 for Lp(a) vs. Lp(a)+E06; for *IL6* P=0,0162 for unstimulated vs Lp(a), P=0.0070 for Lp(a) vs. Lp(a)+E06; for *IL8* P=0,0324 for unstimulated vs Lp(a), P=0.0431 for Lp(a) vs. Lp(a)+E06 (6h stimulation; n=5). **(F)** ECs incubated with 100 mg/dL Lp(a) increased monocyte adhesion (red bars) but co-incubation with E06 diminished Lp(a)-induced adhesion (green bars). Data were analyzed using one-way ANOVA with Tukey's correction. P=0.0342 for unstimulated vs Lp(a), P=0.0324 for Lp(a) vs. Lp(a)+E06 (18h stimulation; n=5). **(G)** Monocyte TEM was increased when ECs were incubated with 100 mg/dL Lp(a) (red bars) and decreased after co-incubation with E06 (green bars). Data were analyzed using one-way ANOVA with Tukey's correction. P=0.0014 for unstimulated vs Lp(a), P=0.0095 for Lp(a) vs. Lp(a)+E06 (18h stimulation; n=5).
TEM, transendothelial migration; 17K, 17K recombinant apolipoprotein(a); 17KΔLBS, 17K recombinant apolipoprotein(a) with a mutation in the lysine binding site; MCP-1, monocyte chemoattractant protein 1; ICAM-1, intercellular adhesion molecule 1; VCAM-1, vascular adhesion molecule 1; IL6, interleukin 6; IL8, interleukin 8; E06, E06, murine IgM monoclonal antibody E06 which binds the PC moiety of oxidized phospholipids. All data are mean ± SEM. *P< 0.05; **P<0.005; ***P< 0.0005; ****P< 0.00005

*PFKFB3-mediated glycolysis drives Lp(a)-induced endothelial inflammation*

Next, we evaluated the metabolic changes in ECs after 17K r-apo(a) or Lp(a) stimulation (Fig. 3A). Expression of the glycolytic enzymes *SLC2A1* (GLUT1), *PFKFB3* and *PFKM* increased 2- to 4-fold, whereas *HK2* expression remained unaltered after 18h incubation with 17K, when compared to EC under control conditions (Fig. 3B; red bars). No significant differences were found for these glycolytic genes between unstimulated cells and 17KΔLBS (Fig. 3B). Since PFKFB3 acts as an important glycolytic regulator, we investigated the upstream regulators of PFKFB3, HIF1?? and KLF2 [26]. As expected, HIF-1α protein expression increased (Online Fig. II-G) and the expression of the negative regulator of HIF1?, KLF2 [27], was decreased after 17K stimulation (Online Fig. II-H). The increase in glycolytic gene expression coincided with enhanced glucose uptake in Lp(a)-ECs, as assessed with labeled 2-NBDG (Fig. 3C and D) and increased lactate production (Fig. 3E). Whereas aforementioned cytokine secretion occurred as early as in 2h in Lp(a)-ECs (Online Fig. I-E), the increase in lactate secretion, observed from 6h onwards (Online Fig. II-I), coincided with a steep increase in "second-wave" cytokine secretion. This suggests an increase in glycolysis downstream of inflammation and substantiates the correlation between inflammation and metabolic reprogramming. Seahorse flux analysis corroborated these findings, revealing an increase in both glycolysis and glycolytic capacity following Lp(a) stimulation (Fig. 3F). In accordance, 17K r-apo(a)-stimulated ECs induced a similar response in ECAR, where the 17KΔLBS r-apo(a) construct showed no significant increase in endothelial glycolysis (Fig. 3G). This increase in glycolysis coincided with only minor changes in endothelial respiration, as reflected by the minimal difference in oxygen consumption rate (OCR) (Fig. 3H). The findings were substantiated by stable isotope $^{13}$C-glucose tracer experiments (Fig. 3I), where an Lp(a)-induced increase in glycolytic metabolic fluxes was observed with a moderate, but significant rise in the appearance of TCA cycle intermediates succinate and fumarate (Fig. 3J). When ECs migrate and proliferate, they predominantly rely on glycolysis [22], therefore we confirmed that the observed increase in glycolytic activity could not be attributed to increased migration nor proliferation of Lp(a)-ECs (Online Fig. II-J).

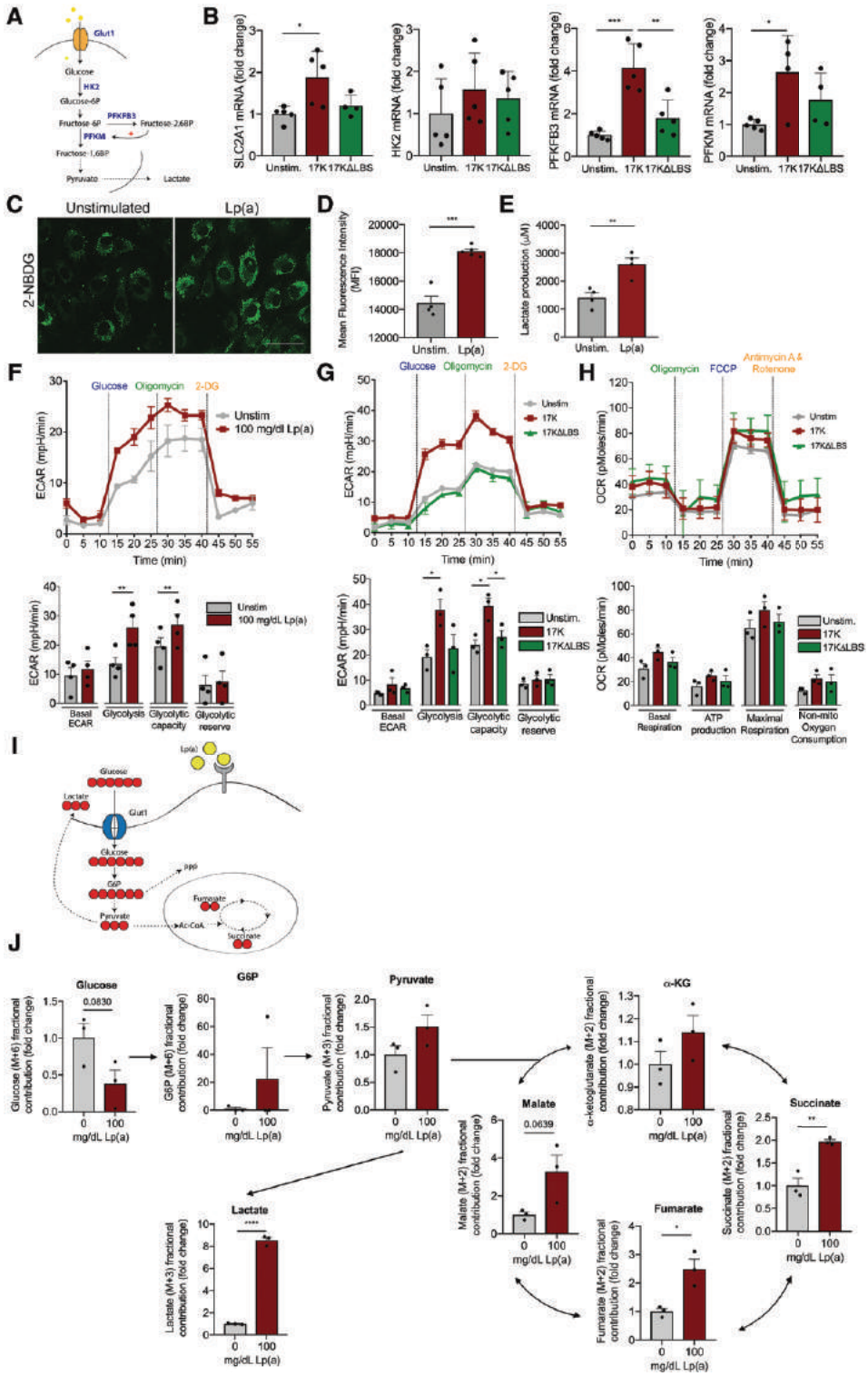
A
Glut1
Glucose
HK2
Glucose-6P
PFKFB3
Fructose-6P
Fructose-2,6BP
PFKM
Fructose-1,6BP
Pyruvate
Lactate
B
SLC2A1 mRNA (fold change)
HK2 mRNA (fold change)
PFKFB3 mRNA (fold change)
PFKM mRNA (fold change)
Unstim.
17K
17KΔLBS
C
Unstimulated
Lp(a)
2-NBDG
D
Mean Fluorescence Intensity (MFI)
E
Lactate production (μM)
F
Glucose
Oligomycin
2-DG
Unstim
100 mg/dl Lp(a)
ECAR (mpH/min)
Time (min)
Basal ECAR
Glycolysis
Glycolytic capacity
Glycolytic reserve
G
17K
17KΔLBS
H
Antimycin A & Rotenone
FCCP
OCR (pMoles/min)
Basal Respiration
ATP production
Maximal Respiration
Non-mito Oxygen Consumption
I
Lp(a)
Glucose
Lactate
Glut1
G6P
PPP
Fumarate
Pyruvate
Ac-CoA
Succinate
J
Glucose
G6P
Pyruvate
α-KG
Malate
Succinate
Lactate
Fumarate
Glucose (M+6) fractional contribution (fold change)
G6P (M+6) fractional contribution (fold change)
Pyruvate (M+3) fractional contribution (fold change)
α-ketoglutarate (M+2) fractional contribution (fold change)
Malate (M+2) fractional contribution (fold change)
Succinate (M+2) fractional contribution (fold change)
Lactate (M+3) fractional contribution (fold change)
Fumarate (M+2) fractional contribution (fold change)
0.0830
0.0639
mg/dL Lp(a)

***Figure 3. Glycolysis drives inflammation in Lp(a)-ECs.*** **(A)** Schematic overview of the EC glycolytic pathway and its key enzymes in blue. **(B)** Glycolytic gene expression profiles of unstimulated EC (grey bars) vs.17K (red bars)- vs. 17KΔLBS-stimulated ECs (green bars). Data were analyzed using one-way ANOVA with Tukey's correction. For *SLC2A1* P=0.0204 for unstimulated vs 17K; for *PFBFB3* P=0.0002 for unstimulated vs 17K, P=0.0013 for 17K vs. 17KΔLBS; for *PFKM* P=0.0332 for unstimulated vs 17K (18h incubation; n=5). **(C)** Representative image of unstimulated ECs (left image) and Lp(a)-ECs (right image), incubated with 50 μM 2-NBDG for 2h. (18h incubation with Lp(a); n=4; white bar, 200 μm). **(D)** Flow cytometric analysis of 2-NBDG uptake (2h) of unstimulated (grey bar) and Lp(a)-stimulated ECs (red bar). Data were analyzed using two-tailed Student unpaired T-test, P=0.0001 (18h incubation with Lp(a); 2h incubation with 50 μM 2-NBDG; n=4). **(E)** Lactate production of unstimulated ECs (grey bars) compared to Lp(a)-ECs. Data were analyzed using two-tailed Student unpaired T-test, P=0.0052 (red bars; n=4). **(F)** Glycolytic flux measurement by Seahorse Flux Analysis of unstimulated ECs (grey line) and Lp(a)-ECs (red line) by recording ECAR after injection of glucose, oligomycin and 2-DG. Glycolytic rate plotted in a bar graph comparing unstimulated ECs (green bars) with Lp(a)-ECs (red bars). Data were analyzed using two-tailed Student unpaired T-test. For glycolysis P=0.0075; for glycolytic capacity P=0.0043 (18h incubation; n=4). **(G)** Graph (left) and bar graph of glycolytic flux of unstimulated (grey line; grey bars), 17K (red line; red bars) and 17KΔLBS (green line; green bars). Data were analyzed using one-way ANOVA with Tukey's correction. For glycolysis P=0.0494 for unstimulated vs 17K; for glycolytic capacity P=0.0139 for unstimulated vs 17K, P=0.0354 for 17K vs. 17KΔLBS; (18h incubation; n=3). **(H)** Oxidative phosphorylation parameters assessed by recording oxygen consumption rate (OCR) after injection of oligomycin, FCCP and rotenone. Unstimulated (grey line; grey bars), 17K (red line; red bars) and 17KΔLBS (green line; green bars). (18h incubation; n=3). **(I)** Schematic overview of $^{13}$C-glucose flux analysis in ECs.**(J)** Bar graphs showing the $^{13}$C metabolic flux analysis with and without 100 mg/dL Lp(a) stimulation after 30 min incubation with isotopically labeled glucose. Arrows indicate the flux. Normalized fractional contribution of intracellular glucose, G6P, pyruvate, lactate, α-KG, succinate, malate and fumarate. Data were analyzed using two-tailed Student unpaired T-test. For succinate P=0.0047; for fumarate P=0.0149; for lactate P<0.0001 (18h incubation with Lp(a); n=3).
GLUT1, glucose transporter 1; HK2, hexokinase 2; PFKFB3, 6-phophofructo-2-kinase/fructose-2,6-biphosphatase; PFKM, 6-phosphofructokinase, muscle; 2-NBDG, 2 2-(N-( 7-Nitrobenz-2-oxa-1,3-diazol-4-yl)Amino)-2-Deoxyglucose; Lp(a), lipoprotein(a); MFI, mean fluorescent intensity; 2-DG, 2-Deoxyglucose; ECAR, extracellular acidification rate; OCR, oxygen consumption rate; FCCP, carbonyl cyanide-4-(trifluoromethoxy)phenylhydrazone; G6P, glucose-6-phosphate; α-KG, α-ketoglutarate.
All data are mean ± SEM. *P< 0.05; **P< 0.005; ***P< 0.0005.

In an *ex vivo* setting in murine aortas, we subsequently assessed if Lp(a) affects the enzyme PFKFB3, acting as a key driver in endothelial glycolysis [22]. In line with our *in vitro* data, *ex vivo* addition of Lp(a) increased aortic endothelial cell PFKFB3 protein expression compared to control aortas, whereas ICAM-1 expression was mildly affected (Fig. 4A and 4B). To validate this *in vivo*, we used transgenic mice expressing both apo(a) and human apoB, which assemble to form Lp(a) (*Lp(a)-Tg*), and mice that express apoB and mutant apo(a) with 2 key point mutations in its LBS lacking OxPL binding capacity (*LBS-Lp(a)-Tg*) [23], and analyzed aortic PFKFB3 expression. A significant increase in endothelial PFKFB3 expression was found in *Lp(a)-Tg* mice compared to *LBS-Lp(a)-Tg* mice (Fig. 4C and 4D), further underlining the importance of PFKFB3 in EC OxPL signaling.
Finally, to also validate this increase in glycolytic activity and inflammatory burden in humans, we investigated human plaques of patients following carotid endarterectomy, included in the Athero-Express Biobank (UMCU, The Netherlands). We measured Lp(a) in 1506 subjects and included subjects with high levels of Lp(a) (>140 mg/dL; n=7) versus low Lp(a) (<20 mg/dL; n=7), matched for BMI, age, systolic blood pressure and year of surgery (Table 1). Subsequently, we analyzed plaques and carotid ECs of Lp(a)-patients displayed increased endothelial PFKFB3 expression (Fig. 4E and 4F). Moreover, endothelial ICAM-1 expression increased, further substantiating the inflammatory-metabolic-axis in patients (Fig. 4E and 4F). Together, these data suggest that Lp(a) activates ECs, coinciding with PFKFB3-mediated increased glycolysis.

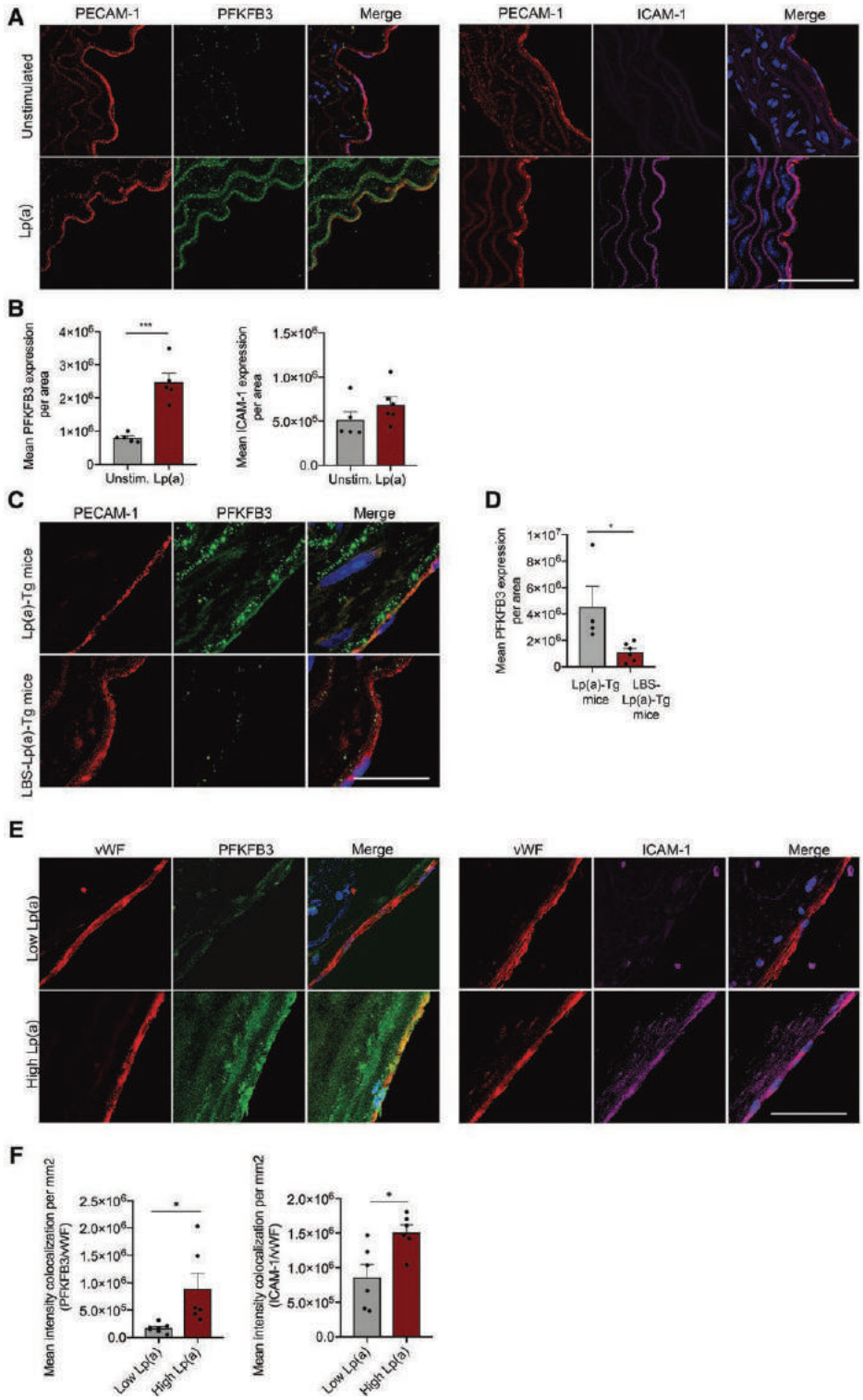
A
PECAM-1
PFKFB3
Merge
PECAM-1
ICAM-1
Merge
Unstimulated
Lp(a)
B
Mean PFKFB3 expression per area
4×10^6
3×10^6
2×10^6
1×10^6
0
***
Unstim.
Lp(a)
Mean ICAM-1 expression per area
1.5×10^6
1.0×10^6
5.0×10^5
0.0
Unstim.
Lp(a)
C
PECAM-1
PFKFB3
Merge
Lp(a)-Tg mice
LBS-Lp(a)-Tg mice
D
Mean PFKFB3 expression per area
1×10^7
8×10^6
6×10^6
4×10^6
2×10^6
0
*
Lp(a)-Tg mice
LBS-Lp(a)-Tg mice
E
vWF
PFKFB3
Merge
vWF
ICAM-1
Merge
Low Lp(a)
High Lp(a)
F
Mean intensity colocalization per mm2 (PFKFB3/vWF)
2.5×10^6
2.0×10^6
1.5×10^6
1.0×10^6
5.0×10^5
0.0
*
Low Lp(a)
High Lp(a)
Mean intensity colocalization per mm2 (ICAM-1/vWF)
2.0×10^6
1.5×10^6
1.0×10^6
5.0×10^5
0.0
*
Low Lp(a)
High Lp(a)

***Figure 4. PFKFB3-expression is increased in murine vessels upon Lp(a) stimulation*** **(A)** Representative images of murine WT aortas *ex vivo* stimulated with (lower images; n=5) and without (upper images; n=6) 100 mg/dL Lp(a) stimulation. Nuclei were stained with DAPI (blue), ECs are stained with PECAM-1 (red), PFKFB3 (green) and ICAM-1 (magenta). (18h incubation; white bar, 200μm) **(B)** Quantification of A. Data were analyzed using two-tailed Student unpaired T-test, P=0.0004. **(C)** Representative images of aortas derived from Lp(a) mice (Lp(a)-Tg; n=4) and mice lacking the lysine binding site which therefore cannot carry OxPLs (LBS-Lp(a)-Tg; n=6) stained for PECAM-1 (red) and PFKFB3 (green), nuclei were stained with DAPI (blue) (white bar, 200μm). **(D)** Quantification of C; EC PFKFB3 expression in aortas of Lp(a)-Tg and LBS-Lp(a)-Tg mice on a chow diet. Data were analyzed using two-tailed Student unpaired T-test, P=0.0354. **(E)** Images representing human carotid plaques derived from patients with low Lp(a) versus high Lp(a) levels. Nuclei were stained with DAPI (blue), ECs are stained with vWF (red), PFKFB3 (green) and ICAM-1 (magenta). (n=6 per group; white bar, 200μm) **(F)** Quantification of E. Data were analyzed using two-tailed Student unpaired T-test; for PFKFB3 P=0.0206; for ICAM1 P=0.0134.
Lp(a), lipoprotein(a); PECAM-1, platelet endothelial cell adhesion molecule 1; PFKFB3, 6-phophofructo-2-kinase/fructose-2,6-biphosphatase; ICAM-1, intercellular adhesion molecule 1; vWF, von Willebrand factor. All data are mean ± SEM. *P< 0.05; ***P< 0.0005

***Table 1. Clinical characteristics of included patients of Athero-Express Biobank.***

| | Lp(a) low (n = 7) | Lp(a) high (n = 7) | p-value |
|---|---|---|---|
| Age, years | 75.3 ± 6.3 | 69.0 ± 7.1 | 0.107 |
| Male | 7 (100%) | 7 (100%) | 1.000 |
| Systolic blood pressure, mmHg | 143 ±25 | 152 ±28 | 0.541 |
| BMI, kg/m$^2$ | 23.6 ±1.7 | 24.5 ±3.6 | 0.589 |
| Current smoker (yes, %) | 2 (28.6%) | 3 (42.9%) | 0.500* |
| Cholesterol lowering medication, (yes, %) | 0 (0%) | 0 (0%) | 1.000 |
| Anti-hypertensive drugs (yes, %) | 1 (14.3%) | 1 (14.3%) | 1.000 |
| Anti-platelet drugs (yes, %) | 1 (14.3%) | 1 (14.3%) | 1.000 |
| Total cholesterol, mmol/L | 4.1 ±1.3 | 5.4 ±0.8 | 0.046 |
| HDL-cholesterol, mmol/L | 0.9 ±0.2 | 1.3 ± 0.3 | 0.019 |
| LDL-cholesterol, mmol/L | 2.2 ± 0.8 | 3.1 ±0.6 | 0.032 |
| Triglycerides, mmol/L | 1.6 [1.0 – 2.0] | 1.2 [1.0 – 1.8] | 0.805 |
| Lipoprotein(a), nmol/L | 7.6 [7.6 – 12.0] | 197.9 [170.2 – 229.0] | 0.001 |
| Lipoprotein(a), mg/dL † | 3.2 [3.2 – 5,0] | 82,5 [70,9 – 95,4] | 0.001 |
| Glucose, mmol/L | 6.2 ±1.0 | 5.6 ±0.9 | 0.415 |

*Chi-Square test, 1-sided. Data are presented as mean ± SD, n (%) or median [min-max].
†To convert Lp(a) in nmol/L to approximate levels in mg/dL, divide by 2.4.
*BMI indicates body mass index; HDL, high-density lipoprotein; LDL, low-density lipoprotein; Lp(a), lipoprotein(a)*

*Inhibiting PFKFB3 in Lp(a)-ECs reverses the inflammatory signature*

Next, we investigated if inhibition of glycolysis leads to a decrease in EC inflammation following Lp(a) stimulation. To this end, we tested and used the commercially available glycolysis inhibitor PFK158 (Online Fig. IV-A and IV-B) [28]. RNA sequencing analysis revealed that PFK158 suppressed transcription of genes in Lp(a)-ECs involved in monocyte TEM (Fig. 5A; Online Fig. III-A and III-B). Validation of EC PFKFB3 knock-down experiments showed that decreased PFKFB3 levels lowered the inflammatory gene expression in Lp(a)-ECs (Fig. 5B). PFK158 treatment of Lp(a)-ECs resulted in a decrease of MCP-1 and IL-6 secretion, while IL-8 levels were unaffected (Fig. 5C). In agreement, PFK158 decreased GLUT1 and ICAM-1 protein expression compared to control ECs (Fig. 5D and E). PFK158 treatment did not result in significantly decreased PFKFB3 protein expression as observed both *in vitro* (Fig. 5D and E) and *ex* vivo (Fig. 5F). However, PFK158 was able to functionally reverse the increased glycolytic rate observed in Lp(a)-ECs (Fig. 5G), leading to decreased lactate production (Online Fig. IV-C). More importantly, our results demonstrate that inhibition of PFKFB3 activity

reverses the Lp(a)-induced increase in monocyte migration by reducing PFKFB3-mediated glycolysis (Fig. 5H and I). Together these data imply that inhibiting increased glycolysis by suppressing PFKFB3-activity in Lp(a)-EC leads to a decrease in inflammation and TEM.

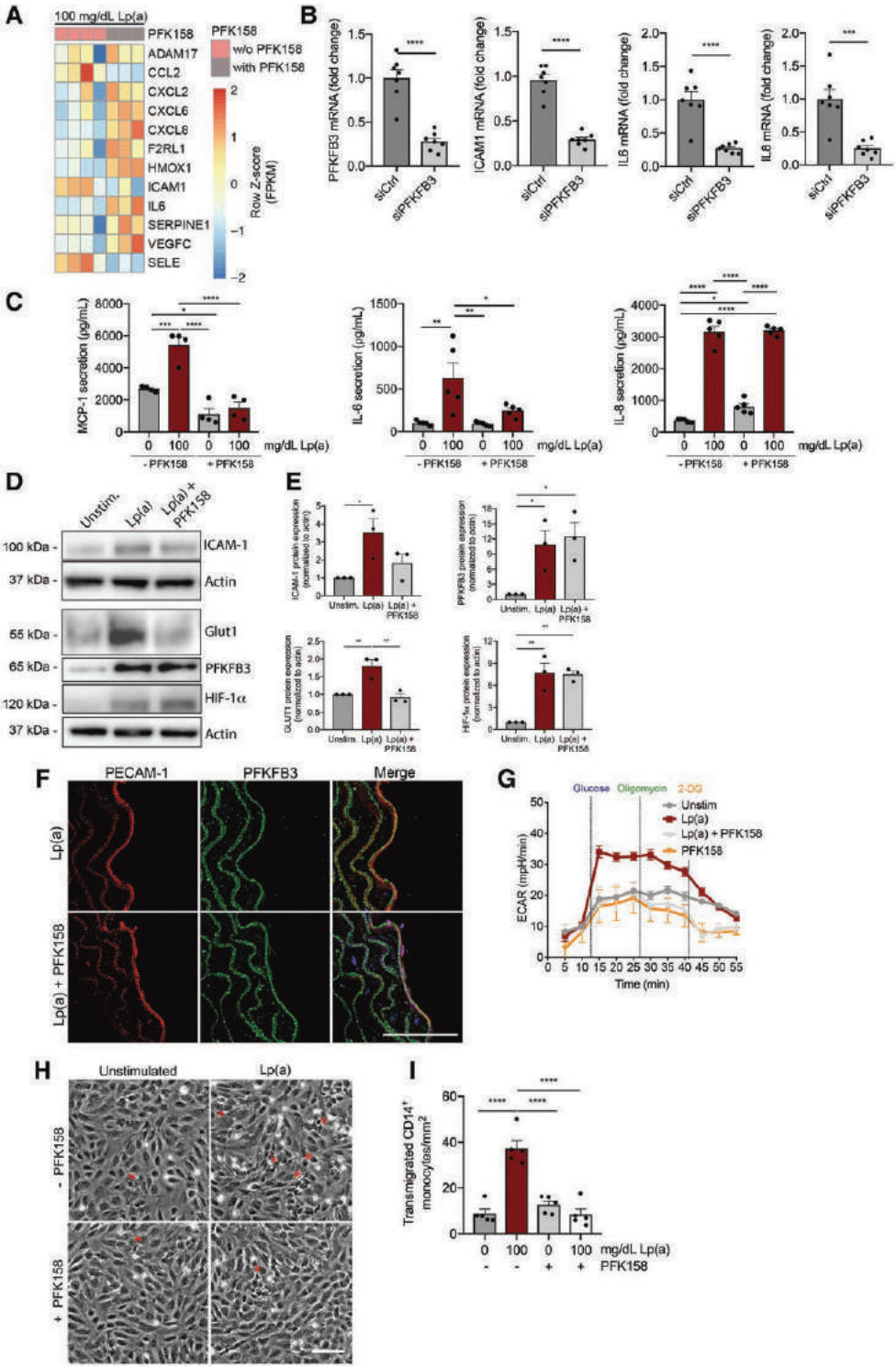
A
100 mg/dL Lp(a)
PFK158
ADAM17
CCL2
CXCL2
CXCL6
CXCL8
F2RL1
HMOX1
ICAM1
IL6
SERPINE1
VEGFC
SELE
PFK158
w/o PFK158
with PFK158
Row Z-score (FPKM)
B
PFKFB3 mRNA (fold change)
ICAM1 mRNA (fold change)
IL6 mRNA (fold change)
IL8 mRNA (fold change)
siCtrl
siPFKFB3
C
MCP-1 secretion (pg/mL)
IL-6 secretion (pg/mL)
IL-8 secretion (pg/mL)
mg/dL Lp(a)
- PFK158
+ PFK158
D
Unstim.
Lp(a)
Lp(a) + PFK158
100 kDa -
ICAM-1
37 kDa -
Actin
55 kDa -
Glut1
65 kDa -
PFKFB3
120 kDa -
HIF-1α
37 kDa -
Actin
E
ICAM-1 protein expression (normalized to actin)
PFKFB3 protein expression (normalized to actin)
GLUT1 protein expression (normalized to actin)
HIF-1α protein expression (normalized to actin)
F
PECAM-1
PFKFB3
Merge
Lp(a)
Lp(a) + PFK158
G
Glucose
Oligomycin
2-DG
Unstim
Lp(a)
Lp(a) + PFK158
PFK158
ECAR (mpH/min)
Time (min)
H
Unstimulated
Lp(a)
- PFK158
+ PFK158
I
Transmigrated CD14+ monocytes/mm2
mg/dL Lp(a)
PFK158

***Figure 5. Inhibition with PFK158 suppresses the glycolytic tone of Lp(a)-ECs and thereby inflammation.*** **(A)** Heatmap of TEM-associated genes in Lp(a)-ECs with (n=3) and without (n=4) inhibition by 5 μM PFK158. (6h incubation). **(B)** Gene expression of Lp(a)-ECs knocked down for PFKFB3 (n=6) and treated with siCtrl (n=7). Data were analyzed using two-tailed Student unpaired T-test. For *PFKFB3* P<0.00001; for *ICAM1* P<0.00001; for *IL6* P<0.00001; for *IL8* P<0.0003(100 mg/dL Lp(a); 6h incubation) **(C)** Cytokine production of unstimulated (grey bars) and 100 mg/dL stimulated ECs (red bars) with and without 5 μM PFK158 Data were analyzed using two-way ANOVA with Tukey's correction. For MCP-1 P=0.0004 0 vs 100 mg/dL Lp(a) (-PFK158); P=0.0170 0 (-PFK158) vs 0 (+PFK158); P<0.0001 100 mg/dL Lp(a) (-PFK158) vs 0 (+PFK158); P<0.0001 100 mg/dL Lp(a) (-PFK158) vs 100 mg/dL Lp(a) (+PFK158). For IL-6 P=0.0044 0 vs 100 mg/dL Lp(a) (-PFK158); P=0.0039 100 mg/dL Lp(a) (-PFK158) vs 0 (+PFK158); P=0.0353 100 (-PFK158) vs 100 (+PFK158). For IL-8 P<0.0001 0 vs 100 mg/dL Lp(a) (-PFK158); P=0.0476 0 (-PFK158) vs 0 (+PFK158); P<0.0001 0 (-PFK158) vs 100 mg/dL Lp(a) (+PFK158); P<0.0001 100 mg/dL Lp(a) (-PFK158) vs 0 (+PFK158); P<0.0001 0 (+PFK158) vs 100 mg/dL Lp(a) (+PFK158) (18h incubation; n=4 for MCP-1; n=5 for IL-6 and IL-8). **(D)** Representative immunoblots of ICAM-1, Glut1, PFKFB3 and HIF-1α protein expression.**(E)** Quantification of immunoblots of ICAM-1 (upper left graph), GLUT1 (lower left graph), PFKFB3 (upper right graph) and HIF-1α (lower right graph) in Lp(a)-ECs (red bars) and 5 μM PFK158-treated Lp(a)-ECs (light grey bars). Actin was used as loading control (100 mg/dL Lp(a); 18h incubation; n=3). Data were analyzed using one-way ANOVA with Tukey's correction. For ICAM-1, P=0.0315 unstimulated vs Lp(a); for PFKFB3 P=0.0226 unstimulated vs Lp(a) and P=0.0416 unstimulated vs. Lp(a)+PFK158; for GLUT1 P=0.0065 unstimulated vs Lp(a) and P=0.0040 Lp(a) vs Lp(a)+PFK158; for HIF-1α P=0.0021 unstimulated vs Lp(a) and P=0.0026 Lp(a) vs Lp(a)+PFK158.**(F)** Aortas of WT mice *ex vivo* incubated with 100 mg/dL Lp(a) and 100 mg/dL Lp(a) + 5 μM PFK158. (Nuclei were stained with DAPI (blue), ECs with PECAM-1 (red) and PFKFB3 was stained (green; 18h incubation; n=5; white bar, 100μm). **(G)** ECAR of unstimulated ECs (grey line/bar), Lp(a)-ECs (red line/bar), Lp(a)-ECs + PFK158 (light grey line/bar) and ECs stimulated with only 5 μM PFK158 (orange line/bar). (100 mg/dL Lp(a); 18h incubation; n=3).**(H)** Representative DIC images TEM assay with unstimulated ECs (upper left), 100 mg/dL ECs (upper-right), Lp(a) + PFK158-stimulated ECs (lower right) and ECs incubated with 5 μM PFK158 (lower left) (18h incubation; white bar, 200 μm).**(I)** Quantification of H; transmigrated monocytes through Lp(a)-ECs co-incubated with and without 5 μM PFK158. Grey bars indicate unstimulated ECs, red bar shows Lp(a)-ECs, light grey indicates Lp(a)-ECs co-incubated with PFK158 and white bars represent PFK158-stimualted ECs. Data were analyzed using two-way ANOVA with Tukey's correction. P<0.0001 0 vs 100 mg/dL Lp(a) (-PFK158); P<0.0001 100 mg/dL Lp(a) (-PFK158) vs 0 (+PFK158); P<0.0001 100 mg/dL Lp(a) (-PFK158) vs 100 mg/dL Lp(a) (+PFK158) vs (100 mg/dL Lp(a); 18h incubation; n=5).
Lp(a), lipoprotein(a); ICAM-1, intercellular adhesion molecule 1; IL6, interleukin 6; IL8, interleukin 8; MCP-1, monocyte chemoattractant protein 1; GLUT1, glucose transporter 1; HIF-1α, hypoxia inducible factor 1α; PECAM-1, platelet endothelial cell adhesion molecule 1; ECAR, extracellular acidification rate; 2-DG, 2-Deoxyglucose. All data are mean ± SEM. *P< 0.05; **P< 0.005; ***P< 0.0005; ****P< 0.00005.

### *Lp(a)-lowering by antisense therapy in humans partly reduces endothelial glycolysis and inflammation*

To investigate the potential of Lp(a) lowering strategies in patients to reduce the pro-inflammatory effects of Lp(a), serum from participants of the IONIS-APO(a)$_{Rx}$ trial with elevated Lp(a) (mean 203.5 mg/dL) were collected before, after 12- and 24 weeks of apo(a)-antisense administration (100-300mg dose) [29]. ECs were incubated with serum samples obtained at baseline (D01), at day 85 (D85) of peak drug effect and after a washout period at day 190 when drug effect was mostly but not completely abolished (D190). Clinically, patients showed a reduction of approximately 80% of plasma Lp(a) levels at day 85, which coincided with an overall reduction of 9-35% in key EC inflammatory markers compared to baseline. However, *VCAM1* and *IL8* did not significantly decrease upon treatment (Fig. 6A). Expression of key glycolytic genes, including *PFKFB3*, *SLC2A1* and *PFKM* decreased at day 85 compared to baseline (Fig. 6B). After the washout period (D190), expression of *MCP1* and *SLC2A1* returned to baseline levels whereas others remained downregulated (Fig. 6A and 6B). In parallel to the changes in gene expression levels, cytokine secretion of MCP-1 and IL-6 decreased in supernatant of ECs incubated with D85 samples compared to baseline, whereas no significant difference was observed in IL-8 secretion (Fig. 6C). Finally, a concomitant decrease in endothelial lactate secretion was observed (Fig. 6D). Collectively, these data support that selective potent Lp(a) lowering in patients

reduces increased EC glycolysis and EC inflammation without achieving complete reversal of the inflammatory activation.

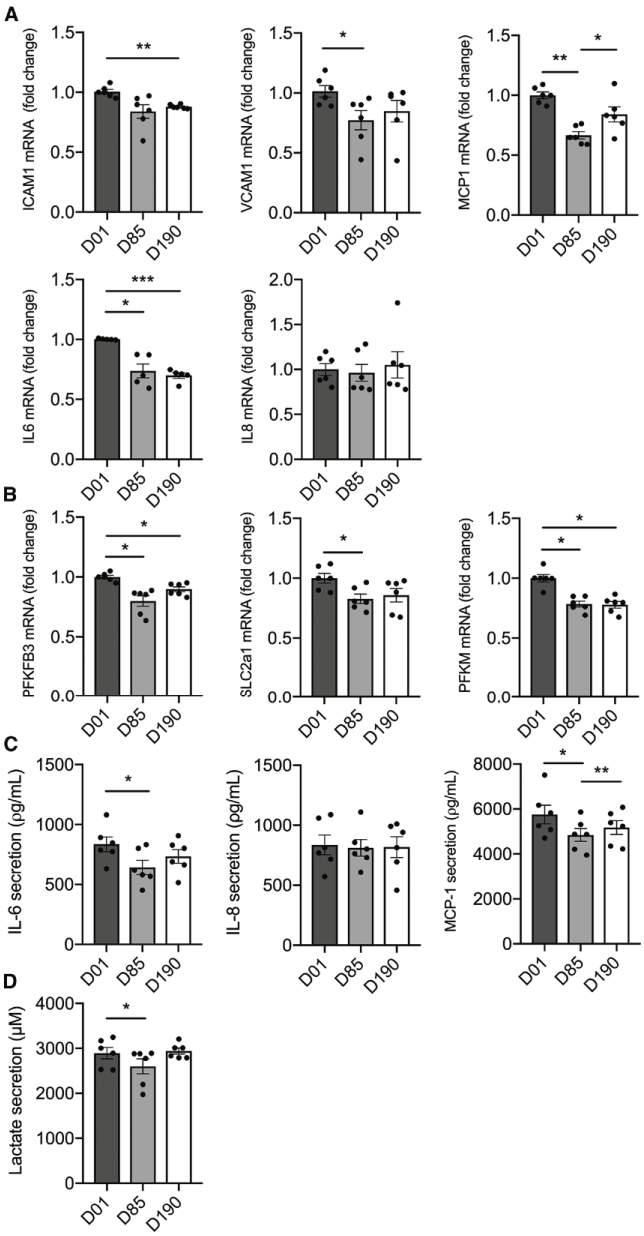


***Figure 6. A strong Lp(a) decrease in human serum partly reduces inflammatory and glycolytic mediators in ECs.*** **(A)** Gene expression of ECs incubated with serum derived from subjects with elevated Lp(a) of the IONIS-APO(a)$_{Rx}$-study (1:1 incubation with endothelial growth medium). Data were analyzed using repeated measures one-way ANOVA with Tukey's correction. For *ICAM1* P=0.0026 D01 vs D190; for *VCAM1* P=0.0338 D01 vs D85; for *MCP1* P=0.0026 D01 vs D85 and P=0.0474 D85 vs D190; for *IL6* P=0.0234 D01 vs D85 and P=0.0006 D01 vs D190. (black bars, D01; grey bars, D85; anthracite bars, D190; n=6; 6h incubation).**(B)** Glycolytic gene expression of *PFKFB3*, *SLC2A1* and *PFKM* revealed a decrease after Lp(a)-lowering in human serum (1:1 incubation with endothelial growth medium). Data were analyzed using repeated measures one-way ANOVA with Tukey's correction. For *PFKFB3* P=0.0196 D01 vs D85 and P=0.0276 D01 vs D190. (n=6; 6h incubation).**(C)** MCP-1, IL-6 and IL-8 secretion in medium of ECs incubated with human serum before and after Lp(a)-lowering. Data were analyzed using repeated measures one-way ANOVA with Tukey's correction. For MCP-1 P=0.0180 D01 vs D85 and P=0.0017 D85 vs D190; for IL-6 P=0.0238 D01 vs D85 (n=6; 18h incubation).**(D)** Lactate secretion in medium of ECs incubated with human serum before and after Lp(a)-lowering therapy. Data were analyzed using repeated measures one-way ANOVA with Tukey's correction. P=0.0160 D01 vs D85 (n=6; 18h incubation).

ICAM-1, intercellular adhesion molecule 1; VCAM-1, vascular adhesion molecule 1; MCP-1, monocyte chemoattractant protein 1; IL6, interleukin 6; IL8, interleukin 8; PFKFB3, 6-phophofructo-2-kinase/fructose-2,6-biphosphatase; PFKM, PFKM, 6-phosphofructokinase, muscle.

All data are mean ± SEM. *P< 0.05; **P< 0.005; ***P< 0.0005

## Discussion

Metabolic pathways are not only crucial in controlling energy balance, but also act as critical determinants in signaling pathways, and hence cellular phenotype [21,30–32]. In this study, we demonstrate that Lp(a) and particularly OxPLs induce EC inflammation,

leading to increased adhesion and transmigration of monocytes. In parallel, we observed a marked increase of glycolytic activity in EC exposed to Lp(a), mainly orchestrated via the glycolytic activator PFKFB3. Inhibition of PFKFB3 not only reverses the increased glycolytic activity in Lp(a)-ECs, but also dampens the inflammatory response and monocyte migration. Finally, using human serum samples from patients who received apo(a) antisense therapy to lower Lp(a), we find a significantly reduced inflammatory signature in ECs *ex vivo*.

OxPLs bound to Lp(a) were shown to induce inflammation in ECs as well as monocytes [4,13]. Monocytes derived from patients with elevated levels of Lp(a) showed increased TEM compared to monocytes derived from healthy subjects. Our data indicate that *in vivo* Lp(a) not only activates monocytes but also endothelial cells [4]. Lp(a) consists of different components, comprising an LDL-like particle, apo(a) and variable amounts of OxPLs present in Lp(a), chiefly on the apo(a) and apoB components [1,2]. We show that absence of Lp(a)-OxPL signaling, using either the OxPL-deficient 17KΔLBS apo(a) construct or the E06 OxPL-blocking antibody, markedly decreases the inflammatory potential of Lp(a). In a similar manner, it was previously shown that E06 could block the ability of OxPL on apoptotic cells to similarly activate endothelial cells [24]. In line, 17K apo(a) lacking OxPLs does not evoke an inflammatory response, which is similar to LDL alone. These data substantiate that OxPLs, rather than the apo(a) or the apoB moiety of the Lp(a) particle, are the main drivers of Lp(a)'s ability to activate ECs.

Lp(a)-OxPLs also induce a profound glycolytic activation in endothelial cells. This increase in glycolysis was manifested by enhanced expression of glycolytic genes and increased glycolytic flux. Aortas from apo(a)-overexpressing mice as well as murine aortas incubated with exogenous Lp(a) displayed increased EC PFKFB3 expression, however Lp(a)-induced PFKFB3 expression was also altered in other cell types (i.e. smooth muscle cells), indicating that glycolytic activation is not restricted to only ECs [33]. In support, Feng *et al.* also reported increased levels of HK2, GLUT1 and PFKFB3 in atheroprone areas in hypercholesterolemic *Apoe*$^{-/-}$ mice [34]. Mechanistically, we found that Lp(a) triggered HIF-1$\alpha$ stabilization, which acts as an upstream regulator of PFKFB3 and GLUT1, suggesting that the HIF-1$\alpha$-PFKFB3-axis fuels inflammation [35,36]. Interestingly, our data show that Lp(a) enhances inflammatory cytokine secretion prior to an increase of lactate secretion, suggesting that the increase in glycolysis is downstream of EC activation. Collectively, this implies that excessive adenosine triphosphate (ATP)-consumption and nucleotide biosynthesis due to EC activation leads to increased ATP generation via glycolysis in order to maintain a state of inflammation. We observed minor changes in glucose oxidation fluxes, although we mainly focused on glycolysis, as ECs rely predominantly on glycolysis (>200-fold higher glucose fluxes as compared to oxidative phosphorylation fluxes) [22].

We validated our findings in human carotid plaques obtained from the Athero-Express database. In line with our *in vitro* and *ex vivo* data, plaques derived from subjects with high levels of Lp(a) showed a profound increase of EC PFKFB3 and ICAM-1 protein levels, suggesting increased activation, despite an advanced atherosclerotic environment in both low- and high Lp(a) groups. Of note, the patients with Lp(a) elevation also had increased levels of LDL-c compared to low Lp(a) patients (3.1 vs. 2.2 mmol/L). However, this increase largely disappears after correction for the Lp(a) elevation, which falsely leads to higher LDL-c laboratory values (LDL-c corrected: approx. 2.5 mmol/L) [37]. Whereas theoretically this minor LDL-c difference may have contributed to a small inflammatory effect, our recent findings in the ANITSCHKOW study make this highly unlikely [38]. Thus, in patients with marked Lp(a) elevation, treatment with a PCSK9-antibody resulting in 60% LDL-c reduction and 14% Lp(a) reduction, did not result in a reduction of the enhanced inflammatory activity in the arterial wall of these patients. In fact, the persistent inflammatory activation was attributed to the marked residual Lp(a) elevation despite PCSK9-antibody treatment [38]. To substantiate the overriding impact of Lp(a) on inflammatory activation as compared to LDL-c, we confirmed the increased inflammatory potency of Lp(a) compared to LDL-c on ECs ex vivo, on equimolar basis.
Several observations in humans underlie the validity of our findings. Thus, Tomas *et al*. found that human 'unstable' atherosclerotic plaques were characterized by an increased glycolytic activity. These unstable plaques displayed increased expression of glycolytic genes *HK2*, *GLUT1* and *PFKM*, comparable with our findings. The activated metabolic state in patients with elevated Lp(a) was corroborated using $^{18}$F-fluorodeoxyglucose (FDG)/computed tomography scans [4], showing a significantly higher glucose uptake in the arterial wall of subjects with Lp(a) elevation. *In vitro* data in human umbilical vein ECs show that oxygen-deprived activated ECs show increased HIF-1$\alpha$-mediated glycolysis and accumulate more $^{18}$F-FDG as compared to control EC [39]. This further indicates that ECs are able to accumulate glucose and increase glycolysis when activated as we observed in human carotid plaques of Lp(a) patients.

In our *ex vivo* incubation experiments, using serum samples of patients with profoundly elevated Lp(a) levels before and after treatment with apo(a)-antisense, we showed a marked pro-inflammatory and glycolytic rise in ECs. Serum obtained from patients after apo(a)-antisense treatment (80% Lp(a) reduction) showed a markedly reduced potential in glycolytic and inflammatory responses in HAECs. This attenuation disappeared using serum obtained after a 185-day washout in these patients, resulting in glycolytic and inflammatory responses comparable to the pretreatment serum samples. These data imply that potent Lp(a) lowering may reduce endothelial inflammation as well as enhanced glycolytic activity in patients with Lp(a) elevation. However, since Lp(a) lowering only partially inhibited the inflammatory responses, interventions beyond Lp(a) lowering may still be required.

Reducing glycolysis via inhibition of PFKFB3 decreased endothelial secretion of IL-6 and MCP-1, with a concomitant decrease of monocyte TEM. Importantly, endothelial knock-down of PFKFB3 does not result in hypometabolism as ECs generate ATP at a normal rate compared to control [40]. Additionally, we show that PFK158 treatment reduces lactate production. Uptake of extracellular lactate stabilizes HIF-1α which in turn increases EC activation in tumor ECs [36]. Thus, Lp(a)-induced lactate production could potentially increase glycolysis through HIF-1**α**-PFKFB3 and thereby affect endothelial inflammation. In summary, inhibiting PFKFB3 reduces the Lp(a)-induced glycolytic increase rendering ECs more quiescent.

*Conclusion*

In the present study, we demonstrate that Lp(a) activates the endothelium, mainly through its OxPL content, thereby facilitating increased monocyte transmigration. Persistent EC activation is induced via PFKFB3-mediated increase of glycolysis. Inhibition of PFKFB3 abolishes the inflammatory potential of OxPLs associated with Lp(a). Since endothelial activation is a hallmark in several pro-atherogenic disease states, including diabetes mellitus, familial hypercholesterolemia and rheumatoid arthritis [41–43], selective endothelial targeting of PFKFB3-mediated glycolysis may offer a new target for future anti-inflammatory therapy in patients at increased cardiovascular risk.

## Acknowledgements and funding

This work was financially supported by the Netherlands Organization for Scientific Research. JK received a VENI grant from ZonMW (91619098). D.P.V.d.K. is supported by The Netherlands Cardiovascular Research Initiative: an initiative with The Netherlands Heart Foundation (CVON 2017-5) and PERSUASIVE EU Horizon 2020 (Taxinomisis 755320). MPJdW is supported by The Netherlands Heart Foundation (CVON 2011/ B019 and CVON 2017-20: Generating the best evidence-based pharmaceutical targets for atherosclerosis [GENIUS I&II]). MPJdW is an established investigator of the Netherlands Heart Foundation (2007T067), is supported by a grant from the Netherlands Heart Foundation and Spark-Holding BV (2015B002), the European Union (ITN-grant EPIMAC), Leducq Transatlantic Network Grant and holds an AMC-fellowship. MvW and RH are supported by the Velux Stiftung (no. 1063). ESGS received funding from the European Union Horizon 2020 research and innovation program REPROGRAM under grant agreement no. 667837. We would like to thank Dr. Han Levels, Stefan Havik and Hans Janssen for their excellent technical support throughout this study.

## Declaration of interests

Dr Tsimikas is a consultant to Boston Heart Diagnostics and has a dual appointment at University of California, San Diego and Ionis Pharmaceuticals. Dr Witztum is a consultant to Ionis Pharmaceuticals. Drs Tsimikas and Witztum are a co-inventors and

receive royalties from patents owned by UCSD on oxidation-specific antibodies and of biomarkers related to oxidized lipoprotein and are co-founders and have an equity interest in Oxitope, Inc and Kleanthi Diagnostics, LLC. The terms of this arrangement have been reviewed and approved by the University of California, San Diego in accordance with its conflict of interest policies. All other authors have nothing to disclose.

## References


1. Bergmark C, Dewan A, Orsoni A, Merki E, Miller ER, Shin M-J, Binder CJ, Horkko S, Krauss RM, Chapman MJ, Witztum JL, Tsimikas S. A novel function of lipoprotein [a] as a preferential carrier of oxidized phospholipids in human plasma. *J Lipid Res* United States; 2008;**49**:2230–2239.
2. Tsimikas S. A Test in Context: Lipoprotein(a): Diagnosis, Prognosis, Controversies, and Emerging Therapies. *J Am Coll Cardiol* United States; 2017;**69**:692–711.
3. Que X, Hung M-Y, Yeang C, Gonen A, Prohaska TA, Sun X, Diehl C, Maatta A, Gaddis DE, Bowden K, Pattison J, MacDonald JG, Yla-Herttuala S, Mellon PL, Hedrick CC, Ley K, Miller YI, Glass CK, Peterson KL, Binder CJ, Tsimikas S, Witztum JL. Oxidized phospholipids are proinflammatory and proatherogenic in hypercholesterolaemic mice. *Nature* England; 2018;**558**:301–306.
4. Valk FM van der, Bekkering S, Kroon J, Yeang C, Bossche J Van den, Buul JD van, Ravandi A, Nederveen AJ, Verberne HJ, Scipione C, Nieuwdorp M, Joosten LAB, Netea MG, Koschinsky ML, Witztum JL, Tsimikas S, Riksen NP, Stroes ESG. Oxidized Phospholipids on Lipoprotein(a) Elicit Arterial Wall Inflammation and an Inflammatory Monocyte Response in Humans. *Circulation* United States; 2016;**134**:611–624.
5. Nordestgaard BG, Langsted A. Lipoprotein (a) as a cause of cardiovascular disease: insights from epidemiology, genetics, and biology. *J Lipid Res* United States; 2016;**57**:1953–1975.
6. Nordestgaard BG, Chapman MJ, Ray K, Boren J, Andreotti F, Watts GF, Ginsberg H, Amarenco P, Catapano A, Descamps OS, Fisher E, Kovanen PT, Kuivenhoven JA, Lesnik P, Masana L, Reiner Z, Taskinen M-R, Tokgozoglu L, Tybjaerg-Hansen A. Lipoprotein(a) as a cardiovascular risk factor: current status. *Eur Heart J* England; 2010;**31**:2844–2853.
7. Kamstrup PR, Tybjaerg-Hansen A, Steffensen R, Nordestgaard BG. Genetically elevated lipoprotein(a) and increased risk of myocardial infarction. *JAMA* United States; 2009;**301**:2331–2339.
8. Langsted A, Kamstrup PR, Nordestgaard BG. High lipoprotein(a) and high risk of mortality. *Eur Heart J* England; 2019;
9. Marcovina SM, Albers JJ, Gabel B, Koschinsky ML, Gaur VP. Effect of the number of apolipoprotein(a) kringle 4 domains on immunochemical measurements of lipoprotein(a). *Clin Chem* England; 1995;**41**:246–255.
10. Utermann G. The mysteries of lipoprotein(a). *Science* United States; 1989;**246**:904–910.
11. Caplice NM, Panetta C, Peterson TE, Kleppe LS, Mueske CS, Kostner GM, Broze GJJ, Simari RD. Lipoprotein (a) binds and inactivates tissue factor pathway inhibitor: a novel link between lipoproteins and thrombosis. *Blood* United States; 2001;**98**:2980–2987.
12. Miller YI, Choi S-H, Wiesner P, Fang L, Harkewicz R, Hartvigsen K, Boullier A, Gonen A, Diehl CJ, Que X, Montano E, Shaw PX, Tsimikas S, Binder CJ, Witztum JL. Oxidation-specific epitopes are danger-associated molecular patterns recognized by pattern recognition receptors of innate immunity. *Circ Res* United States; 2011;**108**:235–248.
13. Pellegrino M, Furmaniak-Kazmierczak E, LeBlanc JC, Cho T, Cao K, Marcovina SM, Boffa MB, Cote GP, Koschinsky ML. The apolipoprotein(a) component of lipoprotein(a) stimulates actin stress fiber formation and loss of cell-cell contact in cultured endothelial cells. *J Biol Chem* United States; 2004;**279**:6526–6533.
14. Ross R. Atherosclerosis--an inflammatory disease. *N Engl J Med* United States; 1999;**340**:115–126.
15. Hahn C, Schwartz MA. The role of cellular adaptation to mechanical forces in atherosclerosis. *Arterioscler Thromb Vasc Biol* United States; 2008;**28**:2101–2107.
16. Xu L, Dai Perrard X, Perrard JL, Yang D, Xiao X, Teng B-B, Simon SI, Ballantyne CM, Wu H. Foamy monocytes form early and contribute to nascent atherosclerosis in mice with hypercholesterolemia. *Arterioscler Thromb Vasc Biol* United States; 2015;**35**:1787–1797.
17. Chistiakov DA, Orekhov AN, Bobryshev Y V. Effects of shear stress on endothelial cells: go with the flow. *Acta Physiol (Oxf)* England; 2017;**219**:382–408.
18. Incalza MA, D'Oria R, Natalicchio A, Perrini S, Laviola L, Giorgino F. Oxidative stress and reactive oxygen species in endothelial dysfunction associated with cardiovascular and metabolic diseases. *Vascul Pharmacol* United States; 2018;**100**:1–19.
19. Cheng S-C, Quintin J, Cramer RA, Shepardson KM, Saeed S, Kumar V, Giamarellos-Bourboulis EJ, Martens JHA, Rao NA, Aghajanirefah A, Manjeri GR, Li Y, Ifrim DC, Arts RJW, Veer BMJW van der, Deen PMT, Logie C, O'Neill LA, Willems P, Veerdonk FL van de, Meer JWM van der, Ng A, Joosten LAB, Wijmenga C, Stunnenberg HG, Xavier RJ, Netea MG. mTOR- and HIF-1alpha-mediated aerobic glycolysis as metabolic basis for trained immunity. *Science* United States; 2014;**345**:1250684.

20. Arts RJW, Novakovic B, Horst R Ter, Carvalho A, Bekkering S, Lachmandas E, Rodrigues F, Silvestre R, Cheng S-C, Wang S-Y, Habibi E, Goncalves LG, Mesquita I, Cunha C, Laarhoven A van, Veerdonk FL van de, Williams DL, Meer JWM van der, Logie C, O'Neill LA, Dinarello CA, Riksen NP, Crevel R van, Clish C, Notebaart RA, Joosten LAB, Stunnenberg HG, Xavier RJ, Netea MG. Glutaminolysis and Fumarate Accumulation Integrate Immunometabolic and Epigenetic Programs in Trained Immunity. *Cell Metab* United States; 2016;**24**:807–819.
21. Smith RL, Soeters MR, Wust RCI, Houtkooper RH. Metabolic Flexibility as an Adaptation to Energy Resources and Requirements in Health and Disease. *Endocr Rev* United States; 2018;**39**:489–517.
22. Bock K De, Georgiadou M, Schoors S, Kuchnio A, Wong BW, Cantelmo AR, Quaegebeur A, Ghesquiere B, Cauwenberghs S, Eelen G, Phng L-K, Betz I, Tembuyser B, Brepoels K, Welti J, Geudens I, Segura I, Cruys B, Bifari F, Decimo I, Blanco R, Wyns S, Vangindertael J, Rocha S, Collins RT, Munck S, Daelemans D, Imamura H, Devlieger R, Rider M, et al. Role of PFKFB3-driven glycolysis in vessel sprouting. *Cell* United States; 2013;**154**:651–663.
23. Leibundgut G, Scipione C, Yin H, Schneider M, Boffa MB, Green S, Yang X, Dennis E, Witztum JL, Koschinsky ML, Tsimikas S. Determinants of binding of oxidized phospholipids on apolipoprotein (a) and lipoprotein (a). *J Lipid Res* United States; 2013;**54**:2815–2830.
24. Chang M-K, Binder CJ, Miller YI, Subbanagounder G, Silverman GJ, Berliner JA, Witztum JL. Apoptotic cells with oxidation-specific epitopes are immunogenic and proinflammatory. *J Exp Med* United States; 2004;**200**:1359–1370.
25. Scipione CA, Sayegh SE, Romagnuolo R, Tsimikas S, Marcovina SM, Boffa MB, Koschinsky ML. Mechanistic insights into Lp(a)-induced IL-8 expression: a role for oxidized phospholipid modification of apo(a). *J Lipid Res* United States; 2015;**56**:2273–2285.
26. Kawanami D, Mahabeleshwar GH, Lin Z, Atkins GB, Hamik A, Haldar SM, Maemura K, Lamanna JC, Jain MK. Kruppel-like factor 2 inhibits hypoxia-inducible factor 1alpha expression and function in the endothelium. *J Biol Chem* United States; 2009;**284**:20522–20530.
27. Doddaballapur A, Michalik KM, Manavski Y, Lucas T, Houtkooper RH, You X, Chen W, Zeiher AM, Potente M, Dimmeler S, Boon RA. Laminar shear stress inhibits endothelial cell metabolism via KLF2-mediated repression of PFKFB3. *Arterioscler Thromb Vasc Biol* United States; 2015;**35**:137–145.
28. Bartrons R, Rodriguez-Garcia A, Simon-Molas H, Castano E, Manzano A, Navarro-Sabate A. The potential utility of PFKFB3 as a therapeutic target. *Expert Opin Ther Targets* England; 2018;**22**:659–674.
29. Viney NJ, Capelleveen JC van, Geary RS, Xia S, Tami JA, Yu RZ, Marcovina SM, Hughes SG, Graham MJ, Crooke RM, Crooke ST, Witztum JL, Stroes ES, Tsimikas S. Antisense oligonucleotides targeting apolipoprotein(a) in people with raised lipoprotein(a): two randomised, double-blind, placebo-controlled, dose-ranging trials. *Lancet (London, England)* England; 2016;**388**:2239–2253.
30. Li X, Kumar A, Carmeliet P. Metabolic Pathways Fueling the Endothelial Cell Drive. *Annu Rev Physiol* United States; 2019;**81**:483–503.
31. Koelwyn GJ, Corr EM, Erbay E, Moore KJ. Regulation of macrophage immunometabolism in atherosclerosis. *Nat Immunol* United States; 2018;**19**:526–537.
32. Ali L, Schnitzler JG, Kroon J. Metabolism: The road to inflammation and atherosclerosis. *Curr Opin Lipidol* England; 2018;**29**:474–480.
33. Kovacs L, Cao Y, Han W, Meadows L, Kovacs-Kasa A, Kondrikov D, Verin AD, Barman SA, Dong Z, Huo Y, Su Y. PFKFB3 in Smooth Muscle Promotes Vascular Remodeling in Pulmonary Arterial Hypertension. *Am J Respir Crit Care Med* United States; 2019;**200**:617–627.
34. Feng S, Bowden N, Fragiadaki M, Souilhol C, Hsiao S, Mahmoud M, Allen S, Pirri D, Ayllon BT, Akhtar S, Thompson AAR, Jo H, Weber C, Ridger V, Schober A, Evans PC. Mechanical Activation of Hypoxia-Inducible Factor 1alpha Drives Endothelial Dysfunction at Atheroprone Sites. *Arterioscler Thromb Vasc Biol* United States; 2017;**37**:2087–2101.
35. Minchenko A, Leshchinsky I, Opentanova I, Sang N, Srinivas V, Armstead V, Caro J. Hypoxia-inducible factor-1-mediated expression of the 6-phosphofructo-2-kinase/fructose-2,6-bisphosphatase-3 (PFKFB3) gene. Its possible role in the Warburg effect. *J Biol Chem* United States; 2002;**277**:6183–6187.
36. Sonveaux P, Copetti T, Saedeleer CJ De, Vegran F, Verrax J, Kennedy KM, Moon EJ, Dhup S, Danhier P, Frerart F, Gallez B, Ribeiro A, Michiels C, Dewhirst MW, Feron O. Targeting the lactate transporter MCT1 in endothelial cells inhibits lactate-induced HIF-1 activation and tumor angiogenesis. *PLoS One* United States; 2012;**7**:e33418.
37. Viney NJ, Yeang C, Yang X, Xia S, Witztum JL, Tsimikas S. Relationship between 'LDL-C', estimated true LDL-C, apolipoprotein B-100, and PCSK9 levels following lipoprotein(a) lowering with an antisense oligonucleotide. *J Clin Lipidol* United States; 2018;**12**:702–710.
38. Stiekema LCA, Stroes ESG, Verweij SL, Kassahun H, Chen L, Wasserman SM, Sabatine MS, Mani V, Fayad ZA. Persistent arterial wall inflammation in patients with elevated lipoprotein(a) despite strong low-density lipoprotein cholesterol reduction by proprotein convertase subtilisin/kexin type 9 antibody treatment. *Eur Heart J* England; 2019;**40**:2775–2781.
39. Paik J-Y, Jung K-H, Lee J-H, Park J-W, Lee K-H. Reactive oxygen species-driven HIF1alpha triggers accelerated glycolysis in endothelial cells exposed to low oxygen tension. *Nucl Med Biol* United States; 2017;**45**:8–14.
40. Bock K De, Georgiadou M, Carmeliet P. Role of endothelial cell metabolism in vessel sprouting. *Cell Metab* United States; 2013;**18**:634–647.
41. Donath MY, Shoelson SE. Type 2 diabetes as an inflammatory disease. *Nat Rev Immunol* England; 2011;**11**:98–107.
42. Bernelot Moens SJ, Neele AE, Kroon J, Valk FM van der, Bossche J Van den, Hoeksema MA, Hoogeveen RM,

Schnitzler JG, Baccara-Dinet MT, Manvelian G, Winther MPJ de, Stroes ESG. PCSK9 monoclonal antibodies reverse the pro-inflammatory profile of monocytes in familial hypercholesterolaemia. *Eur Heart J* England; 2017;
43. Libby P. Inflammation in atherosclerosis. *Arterioscler Thromb Vasc Biol* United States; 2012;**32**:2045–2051.
44. Dobin A, Davis CA, Schlesinger F, Drenkow J, Zaleski C, Jha S, Batut P, Chaisson M, Gingeras TR. STAR: ultrafast universal RNA-seq aligner. *Bioinformatics* England; 2013;**29**:15–21.
45. Heinz S, Benner C, Spann N, Bertolino E, Lin YC, Laslo P, Cheng JX, Murre C, Singh H, Glass CK. Simple combinations of lineage-determining transcription factors prime cis-regulatory elements required for macrophage and B cell identities. *Mol Cell* United States; 2010;**38**:576–589.
46. Love MI, Huber W, Anders S. Moderated estimation of fold change and dispersion for RNA-seq data with DESeq2. *Genome Biol* England; 2014;**15**:550.
47. Alhamdoosh M, Ng M, Wilson NJ, Sheridan JM, Huynh H, Wilson MJ, Ritchie ME. Combining multiple tools outperforms individual methods in gene set enrichment analyses. *Bioinformatics* England; 2017;**33**:414–424.
48. Schnitzler JG, Bernelot Moens SJ, Tiessens F, Bakker GJ, Dallinga-Thie GM, Groen AK, Nieuwdorp M, Stroes ESG, Kroon J. Nile Red Quantifier: a novel and quantitative tool to study lipid accumulation in patient-derived circulating monocytes using confocal microscopy. *J Lipid Res* United States; 2017;**58**:2210–2219.
49. Schneider M, Witztum JL, Young SG, Ludwig EH, Miller ER, Tsimikas S, Curtiss LK, Marcovina SM, Taylor JM, Lawn RM, Innerarity TL, Pitas RE. High-level lipoprotein [a] expression in transgenic mice: evidence for oxidized phospholipids in lipoprotein [a] but not in low density lipoproteins. *J Lipid Res* United States; 2005;**46**:769–778.
50. Verhoeven BAN, Velema E, Schoneveld AH, Vries JPPM de, Bruin P de, Seldenrijk CA, Kleijn DP V de, Busser E, Graaf Y van der, Moll F, Pasterkamp G. Athero-express: differential atherosclerotic plaque expression of mRNA and protein in relation to cardiovascular events and patient characteristics. Rationale and design. *Eur J Epidemiol* Netherlands; 2004;**19**:1127–1133.
51. Sapcariu SC, Kanashova T, Weindl D, Ghelfi J, Dittmar G, Hiller K. Simultaneous extraction of proteins and metabolites from cells in culture. *MethodsX* Netherlands; 2014;**1**:74–80.
52. Fernandez-Fernandez M, Rodriguez-Gonzalez P, Garcia Alonso JI. A simplified calculation procedure for mass isotopomer distribution analysis (MIDA) based on multiple linear regression. *J Mass Spectrom* England; 2016;**51**:980–987.

## Novelty and Significance

What Is Known?

- Genetic and observational data have demonstrated that elevated Lp(a) is a causal risk factor for cardiovascular disease.
- Patients with elevated levels of Lp(a) are hallmarked by increased metabolic activity in the arterial wall on PET/CT.
- Glycolysis is an important source of energy for endothelial cells.

What New Information Does This Article Contribute?

- Lp(a) and its associated OxPLs induce endothelial cell inflammation and thereby facilitate leukocyte transendothelial migration; a hallmark of atherosclerosis.
- Lp(a) activates the endothelium by enhancing PFKFB3-mediated glycolysis; the main glycolytic orchestrator of Lp(a)-induced endothelial inflammation.
- Carotid endarterectomy patients with elevated levels of Lp(a), show increased endothelial PFKFB3 and ICAM-1 expression.
- Inhibition of PFKFB3 abolishes the inflammatory potential of OxPLs associated with Lp(a).
- Selective endothelial targeting of PFKFB3-mediated glycolysis may offer a new target for future anti-inflammatory therapy in patients at increased cardiovascular risk.

Lipoprotein(a) [Lp(a)] and its associated oxidized phospholipids induce endothelial cell inflammation leading to increased leukocyte transendothelial migration. Endothelial cells need to rewire their metabolism in order to meet the energy demand to facilitate an inflammatory state. As a pivotal driver of glycolysis, the glycolytic enzyme PFKFB3 mediates Lp(a)-induced endothelial cell inflammation. Blocking PFKFB3 activity diminishes the

endothelial inflammatory and a marked reduction in leukocyte migration through the vessel wall. From clinical perspective, our findings suggest that selective targeting of endothelial metabolism, in particular PFKFB3-mediated glycolysis, may offer a new promising target for anti-inflammatory therapy in patients at increased cardiovascular risk.

## Supplemental material

### Detailed methods

*Cell culture*

Primary human aortic endothelial cells were purchased from Lonza (Baltimore, MD, the USA) and seeded on fibronectin (30μg/ml; Merck Chemicals, Amsterdam, The Netherlands)-coated, tissue culture-treated culture T75 flasks. HAECs were maintained in EGM-2 medium (Lonza) in a humidified atmosphere of 95% air and 5% $CO_2$ at 37C°. Cells between passage 3-7 were used for experiments.

*Lp(a) and LDL isolation*

Lipoprotein fractions were isolated from plasma of healthy male and female normolipidemic volunteers. All study subjects provided written informed consent prior to enrolment. The study was conducted according to the principles of the International Conference on Harmonization-Good Clinical Practice guidelines. Blood was collected in EDTA (ethylenediaminetetraacetic acid)-containing 10 mL Vacutainer tubes. Plasma was obtained after centrifugation (3000 rpm, 4°C, 15min). Lp(a) and LDL were isolated from 3.5 mL plasma from subjects with either high or normal levels of Lp(a). Lp(a) was isolated by density gradient ultracentrifugation as previously described [4]. Plasma was adjusted to d=1.25 g/mL with solid KBr solution and a discontinuous gradient was formed by layering 2 mL of d=1.225 g/mL KBr, followed by 4 mL of d=1.100 g/mL KBr and subsequently 3 mL of d=1.006 g/mL KBr. Samples were centrifuged in a Beckman centrifuge for 19 hours at 29.000 rpm at 10°C in a SW 41 Ti rotor without brake (Beckman Coulter Inc., CA). Lp(a) and LDL fractions were separated from each other due to the density gradient, cut and dialyzed at least 3 times against phosphate-buffered saline (PBS). Next, samples were filter sterilized (0.2 μm pore size; Sartorius, Göttingen, Germany) and concentrated using Amicon centrifugal filter units filter (10.000 MWCO; Millipore). Subsequently, Lp(a) and apoB concentrations were measured using commercially available immunoturbidimetric enzymatic assays (Lp(a) 21 FS, cat number: Cat. No. 1 7139 99 10 921, Diasys, Holzheim, Germany) on a Selectra system (Sopachem, Ochten, The Netherlands).

*Lp(a), serum, 17K/17KΔLBS and E06 incubation experiments*

A confluent layer of HAECs was incubated with 100 mg/dL Lp(a), 17K/17KΔLBS (a kind gift of dr. Prof. Koschinsky, Robarts Research Institute, Ontario, Canada) and/or 100μg/mL monoclonal antibody E06 (Avanti Polar Lipids, Inc., Alabaster, Alabama, USA, 330001) in EBM2 medium containing 0.5% FBS after a starvation period of 3h in EBM2 medium supplemented with 0.1% FBS. Cells were incubated for 6h and 18h after which sups and cells were stored for further experiments. For the serum incubation experiment obtained from the IONIS-APO(a)$_{Rx}$ trial [29], human serum samples from were kindly provided by Dr. Prof. Tsimikas (UCSD, La Jolla, USA). HAECs were incubated with serum and EBM-2 medium + 0,5% FBS (1:1 ratio) and

cells were harvested after 6h and 18h. Sups were taken for cytokine and lactate measurements. Please see the Major Resources Table in the Supplemental Materials.

*RNA isolation, cDNA synthesis and Real Time quantitative polymerase chain reaction (RT-qPCR)*

HAECs were lysed with TriPure (Roche, Basel, Switzerland) and stored at -80°C prior to RNA isolation. RNA was isolated using manufacturer's instructions. Briefly,1 μg of RNA was used for cDNA synthesis with iScript (BioRad, Veenendaal, The Netherlands). qPCR was performed using Sybr Green Fast (Bioline Meridian Bioscience, Cincinnati, Ohio, USA) on a ViiA7 PCR machine (Applied Biosystems, Bleiswijk, The Netherlands). qPCR was performed for the following genes: *ICAM1, VCAM1, MCP1, IL6, IL8, PFKFB3, SLC2a1, KLF2, HK2, PFKM.* Gene expression was normalized to the housekeeping gene *H36B4*. Primer sequences are outlined in Online Table I. All gene expression graphs indicate fold change of relative gene expression of which values were normalized to the mean of the control group.

*siRNA knockdown*

siRNA duplexes directed against human PFKFB3 (Merck; siRNA sense sequence CAAGAAGUUUGCCAGUGCUdTdT, antisense CAAUGAGGAAGCCAUGAAAdTdT) and ICAM-1 (Thermo Fisher; trifecta Kit, siRNA sense sequence GGAGCAAGACUCAAGACAUtt, antisense AUGUCUUGAGUCUUGCUCCtt) have been described previously [22]. Scrambled siRNA (Thermo Fisher) was used as a control. Transfection medium was prepared according manufacturer's protocol. In short, siPFKFB3/siICAM-1 and transfection medium were prepared separately. siRNA against PFKFB3/ICAM-1 was added to Opti-MEM (Invitrogen, Waltham, Massachusetts, USA) without antibiotics in a 25nM final concentration. Transfection medium was made adding lipofectamine (Invitrogen) to Opti-MEM in a 1:13.5 dilution. All solutions were incubated for 15 minutes at RT and subsequently carefully mixed. The final transfection solution was added to the cells and incubated overnight in a humidified atmosphere of 95% air and 5% $CO_2$ at 37C°. Next, medium was changed and 60h after transfection, cells were incubated in EBM2 medium containing 0.5% fetal bovine serum (FBS; ThermoFisher Scientific) for 2h. Finally, cells were stimulated for the timepoints indicated and both the supernatant and cells were stored at -80C° for further analysis.

*RNA sequencing and library preparation and analysis*

Prior to stimulation, HAECs were starved using EBM-2 medium + 0.1% FBS for 3h at 37C°. Next, Lp(a) was added as indicated using EGM-2 supplemented with 0.5% FBS. After 6h of stimulation, cells were lysed and RNA was isolated as previously mentioned. RNA quality and integrity (RIN-score >8) were determined using Lab-on-a-Chip RNA 6000 Nano on an Agilent Bioanalyzer (Agilent Technologies, Santa Clara, California, USA). Processing of all samples was performed on Illumina HumanHT-12 microarray chips by GenomeScan (Leiden, The Netherlands). RNA-seq libraries were generated from total RNA using the "NEBNext Ultra Directional RNA Library Prep Kit

for Illumina" (NEB #E7420). Briefly, rRNA was depleted from total RNA using the rRNA depletion kit (NEB# E6310). After fragmentation of the depleted RNA, cDNA synthesis was performed. Sequencing adapters were ligated to the cDNA, and the libraries were amplified by PCR. Clustering and DNA sequencing on the Illumina cBot and HiSeq 4000 was performed according to manufacturer's protocols on 2 151-cycle paired-end flow cell lanes. Image analysis, base calling, quality check, and demultiplexing was performed with the Illumina data analysis pipeline RTA (v2.7.7) and Bcl2fastq (v2.20). Reads were aligned to the human genome version hg38 with STAR (v2.5.2b) [44]. Mapped reads were filtered on MAPQ >= 30. Reads were counted in exons and aggregated per gene using HOMER's (v4.9.1) [45] analyzeRepeats.pl script with the following parameters: -count exons -raw. RPKM values were obtained using the same script with the -rpkm flag instead of -raw. Differential expression of genes was assessed with DESeq2 (v1.22.2) [46] in an R (v3.5.1) environment. Briefly, genes were condensed to the highest expressed isoform and filtered to include only genes with median RPKM > 1 in at least one experimental group, after which differential expression was called with the following design formula: '~patient + inhibition + stimulation + inhibition:stimulation'. Results for the relevant contrasts were extracted and visualized using ggplot2 (H. Wickham. ggplot2: Elegant Graphics for Data Analysis. Springer-Verlag New York, 2016.) and pheatmap (Raivo Kolde (2019). pheatmap: Pretty Heatmaps. R package version 1.0.12. https://CRAN.R-project.org/package=pheatmap). Pathway and gene ontology analysis was performed using EGSEA (v1.10.1) [47]. P-values were adjusted for multiple testing using DESeq2 as described with an FDR of 0.1 [46]. Significant differentially expressed genes were included if padj < 0.1 and a member of at least one of the following GO terms: GO_POSITIVE_REGULATION_OF_LEUKOCYTE_MIGRATION; GO_POSITIVE_REGULATION_OF_LEUKOCYTE_CHEMOTAXIS; GO_REGULATION_OF_LEUKOCYTE_MIGRATION.GO_REGULATION_OF_LEUKOCYTE_CHEMOTAXIS. R code is available upon request. The RNA sequencing data generated in this study are available at the NCBI Gene Expression Omnibus (GEO) database under accession number GSE145898.

*Cytokine and lactate measurements*

Cytokine production was measured in supernatants of HAECs using commercial enzyme-linked immunosorbent assay kits for IL-6, IL-8 and MCP-1 (all Thermo Fisher) following the manufacturers' instructions. Lactate was quantified by a coupled reaction, where lactate oxidase was used to react with lactate and convert this to pyruvate and hydrogen peroxide. The hydrogen peroxide is used by Horseradish peroxidase (HRP) to react with Amplex Red so the fluorescent product resorufin is formed. Fluorescence was measured (Fluorstar Ex 570nM, EM:585) and a standard curve was used to calculate the concentrations.

*Immunoblotting*

Samples were lysed in reducing (with β-mercaptoethanol) conditions and analyzed on 4-12% poly-acrylamide gels (BioRad) in MOPS running buffer. Proteins were transferred to PVDF membranes (BioRad) and were blocked using 5% BSA in TBS-T (Tris Buffered Saline – Tween-20). Membranes were then incubated with primary antibodies against PFKFB3 (Cell Signaling Technologies, Danvers, Massachusetts, USA, AB2617178), ICAM-1 (Cell Signaling Technologies, AB2280018), HIF-1α (BD, AB398272), and Actin (Abcam, Cambridge, UK, AB306371). Subsequent protein detection was conducted with streptavidin conjugated to horseradish peroxidase (HRP) from (R & D systems, Minneapolis, USA) and visualized with enhanced chemiluminescence and imaged with ChemiDoc MP Imaging System (BioRad) using Image Lab software (BioRad) (GE, Boston, USA). All protein levels were normalized to the loading control. Please see the Major Resources Table in the Supplemental Materials.

*Monocyte isolation*

Peripheral blood mononuclear cells (PBMCs) were obtained from whole blood samples through density centrifugation using Lymphoprep (Stemcell Technologies, Koln, Germany; D=1.077 g/mL) as described in detail elsewhere [48]. In short, blood was diluted in a 1:1 ratio with PBS/2 mM EDTA and subsequently added to a layer of lymphoprep. Next, cells were centrifuged for 20 minutes at 600x g at RT with slow acceleration and no brake. The PBMC fraction was collected and washed twice with PBS 2 mM EDTA. Next, cells were counted using a Casy Counter (Roche Innovatis Casy TT, Bielefeld, Germany). Subsequently, monocytes were isolated using human CD14 magnetic beads and MACS® cell separation columns according to the manufacturers protocol (Miltenyi, Bergisch Gladbach, Germany). In short, cells were resuspended in MACS buffer (0,5% Bovine Serum Albumin (Sigma-Aldrich, St. Louis, Missouri, USA) in PBS 2 mM EDTA). Next, CD14 MicroBeads (Miltenyi Biotec, Leiden, The Netherlands) were added and incubated for 15 minutes on ice. After incubation, the cells were washed with MACS buffer and resuspended in MACS buffer for CD14 bead isolation using MACS Separation Columns (Miltenyi Biotec). After isolation, cells were counted using a Casy Counter and monocytes were kept at 4°C in RPMI 1640 medium (Thermo Fisher) prior to usage.

*Transendothelial migration assay*

HAEC medium was changed 2h prior to monocyte addition. Next, monocytes ($1*10^5$ monocytes/mL) were added to the monolayer of HAECs and subsequently incubated in a humidified atmosphere of 95% air and 5% $CO_2$ at 37C° for 30 minutes. Then, cells were fixed with 3.7% formaldehyde (Merck), washed with PBS and at least 5 images in duplicate per condition were obtained using a Zeiss Axiovert 200 inverted-microscope (Planapochromat 10x/0.45 M27 Zeiss objective; Carl Zeiss Inc., Jena, Germany). Transmigrated monocytes were distinguished from adhered monocytes by their transitions from bright to dark morphology. Analysis of transmigrated monocytes

was done using ImageJ software and the cell-counter plugin (http://rsb.info.nih.gov/nih-image/).

*2-NBDG uptake assays (flow cytometry and confocal microscopy)*
For flow cytometry, HAECs were incubated for 3h with 0.1% FBS in EBM-2 medium prior addition of Lp(a) in 0.5% FBS in EBM-2 medium. Cells were incubated for 18h in a humidified atmosphere of 95% air and 5% $CO_2$ at 37C°. Next, Lp(a)-rich medium was replaced with 0.1% FBS in EBM-2 medium and was incubated for 1h. 2-NBDG ((2-(*N*-(7-Nitrobenz-2-oxa-1,3-diazol-4-yl)Amino)-2-Deoxyglucose; Thermo Fisher) was added in a final concentration of 50μM for all conditions. After 2h of incubation, the cells were washed twice with pre-cooled PBS and centrifuged at 1200 rpm. Cells remained on ice prior flow cytometric measurements. Fluorescence was measured in the FITC channel with a FACS Canto II (BD) and analyzed with FlowJo software version 7.6.5. (FlowJo, LLC, Ashland, OR). For confocal imaging, HAECs were added to fibronectin-coated (30 μg/mL) glass coverslips and incubated at 37°C, 5% $CO_2$, until they reached full confluency. Then cells were treated as described after which they were fixed with a final concentration of 3.7% formaldehyde and washed with PBS. Imaging was performed on a Leica TCS SP8 Confocal laser scanning microscope.

*Breeding of Lp(a) and LBS- Lp(a) transgenic mice*
Lp(a) and LBS-Lp(a) transgenic mice were bred in the Prof. Tsimikas Laboratory at UCSD. All applicable international, national, and/or institutional guidelines for the care and use of animals were followed. Transgenic mice expressing both apo(a) and human apoB, which assemble to form Lp(a), and mice that express apoB and mutant apo(a) with 2 key point mutations in its lysine binding site (LBS) lacking OxPL binding (LBS-Lp(a)) have been previously described [23,49]. Briefly, Lp(a) transgenic (Lp(a)-Tg) mice express recombinant human apo(a) cDNA encoding kringles IV-1, IV-2, a fusion of IV-3 and IV-5, IV-6 to IV-10, V, and the protease domain (8K-IV apo(a)). LBS-Lp(a)-Tg mice express mutant 8K-IV apo(a) with residues $Asp^{55}$ and $Asp^{57}$ in kringle IV-10 replaced by $Ala^{55}$ and $Ala^{57}$, losing its ability to covalently bind OxPL as verified by lack of E06 immunoreactivity[23]. In this study, all mice were on a *Ldlr*$^{-/-}$ background, fed a regular chow diet, and were 9-12 months of age. A total of 6 (4 males and 2 females) Lp(a)-Tg mice and 6 (3 males and 3 females) LBS-Lp(a)-Tg mice were used in this study.

*Immunofluorescent staining of murine aortas*
All animal experiments were conducted at the Animal Facility of the AMC and approved by the Committee for Animal Welfare (DLV102141-1) of the AMC, Amsterdam, The Netherlands. Aortas of apo(a) transgenic- and wild type mice were dissected using a dissection microscope. The aorta was dissected until 3-5mm before the iliac bifurcation. Directly after sacrifice, aortas were isolated and stored in room temperature EGM-2 medium. Next, every aorta was excised in 5 pieces of approximately 3-5mm. Finally, the aorta rings were incubated in EGM-2 medium in the presence or absence of 100 mg/dL Lp(a) and 5 ?M PFK158 for 24h

(Cayman Chemical, Ann Arbor, Michigan, USA). Please see the Major Resources Table in the Supplemental Materials. Subsequently, aortas were fixed in a final concentration of 3.7% formaldehyde and stored at 4°C. Next, aortas were embedded in paraffin and cut into 10 µm slices. Before staining, the aortas were washed 3x with tris-buffered saline (TBS) and stained for PFKFB3 (Abcam, AB181661), PECAM-1 (Thermo Fisher, AB2631039) and nuclei/DAPI for 2h in blocking buffer (5% BSA in TBS). After primary antibody incubation, samples were washed 3x with TBS prior to 60 min incubation at RT with secondary antibodies (Alexa Fluor 568 (AB2534121) for PFKFB3 and Alexa 633 (AB 2535731) for PECAM-1, Thermo Fisher). The aortas were the fixed on a glass bottom culture dish 35/10mm (GreinerBioOne, Kremsmunster, Austria) and mounted using DAKO mounting medium containing DAPI (Agilent, Santa Clara, USA). Next, samples were visualized on a Leica TCS SP8 Confocal laser scanning microscope and fluorescent intensity was quantified using ImageJ.

*Immunofluorescent staining of human carotid plaques*

The Athero-Express Biobank study design and plaque processing has been previously reported [50]. All patients provided written informed consent. The Athero-Express study protocol conforms to the Declaration of Helsinki and has been approved by the Institution's ethics committee on research on humans. Briefly, this is a prospective ongoing biobank study that includes all patients undergoing carotid or iliofemoral endarterectomy in two referral hospitals in the Netherlands. The sample size of atherosclerotic plaques (Athero-Express) was determined by our stringent selection criteria. We estimated that with a minimum of seven subjects per group, we would be able to identify changes with $p = 0.05$ and a power of 0.9. To minimize for possible influential variables only men, without diabetes and no statin use were included. Plaque sections were dewaxed using xylene and dehydrated in graduated concentration of ethanol (100%, 96% and 70% ethanol). Next, heat-induced epitope retrieval was performed prior blocking with 5% BSA in TBS for 20 min. Sections were subsequently incubated with primary antibody: PFKFB3 rabbit anti-human (Abcam, AB2617178), ICAM-1 mouse anti-human (Abcam, AB2213), von Willebrand Factor mouse anti-human (Agilent, AB2216702). After 2h of incubation at RT, sections were washed and incubated for 1h in the dark at RT with biotinylated secondary antibody: goat anti-rabbit Alexa 488 (ThermoFisher, AB 143165), goat anti-mouse Alexa 488 (ThermoFisher, AB2536161) and goat anti-mouse Alexa 647 (ThermoFisher, AB 2535804). Sections were washed and mounted with DAKO mounting medium containing DAPI (Agilent). Next, sections were imaged on a Leica TCS SP8 Confocal laser scanning microscope and quantified using Leica LAS-X software (Leica Camera, Wetzlar, Germany).

*Seahorse Flux Analysis*

A Seahorse XFe 96 analyzer (Seahorse Bioscience, Billerica, USA) was used to analyze cellular respiration. Prior to stimulation, HAECs were seeded in 80 µL EGM-2 medium at a density of 50,000 cells per well on fibronectin-coated XFe96 microplates (Seahorse Bioscience) and incubated for 48h. The plate was incubated in unbuffered DMEM assay medium (Merck) for 1.5h in a non-$CO_2$ incubator at 37°C. Extracellular acidification rates (ECAR) were measured by three baseline recordings, followed by sequential injection of glucose (10mM), the mitochondrial/ATP synthase inhibitor oligomycin (1.5µM), and the glycolysis inhibitor 2-Deoxy-D-glucose (2-DG; 100mM).

Glycolytic rate is the ECAR of the cell population after the addition of glucose. Glycolytic capacity is the maximum ECAR rate after oligomycin addition, which inhibits oxidative phosphorylation and forces the cell to fully use glycolysis to its maximum capacity. OXPHOS was determined by measuring OCR. In short, cells were stimulated as aforementioned (ECAR determination) and OCR changes were measured in response to oligomycin (1.5µM), FCCP (1.5µM) and rotenone (1.25µM) + antimycin A (2.5µM) injection. Values were corrected for cell count.

*Isotopic labeling of polar metabolites and metabolic flux analysis*

HAECs were seeded 48h prior the start of the experiment in FN coated 6-wells tissue culture plates (Merck, Darmstadt, Germany). Cells (p3) were cultured until a confluent mono layer was formed. After overnight stimulation (20h) in a humidified atmosphere of 95% air and 5% $CO_2$ at 37°C with 100 mg/dL Lp(a) derived from three different donors and 20 mM PFK158 (1h pre-incubation), medium was removed and stored. Cells were washed with PBS before adding glucose free RPMI supplemented with EGM2 singlequots (endothelial growth factors) and 0.5% dialyzed and heat-inactivated FBS and 1mM of labeled [U-$^{13}$C]-glucose (Cambridge Isotope Laboratories, Cambridge, UK) for 30 min. Samples were harvested by two-phase methanol-water/chloroform extraction as described in [51]. Briefly, medium was removed, cells were washed twice with ice-cold 0.9% NaCl, and metabolism was quenched by the addition of 1 mL ice-cold methanol-water (1:1, v/v). Thereafter, the cells were scraped from the well and collected in a 2 mL centrifuge tube. One mL of chloroform was added to the mixture, followed by tip sonication and centrifugation at 10,000 x g for 10 min. After collection of the aqueous phase, the insoluble pellets were re-extracted with 1 mL methanol-water (1:1, v/v). The aqueous phases of both extractions were collected and evaporated. The metabolite residue was dissolved in 100µL 60% (v/v) methanol and analyzed by ultra-high-pressure liquid chromatography system (Thermo Scientific) with a SeQuant ZIC-cHILIC column (100 x 2.1mm, 3 µm particle size; Merck) coupled to a Thermo Q Exactive Plus Orbitrap mass spectrometer (Thermo Scientific). The column was kept at 15°C and the flow rate was 0.250 mL/min. The mobile phase was composed of (A) 9:1 acetonitrile/water with 5 mM ammonium acetate; pH 6.8 and (B) 1:9 acetonitrile/water with 5 mM ammonium acetate; pH 6.8, respectively. The LC gradient program was: start with 100% (A) hold 0-3 min; ramping 3-20 min to 36% (A); ramping from 20-24 min to 20% (A); hold from 24-27 min at 20% (A); ramping from 27-28 min to 100% (A); and re-equilibrate from 28-35 min with 100% (A). Data was acquired in full-scan negative ionization mode. Data interpretation was performed using the Xcalibur software (Thermo Scientific). $^{13}$C enrichment was calculated based on mass isotopomer distribution analysis (MIDA), all results were corrected for their natural $^{13}$C abundance as described in [52].

*Proliferation and apoptosis assay*

HAECs were incubated with 10mM BrdU for 45 min. After incubation, cells were stained using the BrdU kit (Abcam, Cambridge, United Kingdom) according manufacturer's instruction and analyzed using a FACS Canto II (BD) and analyzed with FlowJo software version 7.6.5. (FlowJo). For the 7-AAD apoptosis assay, HAECs were incubated with PFK158 in an increasing dosage as indicated. Then cells were detached using accutase (Stemcell Technologies) and stained for 7-aminoactinomycin D (7-AAD) according manufacturer's protocol (Abcam).

Fluorescence was subsequently determined with a FACS Canto II (BD) and data was analyzed with FlowJo software version 7.6.5. (FlowJo).

*Lp(a) spiking experiments*
Human serum was added 1:1 with EBM-2 medium containing 0.5% FBS to HAECs and was subsequently spiked with 100 mg/dL Lp(a) and incubated for 6h at 37°C, 5% $CO_2$. Both supernatant and cell lysates were stored at -80°C for further experiments.

*Quantification and statistical analysis*
Data are presented as the mean ± standard error of the mean (SEM), unless stated otherwise. To avoid observer bias, the human serum experiments as well as the murine and human plaque analysis were blinded. In brief, an external colleague blinded the samples and after analysis/quantification, samples were deblinded. We tested for normality using the Shapiro-Wilk test and tested for outliers using Grubb's tests. Experiments were assessed with (repeated measures) one- or two-way ANOVA with Tukey's correction and other experiments were analyzed using two-tailed Student unpaired T-test as indicated in the figure legends. No corrections for multiple testing were made across tests, only within-test corrections. Patients were matched using 1-sided Chi-Square test. Representative images were selected based on the value closest to the mean value per group. Statistics were performed using Graphpad Prism (v8.0h; La Jolla, CA) and statistical significance was reported as follows: *P<0.05, **P<0.005, ***P<0.0005, ****P<0.00005.

Online Table I: Primer sequences

| Gene | Forward primer | Reverse Primer |
|---|---|---|
| *H36B4* | ACGGGTACAAACGAGTCCTG | GCCTTGACCTTTTCAGCAAG |
| *ICAM1* | ATGGCAACGACTCCTTCTCG | GCCGGAAAGCTGTAATG GT |
| *VCAM1* | TGTCAATGTTGCCCCCAGA | TGCTCCACAGGATTTTCGGA |
| *MCP1* | TGTCCCAAAGAAGCTGTGATC | ATTCTTGGGTTGTGGAGTGAG |
| *IL6* | CTGCAGAAAAAGGCAAAGAATCT A | GTTGTCATGTCCTGCAGCC |
| *IL8* | TGTTCCACTGTGCCTTGGTTTCTC C | TGCTTCCACATGTCCTCACAACA TCAC |
| *PFKFB3* | GCAGCTGCCTGGACAAAACA | GAGGGCAGGACACAAGCTAA |
| *KLF2* | CATCTGAAGGCGCATCTG | CGTGTGCTTTCGGTAGTGG |

| | | |
|---|---|---|
| *SLC2a1* | CGGGCCAAGAGTGTGCTAAA | TCTTCTCCCGCATCATCTGC |
| *HK2* | CCCCTGCCACCAGACTAAAC | CAAAGTCCCCTCTCCTCTGG |
| *PFKM* | TTGGGGGCTTTGAGGCTTAC | GAGCCAGGGACATTGTTGGA |

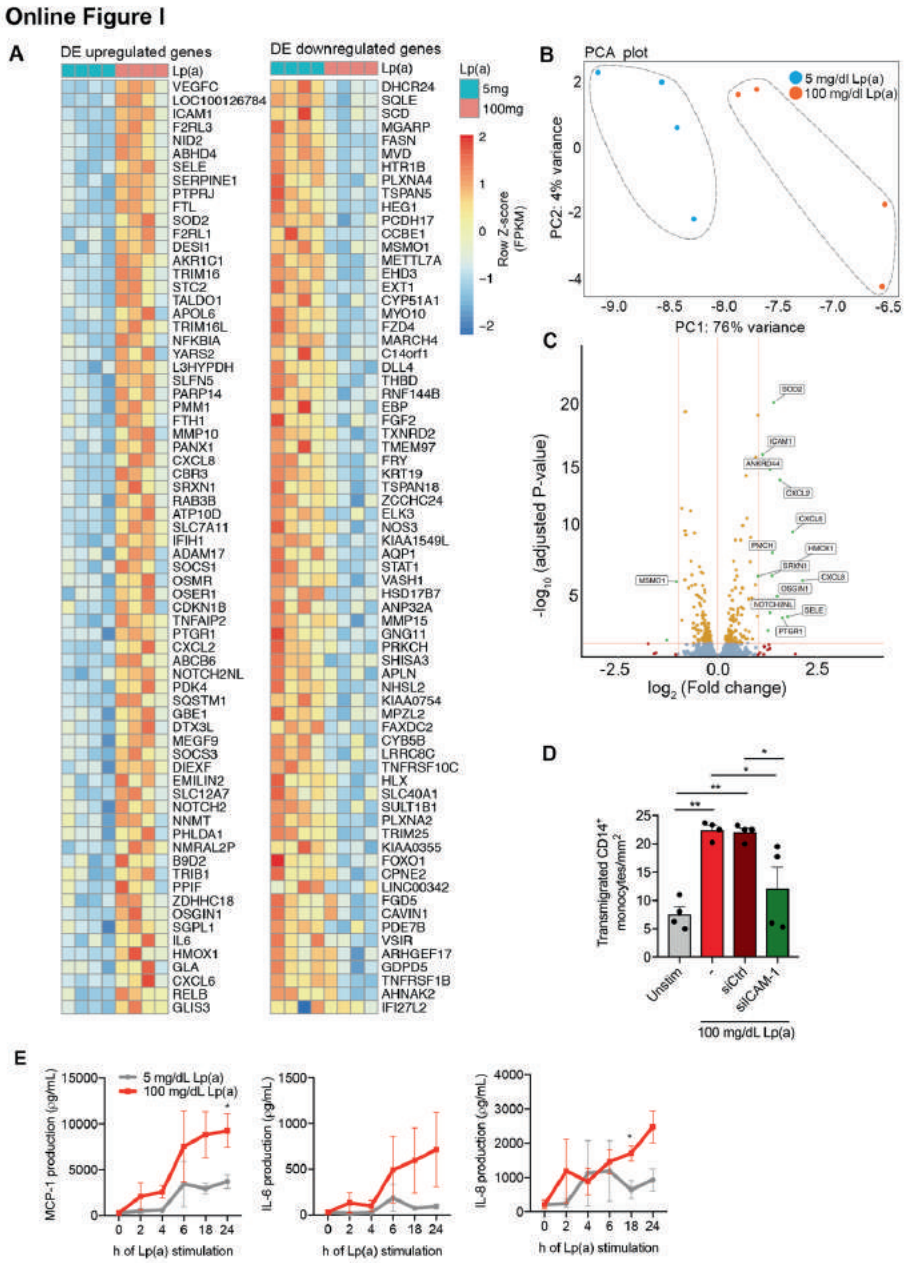


*Online Figure I. Up- and down regulated EC genes with and without Lp(a) stimulation*

**(A)** Heatmap of differentially expressed genes of 100 mg/dL vs 5 mg/dL Lp(a)-incubated ECs. (incubation 6h; n=4) **(B)** PCA plot of EC stimulated with 5 mg/dL (blue) vs 100 mg/dL Lp(a) (red) for 6h (n=4). **(C)** Volcano plot of differentially expressed gene transcripts upon Lp(a) stimulation for 6h. (n=4) **(D)** Monocyte TEM was increased when ECs were incubated with 100 mg/dL Lp(a) (red bars) and decreased after knockdown of ICAM-1 (green bar). Data were analyzed using two-way ANOVA with Tukey's correction. P=0.0054 unstimulated vs Lp(a); P=0.0064 unstimulated vs siCtrl; P=0.0435 Lp(a) vs siICAM-1; P=0.0495 siCtrl vs siICAM-1 (18h stimulation; n=5).**(E)** MCP-1, IL-6 and IL-8 secretion of ECs in medium over time (grey line = ECs stimulated with

5 mg/dL and red line = ECs stimulated with 100 mg/dL Lp(a). Data were analyzed using repeated measures two-way ANOVA with Tukey's correction. For MCP-1 P=0.0481 and for IL-8 P=0.0212. (n=4).
Lp(a), lipoprotein(a); PCA, principal component analysis; ICAM-1, intercellular adhesion molecule 1; MCP-1, monocyte chemoattractant protein 1; IL-6, interleukin 6; IL-8, interleukin 8. All data are mean ± SEM. *P<0.05; **P<0.005.

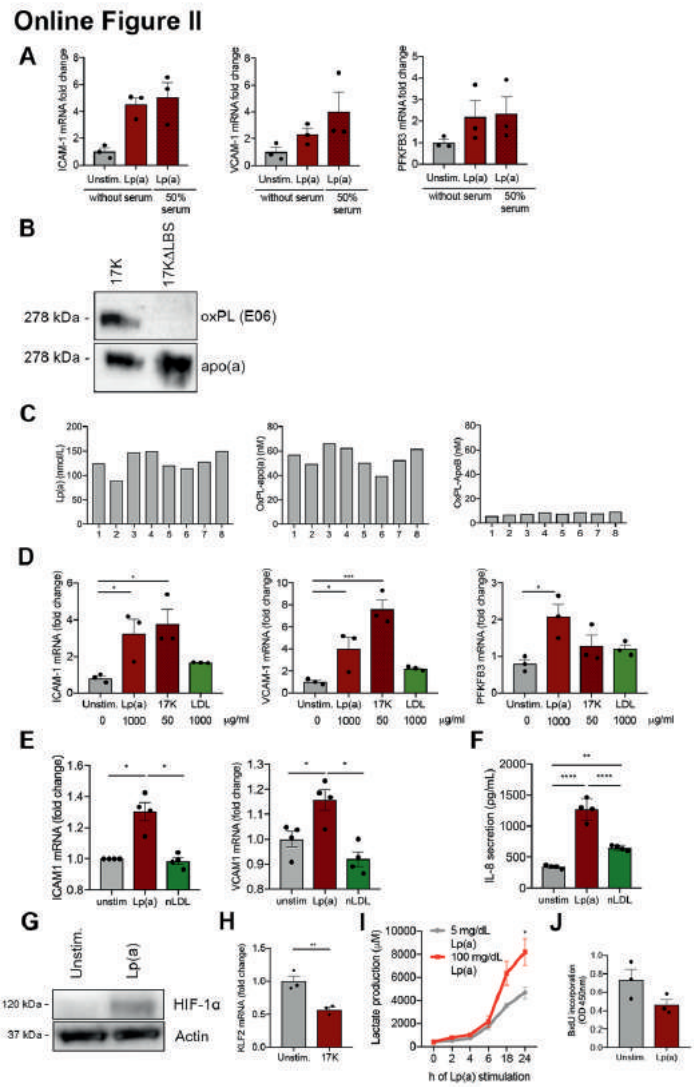


***Online Figure II. Serum and LDL does not affect Lp(a)-EC phenotype and Lp(a)-ECs does not induce proliferation.*** **(A)** Gene expression of Lp(a)-ECs with (right red bar) and without 50% serum addition (left red bar). Data were analyzed using one-way ANOVA with Tukey's correction. For *ICAM1* P=0.0296 unstimulated vs lp(a) and P=0.0155 unstimulated vs Lp(a)+50% serum (6h incubation; n=3) **(B)** Representative immunoblot of E06-detectable OxPLs on r-apo(a) constructs. **(C)** Lp(a) measurement of 8 donors used in this study (left graph). OxPL-apo(a) and OxPL-apoB measurements in Lp(a) fractions after ultracentrifugation (middle and right graph, respectively; n=8).**(D)** *ICAM1*, *VCAM1*, *PFKFB3* expression of ECs stimulated with 100 mg/dL Lp(a) (measured based on apo(a); red bars), 50µM 17K (bordeaux bars) and 100 mg/dL LDL (green bars). Data were analyzed using two-way ANOVA with Tukey's correction. For *ICAM1* P=0.0439 unstimulated vs Lp(a), P=0.0171 unstimulated vs 17K; for *VCAM1* P=0.0451 unstimulated vs Lp(a), P=0.0004 unstimulated vs 17K; for *PFKFB3* P=0.0125 unstimulated vs Lp(a). (6h incubation; n=3) **(E)** *ICAM1* and *VCAM1* expression of ECs stimulated with similar concentration of Lp(a) (measured based on apoB; red

bars) and LDL (green bars). Data were analyzed using one-way ANOVA with Tukey's correction. For *ICAM1* P=0.0283 unstimulated vs Lp(a), P=0.0167 Lp(a) vs nLDL; for *VCAM1* P=0.0266 unstimulated vs Lp(a), P=0.0240 Lp(a) vs nLDL (6h incubation; n=4). **(F)** IL-8 secretion of ECs stimulated with the same concentration of Lp(a) (based on apoB; red bars) and LDL (green bars). P<0.0001 unstimulated vs Lp(a), P=0.0067 unstimulated vs nLDL, P<0.0001 Lp(a) vs nLDL (6h incubation; n=4). **(G)** Representative immunoblot of HIF-1α in ECs incubated with 100 mg/dL Lp(a) (same experiment as showed in Fig. 5D).**(H)** KLF2 gene expression of ECs stimulated with 100 mg/dL Lp(a). Data were analyzed using two-tailed Student unpaired T-test, P=0.0092. (6h incubation; n=3) **(I)** Lactate production of 5 mg/dL-stimulated ECs (grey line) compared to 100 mg/dL Lp(a)-stimulated ECs (red line) over time. Data were analyzed using repeated measures two-way ANOVA with Tukey's correction, P=0.0305 (n=4). **(J)** BrdU-incorporation in unstimulated ECs (grey bar) compared to Lp(a)-ECs (red bar). (24h incubation; n=3)
Lp(a), lipoprotein(a); ICAM-1, intercellular adhesion molecule 1; VCAM-1, vascular adhesion molecule 1; PFKFB3, 6-phophofructo-2-kinase/fructose-2,6-biphosphatase; 17K, 17K recombinant apolipoprotein(a); 17KΔLBS, 17K recombinant apolipoprotein(a) with a mutation in the lysine binding site; OxPL, oxidized phospholipid; E06, E06, murine IgM monoclonal antibody E06 which binds the PC moiety of OxPLs; apo(a), apolipoprotein(a); IL-8, interleukin 8; HIF-1α, hypoxia inducible factor 1α; KLF2, Kruppel like factor 2; BrdU, bromo deoxyuridine; OD, optic density. All data are mean ± SEM. *P< 0.05; **P< 0.005; ***P< 0.0005; ****P<0.00005.

**Online Figure III**

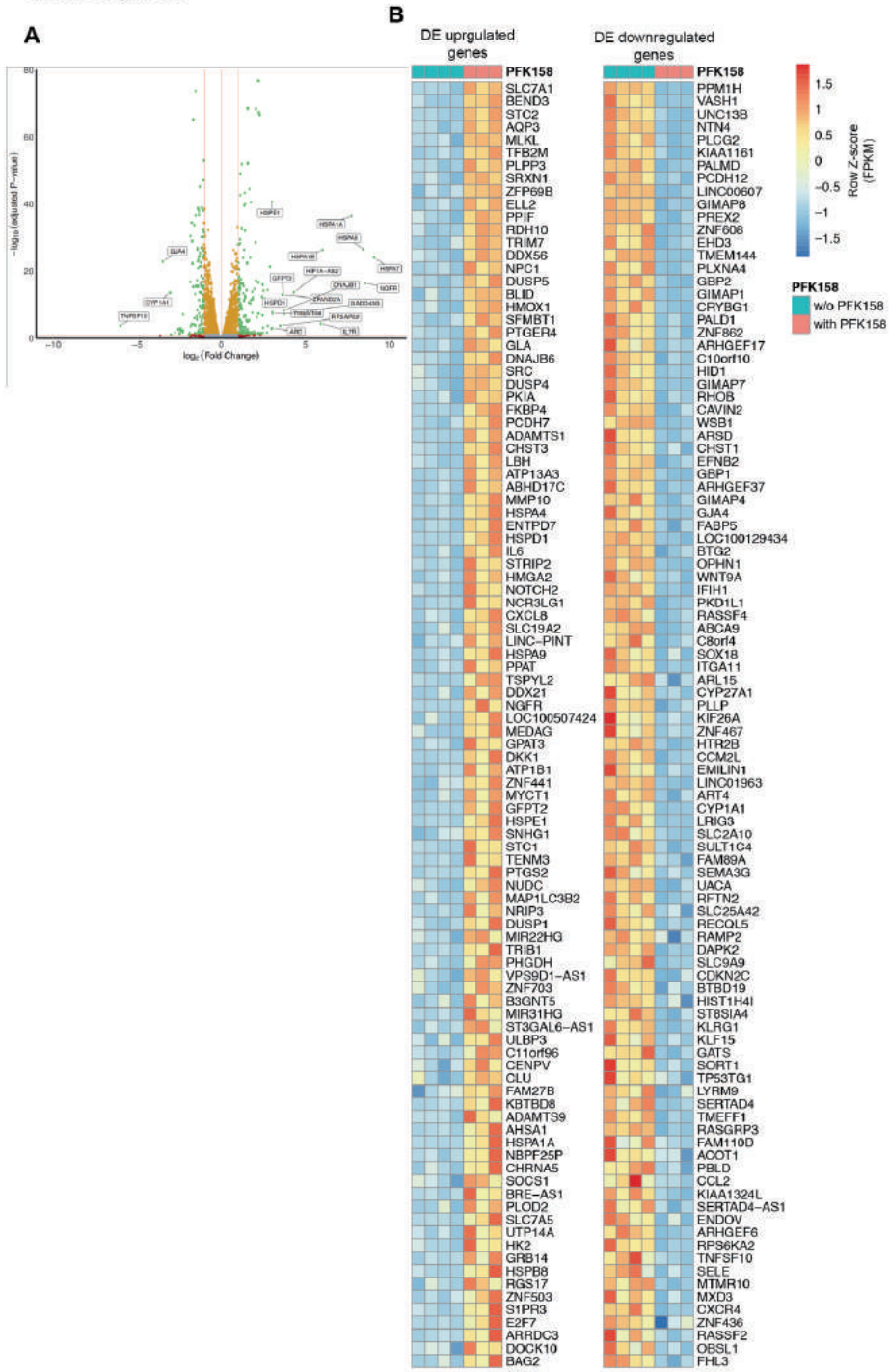

***Online Figure III. Differentially regulated genes in Lp(a)-ECs co-incubated with and without PFK158.*** **(A)** Volcano plot of statistical significance against fold change between Lp(a)-ECs (n=4) and PFK158-treated Lp(a)-ECs (n=3). (6h incubation) **(B)** Heatmap of all differentially expressed genes in Lp(a)-ECs (n=4) and PFK158-treated Lp(a)-ECs (n=3). (6h incubation).

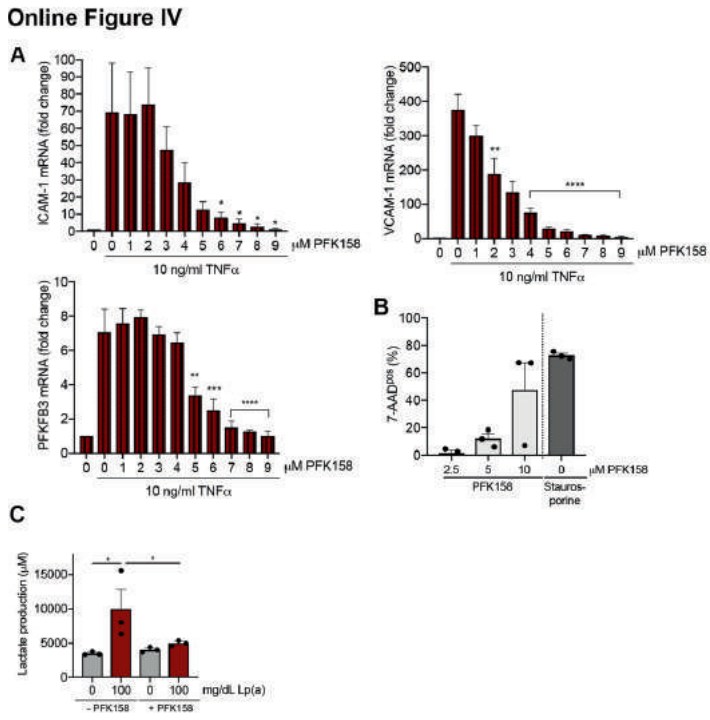


***Online Figure IV. Toxicity of PFK158 in ECs.***
**(A)** Gene expression of ECs incubated with 10 ng/mL TNFα and an increasing dosage of 0-9 μM PFK158. Data was analyzed using repeated measures two-way ANOVA with Tukey's correction. (6h incubation; n=3) **(B)** 7-AAD analysis to indicate apoptotic ECs stimulated with an increasing dosage PFK158. (18h incubation; staurosporine used as positive control; n=3). **(C)** Lactate graph: ECs were stimulated with 100 mg/dL Lp(a) (red bars) and co-incubated with glycolytic inhibitor PFK158 (5 μM). Data was analyzed using repeated measures two-way ANOVA with Tukey's correction. P=0.0386 0 vs 100 mg/dL Lp(a), P=0.0487 100 mg/dL Lp(a) vs 100 mg/dL Lp(a) (+PFK158) (n=3).
TNFα, tumor necrosis factor α; ICAM-1, intercellular adhesion molecule 1; VCAM-1, vascular adhesion molecule 1; PFKFB3, 6-phophofructo-2-kinase/fructose-2,6-biphosphatase; 7-AAD, 7 aminoactinomycin D; Lp(a), lipoprotein(a). All data are mean ± SEM *P<0.05; **P<0.005; ***P<0.0005; ****P<0.00005

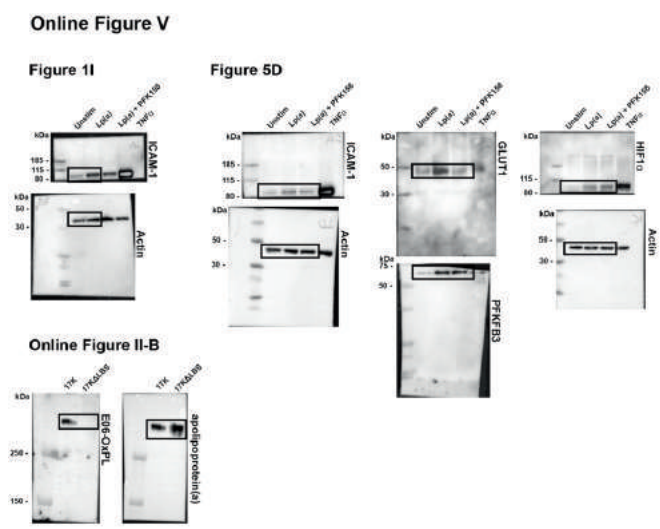


***Online Figure V: whole Western blots.***

# Chapter 9

## Inhibition of PFKFB3 hampers the progression of atherosclerosis and promotes plaque stability

Johan G. Schnitzler*, Kikkie Poels*, Farahnaz Waissi, Johannes H.M. Levels, Erik S.G. Stroes, Mat J.A.P. Daemen, Esther Lutgens, Anne-Marije Pennekamp, Dominique P.V. De Kleijn, Tom T.P. Seijkens# and Jeffrey Kroon#

*Frontiers in Cell and Developmental Biology. 2020, October*

## Abstract

**Aims.** 6-phosphofructo-2-kinase/fructose-2,6-biphosphatase (PFKFB)3-mediated glycolysis is pivotal in driving macrophage- and endothelial cell activation and thereby inflammation. Once activated, these cells play a crucial role in the progression of atherosclerosis. Here, we analyzed the expression of PFKFB-3 in human atherosclerotic lesions and investigated the therapeutic potential of pharmacological inhibition of PFKFB3 in experimental atherosclerosis by using the glycolytic inhibitor PFK158.

**Methods and Results.** PFKFB3 expression was higher in vulnerable human atheromatous carotid plaques when compared to stable fibrous plaques and predominantly expressed in plaque macrophages and endothelial cells. Analysis of advanced plaques of human coronary arteries revealed a positive correlation of PFKFB3 expression with necrotic core area. To further investigate the role of PFKFB3 in atherosclerotic disease progression, we treated six-eight weeks old male *Ldlr*$^{-/-}$ mice. These mice were fed a high cholesterol diet for 13 weeks, of which five weeks treated with the glycolytic inhibitor PFK158 to block PFKFB3 activity. The incidence of fibrous cap atheroma (advanced plaques) was reduced in PFK158-treated mice. Plaque phenotype altered markedly as both necrotic core area and intraplaque apoptosis decreased. This coincided with thickening of the fibrous cap and increased plaque stability after PFK158 treatment. Concomitantly, we observed a decrease in glycolysis in peripheral blood mononuclear cells compared to the untreated group, which alludes that changes in the intracellular metabolism of monocyte and macrophages is advantageous for plaque stabilization.

**Conclusion(s).** High PFKFB3 expression is associated with vulnerable atheromatous human carotid and coronary plaques. In mice, high PFKFB3 expression is also associated with a vulnerable plaque phenotype, whereas inhibition of PFKFB3 activity leads to plaque stabilization. This data implies that inhibition of inducible glycolysis may reduce inflammation, that has the ability to subsequently attenuate atherogenesis.

**Keywords:** Atherosclerosis, glycolysis, PFKFB3, glycolytic inhibition, inflammation

## Introduction

In recent years it has become clear that the development of atherosclerosis coincides with marked metabolic cellular alterations [1,2]. Particularly, inflammatory stimuli modify the intracellular metabolism of multiple cell types involved in atherogenesis, such as macrophages and endothelial cells. These cells are highly dependent on glycolysis for their energy metabolism to regulate cellular function [2–4].This induction in glycolysis could already be observed at regions where the endothelium is subjected to disturbed shear stress, making these early lesions susceptible for endothelial activation by lipoproteins, such as low-density lipoprotein (LDL) and lipoprotein(a) [Lp(a)] [4,5]. Lipid-lowering strategies markedly reduce cardiovascular event rates; however, a marked residual inflammatory risk remains even after potent lipid-lowering therapy in patients [6,7].

Atherogenic stimuli such as Lp(a) have been shown to induce endothelial cell activation through upregulation of key-glycolytic players comprising glucose transporter (GLUT) 1 and hexokinase (Hk) II [4]. This glycolytic switch relies predominantly on the enzyme 6-phosphofructo-2-kinase/fructose-2,6-biphosphatase (PFKFB3), which serves as a potent source for inducible glycolysis [8,9]. Conversely, inhibition of PFKFB3 leads to a marked reduction in the lipoprotein-induced inflammatory signature of endothelial cells and immune cells *in vitro*, pointing to a key role for PFKFB3 in the link between glycolysis and inflammation [4,10]. In addition, partial glycolytic inhibition in *Apoe*$^{-/-}$ mice via silencing of PFKFB3 results in decreased glycolysis in the arterial wall [10]. However, it is currently not known how glycolytic inhibition affects the progression of atherosclerosis.

In the present study, we analysed the expression of PFKFB3 in human atherosclerotic lesions and explored the therapeutic potential of pharmacological inhibition of PFKFB3 in experimental atherosclerosis.

## Materials and methods

*Immunohistochemical analysis of human coronary plaques*

Human coronary artery specimens were obtained after informed written consent of the subjects during autopsies at the Department of Pathology of the Amsterdam University Medical Center (Amsterdam, the Netherlands) and immediately fixed in 10% formalin and processed for paraffin embedding. The use of tissue was in agreement with the 'Code for Proper Secondary Use of Human Tissue in the Netherlands' and was in accordance with the principles as outlined in the Declaration of Helsinki. Based on fibrous cap formation and necrotic core size, specimens were classified as initial or advanced lesion, as described previously [11]. PFKFB3 expression was analyzed by immunohistochemistry. After deparaffinization, slides were blocked for endogenous peroxidase activity in methanol, after which heat induced antigen

retrieval was performed. Slides were then covered with 1:100 dilution of rabbit anti-human PFKFB3 antibody (Abcam, AB2617178) for an hour at room temperature. After washing with Tris-Hcl buffered saline (TBS), a secondary goat anti-rabbit biotin labeled antibody (Dako, E0432) was introduced 1:200 to the slides for 30 minutes, followed by 30 minutes of incubation with 1:200 ABC-HRP (for DAB) or ABC-AP kit (for Vector blue) (Vector, PK-6100, AK-5000). PFKFB3 was visualized with DAB (Vector SK-4105). For the double stainings, PFKFB3 was visualized with Vector blue (Vector, SK-5300), which was followed by 4% FCS block for 30 minutes and additional heat induced epitope retrieval. CD68 (mouse anti-human, Abcam, ab201340, 1:100), CD3 (rat anti-human, AbD Serotec, MCA1477, 1:100), **α**SMA (mouse anti-human, Sigma-Aldrich, F3777, 1:5000) and CD31 (mouse anti-human, Novus Biologicals, NBP2-15202, 1:100) were used, all for 1 hour at RT. Secondary goat anti-mouse biotinylated antibody (Dako, E0433) and rabbit anti-rat biotinylated antibody (Vector, BA-4001) were used at 1:300 for 30 minutes. Slides were covered in 1:200 ABC-HRP kit (Vector laboratories) for 30 minutes. Epitopes were visualized with ImmPACT AMEC red (Vector, SK-4285). Analyses of the slides was performed on a Leica DM3000 microscope with a DFC295 camera and further analysis was done with Adobe Photoshop CS6, Image J, and Las 4.1 software (Leica).

*Carotid Endarterectomy specimens from the Athero-Express Biobank*

The Athero-Express Biobank study design and plaque processing has been reported previously [12,13]. In short, the plaques were randomly selected from patients undergoing a carotid endarterectomy. Percentage of atheroma was estimated by means of visual estimation using Picrosirius red with polarized light in combination with hematoxylin stains. Three groups were considered (n=10 per group), based on the percentage of atheroma in the plaque being present: fibrous plaques containing <10% fat; fibro-atheromatous, 10% to 40%; or atheromatous, >40% fat. Next, the cumulative score for plaque vulnerability was determined by scoring macrophage-, collagen-, smooth muscle cell content and intraplaque hemorrhage. This plaque vulnerability index is scored as follows: macrophages: no/minor (0 points), moderate/heavy (1 point); collagen: moderate/heavy (0 points), no/minor (1 point); smooth muscle cells: moderate/heavy (0 points), no/minor (1 point). Intraplaque hemorrhage was scored as absent (0 points) or present (1 point), as previously described [14]. Sections were subsequently stained as described previously [4]. Briefly, plaque sections were dewaxed in xylene and dehydrated in graduated concentration of ethanol (100-70% ethanol). Heat-induced epitope retrieval was performed before blocking the sections for 20 min with 5% BSA in tris-buffered saline (TBS). Next, the sections were incubated for 2h at room temperature with the following primary antibodies: PFKFB3 rabbit anti-human (Abcam, AB2617178), CD68 (Invitrogen, MA1-80133) and von Willebrand Factor mouse anti-human (Agilent, AB2216702). Next, sections were incubated in the dark at RT with biotinylated secondary antibody: goat anti-rabbit Alexa 488 (ThermoFisher, AB 143165), goat anti-mouse Alexa 564

(ThermoFisher, AB2536161) and goat anti-mouse Alexa 647 (ThermoFisher, AB 2535804). After 1h incubation, the sections were mounted with DAKO mounting medium containing DAPI (Agilent). A Leica TCS SP8 Confocal laser scanning microscope was used to image the sections and quantification was performed using Leica LAS-X software (Leica Camera, Wetzlar, Germany). All patients provided written informed consent. The Athero-Express study protocol conforms to the Declaration of Helsinki and has been approved by the Institution's ethics committee on research on humans.

*Animal experiments*

Male *Ldlr*$^{-/-}$ mice were bred and housed at the local animal facility with normal light/dark cycle and were fed 0.15% cholesterol diet *ad libitum*. At 16 weeks of age mice were injected in the morning 3x/week for 5 weeks with PFK158 (2mg/kg *ip)* or vehicle control (0.1% DMSO). Mice were euthanized by a single intraperitoneal injection of a cocktail of 30mg/kg Sedamun (xylazine 20mg/ml) and 100mg/kg Anesketin (ketamine, 100mg/ml) and death was confirmed by heart puncture. All experiments were approved by the Committee for Animal Welfare of the University of Amsterdam, the Netherlands (protocol 265-AW-1), and comply to the European Regulations as identified in Directive 2010/63/EU on the protection of laboratory animals.

*Lipoprotein separation by fast protein liquid chromatography*

Blood was obtained by venous or cardiac puncture and collected into ethylenediaminetetraacetic acid (EDTA)-containing tubes. Individual lipoprotein levels were determined by fast-performance liquid chromatography (FPLC) as described previously [15]. In short, total cholesterol (TC) and triglyceride (TG) content in the main lipoprotein classes (VLDL, LDL and HDL) was determined using FPLC. The main system consisted of a PU-980 ternary pump with an LG-980-02 linear degasser and an UV-975 UV/VIS detector (Jasco, Tokyo, Japan). After injection of 30 ul plasma (1:1 diluted with TBS) the lipoproteins were separated using a Superose 6 increase 10/30 column (GE Healthcare Hoevelaken, The Netherlands). As eluent TBS pH 7.4 was used at a flow rate of 0.31 ml/min. A second pump (PU-2080i Plus, Jasco, Tokyo Japan) was used for either in-line cholesterol PAP or Triglyceride enzymatic substrate reagent (Sopachem, Ochten, The Netherlands) addition at a flowrate of 0.1 ml/min facilitating TC or TC detection. Commercially available lipid plasma standards (low, medium and high) were used for generation of TC or TG calibration curves for the quantitative analysis (SKZL, Nijmegen, the Netherlands) of the separated lipoprotein fractions. All calculations performed on the chromatograms were carried out with ChromNav chromatographic software, version 1.0 (Jasco, Tokyo, Japan).

*Histology*

At the age of 21 weeks, mice were sacrificed and the arterial tree was perfused with PBS and 1% paraformaldehyde. The aortic arch and organs were isolated and fixed in paraformaldehyde. Longitudinal sections of the aortic arch (4 µm)(n=10/group) and sections of the three valve area in the aortic root (n=14/group) were stained with hematoxylin and eosin and analyzed for plaque extent and phenotype as previously described [16]. One mouse was excluded from aortic arch analysis due to situs inversus. Necrotic core measurements were only performed in advanced plaques. Intimal xanthoma (IX) was defined by a small lesion consisting of foam cells in which no extracellular lipid accumulation can be detected, pathological intimal thickening (PIT) was defined as a larger lesion that mainly consists of macrophage foam cells, but contains small extracellular lipid pools and the first matrix depositions, a fibrous cap atheroma (FCA) was defined as an advanced atherosclerotic lesion with a clear fibrous cap and necrotic cores (extracellular lipid accumulation, cholesterol crystals and/or calcification) [17]. Fibrous cap thickness was measured at the thinnest part of each fibrous cap. Immunohistochemistry was performed for MAC3 (BD Pharmingen), alpha smooth muscle actin (Sigma-Aldrich), CD3 (AbD Serotec), CD8 (eBioscience), Ki67 (Abcam) and TUNEL (in situ apoptosis detection kit, Roche). The stability index was defined as (% **α** smooth muscle actin / % necrotic core). Morphometric analyses were performed on a Leica DM3000 microscope with a DFC 295 camera and Adobe Photoshop CS6, Image J or Las4.0 software (Leica).

*Flow cytometry*

Spleen and lymph nodes were homogenized, and blood and spleen samples were subjected to red blood cell lysis. The cells were stained with fluorescently labelled surface antibodies (CD45, CD3, CD4, CD8, F4/80, Ly6C, Ly6G, MHCI, MHCII, CD44, CD62L, CD19, CD11C, NK1.1; all from BD Biosciences:). For intracellular staining, cells were fixed and permeabilized with fixation/permeabilization buffer (eBioscience) and stained with fluorescent antibodies against Foxp3 (BioLegend). Flow cytometric analysis was performed on a BD Canto II (BD Biosciences).

*Immunofluorescent staining of murine aortas using confocal microscopy*

Abdominal aortas remained intact for *en face* staining with ICAM-1 (Abcam) and VCAM-1 (Abcam) or aortas were dissected until 3-5mm before the iliac bifurcation to obtain transverse sections. For the latter, aortas were embedded in paraffin for subsequent cutting sections into 10 µm slices for immunofluorescent staining. Next, the transverse sections were stained as described previously [4]. In summary, the following antibodies were used: ICAM-1 (Abcam), GLUT-1 (Thermo Fisher) and Alexa Fluor 568 for PFKFB3 and Alexa 633 for GLUT1-1 (both Thermo Fisher). The transverse sections aortas were fixed with DAKO mounting medium containing DAPI (Agilent, Santa Clara, USA). All samples were visualized on a Leica TCS SP8 Confocal laser scanning microscope and quantified using ImageJ.

*RNA isolation, cDNA synthesis and Real Time quantitative polymerase chain reaction*
Tissues were homogenized and lysed with TriPure (Roche, Basel, Switzerland). RNA was isolated according to the manufacturer's instructions. Briefly,1 μg of RNA was used for cDNA synthesis with iScript (BioRad, Veenendaal, The Netherlands). qPCR was performed using Sybr Green Fast (Bioline Meridian Bioscience, Cincinnati, Ohio, USA) on a ViiA7 PCR machine (Applied Biosystems, Bleiswijk, The Netherlands). Gene expression was normalized to the housekeeping gene *H36B4*. Primer sequences are shown in Supplemental Table 1. All gene expression graphs indicate fold change of relative gene expression of which values were normalized to the mean of the control group.

*Murine PBMC isolation and Seahorse Flux Analysis*
Murine peripheral blood mononuclear cells (PBMCs) were obtained from whole blood samples through density centrifugation using Lymphoprep (Stemcell Technologies, Koln, Germany; D=1.077 g/mL) as described in detail previously [18]. In short, blood was diluted in a 1:1 ratio with PBS enriched with 2 mM EDTA and subsequently added to a layer of Lymphoprep. Next, cells were centrifuged for 20 minutes at 600x g at RT with slow acceleration and no brake. The PBMC fraction was collected and washed twice with PBS/2 mM EDTA. Next, cells were counted using a Casy Counter (Roche Innovatis Casy TT, Bielefeld, Germany). Next, PBMCs were seeded in 80 μL EGM-2 medium at a density of 50.000 cells per well on XFe96 microplates (Seahorse Bioscience). The cells were incubated in unbuffered DMEM assay medium (Merck) for 1.5h in a non-$CO_2$ incubator at 37°C. A Seahorse XFe 96 analyzer (Seahorse Bioscience, Billerica, USA) was used to analyze cellular respiration. Extracellular acidification rates (ECAR) were measured after injecting glucose (10mM), the mitochondrial/ATP synthase inhibitor oligomycin (1.5μM), and the glycolysis inhibitor 2-Deoxy-D-glucose (2-DG; 100mM), to determine glycolysis, glycolytic capacity and glycolytic reserve, respectively. Values were corrected for cell count.

*Quantification and statistical analysis*
Data are presented as the mean ± standard error of the mean (SEM), unless stated otherwise. To avoid observer bias, the murine and human plaque analysis were blinded. Experiments were assessed with two-tailed Student T-tests, two-tailed Mann Whitney or One-way ANOVA as indicated in the figure legends. Clinical characteristics of patients from the Athero-Express Biobank were compared between the three plaque phenotypically different groups (fibrous, fibro-atheromatous, and atheromatous plaques). Statistical testing for differences between the three group was done by using a One-way ANOVA test for normally distributed data and a Kruskal-Wallis Rank Sum Test for non-normally distributed data (i.e., triglycerides and lipoprotein (a)). Representative images were selected based on the value closest to the mean value per group. Statistics were performed using Graphpad Prism (v8.0h;

La Jolla, CA) and statistical significance was reported as *P<0.05. The analysis found in the baseline table was performed in R version 3.6.1 (R Foundation, Vienna, Austria). A P-value of <0.05 was considered statistically significant.

## Results

*PFKFB3 expression in macrophages and endothelial cells correlates with plaque instability in human atherosclerosis*

Carotid plaques were obtained from patients undergoing endarterectomy enrolled in the Athero-Express biobank. Plaques were classified as fibrous plaques (containing <10% intraplaque fat), fibro-atheromatous (10% to 40% intraplaque fat) or atheromatous (>40% intraplaque fat) [12,13]. Both fibro-atheromatous and atheromatous plaques had an increased plaque vulnerability index (Table 1) [13]. Further carotid plaque analysis revealed a marked higher PFKFB3 expression when plaque vulnerability is higher (Figure 1A, B). Higher PFKFB3 expression coincides with high number of $CD68^+$ macrophage in atheromatous plaques (Figure 1A, C) that positively correlates with PFKFB3 expression (Figure 1D). These data imply that mainly macrophages show enhanced PFKFB3 expression in atherosclerotic plaques. In line, human coronary atherosclerotic plaques, histologically classified as fibrous cap atheromata (advanced atherosclerosis) express higher levels of $PFKFB3^+$ cells when compared with intimal xanthomas or pathological intimal thickenings (initial/intermediate atherosclerosis) (Figure 1E, F). PFKFB3 expression positively correlates with necrotic core area (Figure 1G), indicating that PFKFB3 expression increases during the progression of atherosclerosis. The majority of $PFKFB3^+$ cells are $CD68^+$ macrophages and $PECAM^+$ endothelial cells (Figure 1H, I). Only few $CD3^+$ T cells and **α** smooth muscle actin (**α**SMA)$^+$ vascular smooth muscle cells express PFKFB3 (Figure 1J, K). Together, these data suggest that PFKFB3 expression increases as plaques become more vulnerable.

*Table 1. Clinical characteristics of included patients of Athero-Express Biobank.*

| | Fibrous (n = 10) | Fibro-Atheromatous (n=10) | Atheromatous (n = 10) | P-value |
|---|---|---|---|---|
| Age | 73.1 (7.5) | 67.7 (8.7) | 69.4 (7.4) | 0.308 |
| Gender (Male, %) | 6 (60.0) | 8 (80.0) | 8 (80.0) | 0.506 |
| Systolic blood pressure, mmHg | 148.3 (33.6) | 174.7 (45.6) | 176.7 (37.3) | 0.316 |
| BMI, $kg/m^2$ | 26.8 (4.5) | 26.0 (2.5) | 27.2 (3.8) | 0.768 |
| Current smoker (yes, %) | 2 (20.0) | 4 (40.0) | 4 (40.0) | 0.549* |
| Cholesterol lowering medication, (yes, %) | 9 (90.0) | 8 (80.0) | 8 (80.0) | 0.787 |
| Total cholesterol, mmol/L | 3.9 (0.7) | 4.3 (0.9) | 4.0 (1.3) | 0.607 |
| HDL-cholesterol, mmol/L | 1.0 (0.3) | 1.1 (0.3) | 1.0 (0.2) | 0.587 |
| LDL-cholesterol, mmol/L | 2.0 (0.3) | 2.3 (1.0) | 2.0 (1.1) | 0.709 |
| Triglycerides, mmol/L | 1.7 [1.3, 2.5] | 1.4 [1.0, 1.8] | 1.3 [0.9, 1.8] | 0.399 |
| Lipoprotein(a), nmol/L | 21.4 [11.1, 44.6] | 49.4 [14.0, 121.5] | 14.2 [12.2, 47.0] | 0.464 |
| Glucose, mmol/L | 5.9 (2.1) | 6.7 (3.5) | 6.8 (3.0) | 0.794 |
| Plaque Vulnerability Index | 0.0 (0.0) | 1.4 (0.5) | 3.8 (0.4) | <0.001 |

*Chi-Square test, 1-sided
Data are presented as mean (SD), n (%) or median [IQR]. BMI, body-mass index; HDL, high density lipoprotein; LDL, low-density lipoprotein.

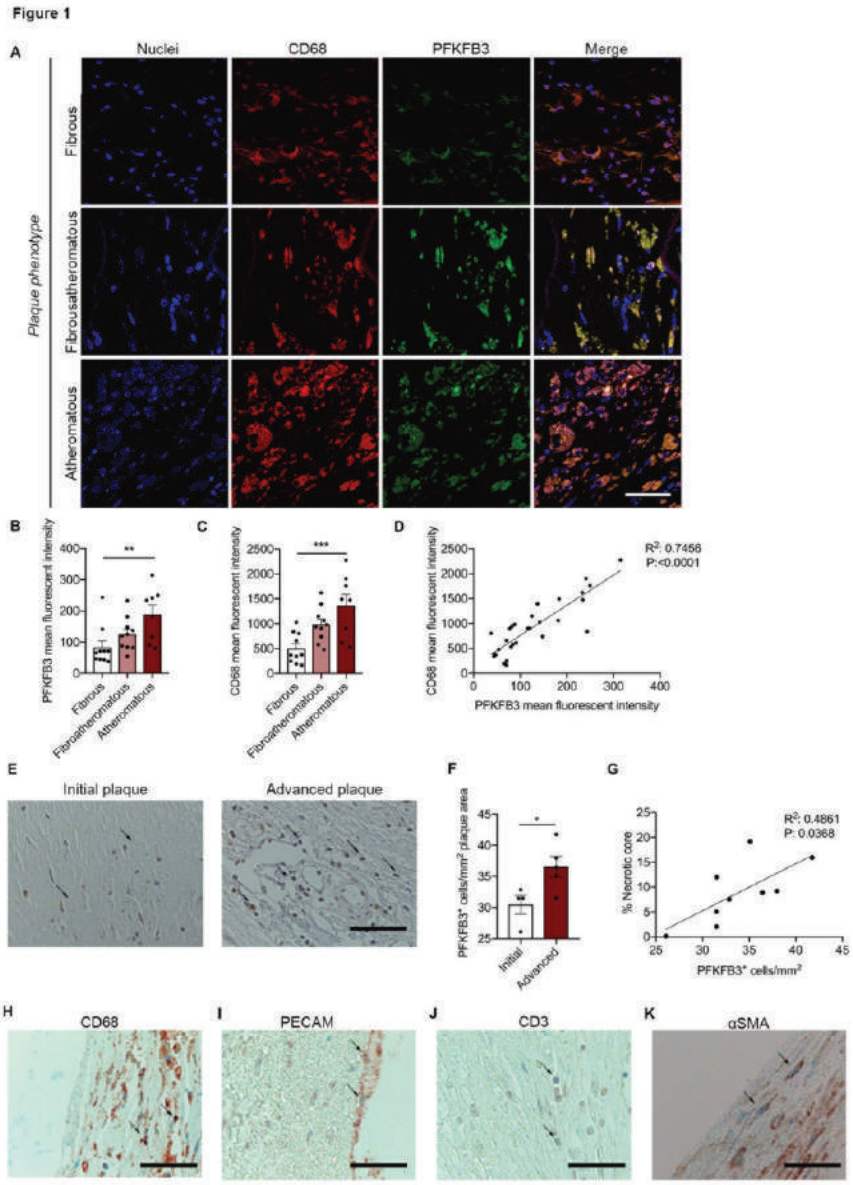


**Figure 1. PFKFB3 expression is increased in advanced atherosclerotic plaques and correlates with CD68⁺ macrophages and necrotic core area. (A + B)** Increased expression of PFKFB3 (green) in atheromatous plaques compared with fibrous carotid plaques. n=10 for fibrous and fibroatheromatous plaques, n=8 for atheromatous plaques; one-way ANOVA, P=0.0078 for fibrous vs atheromatous plaques. Scale bar 50μm **(A + C)** $CD68^+$ macrophages (red) increased in atheromatous carotid plaques. n=10 for fibrous and fibroatheromatous plaques, n=8 for atheromatous plaques; one-way ANOVA, P=0.0008 for fibrous vs atheromatous plaques. Scale bar 50μm **(D)** PFKFB3 expression and CD68 expression correlated significantly. n=28; linear regression analysis, $R^2$=0.7456, P<0.0001. **(E)** Human coronary atherosclerotic advanced plaques showed increased PFKFB3 expression compared to initial plaques. n=4 for initial vs n=5 for advanced plaques; two-tailed unpaired Mann-Whitney,

P=0.0317. Scale bar 200μm **(F)** PFKFB3 expression positively correlated with necrotic core area. n=9; Linear regression analysis $R^2$=0.4861, P=0.0368. **(G)** Immunohistochemistry of PFKFB3$^+$ co-staining with CD68$^+$ macrophages; Scale bar 100μm, **(H)** PECAM$^+$ endothelial cells; Scale bar 100μm, **(I)** CD3$^+$ T cells; Scale bar 100μm and **(J)** and **α** smooth muscle actin (**α**SMA)$^+$ vascular smooth muscle cells; Scale bar 100μm.
Data are shown as mean ± standard error of the mean. *P<0.05. PFKFB3, 6-phophofructo-2-kinase/fructose-2,6-biphosphatase 3; PECAM, platelet endothelial cell adhesion molecule; **α**SMA, **α** smooth muscle actin.

*PFKFB3 inhibition hampers the progression of atherosclerosis and promotes plaque stability*

To investigate the therapeutic potential of PFKFB3 inhibition on atherosclerosis, 6-8 weeks-old *Ldlr*$^{-/-}$ mice received a high fat diet for 8 weeks and were subsequently treated with the PFKFB3 inhibitor PFK158 for 5 weeks (intraperitoneal administration, three times per week, 2mg/kg) (Figure 2A). To assess the efficacy of PFK158, we examined the metabolic signature of peripheral blood mononuclear cells (PBMCs) of PFK158-treated mice which displayed a significant decrease in glycolytic capacity (Figure 2B). PFK158 treatment had no effect on bodyweight and total plasma cholesterol levels, plasma VLDL-, LDL- and HDL-levels (Figure 2C, D). Immune cell distribution in peripheral blood and lymphoid organs was unaffected by PFK158 treatment (Supplemental Fig. 1A-D).

While atherosclerotic lesion size in the aortic arch was not affected by PFK158 treatment (Figure 2E, F), morphological analysis demonstrated that the aortic arch of PFK158-treated mice contained relatively less fibrous cap atheroma (advanced atherosclerotic lesions) (Figure 2G). This is accompanied by an increase in the incidence of intimal xanthomas (initial atherosclerotic lesions) upon PFK158 treatment (Figure 2G), indicating that inhibition of PFKFB3 mitigates progression of atherosclerosis. Interestingly, both the necrotic core area per plaque (Figure 2H) and intraplaque apoptosis (Figure 2I) were reduced in PFK158-treated mice, whilst the number of CD4$^+$ and CD8$^+$ T cells and proliferating Ki67$^+$ cells remained unaffected (Supplemental Fig. 2A-C, respectively). In addition, a trend towards increased plaque macrophage content (Mac3$^+$ area) was observed in PFK158 treated mice (Figure 2J). Interestingly, PFK158 treatment induced a marked increase in vascular smooth muscle content (**α**SMA$^+$) (Figure 2K, L) and thickening of the fibrous cap (Figure 2M. Together this led to a significant rise in stable plaques as shown by an increased plaque stability index (Figure 2N). A similar atherosclerotic phenotype was observed in the aortic roots of PFK158 treated mice (Supplemental Fig. 3A-F). These data indicate that therapeutic inhibition of PFKFB3 inhibits the progression of atherosclerosis and promotes plaque stability.

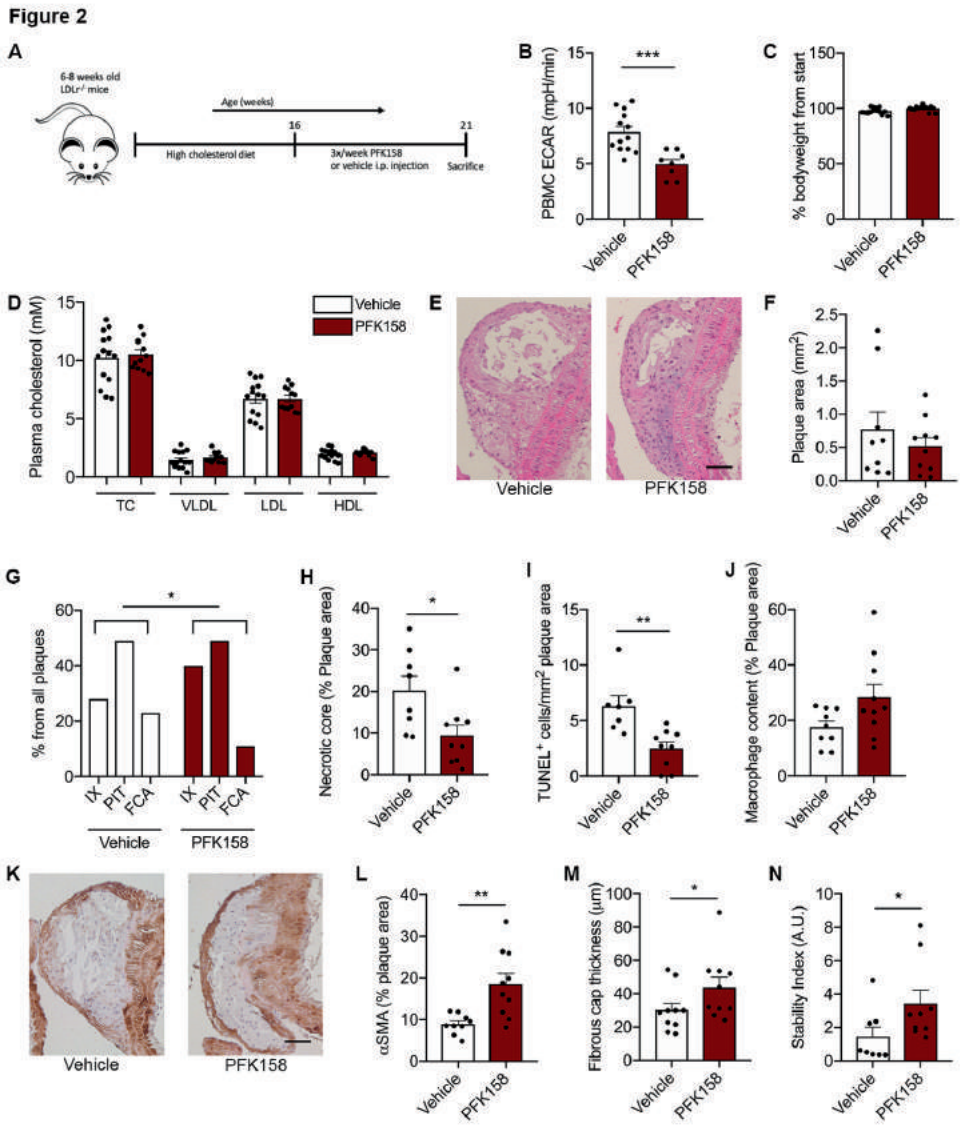


**Figure 2. PFK158 hampers the progression of atherosclerosis and increases plaque stability. (A)** Experimental design: after ten weeks of 0.15% high cholesterol diet male *Ldlr*$^{-/-}$ mice (n = 14/group) were injected three times per week with either PFK158 or vehicle for five weeks. **(B)** Analysis of circulating peripheral blood mononuclear cells revealed an increased extracellular acidification rate in vehicle cells (n=13) compared to their PFK158-treated counterparts (n=8) indicating the effectiveness of glycolytic inhibition. Two-tailed unpaired Student T-test P=0.0007. **(C)** PFK158 treatment did not significantly affect bodyweight. n=10/group **(D)** Plasma cholesterol levels remained similar between groups. n=14/group **(E-F)** Atherosclerotic lesion area in the aortic arch did not change; black bar = 50µm. n=10/group **(G)** Morphological analysis (Virmani classification) revealed a reduced incidence of fibrous cap atheroma in the aortic arch of PFK158 treated mice. The incidence of intimal xanthomas was increased in PFK158-treated mice. Chi-square, P=0.0417. **(H)** Necrotic core area per advanced plaque was reduced in PFK158 treated mice (n=8) vs vehicle (n=9). Unpaired Student T-test P=0.0205. **(I)** PFK158 treatment (n=9) reduced the number of apoptotic (TUNEL$^{+}$) cells compared to vehicle cells (n=7). Two-tailed unpaired Mann-Whitney, P=0.0012. **(J)** A trend towards increased macrophage content was observed in PFK158 treated mice. Two-tailed unpaired Student T-test P=0.0628. **(K-L)** PFK158 increased αSMA content in PFK158 treated mice (n=10) vs vehicle treated mice (n=9; Two-tailed unpaired Student T-test P=0.0033; black bar = 50µm) and **(M)** increased fibrous cap thickness (n=10/group; Two-tailed unpaired Mann-Whitney,

P=0.0410) **(N)** which increased the plaque stability index (n=8 for vehicle and n=9 for PFK158 group; Two-tailed unpaired Mann-Whitney, P=0.0464).
Data are shown as mean ± standard error of the mean. *P<0.05, **P<0.005, *** P<0.0005. TC, total cholesterol; VLDL, Very low-density lipoprotein; LDL, low-density lipoprotein; HDL, high-density lipoprotein; H&E, hematoxylin & eosin; IX, initial xanthoma; PIT, pathologic intimal thickening; FCA, fibrous cap atheroma; **α**SMA, **α** smooth muscle actin; PBMC, peripheral blood mononuclear cell; ECAR extracellular acidification rate.

### *PFK158 does not affect the atherosclerotic phenotype of endothelium*

No differences in ICAM-1 and VCAM-1 expression were observed after PFK158 treatment (Figure 3A). Previously, we have shown that GLUT1 protein expression decreases in arterial ECs after PFK158 treatment [4]; however GLUT1 expression remained unaffected in cross-sections of aortas between groups (Figure 3B). Conversely, homogenates of murine lungs, a highly vascularized organ comprising several types of macrophages, indicated that PFK158 treatment did result in a decrease in the gene expression of inflammatory markers *Il1β* and *Cd36*. Conversely, macrophage marker *F4/80* decreased in the PFK158 group, with a concomitant reduction in *Cd11c*, *Arg1* and *Cd206*, suggesting a lower content of alternatively activated macrophages (Figure 3C). Interestingly, the glycolytic signature of the lung tissue altered upon treatment as *Ctpa1* increased and *G6p* reduced in the treated group (Figure 3C). These data are indicative of an altered metabolic profile in the lung tissue on the level of gene expression after treatment with PFK158.

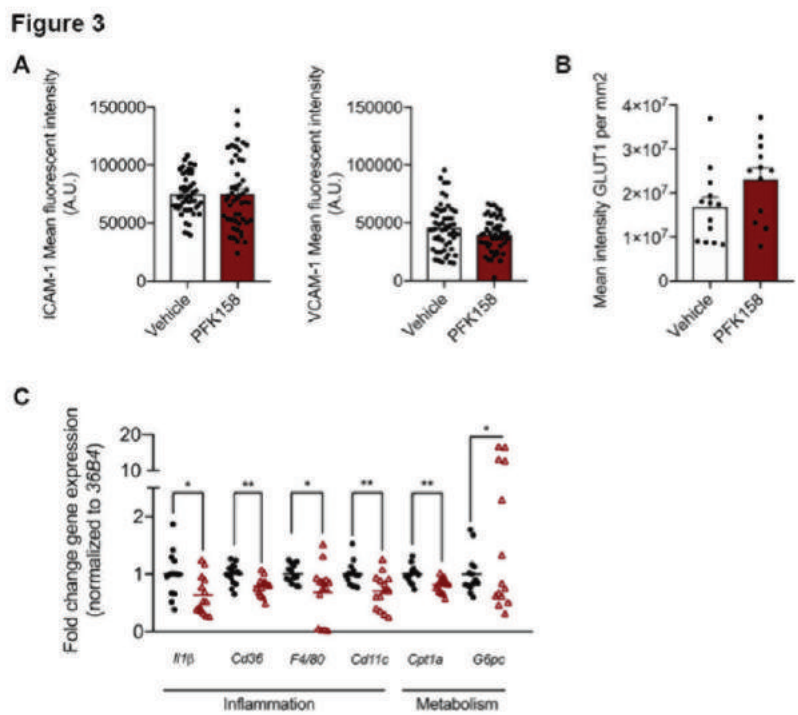


Figure 3. PFK158 alters phenotype of highly vascularized lung tissue but does not affect arterial endothelial phenotype. **(A)** ICAM-1 and VCAM-1 expression per image (n=50 per group) and **(B)** GLUT1 expression in ECs did not significantly alter between groups (n=13 for vehicle and n=12 for PFK158 group). **(C)** Lung tissue indicated several significantly differentially expressed genes. Two-tailed unpaired Student T-test, P=0.012 for *Il1β*, P=0.003 for *Cd36*, P=0.0269 for *F4/80*, P=0.0059 for *Cd11c*, P=0.0021 for *Cpt1a* and P=0.0405 for *G6pc* (n=14 per group).

Data are shown as mean ± standard error of the mean. ICAM-1, intercellular adhesion molecule 1; GLUT1, glucose transporter 1.

## Discussion

In this study, we reveal for the first time that PFKFB3 expression positively correlates with an unstable plaque phenotype in both carotid and coronary plaques in humans. Targeting PFKFB3 with a low-dose glycolytic inhibitor leads a reduction in advanced plaques with a vulnerable phenotype and an increase in stable plaque phenotype in *Ldlr*$^{-/-}$ mice, with a concomitant decrease in glycolytic flux in circulating PBMCs. This data may imply an atheroprotective role for glycolytic inhibition.

In humans, increased plaque vulnerability is characterized by a profound inflammatory and glycolytic phenotype [19] as shown by metabolomic analysis on 156 human carotid endarterectomy plaques. They reported that atherosclerotic plaques with a high risk to rupture are recognized by increased glycophorin A (indicative of intraplaque haemorrhage) and a profound glycolytic phenotype [19]. Here, we find a positive correlation between PFKFB3 expression and necrotic core area in human coronary plaques and a positive correlation between PFBFB3 and high-risk plaques, mainly attributable to high expression of PFKFB3 in macrophages in both human carotid and coronary plaques [20]. In addition, the increasing vulnerability of carotid plaques is positively associated with an increased prevalence of transient ischemic attack and stroke [13]. We also substantiate a marked increase in CD68$^{+}$ macrophage content in advanced carotid plaques [19,21]. Once macrophages are activated, they increase PFKFB3 activity, indicating that inflammation and glycolytic activation are closely intertwined [10]. Conversely, glycolytic inhibition of macrophages using siRNA against PFKFB3 or using 3-[3-pyridinyl]-1-[4-pyridinyl]-2-propen-1-one, a selective inhibitor of PFKFB3, leads to a blockade in macrophage activation [10]. *In vivo,* this translated into decreased $^{18}$F-fluorodexyglucose ($^{18}$F-FDG) uptake in the arterial vessel wall in *Apoe*$^{-/-}$ mice measured with positron emission tomography/computed tomography [22], underscoring attenuated arterial wall inflammation following attenuation of inducible glycolysis in macrophages [23]. In our *LDLr* knockout mice, we show that the progression of atherosclerosis is attenuated upon PFKFB3 inhibition. Plaques from mice treated with PFK158 displayed less fibrous cap atheromas and increased initial- and intermediate plaques, indicative of reduced formation of advanced plaques [5,19]. Thus, PFK158-treated mice displayed an increase in plaque stability index and thickening of the fibrous cap, which can be attributed to enhanced SMC proliferation and/or migration towards the fibrous cap [24].

In mice, we showed that targeting PFKFB3 *in vivo* led to decreased necrotic core area, a phenomenon that could be attributed to the significant loss of apoptotic cells in the PFK158-treaded mice compared to the control group. In advanced stages of atherosclerotic plaques, macrophage apoptosis contributes to necrotic core

formation, furthermore implying that glycolytic inhibition leads to plaque stabilization [5,25–27].

As plaque progression is dependent on the influx of immune cells, we have investigated the metabolic state of PBMCs. The PBMC fraction comprises monocytes, which are key orchestrators in the development of atherosclerosis [28–31]. In patients with severe symptomatic coronary atherosclerosis, monocytes display a distinct glycolytic phenotype by overexpressing hexokinase 2 and PFKFB3 [20]. We corroborated these findings as partial inhibition of PFKFB3 decreased glycolytic flux in PBMCs indicating that these cells were metabolically inhibited which in turn alleviated atherosclerotic burden in mice. However, as PBMCs include a variety of cells, such as monocytes and lymphocytes, it would be interesting to investigate which cell subset plays a predominant role in our model [32].

The other pivotal cell type, the endothelial cells covering the atherosclerotic plaques, did not seem to be affected by glycolytic inhibition as ICAM-1, VCAM-1 and GLUT1 expression did not alter after treatment. This might be a result of treating the mice in this study with a low dose of PFK158, whereas *in vitro* studies used increased concentrations [4]. Concomitantly, we found increased plaque stability and thickening of the fibrous cap which may be consequences of either a decrease in SMC apoptosis or increased SMC proliferation. Loss of these cells contribute to plaque destabilization once exposed to increased endoplasmic reticulum stress which facilitates apoptosis of SMCs [33].
In summary, this study demonstrates that intraplaque PFKFB3 levels are associated with plaque stability and glycolytic inhibition leads to a decrease in plaque vulnerability of vulnerable plaque characteristics and increases plaque stabilization. The present study identifies PFKFB3 inhibition as a novel target potentially suitable to further attenuate atherosclerotic development.

## Conflict of Interest

The authors declare that the research was conducted in the absence of any commercial or financial relationships that could be construed as a potential conflict of interest.

## Author contributions

J.G.S., K.P., T.T.P.S., J.K., conceived and planned the experiments. J.G.S., K.P., A.M.P., T.T.P.S., J.K., carried out the experiments and data analysis. J.G.S., K.P., T.T.P.S., J.K.wrote the manuscript. All authors provided critical feedback and helped shape the research, analysis and manuscript.

## Funding

This work was supported by the Netherlands Organization for Scientific Research. JK received a VENI grant from ZonMW (91619098). This study was also supported by the Dutch Heart Foundation (Dr. Dekker Physician-in-specialty-training grant to T.T.P.S.). This work was also financially supported by The Netherlands CardioVascular Research Initiative: the Dutch Heart Foundation, Dutch Federation of University Medical Centers, the Netherlands, Organization for Health Research and Development and the Royal Netherlands Academy of Sciences for the GENIUS-II project 'Generating the best evidence-based pharmaceutical targets for atherosclerosis-II' (CVON 2017-20 to ESGS). Funding was also obtained from the Dutch Heart Foundation, CVON 2017-05 pERSUASIVE and EU 755320 Taxinomisis grant to D.P.V.d.K.

## Acknowledgements

We would like to thank Myrthe Den Toom, Cindy van Roomen, Linda Beckers and Laurens F. Reeskamp for their technical assistance.

## References


1. Ali L, Schnitzler JG, Kroon J. Metabolism: The road to inflammation and atherosclerosis. *Curr Opin Lipidol* England; 2018;**29**:474–480.

2. Riksen NP, Stienstra R. Metabolism of innate immune cells: impact on atherosclerosis. *Curr Opin Lipidol* England; 2018;**29**:359–367.

3. Bekkering S, Arts RJW, Novakovic B, Kourtzelis I, Heijden CDCC van der, Li Y, Popa CD, Horst R Ter, Tuijl J van, Netea-Maier RT, Veerdonk FL van de, Chavakis T, Joosten LAB, Meer JWM van der, Stunnenberg H, Riksen NP, Netea MG. Metabolic Induction of Trained Immunity through the Mevalonate Pathway. *Cell* United States; 2018;**172**:135-146.e9.

4. Schnitzler JG, Hoogeveen RM, Ali L, Prange KH, Waissi F, Weeghel M van, Bachmann JC, Versloot M, Borrelli MJ, Yeang C, Kleijn D de, Houtkooper RH, Koschinsky M, Winther MP de, Groen AK, Witztum JL, Tsimikas S, Stroes ES, Kroon J. Atherogenic Lipoprotein(a) Increases Vascular Glycolysis, Thereby Facilitating Inflammation and Leukocyte Extravasation. *Circ Res* United States; 2020;

5. Libby P. Inflammation in atherosclerosis. *Arterioscler Thromb Vasc Biol* United States; 2012;**32**:2045–2051.

6. Ridker PM. Residual inflammatory risk: addressing the obverse side of the atherosclerosis prevention coin. *Eur Heart J* England; 2016;**37**:1720–1722.

7. Stiekema LCA, Stroes ESG, Verweij SL, Kassahun H, Chen L, Wasserman SM, Sabatine MS, Mani V, Fayad ZA. Persistent arterial wall inflammation in patients with elevated lipoprotein(a) despite strong low-density lipoprotein cholesterol reduction by proprotein convertase subtilisin/kexin type 9 antibody treatment. *Eur Heart J* England; 2019;**40**:2775–2781.

8. Bock K De, Georgiadou M, Schoors S, Kuchnio A, Wong BW, Cantelmo AR, Quaegebeur A, Ghesquiere B, Cauwenberghs S, Eelen G, Phng L-K, Betz I, Tembuyser B, Brepoels K, Welti J, Geudens I, Segura I, Cruys B, Bifari F, Decimo I, Blanco R, Wyns S, Vangindertael J, Rocha S, Collins RT, Munck S, Daelemans D, Imamura H, Devlieger R, Rider M, et al. Role of PFKFB3-driven glycolysis in vessel sprouting. *Cell* United States; 2013;**154**:651–663.

9. Cantelmo AR, Conradi L-C, Brajic A, Goveia J, Kalucka J, Pircher A, Chaturvedi P, Hol J, Thienpont B, Teuwen L-A, Schoors S, Boeckx B, Vriens J, Kuchnio A, Veys K, Cruys B, Finotto L, Treps L, Stav-Noraas TE, Bifari F, Stapor P, Decimo I, Kampen K, Bock K De, Haraldsen G, Schoonjans L, Rabelink T, Eelen G, Ghesquiere B, Rehman J, et al. Inhibition of the Glycolytic Activator PFKFB3 in Endothelium Induces Tumor Vessel Normalization, Impairs Metastasis, and Improves Chemotherapy. *Cancer Cell* United States; 2016;**30**:968–985.

10. Tawakol A, Singh P, Mojena M, Pimentel-Santillana M, Emami H, MacNabb M, Rudd JHF, Narula J, Enriquez JA, Traves PG, Fernandez-Velasco M, Bartrons R, Martin-Sanz P, Fayad ZA, Tejedor A, Bosca L. HIF-1alpha and PFKFB3 Mediate a Tight Relationship Between Proinflammatory Activation and Anerobic Metabolism in Atherosclerotic Macrophages. *Arterioscler Thromb Vasc Biol* United States; 2015;**35**:1463–1471.

11. Seijkens TTP, Poels K, Meiler S, Tiel CM van, Kusters PJH, Reiche M, Atzler D, Winkels H, Tjwa M, Poelman H, Slutter B, Kuiper J, Gijbels M, Kuivenhoven JA, Matic LP, Paulsson-Berne G, Hedin U, Hansson GK, Nicolaes GAF, Daemen MJAP, Weber C, Gerdes N, Winther MPJ de, Lutgens E. Deficiency of the T cell regulator Casitas B-cell lymphoma-B aggravates atherosclerosis by inducing CD8+ T cell-mediated macrophage death. *Eur Heart J* England; 2019;**40**:372–382.

12. Verhoeven BAN, Velema E, Schoneveld AH, Vries JPPM de, Bruin P de, Seldenrijk CA, Kleijn DP V de, Busser E, Graaf Y van der, Moll F, Pasterkamp G. Athero-express: differential atherosclerotic plaque expression of mRNA and protein in relation to cardiovascular events and patient characteristics. Rationale and design. *Eur J Epidemiol* Netherlands; 2004;**19**:1127–1133.

13. Verhoeven B, Hellings WE, Moll FL, Vries JP de, Kleijn DP V de, Bruin P de, Busser E, Schoneveld AH, Pasterkamp G. Carotid atherosclerotic plaques in patients with transient ischemic attacks and stroke have unstable characteristics compared with plaques in asymptomatic and amaurosis fugax patients. *J Vasc Surg* United States; 2005;**42**:1075–1081.

14. Hellings WE, Peeters W, Moll FL, Piers SRD, Setten J van, Spek PJ Van der, Vries J-PPM de, Seldenrijk KA, Bruin PC De, Vink A, Velema E, Kleijn DP V de, Pasterkamp G. Composition of carotid atherosclerotic plaque is associated with cardiovascular outcome: a prognostic study. *Circulation* United States; 2010;**121**:1941–1950.

15. Fedoseienko A, Wijers M, Wolters JC, Dekker D, Smit M, Huijkman N, Kloosterhuis N, Klug H, Schepers A, Willems

van Dijk K, Levels JHM, Billadeau DD, Hofker MH, Deursen J van, Westerterp M, Burstein E, Kuivenhoven JA, Sluis B van de. The COMMD Family Regulates Plasma LDL Levels and Attenuates Atherosclerosis Through Stabilizing the CCC Complex in Endosomal LDLR Trafficking. *Circ Res* United States; 2018;**122**:1648–1660.

16. Seijkens TTP, Tiel CM van, Kusters PJH, Atzler D, Soehnlein O, Zarzycka B, Aarts SABM, Lameijer M, Gijbels MJ, Beckers L, Toom M den, Slutter B, Kuiper J, Duchene J, Aslani M, Megens RTA, 't Veer C van, Kooij G, Schrijver R, Hoeksema MA, Boon L, Fay F, Tang J, Baxter S, Jongejan A, Moerland PD, Vriend G, Bleijlevens B, Fisher EA, Duivenvoorden R, et al. Targeting CD40-Induced TRAF6 Signaling in Macrophages Reduces Atherosclerosis. *J Am Coll Cardiol* United States; 2018;**71**:527–542.

17. Virmani R, Kolodgie FD, Burke AP, Farb A, Schwartz SM. Lessons from sudden coronary death: a comprehensive morphological classification scheme for atherosclerotic lesions. *Arterioscler Thromb Vasc Biol* United States; 2000;**20**:1262–1275.

18. Schnitzler JG, Bernelot Moens SJ, Tiessens F, Bakker GJ, Dallinga-Thie GM, Groen AK, Nieuwdorp M, Stroes ESG, Kroon J. Nile Red Quantifier: a novel and quantitative tool to study lipid accumulation in patient-derived circulating monocytes using confocal microscopy. *J Lipid Res* United States; 2017;**58**:2210–2219.

19. Tomas L, Edsfeldt A, Mollet IG, Perisic Matic L, Prehn C, Adamski J, Paulsson-Berne G, Hedin U, Nilsson J, Bengtsson E, Goncalves I, Bjorkbacka H. Altered metabolism distinguishes high-risk from stable carotid atherosclerotic plaques. *Eur Heart J* England; 2018;**39**:2301–2310.

20. Bekkering S, Munckhof I van den, Nielen T, Lamfers E, Dinarello C, Rutten J, Graaf J de, Joosten LAB, Netea MG, Gomes MER, Riksen NP. Innate immune cell activation and epigenetic remodeling in symptomatic and asymptomatic atherosclerosis in humans in vivo. *Atherosclerosis* Ireland; 2016;**254**:228–236.

21. Moore KJ, Sheedy FJ, Fisher EA. Macrophages in atherosclerosis: a dynamic balance. *Nat Rev Immunol* England; 2013;**13**:709–721.

22. Singh P, Gonzalez-Ramos S, Mojena M, Rosales-Mendoza CE, Emami H, Swanson J, Morss A, Fayad ZA, Rudd JHF, Gelfand J, Paz-Garcia M, Martin-Sanz P, Bosca L, Tawakol A. GM-CSF Enhances Macrophage Glycolytic Activity In Vitro and Improves Detection of Inflammation In Vivo. *J Nucl Med* United States; 2016;**57**:1428–1435.

23. Tarkin JM, Joshi FR, Rudd JHF. PET imaging of inflammation in atherosclerosis. *Nat Rev Cardiol* England; 2014;**11**:443–457.

24. Allahverdian S, Chaabane C, Boukais K, Francis GA, Bochaton-Piallat M-L. Smooth muscle cell fate and plasticity in atherosclerosis. *Cardiovasc Res* England; 2018;**114**:540–550.

25. Gonzalez L, Trigatti BL. Macrophage Apoptosis and Necrotic Core Development in Atherosclerosis: A Rapidly Advancing Field with Clinical Relevance to Imaging and Therapy. *Can J Cardiol* England; 2017;**33**:303–312.

26. Tabas I, Bornfeldt KE. Macrophage Phenotype and Function in Different Stages of Atherosclerosis. *Circ Res* United States; 2016;**118**:653–667.

27. Tabas I. Macrophage death and defective inflammation resolution in atherosclerosis. *Nat Rev Immunol* England; 2010;**10**:36–46.

28. Laan AM van der, Horst EN Ter, Delewi R, Begieneman MP V, Krijnen PAJ, Hirsch A, Lavaei M, Nahrendorf M, Horrevoets AJ, Niessen HWM, Piek JJ. Monocyte subset accumulation in the human heart following acute myocardial infarction and the role of the spleen as monocyte reservoir. *Eur Heart J* England; 2014;**35**:376–385.

29. Nahrendorf M, Swirski FK. Innate immune cells in ischaemic heart disease: does myocardial infarction beget myocardial infarction? *Eur Heart J* England; 2016;**37**:868–872.

30. Sotiriou SN, Orlova V V, Al-Fakhri N, Ihanus E, Economopoulou M, Isermann B, Bdeir K, Nawroth PP, Preissner KT, Gahmberg CG, Koschinsky ML, Chavakis T. Lipoprotein(a) in atherosclerotic plaques recruits inflammatory cells through interaction with Mac-1 integrin. *FASEB J Off Publ Fed Am Soc Exp Biol* United States; 2006;**20**:559–561.

31. Schnitzler JG, Dallinga-Thie GM, Kroon J. The Role of (Modified) Lipoproteins in Vascular Function: A Duet Between Monocytes and the Endothelium. *Curr Med Chem* United Arab Emirates; 2019;**26**:1594–1609.

32. Kleiveland CR. Peripheral Blood Mononuclear Cells. In: Verhoeckx K, Cotter P, Lopez-Exposito I, Kleiveland C, Lea T, Mackie A, Requena T, Swiatecka D, Wichers H, eds. Cham (CH); 2015. p. 161–167.

33. Myoishi M, Hao H, Minamino T, Watanabe K, Nishihira K, Hatakeyama K, Asada Y, Okada K, Ishibashi-Ueda H, Gabbiani G, Bochaton-Piallat M-L, Mochizuki N, Kitakaze M. Increased endoplasmic reticulum stress in atherosclerotic plaques associated with acute coronary syndrome. *Circulation* United States; 2007;**116**:1226–1233.

## Supplemental material

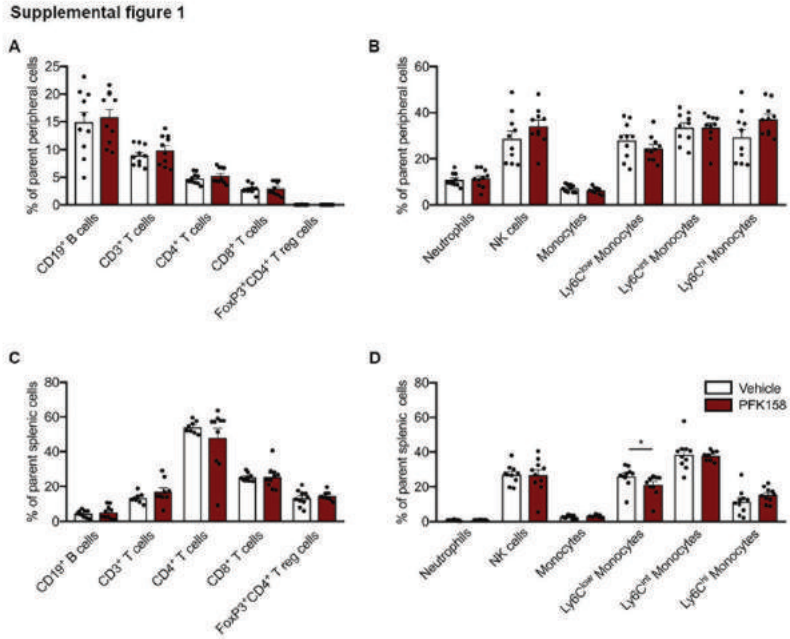


**Supplemental figure 1. PFK158 treatment does not affect peripheral and splenic cell count. (A)** Peripheral lymphoid (n=10/group) and **(B)** peripheral myeloid cell subsets do not differ between groups (n=10/group) **(C)** Splenic lymphoid cells remain unaffected (n=10/group). (D) No changes in splenic myeloid subsets, only Ly6C$^{low}$ monocytes decreased after PFK158 treatment (n=10/group). All tests were performed using Two-tailed unpaired Mann-Whitney, P=0.0156 for Ly6C$^{low}$ monocytes. Data are shown as mean ± standard error of the mean. *P<0.05.

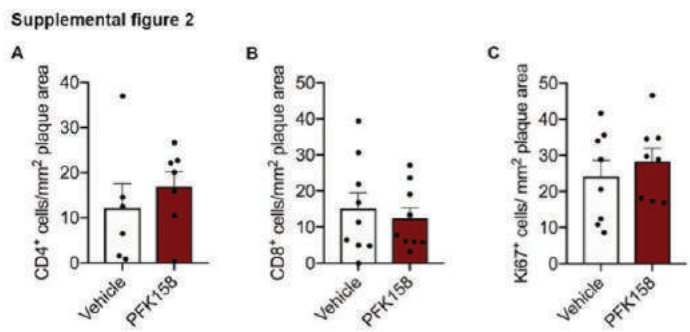


**Supplemental figure 2. No differences in lymphoid and proliferating cells in the plaque. (A)** The number of CD4$^+$ T cells (n=6 for vehicle; n=7 for PFK158), **(B)** CD8$^+$ T cells (n=9/group) and **(C)** proliferating Ki67$^+$ cells in the plaques do not alter after treatment with PFK158 (n=8) compared to vehicle (n=8). All tests were performed using Two-tailed unpaired Mann-Whitney. Data are shown as mean ± standard error of the mean.

**Supplemental figure 3**

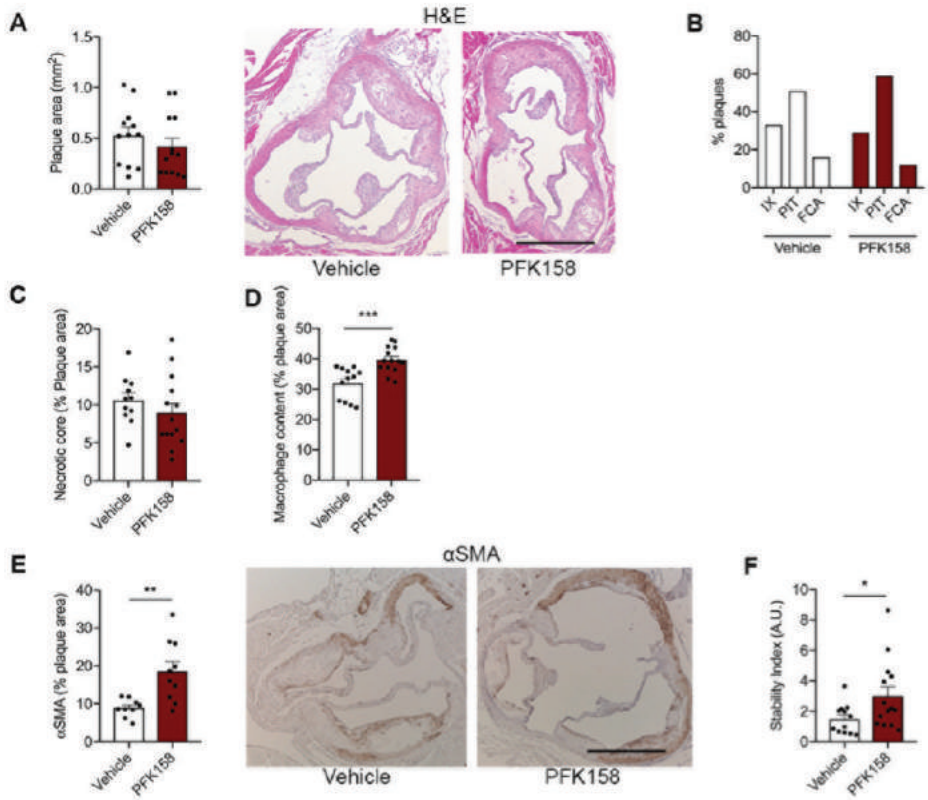


**Supplemental figure 3. Increased plaque stability in aorta roots. (A)** Atherosclerotic lesion area in the aortic roots was similar between groups (n=12 vehicle vs n=13 PFK158; black bar = 500 µm **(B)** Morphological analysis displayed no significant differences. **(C)** Necrotic core area was not affected by PFK158 treatment (n=11 vehicle vs n=14 PFK158). **(D)** Macrophage content increased in PFK158 treated mice (n=12 vehicle vs n=14 PFK158). Two-tailed unpaired Student T-test P=0.0004. **(E)** PFK158 induced a trend towards increased **α**SMA content (n=9 vehicle vs n=10 PFK158. Two-tailed unpaired Student T-test P=0.051; black bar = 500 µm. **(F)** Plaque stability index showed increased the plaque stability in PFK158 treated mice (n=13 vehicle vs n=14 PFK158. Two-tailed unpaired Mann-Whitney, P=0.027.
Data are shown as Mean ± standard error of the mean. *P<0.05, **P<0.005, *** P<0.0005 Hematoxylin & eosin, H&E; initial xanthoma, IX; pathologic intimal thickening, PIT; fibrous cap atheroma, FCA; **α** smooth muscle actin, **α**SMA

**Supplemental table 1. Primer sequences**

| Primer | Sequence |
|---|---|
| *Il1beta* | Fw: GCAACTGTTCCTGAACTCAACT<br>Rv: ATCTTTTGGGGTCCGTCAACT |
| *Cd36* | Fw: TGGCTAAATGAGACTGGGACC<br>Rv: GGCCATCTCTACCATGCCAA |
| *F4/80* | Fw: TGACAACCAGACGGCTTGTG<br>Rv: GCAGGCGAGGAAAAGATAGTGT |
| *Cd11c* | Fw: CGTCAGTACAAGGAGATGTTGGA<br>Rv: TCCTATTGCAGAATGCTTCTTTACC |
| *Cpt1a* | Fw: AGA GGG GAG GAC AGA GAC TG<br>Rv: TCT GCT CTG CCG TTG TTG TG |
| *G6pc* | Fw: CCG GTG TTT GAA CGT CAT CT<br>Rv: CAA TGC CTG ACA AGA CTC CA |

# CHAPTER 10

Summary and discussion

## Summary and discussion

This thesis describes two important components of atherosclerosis. **Part I** addresses how different sets of lipoproteins affect monocytes and **part II** focusses on the link between inflammation and metabolism in endothelial cells.

**Chapter 2** describes how lipoproteins such as LDL, remnant cholesterol and Lp(a) affect both monocytes and endothelial cells. These cells play a central role in the progression of atherosclerosis as both cell types are the key players in the process of transendothelial migration. The latter is characterized by endothelial cells that become activated at sites of disturbed blood flow, observed at bifurcations in the arteries. Furthermore, we dive more into the inflammatory phenotype of monocytes upon exposure to lipoproteins such as Lp(a) and LDL. For example, Lp(a) activates monocytes via its OxPL content by increasing adhesion structures CD11b and CD11c, which are important in de process of TEM, thereby driving atherogenesis [1]. LDL on the other hand is actively taken up intracellularly in the periphery. This peripheral lipid uptake by monocytes alters their phenotype toward an inflammatory state which coincides with an increased intracellular lipid droplet (LD) content as we also have verified patients with FH (this thesis)[2]. In this study we found a positive correlation between CCR2 expression and the content of lipid droplets in peripheral monocytes. These distinct inflammatory signatures (i.e. CD11b, CD11c, lipid droplet content of circulating monocytes) serve as important biomarkers for atherosclerotic plaque vulnerability [3–5]. However, determination of lipid content of circulating monocytes is not very well established.

*Low-density lipoprotein*

Therefore, in **chapter 3**, we reveal how the immunofluorescent dye Nile Red (NR) stains neutral LDs and can be imaged using confocal microscopy [6]. LD content is an important feature to determine the activated state of peripheral monocytes. Gower showed that LD content positively correlates with CD11b and CD11c. To further investigate LD formation and to quantify this, we developed NR Quantifier (NRQ), a novel quantification method to assess LD content in monocytes derived from patients. We isolated circulating monocytes from the blood and applied the NR staining procedure. In monocytes stained with NR, we clearly distinguished, based on 3D imaging, phospholipids and exclusively intracellular neutral lipids. Next, we developed and validated NRQ, a semi-automated quantification program in MATLAB that detects alterations in lipid accumulation in monocytes. NRQ was able to detect

monocyte LD content alterations upon *ex vivo* exposure LDL in a time- and dose-dependent manner. Finally, we validated NRQ in patients with familial hypercholesterolemia and obese subjects in pre- and postprandial state [6]. This study shows that peripheral lipid uptake is increased in FH-patients indicating that high levels of LDL increase lipid uptake by circulating monocytes. Additionally, FH-patients have monocytes characterized by increased C-C chemokine receptor (CCR) 2, scavenger receptor (SR) A and SR CD36 surface expression, all indicative of a pro-inflammatory state [2]. Especially, increased SRA and CD36 expression corroborate our findings as these structures are associated with lipid uptake as well as increased expression of the lipid efflux mediators ABCA1 and ABCG1 [7]. These mechanisms are likely to play a dominant role in the observed increased neutral LDs in circulating monocytes of FH-patients. Using lipid lowering protein convertase subtilisin/kexin type 9 (PCSK9) inhibitors in FH-patients, a strong decrease in LDL-levels was observed which was accompanied by decreased LD-content (>20% decrease) and a two-fold reduction in transendothelial migration (TEM), indicating the link between LD content and inflammatory state of monocytes [2]. These studies for the first time provide convincing evidence that increased uptake of plasma LDL in circulating (innate) immune cells predisposes towards an activated, pro-inflammatory phenotype of these cells. The latter may be an understudied, yet important link contributing to the persistent pro-inflammatory state in dyslipidemic patients. With the NRQ-tool currently available it would be interesting to see if in other disease settings such as elevated Lp(a) or increased remnant cholesterol, lipid accumulation occurs in circulating monocytes. Furthermore, as Lp(a) is an LDL-like particle but is known to signal via its OxPL content [8], it would be interesting to investigate if Lp(a) is actively being taken up in monocytes (as we see in patients with FH [2]) or solely has signaling capacity.

*Remnant cholesterol*

The increase in peripheral monocyte LD-content was also observed in patients with elevated levels of remnant cholesterol as described in **chapter 4** [9]. In this study, we evaluated the impact of remnant cholesterol on arterial wall inflammation and circulating monocytes in patients with familial dysbetalipoproteinemia (FD); a genetic disorder characterized by increased remnant cholesterol levels [10]. Similar to FH-patients, the subjects in this study were characterized by increased monocyte surface integrins CD11b, CD11c and CD18 which are important structures involved in the process of TEM [11]. Besides activation of circulating monocytes, we observed increased leukocyte counts with a marked monocytosis in FD patients. Earlier

experimental pre-clinical studies in *Apoe*$^{-/-}$ mice showed that mice exhibited excessive proliferation and myeloid skewing of hematopoietic stem and progenitor cells (HSPC)s as a result of cholesterol trapping [7]. Our *ex vitro* experiments substantiated the finding that remnant cholesterol accumulates in bone marrow-derived HSPCs, a phenomenon that coincided with myeloid skewing. This myeloid skewing implies increased generation of immune cells towards myeloid cells such as monocytes and macrophages [12]. $^{18}$F-fluordeoxy glucose positron emission tomography/computed tomography (FDG PET/CT) imaging in these patients showed increased bone marrow activation [9]. This insinuates a link between *in vitro* cholesterol trapping in isolated HSPCs and bone marrow activity in FD patients. Interestingly, the large impact of remnant cholesterol particles on inflammation was higher than anticipated, since in plasma the concentration of remnant particles is numerically much lower than their LDL counterparts. However, perhaps the atherogenicity of TRL-particles is increased per particle if compared to the LDL particle. In this respect, Varbo/Nordestgaard showed in Mendelian randomisation studies that increased TRL particles associated with higher levels of the acute inflammatory protein CRP, whereas LDL does not [13]. Thus, it has been suggested that the TRL particle not only delivers it's atherogenic cholesterol load (comparable to LDL) but is also ignites an inflammatory response by the local release of free fatty acids due to LPL-mediated TG lipolysis of the TRL particle[13]. Other recent data imply that this activated state of the bone marrow plays a pivotal role in residual risk for developing future events [14]. The mechanism behind this phenomenon was elegantly shown in hypercholesterolemic *Apoe*$^{-/-}$ mice that activate the bone marrow microenvironment and skew development towards myeloid lineages resulting in monocytosis. HSPCs derived from these mice revealed an enhanced propensity to develop pro-inflammatory Ly6C$^{high}$ monocytes which was persistent as this phenotype was also expressed in normocholesterolemic mice [12].

*Lipoprotein(a)*

In contrast to elevated LDL levels in mice, it remained enigmatic whether elevated Lp(a) levels can persistently activate the bone marrow. In patients with elevated Lp(a) levels it was found that $^{18}$F- FDG uptake was increased. In hypercholesterolemic mice it was found that even after bone marrow transplantation with normocholesterolemic, myeloid skewing and production of inflammatory monocytes was persistent. This insinuates that if LDL is lowered in patients with for example FH, lowering LDL alone would not be sufficient as the activated bone marrow still produces activated monocytes which contribute to anthogenesis. However, if a similar mechanism is

attributed to Lp(a) remains unknown. Therefore, in **chapter 5**, we investigated the bone marrow of Lp(a) transgenic mice. These mice have increased levels of Lp(a) [8]. In this study, we show that murine HSPCs stimulated with Lp(a) produce pro-inflammatory monocytes, indicating that interaction of Lp(a) with monocytes in the circulation leads to monocyte activation, but also that Lp(a) affects their production on the bone marrow level. In contrast to long-term *in vivo* priming of HSPCs by LDL [12], Lp(a) exposure did not induce long-term priming of HSPCs in mice which led to the hypothesis that this is attributed to the relative low concentrations of Lp(a) compared to LDL concentrations used in other studies and therefore the lack of Lp(a)-induced priming [15]. A possible explanation for this phenomenon is that this mainly relies on the inflammatory effects of Lp(a) orchestrated primarily via the signaling capacity of its OxPL content and not due to NLRP3 inflammasome activation resulting from intracellular cholesterol accumulation. The latter is the mechanism of LDL-induced intrinsic priming of myeloid cells and their progenitors [16,17]. Furthermore, the LDL-entity of Lp(a) and its apo(a) tail do not induce cellular activation without presence of OxPLs based on colony formation assays [18,19]. In line with this, Lp(a) was able to activate HSPCs directly (i.e. 24 h and 7 days), however, once the Lp (a) stimulus was absent (i.e. 24 h stimulation and 6 days without stimulus or BMT experiment) HSPC activity exerted normal function further indicating that Lp(a) does not induce NLRP3 activation but its mode of action is via OxPLs. Our data imply that depleting the HSPC microenvironment of Lp (a) will lead to a rapid reversal of the activated monocyte profile that is attributed to elevated Lp(a) levels, while the LDL-induced hematopoietic effects will persist for a much longer period following LDL-C reduction. This concept concurs with the attenuation of transendothelial migration of monocytes by an approximately 70% Lp(a) reduction following 12 weeks of apo(a) antisense therapy in Lp(a) patients, whereas an approximately 44% LDL-C reduction following 14 weeks of statin therapy is still characterized by an unchanged, hyperinflammatory monocyte phenotype in patients with FH [20,21]. These data indicate the distinct mode of action of both LDL and Lp(a) to induce a pro-inflammatory state. In contrast to LDL, long-term Lp(a) exposure does not lead to persistent activation of the bone marrow. Once the Lp(a) stimulus is absent, HSPCs do not skew towards a myeloid lineage. It indicates hat LDL-lowering alone in patients may not be sufficient to decrease monocyte production by the bone marrow, however this is seemingly not the case for Lp(a). Our study indicates that if Lp(a)-lowering therapies may have direct effects, especially with regards to diminished bone marrow activation and therefore decreased monocyte production.

*Triglycerides*

Post-prandial inflammation is a state in which oral food intake leads to systemic low-grade inflammation [22]. In patients with metabolic syndrome, triglyceride levels increase markedly upon oral food intake [23]. We have proposed that the increased triglyceride levels after an oral fat load lead to lipopolysaccharide (LPS) translocation from the gut towards plasma (**chapter 6)**. In this chapter, we furthermore investigated the effect of manipulation of the gut microbiota on the inflammatory response in the postprandial state. Despite large shifts fecal microbiota composition featured with a marked increase in Gram-negative bacteria and a concomitant significant elevation in fasting LPS, we did not observe a change in several postprandial inflammatory markers after a high-fat meal in lean and obese subjects with metabolic syndrome. This suggests that the LPS translocation may not play a large role in the short-term postprandial response in these groups [24]. Post-prandial IL-6 and LPS elevations have been found in previous studies. However, these studies indicate that after a high-fat meal plasma LPS as well as inflammatory markers increase, but they cannot confer, which is similar to our study, a causal relationship between postprandial LPS translocation from the gut to the plasma and low-grade inflammation observed after acute consumption of dietary fat [25,26]. Therefore, a state of postprandial inflammation is more likely attributed to elevated levels of triglycerides instead of elevated LPS levels after increased translocation from the intestines.

Together **chapters 2-6** indicate the pivotal role of lipoproteins in the onset of inflammation in CVD pathogenesis. The question arises what this implies for the machinery of cells involved in the context of metabolism. Once cells become active in a state of inflammation one can imagine that this appeals to an increase in metabolism to meet the elevated need of energy. In **part II** of this thesis, we investigate how a state of inflammation is linked to an altered metabolic cellular phenotype during atherosclerotic disease.

In **chapter 7**, we describe that cellular metabolism comprises an intricate network of many different metabolites and enzymes necessary for the generation of nucleic acids, proteins, lipids, carbohydrates which together provide energy for the cell [27]. Metabolism plays a pivotal role in maintaining homeostasis, proliferation and cellular activation. The need to produce energy in the form of ATP for cellular function is essential for both quiescent as well as activated cells and is tightly orchestrated by the integrated metabolic pathways of glycolysis, the tricarboxylic acid (TCA) cycle and the pentose-phosphate pathway (PPP) [27].

Early studies in the field metabolism focused on oncology and provided researchers with fundamental insights on how alterations in the cell's metabolism steers the fate of the cell. Where glucose via the glycolytic pathway feeds into the TCA cycle and thereby drives mitochondrial oxidative phosphorylation (OXPHOS), highly proliferative tumor cells in cancer rely predominantly on glycolysis. This is remarkable, since sufficient oxygen is present to sustain the OXPHOS pathway; a phenomenon known as 'the Warburg effect' [28]. In addition, recent findings show that the Warburg is also crucial in endothelial cells (EC) cells, monocytes and macrophages [29,30]. This interplay between metabolism and immunology is rapidly emerging due to recent insights revealing that cellular metabolism has a major impact on the functional behavior of cells.

However, the role of metabolism in endothelial cells has been done by pioneering research by the group of Prof. dr. Carmeliet who indicated glycolysis and not OXPHOS as the main source of ATP during angiogenic sprouting of ECs and even show a high glycolytic flux when in quiescent state. It was shown that ECs have relatively low mitochondrial content (2-6% of total cytoplasm volume). This substantiates the finding why ECs rely on glycolysis to generate 2 ATP molecules and lactate per glucose molecule [31,32] and underpin the importance of glycolysis as primary energy source in these cells [33]. However, the role of endothelial cell metabolism in the context of cardiovascular disease, especially the role of EC glycolysis in dictating disease progression, remains elusive to date.

In light of this, Feng and colleagues showed that atheroprone regions are featured with increased glycolysis. As such, expression of the glycolytic regulators hexokinase (HK) 2, enolase 2, glucose transporter (GLUT) 1 and 6-phosphofructo-2-kinase/fructose-2,6-biphosphatase (PFKFB) 3 were increased and (as a direct measurement for glycolysis) an increased extracellular acidification rate (ECAR). Furthermore, IκBα overexpression in ECs led to diminished nuclear factor κB (NFκB) activity and reduced hypoxia-inducible factor (HIF)1α expression, a regulator allowing rapid ATP generation [34,35]. These data imply a direct link between the endothelial metabolic and inflammatory axis. In addition, the carotid arteries of hypercholesterolemic *Apoe*$^{-/-}$ mice displayed a distinct glycolytic phenotype which was featured with increased mRNA levels of HK2, enolase 2, GLUT1 and PFKFB3. Interestingly, this metabolic profile coincided with a 50% increase in carotid lesion size compared to mice with an endothelial specific deletion of HIF1α (HIF1α$^{EC\text{-}cKO}$

*Apoe*$^{-/-}$) which thereby validated that metabolic alterations underlie experimental atherosclerotic progression *in vivo* [36].

In **chapter 8** we investigated endothelial metabolism in the context of atherogenesis and hypothesized that Lp(a) induces endothelial inflammation via rewiring EC metabolism. In this chapter, it is proposed that Lp(a) and particularly OxPLs induce EC inflammation, leading to increased adhesion and transmigration of monocytes. This is in line with previous data from our group showing that monocytes derived from patients with elevated levels of Lp(a) showed increased TEM compared with monocytes derived from healthy subjects. Lp(a) consists of different components and therefore we set out to investigate what entity of Lp(a) acts as driver of inflammation. The Lp(a) lipoprotein comprises an LDL-like particle, apolipoprotein (apo)(a), and variable amounts of OxPLs present in Lp(a), chiefly on the apo(a) and apoB components [37]. We show that the absence of Lp(a)-OxPL signaling, using either OxPL-deficient recombinant apo(a) or the E06 OxPL-blocking antibody, markedly decreases the inflammatory potential of Lp(a) in ECs. These data indicate that Lp(a)'s atherogenicity is mainly attributed to the OxPL-component and not to the LDL or apo(a) entities. OxPLs, amongst other derived from apoptotic cells, are able to activate EC and can be blocked using E06 which further implies the activating trait of OxPLs [38]. Most pivotal finding of this study is OxPLs associated with Lp(a) induce a profound glycolytic activation in ECs with PFKFB3 acting as the main orchestrator. PFKFB3 is highly expressed in ECs stimulated with Lp(a) which resulted in a marked increase in glycolytic flux as measured by extracellular acidification rate. We additionally show in human carotid plaques obtained from the Athero-Express database that PFKFB3 is highly expressed in ECs of Lp(a)-patients. ICAM-1 protein levels were also increased in human specimen, suggesting increased activation, despite an advanced atherosclerotic environment in both low and high Lp(a) groups [19]. Although the LDL difference may have contributed to a small inflammatory effect, our recent findings in the ANITSCHKOW study showed in patients with marked Lp(a) elevation, that treatment with a PCSK9 antibody resulted in 60% LDL reduction and 14% Lp(a) reduction but not a reduction of the enhanced inflammatory activity in the arterial wall of these patients. In fact, the persistent inflammatory activation was attributed to the marked residual Lp(a) elevation despite PCSK9 antibody treatment [39]. Furthermore, Tomas *et al* found that human unstable atherosclerotic plaques were characterized by an increased glycolytic activity [40]. These unstable plaques displayed increased expression of glycolytic genes *HK2*, *GLUT1*, and *PFKM*, which is highly comparable with our findings. The activated metabolic state in patients with elevated

Lp(a) was corroborated using $^{18}$F-fluorodeoxyglucose/computed tomography scans, showing a significantly higher glucose uptake in the arterial wall of subjects with Lp(a) elevation [18]. *In vitro* data in human umbilical vein ECs show that oxygen-deprived activated ECs show increased HIF1α-mediated glycolysis which lead to increased accumulation of $^{18}$F-FDG as compared with control ECs [41]. This further substantiates that ECs are very well able to accumulate glucose to subsequently increase glycolysis when activated as we observed in human carotid plaques of Lp(a) patients. These data, as a consequence raise the question whether inhibition of glycolysis may lead to a decrease in inflammation to subsequently reduce atherogenesis. Answering this question, we show that inhibition of PFKFB3 not only reverses the increased glycolytic activity in Lp(a)-ECs but also dampens the inflammatory response via amongst others reduction of endothelial secretion of IL-6 and MCP-1 leading to a concomitant decrease of healthy monocyte TEM. As glycolysis is an important energy provider, it may seem unwise to inhibit this process however, endothelial knockdown of PFKFB3 does not result in hypometabolism as ECs generate ATP at a normal rate compared with control [34]. Finally, using human serum samples from patients who received apo(a) antisense therapy to lower Lp(a) (<80%) [20], we find a significantly reduced inflammatory signature in ECs *ex vivo*. This attenuation disappeared using serum obtained after a washout in these patients, resulting in glycolytic and inflammatory responses comparable to the pretreatment serum samples. These data imply that potent Lp(a) lowering may reduce endothelial inflammation and enhanced glycolytic activity in patients with Lp(a) elevation. However, since Lp(a) lowering only partially inhibited the inflammatory responses, interventions beyond Lp(a) lowering may still be required. This indicates that inhibition of metabolism by targeting PFKFB3 may serve as interesting therapy to attenuate atherogenesis. Specific targeting of activated endothelial cells via for example VCAM-1 of ICAM-1-coated nanoparticles containing a PFKFB3-inhibitor offers a promising intervention for CVD patients [42].

To translate the concept of inhibiting glycolysis in atherosclerosis to an *in vivo* setting, we used an atherosclerotic *Ldlr*$^{-/-}$ mouse model with increased levels of cholesterol in chapter 9. Firstly, we show that PFKFB3 expression positively correlates with an unstable plaque phenotype in both carotid and coronary plaques in humans. Previous studies in humans showed that, increased plaque vulnerability is characterized by a profound inflammatory and glycolytic phenotype as shown by metabolomic analysis on 156 human carotid endarterectomy plaques [40]. In this study an increase of glycophorin A presence was found (indicative of intraplaque haemorrhage), a finding which we corroborated by demonstrating a positive correlation between PFKFB3

expression and necrotic core area in human coronary plaques and a positive correlation between PFBFB3 and high-risk plaques, mainly attributable to high expression of PFKFB3 in $CD68^+$ macrophages in both human carotid and coronary plaques [43]. This increased carotid plaque vulnerability is positively associated with an increased prevalence of transient ischemic attack and stroke [44]. Previous data indicated that targeting glycolysis rendered macrophages in a more quiescent state [45]. We corroborated these findings in atherosclerotic *LDLr* knockout mice, showing that the progression of atherosclerosis is attenuated upon PFKFB3 inhibition. Plaques from mice treated with glycolytic inhibitor displayed less fibrous cap atheromas and increased initial- and intermediate plaques, indicative of reduced formation of advanced plaques [40,46]. Plaques of these mice furthermore displayed decreased necrotic core area, a phenomenon that could be attributed to the significant loss of apoptotic cells in the treaded mice compared to the control group. In advanced stages of atherosclerotic plaques, macrophage apoptosis contributes to necrotic core formation, which implies that glycolytic inhibition leads to plaque stabilization [46–49]. As plaque progression is dependent on the influx of immune cells, we have investigated the metabolic state of peripheral blood mononuclear cells (PBMCs). The PBMC fraction comprises monocytes, which are key orchestrators in the development of atherosclerosis [11,50–52]. In patients with severe symptomatic coronary atherosclerosis, monocytes display a distinct glycolytic phenotype by overexpressing hexokinase 2 and PFKFB3 [43]. We validated these findings as partial inhibition of PFKFB3 decreased glycolytic flux in murine PBMCs indicating that these cells were metabolically inhibited which in turn alleviated atherosclerotic burden in mice [19].

*Conclusion*

In summary, the first part of this thesis describes how a variety of lipoproteins is able to induce inflammation which accelerates atherogenesis. The second part reveals that a common mechanism in the form of an altered metabolism underlies this general inflammatory state which is driven by PFKFB3 (displayed in the graphical summary in figure 1 of the general introduction*)*. Therefore, inhibition of the latter or other metabolic mediators may therefore serve as interesting novel targets to further attenuate atherosclerotic CVD.

# REFERENCES


1. Valk FM Van Der, Bekkering S, Kroon J, Yeang C, Bossche J Van Den, Buul JD Van, Ravandi A, Nederveen AJ, Verberne HJ, Scipione C, Nieuwdorp M, Joosten LAB, Netea MG, Koschinsky ML, Witztum JL, Tsimikas S, Riksen NP, Stroes ESG. Oxidized phospholipids on Lipoprotein(a) elicit arterial wall inflammation and an inflammatory monocyte response in humans. *Circulation* 2016;**134**.
2. Bernelot Moens SJ, Neele AE, Kroon J, Valk FM van der, Bossche J Van den, Hoeksema MA, Hoogeveen RM, Schnitzler JG, Baccara-Dinet MT, Manvelian G, Winther MPJ de, Stroes ESG. PCSK9 monoclonal antibodies reverse the pro-inflammatory profile of monocytes in familial hypercholesterolaemia. *Eur Heart J* England; 2017;
3. Passacquale G, Giosia P Di, Ferro A. The role of inflammatory biomarkers in developing targeted cardiovascular therapies: lessons from the cardiovascular inflammation reduction trials. *Cardiovasc Res* England; 2016;**109**:9–23.
4. Kashiwagi M, Imanishi T, Tsujioka H, Ikejima H, Kuroi A, Ozaki Y, Ishibashi K, Komukai K, Tanimoto T, Ino Y, Kitabata H, Hirata K, Akasaka T. Association of monocyte subsets with vulnerability characteristics of coronary plaques as assessed by 64-slice multidetector computed tomography in patients with stable angina pectoris. *Atherosclerosis* Ireland; 2010;**212**:171–176.
5. Gower RM, Wu H, Foster GA, Devaraj S, Jialal I, Ballantyne CM, Knowlton AA, Simon SI. CD11c/CD18 expression is upregulated on blood monocytes during hypertriglyceridemia and enhances adhesion to vascular cell adhesion molecule-1. *Arterioscler Thromb Vasc Biol* United States; 2011;**31**:160–166.
6. Schnitzler JG, Bernelot Moens SJ, Tiessens F, Bakker GJ, Dallinga-Thie GM, Groen AK, Nieuwdorp M, Stroes ESG, Kroon J. Nile Red Quantifier: a novel and quantitative tool to study lipid accumulation in patient-derived circulating monocytes using confocal microscopy. *J Lipid Res* United States; 2017;**58**:2210–2219.
7. Tall AR, Yvan-Charvet L. Cholesterol, inflammation and innate immunity. *Nat Rev Immunol* England; 2015;**15**:104–116.
8. Leibundgut G, Scipione C, Yin H, Schneider M, Boffa MB, Green S, Yang X, Dennis E, Witztum JL, Koschinsky ML, Tsimikas S. Determinants of binding of oxidized phospholipids on apolipoprotein (a) and lipoprotein (a). *J Lipid Res* United States; 2013;**54**:2815–2830.
9. Bernelot Moens SJ, Verweij SL, Schnitzler JG, Stiekema LCA, Bos M, Langsted A, Kuijk C, Bekkering S, Voermans C, Verberne HJ, Nordestgaard BG, Stroes ESG, Kroon J. Remnant Cholesterol Elicits Arterial Wall Inflammation and a Multilevel Cellular Immune Response in Humans. *Arterioscler Thromb Vasc Biol* United States; 2017;
10. Marais AD, Solomon GAE, Blom DJ. Dysbetalipoproteinaemia: a mixed hyperlipidaemia of remnant lipoproteins due to mutations in apolipoprotein E. *Crit Rev Clin Lab Sci* England; 2014;**51**:46–62.
11. Schnitzler JG, Dallinga-Thie GM, Kroon J. The Role of (Modified) Lipoproteins in Vascular Function: A Duet Between Monocytes and the Endothelium. *Curr Med Chem* United Arab Emirates; 2019;**26**:1594–1609.
12. Seijkens T, Hoeksema MA, Beckers L, Smeets E, Meiler S, Levels J, Tjwa M, Winther MPJ de, Lutgens E. Hypercholesterolemia-induced priming of hematopoietic stem and progenitor cells aggravates atherosclerosis. *FASEB J Off Publ Fed Am Soc Exp Biol* United States; 2014;**28**:2202–2213.
13. Nordestgaard BG, Varbo A. Triglycerides and cardiovascular disease. *Lancet (London, England)* England; 2014;**384**:626–635.
14. Dutta P, Courties G, Wei Y, Leuschner F, Gorbatov R, Robbins CS, Iwamoto Y, Thompson B, Carlson AL, Heidt T, Majmudar MD, Lasitschka F, Etzrodt M, Waterman P, Waring MT, Chicoine AT, Laan AM van der, Niessen HWM, Piek JJ, Rubin BB, Butany J, Stone JR, Katus HA, Murphy SA, Morrow DA, Sabatine MS, Vinegoni C, Moskowitz MA, Pittet MJ, Libby P, et al. Myocardial infarction accelerates atherosclerosis. *Nature* England; 2012;**487**:325–329.
15. Tsimikas S. A Test in Context: Lipoprotein(a): Diagnosis, Prognosis, Controversies, and Emerging Therapies. *J Am Coll Cardiol* United States; 2017;**69**:692–711.
16. Que X, Hung M-Y, Yeang C, Gonen A, Prohaska TA, Sun X, Diehl C, Maatta A, Gaddis DE, Bowden K, Pattison J, MacDonald JG, Yla-Herttuala S, Mellon PL, Hedrick CC, Ley K, Miller YI, Glass CK, Peterson KL, Binder CJ, Tsimikas S, Witztum JL. Oxidized phospholipids are proinflammatory and proatherogenic in hypercholesterolaemic mice. *Nature* England; 2018;**558**:301–306.
17. Christ A, Günther P, Lauterbach MAR, Duewell P, Biswas D, Pelka K, Scholz CJ, Oosting M, Haendler K, Baßler K, Klee K, Schulte-Schrepping J, Ulas T, Moorlag SJCFM, Kumar V, Park MH, Joosten LAB, Groh LA, Riksen NP, Espevik T, Schlitzer A, Li Y, Fitzgerald ML, Netea MG, Schultze JL, Latz E. Western Diet Triggers NLRP3-Dependent Innate Immune Reprogramming. *Cell* 2018;**172**:162-175.e14.
18. Valk FM van der, Bekkering S, Kroon J, Yeang C, Bossche J Van den, Buul JD van, Ravandi A, Nederveen AJ, Verberne HJ, Scipione C, Nieuwdorp M, Joosten LAB, Netea MG, Koschinsky ML, Witztum JL, Tsimikas S, Riksen NP, Stroes ESG. Oxidized Phospholipids on Lipoprotein(a) Elicit Arterial Wall Inflammation and an Inflammatory Monocyte Response in Humans. *Circulation* United States; 2016;**134**:611–624.
19. Schnitzler JG, Hoogeveen RM, Ali L, Prange KH, Waissi F, Weeghel M van, Bachmann JC, Versloot M, Borrelli MJ, Yeang C, Kleijn D de, Houtkooper RH, Koschinsky M, Winther MP de, Groen AK, Witztum JL, Tsimikas S, Stroes ES, Kroon J. Atherogenic Lipoprotein(a) Increases Vascular Glycolysis, Thereby Facilitating Inflammation and Leukocyte Extravasation. *Circ Res* United States; 2020;
20. Viney NJ, Capelleveen JC van, Geary RS, Xia S, Tami JA, Yu RZ, Marcovina SM, Hughes SG, Graham MJ, Crooke RM, Crooke ST, Witztum JL, Stroes ES, Tsimikas S. Antisense oligonucleotides targeting apolipoprotein(a) in people with raised lipoprotein(a): two randomised, double-blind, placebo-controlled, dose-ranging trials. *Lancet (London, England)* England; 2016;**388**:2239–2253.

21. Bekkering S, Stiekema LCA, Bernelot Moens S, Verweij SL, Novakovic B, Prange K, Versloot M, Roeters van Lennep JE, Stunnenberg H, Winther M de, Stroes ESG, Joosten LAB, Netea MG, Riksen NP. Treatment with Statins Does Not Revert Trained Immunity in Patients with Familial Hypercholesterolemia. Cell Metab. United States; 2019. p. 1–2.
22. Gower RM, Wu H, Foster GA, Devaraj S, Jialal I, Ballantyne CM, Knowlton AA, Simon SI. CD11c/CD18 Expression Is Upregulated on Blood Monocytes During Hypertriglyceridemia and Enhances Adhesion to Vascular Cell Adhesion Molecule-1. *Arterioscler Thromb Vasc Biol* 2011;**31**:160–166.
23. Kallio P, Kolehmainen M, Laaksonen DE, Pulkkinen L, Atalay M, Mykkänen H, Uusitupa M, Poutanen K, Niskanen L. Inflammation markers are modulated by responses to diets differing in postprandial insulin responses in individuals with the metabolic syndrome. *Am J Clin Nutr* 2008;**87**:1497–1503.
24. Bakker GJ, Schnitzler JG, Bekkering S, Clercq NC de, Koopen AM, Hartstra A V, Meessen ECE, Scheithauer TP, Winkelmeijer M, Dallinga-Thie GM, Cani PD, Kemper EM, Soeters MR, Kroon J, Groen AK, Raalte DH van, Herrema H, Nieuwdorp M. Oral vancomycin treatment does not alter markers of postprandial inflammation in lean and obese subjects. *Physiol Rep* 2019;**7**:e14199.
25. Nappo F, Esposito K, Cioffi M, Giugliano G, Molinari AM, Paolisso G, Marfella R, Giugliano D. Postprandial endothelial activation in healthy subjects and in type 2 diabetic patients: role of fat and carbohydrate meals. *J Am Coll Cardiol* United States; 2002;**39**:1145–1150.
26. Harte AL, Varma MC, Tripathi G, McGee KC, Al-Daghri NM, Al-Attas OS, Sabico S, O'Hare JP, Ceriello A, Saravanan P, Kumar S, McTernan PG. High fat intake leads to acute postprandial exposure to circulating endotoxin in type 2 diabetic subjects. *Diabetes Care* 2012;**35**:375–382.
27. Ali L, Schnitzler JG, Kroon J. Metabolism: The road to inflammation and atherosclerosis. *Curr Opin Lipidol* England; 2018;**29**:474–480.
28. Warburg O, Wind F, Negelein E. THE METABOLISM OF TUMORS IN THE BODY. *J Gen Physiol* United States; 1927;**8**:519–530.
29. Stienstra R, Netea-Maier RT, Riksen NP, Joosten LAB, Netea MG. Specific and Complex Reprogramming of Cellular Metabolism in Myeloid Cells during Innate Immune Responses. *Cell Metab* United States; 2017;**26**:142–156.
30. Koelwyn GJ, Corr EM, Erbay E, Moore KJ. Regulation of macrophage immunometabolism in atherosclerosis. *Nat Immunol* United States; 2018;**19**:526–537.
31. Mertens S, Noll T, Spahr R, Krutzfeldt A, Piper HM. Energetic response of coronary endothelial cells to hypoxia. *Am J Physiol* United States; 1990;**258**:H689-94.
32. Dobrina A, Rossi F. Metabolic properties of freshly isolated bovine endothelial cells. *Biochim Biophys Acta* Netherlands; 1983;**762**:295–301.
33. Bock K De, Georgiadou M, Schoors S, Kuchnio A, Wong BW, Cantelmo AR, Quaegebeur A, Ghesquiere B, Cauwenberghs S, Eelen G, Phng L-K, Betz I, Tembuyser B, Brepoels K, Welti J, Geudens I, Segura I, Cruys B, Bifari F, Decimo I, Blanco R, Wyns S, Vangindertael J, Rocha S, Collins RT, Munck S, Daelemans D, Imamura H, Devlieger R, Rider M, et al. Role of PFKFB3-driven glycolysis in vessel sprouting. *Cell* United States; 2013;**154**:651–663.
34. Bock K De, Georgiadou M, Carmeliet P. Role of endothelial cell metabolism in vessel sprouting. *Cell Metab* United States; 2013;**18**:634–647.
35. Eelen G, Zeeuw P de, Simons M, Carmeliet P, Zeeuw P de, Simons M, Carmeliet P. Endothelial cell metabolism in normal and diseased vasculature. *Circ Res* 2016;**116**:1231–1244.
36. Feng S, Bowden N, Fragiadaki M, Souilhol C, Hsiao S, Mahmoud M, Allen S, Pirri D, Ayllon BT, Akhtar S, Thompson AAR, Jo H, Weber C, Ridger V, Schober A, Evans PC. Mechanical Activation of Hypoxia-Inducible Factor 1alpha Drives Endothelial Dysfunction at Atheroprone Sites. *Arterioscler Thromb Vasc Biol* United States; 2017;**37**:2087–2101.
37. Bergmark C, Dewan A, Orsoni A, Merki E, Miller ER, Shin M-J, Binder CJ, Horkko S, Krauss RM, Chapman MJ, Witztum JL, Tsimikas S. A novel function of lipoprotein [a] as a preferential carrier of oxidized phospholipids in human plasma. *J Lipid Res* United States; 2008;**49**:2230–2239.
38. Chang M-K, Binder CJ, Miller YI, Subbanagounder G, Silverman GJ, Berliner JA, Witztum JL. Apoptotic cells with oxidation-specific epitopes are immunogenic and proinflammatory. *J Exp Med* United States; 2004;**200**:1359–1370.
39. Stiekema LCA, Stroes ESG, Verweij SL, Kassahun H, Chen L, Wasserman SM, Sabatine MS, Mani V, Fayad ZA. Persistent arterial wall inflammation in patients with elevated lipoprotein(a) despite strong low-density lipoprotein cholesterol reduction by proprotein convertase subtilisin/kexin type 9 antibody treatment. *Eur Heart J* England; 2019;**40**:2775–2781.
40. Tomas L, Edsfeldt A, Mollet IG, Perisic Matic L, Prehn C, Adamski J, Paulsson-Berne G, Hedin U, Nilsson J, Bengtsson E, Goncalves I, Bjorkbacka H. Altered metabolism distinguishes high-risk from stable carotid atherosclerotic plaques. *Eur Heart J* England; 2018;**39**:2301–2310.
41. Paik J-Y, Jung K-H, Lee J-H, Park J-W, Lee K-H. Reactive oxygen species-driven HIF1alpha triggers accelerated glycolysis in endothelial cells exposed to low oxygen tension. *Nucl Med Biol* United States; 2017;**45**:8–14.
42. Schnitzler JG, Dzobo KE, Nurmohamed NS, Stroes ESG, Kroon J. Surmounting the endothelial barrier for delivery of drugs and imaging tracers. *Atherosclerosis* 2020;
43. Bekkering S, Munckhof I van den, Nielen T, Lamfers E, Dinarello C, Rutten J, Graaf J de, Joosten LAB, Netea MG, Gomes MER, Riksen NP. Innate immune cell activation and epigenetic remodeling in symptomatic and asymptomatic atherosclerosis in humans in vivo. *Atherosclerosis* Ireland; 2016;**254**:228–236.
44. Verhoeven B, Hellings WE, Moll FL, Vries JP de, Kleijn DP V de, Bruin P de, Busser E, Schoneveld AH, Pasterkamp G.

Carotid atherosclerotic plaques in patients with transient ischemic attacks and stroke have unstable characteristics compared with plaques in asymptomatic and amaurosis fugax patients. *J Vasc Surg* United States; 2005;**42**:1075–1081.
45. Tawakol A, Singh P, Mojena M, Pimentel-Santillana M, Emami H, MacNabb M, Rudd JHF, Narula J, Enriquez JA, Traves PG, Fernandez-Velasco M, Bartrons R, Martin-Sanz P, Fayad ZA, Tejedor A, Bosca L. HIF-1alpha and PFKFB3 Mediate a Tight Relationship Between Proinflammatory Activation and Anerobic Metabolism in Atherosclerotic Macrophages. *Arterioscler Thromb Vasc Biol* United States; 2015;**35**:1463–1471.
46. Libby P. Inflammation in atherosclerosis. *Arterioscler Thromb Vasc Biol* United States; 2012;**32**:2045–2051.
47. Gonzalez L, Trigatti BL. Macrophage Apoptosis and Necrotic Core Development in Atherosclerosis: A Rapidly Advancing Field with Clinical Relevance to Imaging and Therapy. *Can J Cardiol* England; 2017;**33**:303–312.
48. Tabas I, Bornfeldt KE. Macrophage Phenotype and Function in Different Stages of Atherosclerosis. *Circ Res* United States; 2016;**118**:653–667.
49. Tabas I. Macrophage death and defective inflammation resolution in atherosclerosis. *Nat Rev Immunol* England; 2010;**10**:36–46.
50. Laan AM van der, Horst EN Ter, Delewi R, Begieneman MP V, Krijnen PAJ, Hirsch A, Lavaei M, Nahrendorf M, Horrevoets AJ, Niessen HWM, Piek JJ. Monocyte subset accumulation in the human heart following acute myocardial infarction and the role of the spleen as monocyte reservoir. *Eur Heart J* England; 2014;**35**:376–385.
51. Nahrendorf M, Swirski FK. Innate immune cells in ischaemic heart disease: does myocardial infarction beget myocardial infarction? *Eur Heart J* England; 2016;**37**:868–872.
52. Sotiriou SN, Orlova V V, Al-Fakhri N, Ihanus E, Economopoulou M, Isermann B, Bdeir K, Nawroth PP, Preissner KT, Gahmberg CG, Koschinsky ML, Chavakis T. Lipoprotein(a) in atherosclerotic plaques recruits inflammatory cells through interaction with Mac-1 integrin. *FASEB J Off Publ Fed Am Soc Exp Biol* United States; 2006;**20**:559–561.

# AUTHORS AND AFFILIATIONS


L. Ali
Amsterdam UMC, University of Amsterdam, Department of Experimental Vascular Medicine, Amsterdam Cardiovascular Sciences, Meibergdreef 9, Amsterdam, The Netherlands.

J.C. Bachmann
Amsterdam UMC, University of Amsterdam, Department of Experimental Vascular Medicine, Amsterdam Cardiovascular Sciences, Meibergdreef 9, Amsterdam, The Netherlands.

G.J. Bakker
Amsterdam UMC, University of Amsterdam, Department of Vascular Medicine, Amsterdam Cardiovascular Sciences, Meibergdreef 9, Amsterdam, The Netherlands.

S. Bekkering
Department of Experimental Internal Medicine, Radboud University Medical Centre, Nijmegen, The Netherlands.

S.J. Bernelot Moens
Amsterdam UMC, University of Amsterdam, Department of Vascular Medicine, Amsterdam Cardiovascular Sciences, Meibergdreef 9, Amsterdam, The Netherlands.

M. Bos
Amsterdam UMC, University of Amsterdam, Department of Vascular Medicine, Amsterdam Cardiovascular Sciences, Meibergdreef 9, Amsterdam, The Netherlands.

P.D. Cani
WELBIO – Walloon Excellence in Life Sciences and BIOtechnology, Louvain Drug Research Institute, Université Catholique de Louvain, Brussels, Belgium.

N.C. De Clercq
Amsterdam UMC, University of Amsterdam, Department of Vascular Medicine, Amsterdam Cardiovascular Sciences, Meibergdreef 9, Amsterdam, The Netherlands.

M.J.A.P. Daemen
Amsterdam UMC, University of Amsterdam, Department of Pathology, Amsterdam Cardiovascular Sciences, Meibergdreef 9, Amsterdam, The Netherlands.

G.M. Dallinga-Thie
Amsterdam UMC, University of Amsterdam, Department of Vascular Medicine, Amsterdam Cardiovascular Sciences, Meibergdreef 9, Amsterdam, The Netherlands.

Amsterdam UMC, University of Amsterdam, Department of Experimental Vascular Medicine, Amsterdam Cardiovascular Sciences, Meibergdreef 9, Amsterdam, The Netherlands.

A.K. Groen
Amsterdam UMC, University of Amsterdam, Department of Vascular Medicine, Amsterdam Cardiovascular Sciences, Meibergdreef 9, Amsterdam, The Netherlands.

Department of Pediatrics, Laboratory of Metabolic Diseases, University of Groningen, UMCG, Groningen, The Netherlands.

A.V. Hartstra
Amsterdam UMC, University of Amsterdam, Department of Vascular Medicine, Amsterdam Cardiovascular Sciences, Meibergdreef 9, Amsterdam, The Netherlands.

H. Herrema
Amsterdam UMC, University of Amsterdam, Department of Experimental Vascular Medicine, Amsterdam Cardiovascular Sciences, Meibergdreef 9, Amsterdam, The Netherlands.

R.M. Hoogeveen
Amsterdam UMC, University of Amsterdam, Department of Vascular Medicine, Amsterdam Cardiovascular Sciences, Meibergdreef 9, Amsterdam, The Netherlands.

R.H. Houtkooper
Laboratory Genetic Metabolic Diseases, Amsterdam Gastroenterology & Metabolism, Amsterdam Cardiovascular Sciences, Amsterdam UMC, University of Amsterdam, Amsterdam, 1105 AZ, The Netherlands.

Y. Kaiser
Amsterdam UMC, University of Amsterdam, Department of Vascular Medicine, Amsterdam Cardiovascular Sciences, Meibergdreef 9, Amsterdam, The Netherlands.

E.M. Kemper
Department of Clinical Pharmacy, Amsterdam University Medical Centers, Amsterdam, The Netherlands.

D.P.V. De Kleijn
Department of Vascular Surgery, Netherlands & Netherlands Heart Institute, UMC Utrecht, University Utrecht, Utrecht, 3584 CS, The Netherlands.

A.M. Koopen
Amsterdam UMC, University of Amsterdam, Department of Vascular Medicine, Amsterdam Cardiovascular Sciences, Meibergdreef 9, Amsterdam, The Netherlands.

M.L. Koschinsky
Robarts Research Institute, Schulich School of Medicine & Dentistry, University of Western Ontario, London, Ontario, ON N6A 5C1, Canada.

J. Kroon
Amsterdam UMC, University of Amsterdam, Department of Experimental Vascular Medicine, Amsterdam Cardiovascular Sciences, Meibergdreef 9, Amsterdam, The Netherlands.

C. Kuijk
Department of Hematopoiesis, Sanquin Research and Landsteiner Laboratory, University of Amsterdam, The Netherlands.

A. Langsted
The Copenhagen General Population study and Department of Clinical Biochemistry, Herlev and Gentofte Hospital, Copenhagen University Hospital, Denmark.

J.H.M. Levels
Amsterdam UMC, University of Amsterdam, Department of Experimental Vascular Medicine, Amsterdam Cardiovascular Sciences, Meibergdreef 9, Amsterdam, The Netherlands.

E. Lutgens
Department of Medical Biochemistry, Amsterdam Cardiovascular Sciences, Amsterdam UMC, University of Amsterdam, Amsterdam, 1105 AZ, The Netherlands.

Institute for Cardiovascular Prevention (IPEK), Ludwig Maximilians University, Petterkoferstraße 8a &9, 80336 Munich, Germany and German Center for Cardiovascular Research (DZHK), partner site Munich Heart Alliance, Munich, Germany.

E.C.E. Meessen
Department of Endocrinology and Metabolism, Amsterdam University Medical Centers, Amsterdam, The Netherlands.

M. Nieuwdorp
Amsterdam UMC, University of Amsterdam, Department of Vascular Medicine, Amsterdam Cardiovascular Sciences, Meibergdreef 9, Amsterdam, The Netherlands.

Department of Experimental Vascular Medicine, Amsterdam University Medical Centers, Amsterdam, The Netherlands.

Diabetes Center, Department of Internal Medicine, Amsterdam University Medical Centers, Amsterdam, The Netherlands.

Wallenberg Laboratory, Department of Molecular and Clinical Medicine, Sahlgrenska Academy, University of Gothenburg, Gothenburg, Sweden.

ICaR, Amsterdam University Medical Centers, Amsterdam, The Netherlands.

B.G. Nordestgaard
The Copenhagen General Population study and Department of Clinical Biochemistry, Herlev and Gentofte Hospital, Copenhagen University Hospital, Denmark.

A.M. Pennekamp
Amsterdam UMC, University of Amsterdam, Department of Experimental Vascular Medicine, Amsterdam Cardiovascular Sciences, Meibergdreef 9, Amsterdam, The Netherlands.

K. Poels
Department of Medical Biochemistry, Amsterdam Cardiovascular Sciences, Amsterdam UMC, University of Amsterdam, Amsterdam, 1105 AZ, The Netherlands.

K.H.M. Prange
Department of Medical Biochemistry, Amsterdam Cardiovascular Sciences, Amsterdam UMC, University of Amsterdam, Amsterdam, 1105 AZ, The Netherlands.

D.H. Van Raalte
Diabetes Center, Department of Internal Medicine, Amsterdam University Medical Centers, Amsterdam, The Netherlands.

T.P. Scheithauer
Amsterdam UMC, University of Amsterdam, Department of Vascular Medicine, Amsterdam Cardiovascular Sciences, Meibergdreef 9, Amsterdam, The Netherlands.

T.T.P. Seijkens
Department of Medical Biochemistry, Amsterdam Cardiovascular Sciences, Amsterdam UMC, University of Amsterdam, Amsterdam, 1105 AZ, The Netherlands.

M.R. Soeters
Department of Endocrinology and Metabolism, Amsterdam University Medical Centers, Amsterdam, The Netherlands.

L.C.A. Stiekema
Amsterdam UMC, University of Amsterdam, Department of Vascular Medicine, Amsterdam Cardiovascular Sciences, Meibergdreef 9, Amsterdam, The Netherlands.

E.S.G. Stroes
Amsterdam UMC, University of Amsterdam, Department of Vascular Medicine, Amsterdam Cardiovascular Sciences, Meibergdreef 9, Amsterdam, The Netherlands.

F. Tiessens
Amsterdam UMC, University of Amsterdam, Department of Vascular Medicine, Amsterdam Cardiovascular Sciences, Meibergdreef 9, Amsterdam, The Netherlands.

S.Tsimikas
Sulpizio Cardiovasc ular Center, Vascular Medicine Program, University of California San Diego, La Jolla, CA, USA.

H.J. Verberne
Amsterdam UMC, University of Amsterdam,Department of Nuclear Medicine, Meibergdreef 9, Amsterdam, The Netherlands.

M. Versloot
Amsterdam UMC, University of Amsterdam, Department of Experimental Vascular Medicine, Amsterdam Cardiovascular Sciences, Meibergdreef 9, Amsterdam, The Netherlands.

C. Voermans
Department of Hematopoiesis, Sanquin Research and Landsteiner Laboratory, University of Amsterdam, The Netherlands.

F. Waissi
Department of Vascular Surgery, Netherlands & Cardiology, UMC Utrecht, University Utrecht, Utrecht, 3584 CS, The Netherlands.

M. Van Weeghel
Laboratory Genetic Metabolic Diseases, Amsterdam Gastroenterology & Metabolism, Amsterdam Cardiovascular Sciences, Amsterdam UMC, University of Amsterdam, Amsterdam, 1105 AZ, The Netherlands.

Core Facility Metabolomics, Amsterdam UMC, University of Amsterdam, Amsterdam, 1105 AZ, The Netherlands.

M.P.J. De Winther
Department of Medical Biochemistry, Amsterdam Cardiovascular Sciences, Amsterdam UMC, University of Amsterdam, Amsterdam, 1105 AZ, The Netherlands.

Institute for Cardiovascular Prevention (IPEK), Munich, 80336, Germany.

J.L. Witztum
Division of Endocrinology and Metabolism, Department of Medicine, University of California San Diego, La Jolla, CA., 92093, USA.

C.Yeang
Sulpizio Cardiovasc ular Center, Vascular Medicine Program, University of California San Diego, La Jolla, CA, USA.

# PORTFOLIO

| | |
|---|---|
| Name PhD student: | Johan Gustaaf Schnitzler |
| PhD period: | June 2016 – March 2020 |
| Name promotor: | Prof. dr. E.S.G. Stroes |
| Name co-promotor: | Dr. J. Kroon |

| | Year | ECTS |
|---|---|---|
| **Courses** | | |
| Laboratory animal science (artikel 9) | 2017 | 3.9 |
| Advanced PCR | 2017 | 0.7 |
| Systems Medicine | 2017 | 1.4 |
| Career Development | 2019 | 0.8 |
| **Seminars, workshops and masterclasses** | | |
| Weekly journal club, dept. of Vascular Medicine, AMC | 2016-2020 | 4 |
| Laboratory meetings | 2016-2020 | 2 |
| Clinical Education | 2016-2020 | 1 |
| Masterclass Prof. dr. Ira Goldberg, Amsterdam, The Netherlands | 2018 | 0.2 |
| Monthly Amsterdam Cardiovascular Science (ACS) meeting | 2019-2020 | 0.2 |
| **Presentations** | | |
| *Oral* | | |
| European Atherosclerosis Society, Lisbon, Portugal | 2018 | 0.5 |
| ACS Annual Meeting, Amsterdam, The Netherlands | 2019 | 0.5 |
| European Atherosclerosis Society, Maastricht, The Netherlands | 2019 | 0.5 |
| ACS PhD Retreat, Soesterberg, The Netherlands | 2019 | 0.5 |
| *Poster* | | |
| Rembrandt Symposium, Noordwijkerhout, The Netherlands | 2016 | 0.5 |
| European Atherosclerosis Society, Prague, Czech Republic | 2017 | 0.5 |
| American Society for Cell Biology, Philadelphia, USA | 2017 | 0.5 |
| Joint Dutch German Vascular Biology Meeting, Amsterdam, The Netherlands | 2018 | 0.5 |
| **Conferences** | | |
| Rembrandt Symposium, Noordwijkerhout, The Netherlands | 2016-2018 | 0.25 |

| | | |
|---|---|---|
| Dutch Endothelial Biology Society (DEBS) Fall meeting, Biezenmortel, The Netherlands | 2017 | 0.25 |
| European Atherosclerosis Society, Prague, Czech Republic | 2017 | 0.25 |
| American Society for Cell Biology, Philadelphia, USA | | |
| European Atherosclerosis Society, Lisbon, Portugal | 2018 | 0.25 |
| Joint Dutch German Vascular Biology Meeting, Amsterdam, The Netherlands | 2018 | 0.5 |
| European Atherosclerosis Society, Maastricht, The Netherlands | 2019 | 0.25 |
| ACS PhD Retreat, Soesterberg, The Netherlands | 2019 | 0.25 |
| ACS Annual Meeting, Amsterdam, The Netherlands | 2019 | 0.25 |

## Teaching

*Tutoring, mentoring and supervising*

| | | |
|---|---|---|
| Master student: E. van der Kooij (7 months) | 2018 | 2 |
| Bachelor student: J. ter Mors (9 months) | 2019 | 2.5 |
| Bachelor student: K. Kass (9 months) | 2019 | 2.5 |
| Bachelor students Medicine UvA (5 weeks) | 2019 | 0.5 |

## Parameters of Esteem

| | |
|---|---|
| Award for best oral presentation, ACS PhD retreat, Soesterberg, The Netherlands | 2019 |

# PUBLICATION LIST

1. Potent lipoprotein(a) lowering following apolipoprotein(a) antisense treatment reduces the pro-inflammatory activation of circulating monocytes in patients with elevated lipoprotein(a). Stiekema LCA, Prange KHM, Hoogeveen RM, Verweij SL, Kroon J, **Schnitzler JG**, Dzobo KE, Cupido AJ, Tsimikas S, Stroes ESG, de Winther MPJ, Bahjat M. Eur Heart J. 2020 Apr 8:ehaa171. doi: 10.1093/eurheartj/ehaa171. Online ahead of print. PMID: 32268367

2. Nile Red Quantifier: a novel and quantitative tool to study lipid accumulation in patient-derived circulating monocytes using confocal microscopy. **Schnitzler JG**, Bernelot Moens SJ, Tiessens F, Bakker GJ, Dallinga-Thie GM, Groen AK, Nieuwdorp M, Stroes ESG, Kroon J.J Lipid Res. 2017 Nov;58(11):2210-2219. doi: 10.1194/jlr.D073197. Epub 2017 Sep 28.PMID: 28972117

3. Surmounting the endothelial barrier for delivery of drugs and imaging tracers. **Schnitzler JG**, Dzobo KE, Nurmohamed NS, Stroes ESG, Kroon J.Atherosclerosis. 2020 May 11:S0021-9150(20)30239-2. doi: 10.1016/j.atherosclerosis.2020.04.025. Online ahead of print. PMID: 32444105 Review.

4. Remnant Cholesterol Elicits Arterial Wall Inflammation and a Multilevel Cellular Immune Response in Humans. Bernelot Moens SJ, Verweij SL, **Schnitzler JG**, Stiekema LCA, Bos M, Langsted A, Kuijk C, Bekkering S, Voermans C, Verberne HJ, Nordestgaard BG, Stroes ESG, Kroon J.Arterioscler Thromb Vasc Biol. 2017 May;37(5):969-975. doi: 10.1161/ATVBAHA.116.308834. Epub 2017 Mar 23.PMID: 28336558 Clinical Trial.

5. Atherogenic Lipoprotein(a) Increases Vascular Glycolysis, Thereby Facilitating Inflammation and Leukocyte Extravasation. **Schnitzler JG**, Hoogeveen RM, Ali L, Prange KHM, Waissi F, van Weeghel M, Bachmann JC, Versloot M, Borrelli MJ, Yeang C, De Kleijn DPV, Houtkooper RH, Koschinsky ML, de Winther MPJ, Groen AK, Witztum JL, Tsimikas S, Stroes ESG, Kroon J.Circ Res. 2020 May 8;126(10):1346-1359. doi: 10.1161/CIRCRESAHA.119.316206. Epub 2020 Mar 12.PMID: 32160811

6. The maturation of a 'neural-hematopoietic' inflammatory axis in cardiovascular disease. Stiekema LCA, **Schnitzler JG**, Nahrendorf M, Stroes

ESG.Curr Opin Lipidol. 2017 Dec;28(6):507-512. doi: 10.1097/MOL.0000000000000457.PMID: 28877089 Review.

7. The Role of (Modified) Lipoproteins in Vascular Function: A Duet Between Monocytes and the Endothelium. **Schnitzler JG**, Dallinga-Thie GM, Kroon J.Curr Med Chem. 2019;26(9):1594-1609. doi: 10.2174/0929867325666180316121015.PMID: 29546830 Review.

8. Oral vancomycin treatment does not alter markers of postprandial inflammation in lean and obese subjects. Bakker GJ, **Schnitzler JG**, Bekkering S, de Clercq NC, Koopen AM, Hartstra AV, Meessen ECE, Scheithauer TP, Winkelmeijer M, Dallinga-Thie GM, Cani PD, Kemper EM, Soeters MR, Kroon J, Groen AK, van Raalte DH, Herrema H, Nieuwdorp M.Physiol Rep. 2019 Aug;7(16):e14199. doi: 10.14814/phy2.14199.PMID: 31423751

9. PCSK9 monoclonal antibodies reverse the pro-inflammatory profile of monocytes in familial hypercholesterolaemia. Bernelot Moens SJ, Neele AE, Kroon J, van der Valk FM, Van den Bossche J, Hoeksema MA, Hoogeveen RM, **Schnitzler JG**, Baccara-Dinet MT, Manvelian G, de Winther MPJ, Stroes ESG.Eur Heart J. 2017 May 21;38(20):1584-1593. doi: 10.1093/eurheartj/ehx002.PMID: 28329114

10. Lipoprotein(a) as Orchestrator of Calcific Aortic Valve Stenosis. **Schnitzler JG**, Ali L, Groenen AG, Kaiser Y, Kroon J.Biomolecules. 2019 Nov 21;9(12):760. doi: 10.3390/biom9120760.PMID: 31766423 Review.

11. N-Glycosylation Defects in Humans Lower Low-Density Lipoprotein Cholesterol Through Increased Low-Density Lipoprotein Receptor Expression. Van den Boogert MAW, Larsen LE, Ali L, Kuil SD, Chong PLW, Loregger A, Kroon J, **Schnitzler JG**, Schimmel AWM, Peter J, Levels JHM, Steenbergen G, Morava E, Dallinga-Thie GM, Wevers RA, Kuivenhoven JA, Hand NJ, Zelcer N, Rader DJ, Stroes ESG, Lefeber DJ, Holleboom AG. Circulation. 2019 Jul 23;140(4):280-292. doi: 10.1161/CIRCULATIONAHA.118.036484. Epub 2019 May 23.PMID: 31117816

12. Metabolism: The road to inflammation and atherosclerosis. **Schnitzler JG**, Ali L, Kroon J.Curr Opin Lipidol. 2018 Dec;29(6):474-480. doi: 10.1097/MOL.0000000000000550.PMID: 30234554 Review.

13. Low Hdl-Cholesterol Levels Are Associated With A Decreased Monocyte Activity And Inflammation In Carriers Of Lcat Mutation. Pavanello C, Zheng,

KH, **Schnitzler JG**, Kroon J, Versloot M, Levels JHM, Calabresi L, Stroes ESG, Bekkering S. Atherosclerosis. 2019 Aug 03, doi.org/10.1016/j.atherosclerosis.2019.06.067

14. *Elevated Lipoprotein(a) levels increase risk of secondary Major Adverse Cardiovascular Events in patients following carotid endarterectomy*. Waissi F, Dekker M, Timmerman N, Hoogeveen RM, Van Bennekom J, Dzobo K, **Schnitzler JG**, Pasterkamp G, Grobbee D, De Borst G, Stroes ESG, De Kleijn DPV and Kroon J. Accepted Stroke, Jun 2020.

15. Short-term Regulation of Hematopoiesis by Lipoprotein(a) Results in the Production of Pro-Inflammatory Monocytes. Johan G Schnitzler, Kikkie Poels, Lotte C A Stiekema, Calvin Yeang, Sotirios Tsimikas, Jeffrey Kroon, Erik S G Stroes, Esther Lutgens, Tom T P Seijkens PMID: 32387421 DOI: 10.1016/j.ijcard.2020.05.008

# ADDENDUM

# Nederlandse samenvatting en discussie

Dit proefschrift beschrijft twee belangrijke componenten van atherosclerose. **Deel I** beschrijft hoe verschillende soorten lipoproteïnen monocyten beïnvloeden en **deel II** richt zich op het verband tussen ontsteking en het metabolisme van endotheelcellen.

In **Hoofdstuk 2** staat hoe lipoproteïnen zoals LDL, remnant cholesterol en lipoproteine(a) [Lp(a)] zowel de monocyten als de endotheelcellen beïnvloeden. Deze cellen spelen een centrale rol in de progressie van atherosclerose, aangezien beide celtypes erg belangrijke componenten zijn in het proces van transendotheliale migratie (TEM). Dit proces wordt gekenmerkt door activatie van endotheelcellen op plaatsen waar de bloedstroom verstoord is, maar ook wanneer monocyten worden blootgesteld aan verhoogde bloedwaarden van verschillende lipoproteïnen. Het ontstekingsprofiel van de circulerende monocyten kan dienen als een belangrijke biomarker om de kwetsbaarheid van atherosclerotische plaques te kunnen bepalen. Opname van lipiden door monocyten verandert het fenotype in een ontstekingsstaat die samenvalt met een verhoogd gehalte aan intracellulaire lipidedruppels (LD). De bepaling van het LD-gehalte in circulerende monocyten is echter niet goed te meten. In **hoofdstuk 3** bespreken we hoe de immunofluorescerende kleurstof Nile Red (NR) neutrale LD's kleurt en vervolgens met behulp van confocale microscopie in beeld kan worden gebracht. Verder hebben we NR Quantifier (NRQ) ontwikkeld, een nieuwe kwantificeringsmethode om het LD-gehalte in monocyten te meten. Om dit te onderzoeken hebben we monocyten uit het bloed geïsoleerd en de NR-kleuring toegepast. In monocyten gekleurd met NR hebben wij op basis van 3D-beeldvorming duidelijk onderscheid gemaakt tussen fosfolipiden en intracellulaire neutrale lipiden. Vervolgens hebben wij NRQ ontwikkeld; een semiautomatisch kwantificatieprogramma dat veranderingen in lipidenaccumulatie van monocyten detecteert. NRQ was in staat om veranderingen in het LD-gehalte van monocyten te detecteren na *ex vivo* blootstelling aan LDL dat zowel tijd- als dosisafhankelijk was. Tenslotte hebben we NRQ gevalideerd bij patiënten met familiale hypercholesterolemie (FH) en obesitas in pre- en postprandiale toestand. Deze studie toont aan dat de lipidenopname verhoogd is bij FH-patiënten, wat aangeeft dat hoge niveaus van LDL de lipidenopname verhogen in de circulatie door monocyten. FH-patiënten worden gekenmerkt door monocyten met een verhoogde C-C chemokine receptor (CCR) 2, scavenger receptor A (SRA) en scavenger receptor CD36, indicatief voor een proinflammatoire toestand. Ook kwam naar voren dat monocyten van FH-patiënten gekarakteriseerd werden door verhoogde neutrale LD-inhoud in circulerende monocyten. Met behulp van lipidenverlagende eiwitconversie subtilisine/kexine type 9 (PCSK9) remmers in FH-patiënten verzorgde een sterke afname van LDL dat gepaard ging met een verminderde LD-inhoud (>20% afname)

en een sterke reductie in TEM, wat duidt op het verband tussen LD-inhoud en de ontstekingsstaat van monocyten.

De toename in LD-content van monocyten werd ook waargenomen bij patiënten met een verhoogd remnant cholesterolgehalte zoals beschreven in **hoofdstuk 4**. In deze studie evalueerden we de impact van remnant cholesterol op arteriële vaatwandontsteking en circulerende monocyten bij patiënten met familiaire dysbetalipoproteïnemie (FD), een genetische aandoening die gekenmerkt wordt door een verhoogd remnant cholesterolgehalte. Net als bij FH-patiënten werden de proefpersonen in deze studie gekenmerkt door verhoogde oppervlakte-integrines CD11b, CD11c en CD18 op monocyten. Naast activatie van circulerende monocyten, zagen we een verhoogd leukocytaantal gepaard met een duidelijke monocytose bij FD-patiënten. Experimentele pre-klinische studies toonden eerder aan dat *Apoe*$^{-/-}$ muizen overmatige proliferatie en myeloïde groei van hematopoëtische stam- en voorlopercellen (HSPC's) vertoonden als gevolg van cholesterol accumulatie. Onze *in vitro* experimenten onderbouwden dat remnant cholesterol zich ophoopt in HSPC's, afkomstig uit het beenmerg, en samenvalt met myeloïde bias in celontwikkeling. Deze myeloïde bias impliceert een verhoogde ontwikkeling van de immuuncellen naar een myeloïde lijn die onder andere monocyten genereert. Bij onze FD-patiënten vonden we dat het beenmerg van deze patiënten werd geactiveerd (gemeten met 18F-fluordeoxy glucose positron emissie tomografie/computed tomography (FDG PET/CT)). Meer recente gegevens indiceren dat deze geactiveerde toestand van het beenmerg een centrale rol speelt in het restrisico voor het ontwikkelen van toekomstige voorvallen. Als zodanig, in hypercholesterolemische *Apoe*$^{-/-}$ muizen is de micro-omgeving van het beenmerg geactiveerd en is er myeloïde ontwikkeling wat resulteert in monocytose. HSPC's van deze muizen toonden een verhoogde neiging om pro-inflammatoire Ly6C$^{high}$ monocyten te ontwikkelen, wat hardnekkig bleek omdat dit fenotype ook tot uiting kwam in normocholesterolemische muizen.

In tegenstelling tot verhoogde LDL-niveaus in het bloed blijft het raadselachtig of Lp(a het beenmerg kan primen. In **hoofdstuk 5** hebben we het beenmerg van Lp(a) transgene muizen onderzocht die als gevolg daarvan een verhoogd Lp(a) gehalte hebben. In deze studie tonen we aan dat HSPC's uit muizen die gestimuleerd worden met Lp(a), proinflammatoire monocyten produceren. Dit toont aan dat naast interactie van Lp(a) met monocyten in de circulatie, ook op beenmergniveau) de productie van monocyten beïnvloed wordt door Lp(a). In tegenstelling tot de langdurige priming van HSPC's door LDL, leidde blootstelling aan Lp(a) niet tot langdurige priming van HSPC's, wat resulteerde in de hypothese dat de relatief lage concentraties van Lp(a) in vergelijking met LDL die in andere studies worden gebruikt leidt tot het gebrek aan Lp(a)-geïnduceerde priming. De ontstekingseffecten van Lp(a) zijn voornamelijk gereguleerd via de signaalcapaciteit van geoxideerde fosfolipiden op Lp(a) en niet door NLRP3 ontstekingsactiviteit als gevolg van

intracellulaire cholesterolaccumulatie, wat het mechanisme is van LDL-geïnduceerde intrinsieke priming van myeloïde cellen en hun voorlopers. Bovendien induceren zowel de LDL-entiteit van Lp(a) als de apo(a)-staart van Lp(a) niet tot cellulaire activatie zonder de aanwezigheid van OxPL's. Lp (a) was dan ook in staat om direct HSPC's te HSPC's (d.w.z. na 24 uur en na 7 dagen), maar zodra de Lp(a)-stimulus afwezig was (na 24 uur stimulatie en na 6 dagen zonder stimulus of beenmergtransplantatie) vertoonden HSPC's normale activiteit wat aangeeft dat Lp (a) geen NLRP3 activatie induceert, maar via OxPLs signaleert. Onze gegevens impliceren dat zonder de aanwezigheid van Lp(a), de HSPC-micro-omgeving zich snel ontdoet van de geactiveerde monocytenstaat, terwijl de LDL-geïnduceerde hematopoëtische effecten aanwezig zullen blijven zijn, ook na LDL-C-reductie. Dit concept komt overeen met de vermindering van de TEM van monocyten dat toe te schrijven is aan een 70% Lp(a)-reductie na 12 weken apo(a)-antisense-therapie bij Lp(a)-patiënten. Een 44% LDL-C-reductie na 14 weken statine-therapie blijft nog steeds wordt gekenmerkt door een onveranderd, hyperinflammatoir monocytenfenotype bij patiënten met FH. Deze data geven duidelijk aan dat zowel LDL als Lp(a) een eigen mechanisme hebben om een proinflammatoire staat te induceren.

Postprandiale ontsteking is een staat waarin voedselopname leidt tot systemische laagdurige ontsteking. We hebben onderzocht of de verhoogde triglyceridenniveaus na een orale vetinname leiden tot lipopolysaccharide (LPS) translocatie vanuit de darm in **hoofdstuk 6**. In dit hoofdstuk beschrijven we het effect van manipulatie van de darmmicrobiota op de ontstekingsreactie in de postprandiale staat. Ondanks grote verschuivingen in de samenstelling van de fecale microbiota met een groei van Gram-negatieve bacteriën en een daarmee gepaard gaande significante toename van LPS, hebben we geen verandering waargenomen in een aantal postprandiale inflammatoire markers na een vetrijke maaltijd bij magere en obese proefpersonen met het metabool syndroom. Dit suggereert dat de LPS-translocatie mogelijk geen grote rol speelt in de kortetermijnpostprandiale respons in deze groepen. Postprandiale IL-6- en LPS-stijgingen zijn beschreven door andere studies, maar deze studies geven aan dat na een vetrijke maaltijd zowel LPS als inflammatoire markers kunnen toenemen, maar dat er geen oorzakelijk verband is tussen postprandiale LPS-translocatie en ontsteking.

Samen geven deze hoofdstukken de centrale rol aan van lipoproteïnen die betrokken zijn bij het ontstaan van ontsteking in CVD-pathogenese. De vraag rijst wat dit betekent voor de machinerie van cellen die betrokken zijn bij de stofwisseling. In **deel II** van dit proefschrift onderzoeken we hoe een staat van ontsteking gekoppeld is aan een veranderd metabool cellulair fenotype.

In **hoofdstuk 7** beschrijven we dat het metabolisme van cellen bestaat uit een ingewikkeld netwerk van vele verschillende metabolieten en enzymen die nodig zijn

voor het genereren van nucleïnezuren, eiwitten, lipiden, koolhydraten en energie voor de cel. Metabolisme speelt een centrale rol in het behoud van homeostase, proliferatie en de cellulaire activering. Het is algemeen erkend dat verstoringen in de metabole paden aan de basis liggen van een grote verscheidenheid aan ziekten. De noodzaak om energie te produceren in de vorm van adenosine trifosfaat (ATP) voor de cellulaire functie is essentieel voor zowel cellen in rust als voor geactiveerde cellen. Dit proces wordt strak gereguleerd door de geïntegreerde metabole paden van de glycolyse, de tricarboxylzuurcyclus (TCA) en de pentose-fosfaatroute (PPP).

Vroege metabolismestudies richtten zich op oncologie en verschaften de onderzoekers fundamentele inzichten over hoe veranderingen in cellulair metabolisme het lot van de cel kan sturen. Waar glucose via de glycolyse in de TCA-cyclus terechtkomt en zo mitochondriale oxidatieve fosforylering (OXPHOS) aanstuurt, zijn zeer proliferatieve tumorcellen voornamelijk afhankelijk van glycolyse. Dit is opmerkelijk, aangezien er voldoende zuurstof aanwezig is om de OXPHOS-route te volgen, dit wordt ook wel het Warburgeffect genoemd. Bovendien blijkt uit recente bevindingen dat het Warburgeffect ook cruciaal is in endotheelcellen (EC), monocyten en macrofagen. Dit samenspel tussen metabolisme en immunologie wordt steeds vaker onderzocht en het wordt aangetoond dat metabolisme een grote invloed heeft op het functionele gedrag van cellen.

De rol van het metabolisme in EC is voornamelijk gedaan door baanbrekend onderzoek door de groep van Prof. Carmeliet in België die glycolyse, en niet het efficiëntere oxidatieve fosforylatie, aanduidde als de belangrijkste bron van ATP tijdens angiogenese van EC die zelfs in rusttoestand een hoge glycolytische flux lieten zien. Er werd aangetoond dat EC een relatief laag aantal mitochondriën hebben (2-6% van het totale cytoplasma volume). Dit onderbouwt waarom EC zo afhankelijk zijn van glycolyse om 2 ATP-moleculen en lactaat per glucosemolecuul te genereren en toont het belang van glycolyse als primaire energiebron in deze cellen. Echter, over de rol van het endotheelcelmetabolisme in de context van hart- en vaatziekten, en dan met name de rol van de EC-glycolyse bij het dicteren van de ziekteprogressie, is vooralsnog weinig bekend.

Feng en collega's toonden aan dat atherosclerosegevoelige regio's in de vaten gekenmerkt worden door een verhoogde glycolyse. Zo was de expressie van de glycolytische regulatoren hexokinase (HK) 2, enolase 2, glucose transporter (GLUT) 1 en 6-fosphofructo-2-kinase/fructose-2,6-bifosfatase (PFKFB) 3 verhoogd en een verhoogde extracellulaire verzuringsgraad. Bovendien leidde IκBα-overexpressie in EC tot een verminderde nuclear factor κB (NFκB) activiteit en een verminderde hypoxie-induceerbare factor (HIF)1 expressie, dat fungeert als een regulator die een snelle ATP-generatie mogelijk maakt. Hiermee laten we een direct verband tussen de endotheliale metabole- en inflammatoire as. Bovendien vertoonden de halsslagaders

van hypercholesterolemische *Apoe*$^{-/-}$ muizen een duidelijk glycolytisch fenotype (verhoogde mRNA-waarden van HK2, enolase 2, GLUT1 en PFKFB3). Dit viel samen met een 50% verhoogde plaquegrootte in de halsslagaders in vergelijking met muizen met een endotheelspecifieke deletie van HIF1α (HIF1αEC-cKO *ApoE*$^{-/-}$) waarmee gevalideerd werd dat metabole veranderingen ten grondslag liggen aan experimentele *in vivo* atherosclerotische progressie.

In **hoofdstuk 8** onderzoeken we het metabolisme van EC verder en veronderstellen we dat Lp(a) een ontsteking veroorzaakt in deze cellen dat gereguleerd is via het EC-metabolisme. In dit hoofdstuk wordt de hypothese getest dat Lp(a) en met name OxPL's op Lp(a) EC-ontsteking veroorzaken, wat leidt tot een verhoogde adhesie en transmigratie van monocyten. Eerdere data van onze groep laten zien dat monocyten afkomstig van patiënten met verhoogde Lp(a)-waarden een verhoogde TEM vertoonden in vergelijking met monocyten afkomstig van gezonde personen. Het Lp(a)-deeltje bestaat uit verschillende componenten en zijn we gaan onderzoeken welke entiteit van Lp(a) ontsteking drijft. De Lp(a)-lipoproteïne bestaat uit een LDL-achtig deeltje, apolipoproteïne (apo)(a), en variabele hoeveelheden OxPLs voornamelijk op de apo(a) en apoB componenten. We tonen aan dat de afwezigheid van Lp(a)-OxPL-signalering, met behulp van ofwel OxPL-deficiënte recombinante apo(a) of het E06 OxPL-blokkerende antilichaam, het ontstekingspotentieel van Lp(a) in de EC duidelijk vermindert. Hiermee tonen wij aan dat de atherogeniciteit van Lp(a) hoofdzakelijk kan worden toegeschreven aan de OxPL-component en niet aan de LDL- of apo(a)-entiteiten. OxPL's, onder andere afkomstig van apoptotische cellen, zijn dus in staat om EC te activeren en kunnen worden geblokkeerd met behulp van E06, wat verder de activerende eigenschap van OxPL's impliceert. De belangrijkste bevinding van deze studie is dat OxPLs geassocieerd met Lp(a) een glycolytische activatie in EC induceren dat gemedieerd wordt via PFKFB3. Dit enzym komt sterk tot expressie in EC gestimuleerd met Lp(a), wat resulteerde in een duidelijke toename van de glycolytische flux. Via de Athero-Express database, tonen we daarnaast een potente toename in EC PFKFB3-expressie in halsslagaders van Lp(a)-patiënten aan. ICAM-1-eiwitniveaus (als maat voor inflammatie) waren tegelijkertijd verhoogd wat wijst op een verhoogde activatie van EC, ondanks een al verhoogde atherosclerotische omgeving in zowel patiënten met lage als hoge Lp(a)-waarden. Hoewel het verschil in LDL kan hebben bijgedragen aan een klein ontstekingseffect, onze recente bevindingen in de ANITSCHKOW-studie maken dit zeer onwaarschijnlijk. Deze studie toonde namelijk bij patiënten met een sterke Lp(a) verhoging aan dat behandeling met een PCSK9 antilichaam resulteerde in 60% LDL-reductie en 14% Lp(a) reductie, maar niet in een reductie van de verhoogde ontstekingsactiviteit in de slagaderwand van deze patiënten. Hierdoor werd de aanhoudende ontstekingsactivatie toegeschreven aan de residuele Lp(a)-verhoging ondanks de PCSK9-antilichaambehandeling en dus LDL-verlaging. Verschillende waarnemingen valideren deze studies. Zo vonden Tomas e.a. dat onstabiele

atherosclerotische plaques in mensen gekenmerkt werden door verhoogde glycolytische activiteit. Deze onstabiele plaques vertoonden een verhoogde expressie van de glycolytische genen HK2, GLUT1 en PFKM, vergelijkbaar met onze bevindingen. De geactiveerde metabole toestand werd bij patiënten met een verhoogde Lp(a) bevestigd met behulp van $^{18}$F-fluorodeoxyglucose (FDG)/gecomputeerde tomografie scans, die significante hogere glucose opname in de arteriële wand van Lp(a)-patiënten lieten zien. *In vitro* data van menselijke EC uit navelstrengen laten zien dat geactiveerde EC bij zuurstofgebrek een verhoogde HIF1$\alpha$-gemedieerde glycolyse vertonen en meer $^{18}$F-FDG accumuleren in vergelijking met de gezonde EC. Hiermee wordt aangetoond dat EC in staat zijn om glucose te accumuleren en vervolgens glycolyse verhogen wanneer ze geactiveerd worden, zoals we hebben waargenomen bij menselijke halsslagaderplaques van Lp(a) patiënten. Bij deze data ontstaat de vraag of remming van glycolyse kan leiden tot een afname van de ontsteking en daarmee tot een verminderde atherogenese. Onze studie toont aan dat inhibitie van PFKFB3 niet alleen de verhoogde glycolytische activiteit in Lp(a)-ECs omkeert, maar ook de ontstekingsreactie en de migratie van monocyten dempt. Het remmen van glycolyse via PFKFB3 leidt tot verminderde endotheliale secretie van IL-6 en MCP-1, en bovendien een afname van monocyt TEM. Belangrijk is dat endotheelspecifieke knockdown van PFKFB3 niet resulteert in hypometabolisme, omdat EC ATP genereren in een normaal tempo in vergelijking met controle cellen. Tot slot, met behulp van menselijk serummonsters van Lp(a)-patiënten die apo(a)-antisense-therapie kregen waarmee Lp(a) verlaagd werd (<80%), vinden we een significant verminderde inflammatoire fenotype in EC *ex vivo* gestimuleerd. Deze reductie verdween geleidelijk na het stoppen van de medicatie bij deze patiënten, wat resulteerde in EC-fenotype zoals vóór interventie. Deze gegevens impliceren dat krachtige Lp(a)-verlaging endotheelontsteking en de verhoogde glycolytische activiteit kan verminderen bij Lp(a)-patiënten. Aangezien Lp(a)-verlaging de EC-ontstekingsreacties echter slechts gedeeltelijk heeft geremd, zijn er nog steeds interventies nodig zijn die verder gaan dan alleen Lp(a)-verlaging.

Het concept van glycolyse remmen in atherosclerose is in **hoofdstuk 9** vertaalt naar een *in vivo* setting. Hier beschrijven we een atherosclerotisch *Ldlr*$^{-/-}$ muismodel met een verhoogd cholesterolwaarden. Eerst laten we zien dat PFKFB3-expressie positief correleert met een onstabiel plaquefenotype in zowel de halsslagader- als de coronaire plaques bij de mens. Bij de mens wordt de verhoogde kwetsbaarheid van de plaque gekenmerkt door een sterk inflammatoir en glycolytisch fenotype, zoals blijkt uit metabole analyse van 156 humane carotis endarterectomie plaques. Zij vonden een verhoogde aanwezigheid van glycoforine A (indicatief voor intraplaque bloeding), wat we bevestigden door het vinden van een positieve correlatie tussen PFKFB3 expressie en necrotische gebied in menselijke coronaire plaques. Daarnaast vonden we een positieve correlatie tussen PFBFB3 en hoog-risico plaques, dat voornamelijk toe te schrijven is aan hoge expressie van PFKFB3 in macrofagen in

zowel de menselijke halsslagader- als de coronaire plaques. De verhoogde kwetsbaarheid van de halsslagaderplaques is positief geassocieerd met een verhoogde prevalentie van ischemische voorvallen en beroertes. Eerdere studies richtten zich op het remmen van glycolyse in macrofagen dat leidde tot een verminderde actieve staat van deze cellen. Wij bevestigden deze bevindingen in atherosclerotische *LDLr* knock-out muizen waarin de progressie van atherosclerose wordt verzwakt door PFKFB3-inhibitie. Plaques van muizen die behandeld zijn met een glycolytische remmer vertoonden minder fibreuze kap atheroma's en verhoogde initiële en intermediaire plaques, wat duidt op een verminderde vorming van geavanceerde plaques. Plaques van deze muizen vertoonden bovendien een afname van het necrotische gebied, een fenomeen dat kan worden toegeschreven aan het aanzienlijke verlies van apoptotische cellen in de behandelde muizen in vergelijking met de controlegroep. In gevorderde stadia van atherosclerotische plaques draagt macrofaagapoptose bij aan de vorming van necrose wat impliceert dat glycolytische remming leidt tot stabilisatie van de plaque. Doordat de plaqueprogressie afhankelijk is van de instroom van immuuncellen, hebben we de metabole staat van perifere bloed mononucleaire cellen (PBMC's) onderzocht. De PBMC-fractie bestaat o.a. uit monocyten, die een belangrijke rol spelen bij de ontwikkeling van atherosclerose. Bij patiënten met ernstige symptomatische coronaire atherosclerose vertonen de monocyten een duidelijk glycolytisch fenotype door overexpressie van hexokinase 2 en PFKFB3 35. We hebben deze bevindingen gevalideerd en remming van PFKFB3 verminderde glycolytische flux in PBMC's wat aangeeft dat deze cellen metabolisch werden geremd, wat op zijn beurt de atherosclerotische belasting bij muizen verlichtte.

Samengevat beschrijft het eerste deel van dit proefschrift hoe verschillende soorten lipoproteïnen in staat zijn om ontsteking te veroorzaken dat leidt tot versnelde atherogenese. Het tweede deel laat zien dat een gemeenschappelijk mechanisme in de vorm van een aangepast metabolisme ten grondslag ligt aan deze ontstekingsstaat dat wordt aangedreven door PFKFB3. In de toekomst kan remming van metabolisme daarom een interessant nieuw doelwit zijn om atherosclerotische CVD verder te verminderen.

# DANKWOORD

Dit proefschrift is een product mede mogelijk gemaakt door de vele mensen die hebben bijgedragen aan het onderzoek waar ik de afgelopen jaren met zoveel plezier aan heb gewerkt. Zonder hen, was het voor mij onmogelijk geweest dit proefschrift te kunnen voltooien. Hoewel het onmogelijk is om iedereen te danken, ga ik toch een poging wagen.

Allereerst wil ik graag mijn promotor prof. dr. Stroes, **Erik**, enorm bedanken voor het geven van de kans om een PhD te kunnen doen op deze fantastische afdeling. Fleur van der Valk benaderde mij voor een positie als PhD gedurende mijn stage en zodoende gingen wij een kop koffie drinken en plots was jij daar ook en dat bleek ook direct mijn sollicitatiegesprek te zijn. Zo kan het ook! Al vanaf moment één ben ik onder de indruk van je altijd-parate kennis, het vermogen om door te pakken en te innoveren. Daarnaast heb je mij geleerd om niet te snel genoegen te nemen in bepaalde situaties en daar ben ik je dan ook erg dankbaar voor.

De grootste rol in het tot stand komen van mijn proefschrift is toe te wijzen aan dr. Kroon, **Jeff**, El Jefe, Jaf/2, Sjeffrey. Wij kwamen op hetzelfde moment werken op de afdeling, jij als post doc en ik als PhD-student. Dit was tevens het moment waarop wij onafscheidelijk bleken te zijn en zo ook vrij snel de naam Jaf vergaarden. Gaandeweg heb ik zoveel mogen leren van jou. Ik ben zeer te spreken over je eindeloze enthousiasme, creativiteit en pragmatisme. Hoe jij zaken voor elkaar krijgt (ook bij mij) en de juiste mensen weet te benaderen, heb ik diep respect. Het maakt mij dan ook trots dat wij samen (met heel veel anderen) een prachtig Circ. Res. paper hebben geschreven waar wij van begin tot het einde al onze ziel en zaligheid aan hebben gegeven. Ik heb daarnaast ook genoten van de ontelbare borrels waar jij, al dan niet met zelf-gebrouwen bier, de slingers ophing. Ik ben je gaandeweg gaan beschouwen als zeer goede vriend en voorzie in de toekomst voor jou een mooie positie als prof. dr. Kroon.

Grote dank gaat ook uit naar de commissieleden **prof. dr. R.H.L. Houtkooper**, **prof. dr. M.P.J. de Winther**, **dr. S. Huveneers**, **prof. dr. J.J.P. Kastelein**, **prof. dr. C.J.M. de Vries** en **prof. dr. G. Pasterkamp** voor het kritisch beoordelen van mijn proefschrift. Ik kijk erg uit naar een interessante en uitdagende gedachtewisseling gedurende de verdediging.

Daarnaast ben ik alle **co-auteurs** zeer erkentelijk die hebben bijgedragen aan de totstandkoming van de papers waaraan ik gewerkt heb. Voor iedereen geldt dat het een bijzonder prettige samenwerking was.

In de afgelopen jaren heb ik ook erg mogen genieten van al mijn directe collega's, zowel op het lab als op F4. Er werd altijd op Champions League-niveau gewerkt maar ook zeker op idem dito niveau geborreld. Wat ben ik jullie dankbaar en wat was het prachtig met jullie!

Allereerst wil ik graag **Fleur** bedanken voor het denken aan mij toen er een PhD-positie vrijkwam in de groep van Erik. Daarnaast iedereen in deze researchgroep, te beginnen bij **Sophie**, hoewel je al in opleiding was, droeg je nog steeds je steentje bij gedurende de meetings. **Kang**, altijd scherp en zoals vaker in deze sectie beschreven wordt, de chillheid zelve, in welke situatie dan ook, daar kan ik nog wat van leren. Wat heb ik ook veel geleerd van jou **Siroon**, altijd in om even een capu te drinken bij Maria op het Voetenplein waar we dan over echt alles praatte. **Lotte**, samen tot diep in de nacht een muizenstudie volbrengen, alsjeblieft nooit meer, volgende keer gewoon weer de glitterbal op 's nachts! Ik ben ook zeer onder de indruk geraakt van de professionele selfies die je maakt, ik kom graag een keer een cursus selfiegrafie bij je doen. Lotte noem je natuurlijk in een adem met **Renate** a.k.a. de koala, prachtmens ben je! Samen vele miljarden PBMCs geïsoleerd maar ook zeker zoveel gelachen samen en ook met Lotte vele spierbal-adjes mogen doen. Zonder jullie waren de vele borrels, plateaupieken en ski-reizen niet zo onvergetelijk geworden, *love your work* en grote dank! Over spierballen gesproken, op **Rutger** kon ik ook altijd rekenen, zo waren er naast het onderzoek nog wel een aantal zaken die zeker besproken moesten worden, met name een bepaald onderwerp. En dan nog een wandelende encyclopedie, **Rens**, als ik ook maar iets te vragen had over cholesterol (of wat dan ook eigenlijk), kon jij mij voorzien van een perfect antwoord. Ik denk dat in de nabije toekomst LDL geen schijn van kans meer maakt tegen jou. Ook heb ik nog samen met jou en Renaat op G1-115 mogen zitten wat ook een ontzettend leuke periode was.

Als we het dan toch over roomies hebben, wil ik ook graag **Moritz**, **Elena** en (daar-is-ie-weer) **Jeff** bedanken voor de mooie jaren in het AMC. Al mijn roomies waren altijd in om het over wetenschap te hebben, maar ook zeker om de momenten van de avond ervoor te evalueren (of de flarden daarvan). Hetzelfde geldt ook voor **Yannick** en **Nick** die vaak kwamen buurten.

Verder wil ik iedereen bedanken op F4 met wie ik heb kunnen sparren, op congres ben gegaan, en op wintersport ben gegaan. **Kristien**, **Nico**, **Simone**, **Merel**, **AF**, **Casper**, **Guido**, **Casper**, **Ilias**, **Noémie**, **Madelief**, **Arjen**, **Julia**, **Stijn**, **Ömrüm**, **Thijs**, **Veera**, **Ulrika**, **Floris** en **Frits**, wat was het een mooie tijd met jullie!

Wat ben ik ook blij dat ik heb mogen werken op het lab van G1! Een mooie samenstelling van verschillende mensen die erg goed bij elkaar passen, behalve **Jorge**. Nee, ook zeker Jorge hoort hierbij want hij is toch wel de gangmaker van het

lab, altijd in om te helpen en ook zeker in om de dag af te sluiten met een koud biertje. Niet geheel verrassend waren de knuffelberen **Hans** en **Han** hier ook altijd wel voor te porren. Hans, dank voor de 813324 Lp(a)-metingen die je hebt gedaan en Han voor je expertise in chromatografie. **Miranda**, Mier, zonder jou had ik hier niet gestaan, je hebt zoveel experimenten voor mij gedaan waar ik je erg dankbaar ben! **Alinda**, Alin, de grote strijder van het lab, wat heb jij een geweldig arbeidsethos (ook gedurende de borrels). **Wil**, je zat er altijd bovenop en **Stefan**, dank voor helpen met de vele kleuringen. Ook **Maaike** wil ik graag bedanken, je was altijd een luisterend oor als ik weer eens aan het klagen was en daarnaast heb je ook keihard gewerkt gedurende het PPI-project, waarvoor hulde! **Anne-Marije**, nog zo'n ontzettende topper, wat ben jij een aanwinst voor het lab. Je bent altijd het zonnetje en brengt de nodige reuring aan de afdeling! Ook bij jou, **Agnes**, kon ik altijd terecht. **Lubna**, samen hebben wij een paar mooie stukken bij elkaar gepipetteerd, waarvoor dank. Als er iemand is die nooit over zich heen laat lopen ben jij dat, **Kim**, dat vind ik heel tof aan je. **Torsten**, when your mind is set, you'll go all in (both professionally as during all the borrels we have had). I think the lab is very happy to have a scientist like you. Prof. dr. Groen, **Bert**, jouw scherpe analyses en ontnuchterende kijk op de wetenschap had een uiterst positief effect op de kwaliteit van mijn onderzoek. Hetzelfde geldt voor **Geesje**, jouw deur stond altijd open, je bent zeer kritisch doch rechtvaardig, dank voor al je feedback afgelopen jaren. **Lars**, ouwe Deen, vriend en paranymf, samen kwamen wij van de studie biomedische wetenschappen en samen begonnen wij een PhD op de afdeling. Onze diners zijn door jouw kookkunsten altijd een groot succes, laten we dit blijven doen in de toekomst. Last but not least, **Julian**, Chris, you were a driving factor in our research group and had major impact on the remain-study. Both professionally and at personal level, we were aligned, Thanks for an amazing time and Julian, I'm still sorry for that time at the terrace (so sorry, not sorry).

Gelukkig was er gedurende afgelopen jaren ook nog wel wat tijd voor ontspanning. **Gunth**, hoewel je altijd in het tropische Singapore was, hadden wij dagelijks (vrijwel altijd hilarisch) contact. Zodra ik achter mijn computer zat, kon ik altijd wel weer een bericht van je verwachten. Een jaar nadat ik was begonnen in het AMC, heb ik **Annick**, Annie, en **Mike**, el Magico, leren kennen. Binnen afzienbare tijd hebben we een zeer hechte vriendschap ontwikkeld waar wij ons leven lang nog plezier van gaan hebben. Uiteraard zijn er nog vele anderen die ik wil noemen, vrienden van vroeger, jaargenoten, dispuutgenoten, boksteam Behdad van Kops, AFC8, Wildeburg hartjes etc., dank voor alles.

De Schnitzler-familie was ook altijd uiterst geïnteresseerd in mijn promotie-traject. Met name tijdens de kerstdiners en de muziekavonden met mijn ooms en mijn vader. **Guus** en **Marceline**, pap en mam, ik kan het niet vaak genoeg zeggen, zonder jullie was dit nooit mogelijk geweest. Dank voor het geloof houden in mij, ik ben trots op

het feit dat jullie mijn ouders zijn. Ook Der Wally, **Wouter**, mijn broertje, beste vriend en paranymf, met jou en **Laurens-Jan**, Lau, hebben we eindeloze gesprekken gehad en mooie avonden gehad waarvan ik hoop dat we deze nog veel gaan hebben. Jullie staan altijd klaar voor mij en konden alles goed relativeren middels een goede portie humor. Jullie zijn altijd actief bezig geweest met mijn persoonlijke leven en mijn carrière, enorm veel dank hiervoor.

Tenslotte, lieve **Marit**, Mit, voor jou schieten woorden tekort maar ik zal het toch proberen. Jij hebt mijn leven vanaf moment één enorm verrijkt. Bij jou kan ik altijd terecht voor wat dan ook. Je hebt een scherpe kijk op bepaalde aspecten van het leven, je bent totaal authentiek, je bent mooi en je hebt een verdomd goed gevoel voor humor. Ik houd van onze gesprekken, je levendigheid en hoe je mij aan het denken zet. Daar kan ik het nog wel even mee uithouden;) Ik kijk uit om de toekomst met jou te delen met alles wat nog komen gaat. Dank dat je in mijn leven bent. Ik houd van jou!

**Jan**

# ABOUT THE AUTHOR

Johan Gustaaf Schnitzler (Jan) was born in Naarden, The Netherlands. Together with his brother Wouter, he grew up in Groenekan near Utrecht. After high school at the Sint Gregorius College in Utrecht, he obtained his bachelor's degree in 2013 and decided to travel through Tanzania for five months. After his travels he started his master Biomedical Sciences at the Vrije Universiteit in Amsterdam and specialized in cardiovascular disease and immunology. Under supervision of Prof. dr. Lutgens, he finished his first internship and was offered a PhD-trajectory in the group of Prof. dr. Stroes, where he and dr. Kroon focused on inflammation and vascular metabolism in atherosclerosis. In August 2020, Jan started his job as consultant in curative healthcare at Q-Consult in Utrecht. Jan and Marit live in Amsterdam and enjoy life there near the beautiful Westerpark. They both enjoy traveling, walking, cooking, music and renovating their new home and so much more. As for other hobbies, he focuses on sports such as boxing, fitness, football and running. Besides sports, he enjoys being among friends and family and enjoys the bi-annual 'muziekavond' with his uncles and father.